MICROFLUIDIC BASED INJECTION SYSTEMS FOR CAPILLARY ELECTROPHORESIS COUPLED TO CONTACTLESS CONDUCTIVITY, FLUORESCENCE AND MASS SPECTROMETRIC DETECTION

INAUGURALDISSERTATION

ZUR

ERLANGUNG DER WÜRDE EINES DOKTORS DER PHILOSOPHIE

VORGELEGT DER

PHILOSOPHISCH-NATURWISSENSCHAFTLICHEN FAKULTÄT

DER UNIVERSITÄT BASEL

VON

JASMINE FURTER

Basel, 2022

Genehmigt von der Philosophisch-Naturwissenschaftlichen Fakultät
auf Antrag von

Prof. Peter C. Hauser

Prof. Daniel Häussinger

Prof. Serge Rudaz

Basel, den 22.06.21

Prof. Dr. Marcel Mayor
Dekan

ABSTRACT

This thesis focuses on the development of novel injection systems for capillary electrophoresis based on microfluidics driven through pressurization combined to different detection methods as well as the coupling to and the use of different ionization methods for mass spectrometry.

At first, an ambient ionization method based on a cold plasma, which is called dielectric barrier discharge, was coupled to a mass spectrometer. The ambient plasma source was low-cost and the circuitry can easily be replicated. The plasma source was characterised in terms of electronic and optical properties. The ionization method was used to qualitatively and quantitatively analyse substances from different application areas such as pharmaceuticals, illegal drugs and food samples.

As second project a new capillary electrophoresis system based on microfluidics was developed. The injection system was solely based on the application of one fixed pressure, while the flow rates were varied by the implementation of flow restrictors. The feasibility of the instrument was demonstrated by the fast separation of different inorganic cations using a thin capillary with an inner diameter of 10 µm. Nine ions were separated in only 25 seconds. Good reproducibility and detection limits could be achieved.

The third project was the development of a graphical user interface for controlling analytical instruments. The software was written in Java programming language and enables the communication with a microcontroller running Forth code. The graphical user interface sends commands in the interpreted programming language Forth to the microcontroller. This approach is simple and improves at the same time the user friendliness of the device operation. This project was published as part of a tutorial about the usage of Forth on microcontrollers for controlling analytical instruments. The graphical user interface was tested by reading and saving analogue values from an alcohol sensor as well as displaying the results in a real time graph.

The fourth project was the development of a low-cost fluorescence detector for capillary electrophoresis. The detector based on a laser diode was assembled from different commercially available parts. The focused light was coupled to the separation capillary and the arising fluorescence converted to a current by using a photomultiplier. The resulting current was amplified and converted to a voltage by using a transimpedance amplifier. The performance of the detector was demonstrated in the scope of a collaboration with

the group of Prof. Dr. Than Duc Mai. A new method was developed for detecting different oligosaccharides labelled with a fluorescent tag by using the detector. The results were compared to the performance of a commercially available instrument.

In the scope of the fifth project, an open source capillary electrophoresis instrument was developed. The design of the instrument was kept as simple as possible. Three modules contained an electronic part for instrument control, a pneumatic part for driving the liquids in the tubes at controlled flow rates and a microfluidic part responsible for all fluid handling actions necessary for sample injection. The performance of the instrument was demonstrated showing the separation of alkaline, alkaline earth metals and different heavy metals. In addition, a method was developed for separating different inorganic ions responsible for honey quality. Four honey samples were analysed quantitatively. This project resulted in a collaboration with the company SensorFactory in the Netherlands.

The last project was the development of an automated capillary electrophoresis instrument for the coupling to a mass spectrometer by using an interface free sheathless nanoelectrospray. The microfluidic part responsible for sample injection contained no electronics to avoid damage of the devices due to the high voltage applied to the injection end. Instead, pneumatic valves and different pressures were used for the injection process. A capillary with an internal diameter of 15 µm was employed for obtaining good resolution. Volatile buffers based on acetic acid were used to achieve acceptable separation and ionization of the analytes. The feasibility of the set-up was demonstrated by separating three benzalkonium chloride homologues qualitatively. Good resolution and detection limits were obtained for the quantitative measurements of four pesticides in spiked grape juice.

„Mut brüllt nicht immer nur.
Mut kann auch die leise Stimme am
Ende des Tages sein, die sagt:
Morgen versuche ich es nochmal."

Mary Anne Radmacher

ACKNOWLEDGEMENTS

Without the help of so many people, it would be not possible to conduct this PhD thesis. First of all, I'd like to sincerely thank Prof. Dr. Peter Hauser for accepting me as a PhD student and for his valuable supervision and helpful guidance during these four years. I really appreciated to work on the various interesting projects and valued their interdisciplinary character. I'm grateful that Prof. Dr. Daniel Häussinger accepted to be second supervisor and for his helpful advices and support during the annual meetings. I would like to thank Prof. Dr. Serge Rudaz for being co-examiner to this work.

Many thanks to all members of the workshop, Andres Koller, Philipp Knöpfel, Grischa Martin and their apprentices. Their great knowledge and technical assistance was very important for building the analytical instruments. I would also like to acknowledge Markus Ast, Hisni Meha and Andreas Sohler for taking care of the whole building and always being very quick on-site for helping out whenever help was needed. I'm very grateful to Marina Mambelli-Johnson for taking care of all administrative matters and to the University of Basel for the financial support. I would to especially thank all present members of the group including Kanchalar Keeratirawee, Nattapong Chantipmanee, Sophia Rehm, Marc Aurèle-Boillat, Andrei Hutanu and also to the former members for a nice working atmosphere, helpful suggestions and support whenever needed and for just having a great time together in these four years. I thank my students Claire, Caroline, Björn and Marc. I would like to acknowledge Prof. Dr. Joao Petruci and Dr. Joel Koenka for correcting my thesis. I would like to appreciate the co-authors, Prof. Than Duc Mai and his group from the university of Paris for the interesting collaboration.

My warmest gratitude belongs to Jakob. You were always on my side during the last years. Thank you for all the love and your enormous support. I'm deeply grateful to my whole family and my friends for their support and encouragement. Without you all, I would not be here today. I'd like to thank in particular my parents Rene and Elisabeth for their tremendous support during my undergraduate and graduate studies and always believing in me.

CONTENTS

I INTRODUCTION 1

1 CAPILLARY ELECTROPHORESIS 3
- 1.1 History . . . 3
- 1.2 Basic Principles and Concepts . . . 4
  - 1.2.1 Instrumental set-up . . . 4
  - 1.2.2 Electroosmotic flow . . . 6
  - 1.2.3 Electromigration . . . 8
  - 1.2.4 Band broadening effects . . . 9
- 1.3 Modes of capillary electrophoresis . . . 10
- 1.4 Detection Methods . . . 12
  - 1.4.1 Mass Spectrometry . . . 13
  - 1.4.2 Optical Detection . . . 13
  - 1.4.3 Electrochemical Detection . . . 15

2 MASS SPECTROMETRY 19
- 2.1 Basic Principles . . . 19
  - 2.1.1 Mass Spectrum . . . 19
- 2.2 Mass Spectrometer . . . 20
  - 2.2.1 Ion sources . . . 20
  - 2.2.2 Mass analyser . . . 24
  - 2.2.3 Hyphenated Methods . . . 25

3 PURPOSE-MADE CAPILLARY ELECTROPHORESIS SYSTEMS 29
- 3.1 Introduction . . . 29
- 3.2 Design of purpose-made microfluidic CE instruments . . . 31

II RESULTS AND DISCUSSION 35

4 PROJECTS 37
- 4.1 DBD ionization source for mass spectrometry . . . 37
- 4.2 Flow restrictor based injection system for CE . . . 51
- 4.3 Forth for controlling analytical instruments . . . 57
- 4.4 Modular instrumentation for CE with LIF . . . 71
- 4.5 Low-cost open-source automated CE instrument . . . 81
- 4.6 Injection system for mass spectrometry based on pneumatic control . . . 93

III REFERENCES 131

IV LIST OF PUBLICATIONS AND POSTERS 137

V APPENDIX 141

LIST OF FIGURES

Figure 1 CE instrument set-up 5
Figure 2 Scheme of the electric double layer in a fused silica capillary 6
Figure 3 Hydrodynamic flow profiles 7
Figure 4 Schematic drawing of the C^4D detector 16
Figure 5 Electronic circuitry of a C^4D detector 17
Figure 6 Detection circuitry of a C^4D detector 17
Figure 7 Schematic drawing of the ESI with Taylor cone 22
Figure 8 Application ranges of different API methods 23
Figure 9 Schematic drawing of a split injector 33

LIST OF ABBREVIATIONS

AC alternating current

ADC analog-to-digital converter

ADI ambient desorption/ionization

APCI atmospheric pressure chemical ionization

API atmospheric pressure ionization

APPI atmospheric pressure photoionization

APTS 8-aminopyrene-1,3,6-trisulfonic acid

BGE background electrolyte

BR buffer reservoir

CE capillary electrophoresis

CGE capillary gel electrophoresis

CI chemical ionization

cIEF capillary isoelectric focusing

CMC critical micelle concentration

CZE capillary zone electrophoresis

C^4D capacitively coupled contactless conductivity detection

DAD diode array detector

DBD dielectric barrier discharge

DC direct current

DNA deoxyribonucleic acid

EI electron ionization

EOF electroosmotic flow

ESI electrospray ionization

FAB fast atom bombardment

FIA flow injection analysis

FT-ICR fourier-transform ion cyclotron resonance

GE slab gel electrophoresis

GUI graphical user interface

HPCE high performance capillary electrophoresis

HPLC high performance liquid chromatography

HV high voltage

ID inner diameter

IDE integrated development environment

ITP isotachophoresis

I²C inter-integrated circuit

LASER light amplification by stimulated emission of radiation

LED light emitting diode

LIF laser induced fluorescence

LOAR lab on a robot

LOC lab on a chip

LOD limit of detection

LTE local thermal equilibrium

LTP low temperature plasma

MALDI matrix-assisted laser desorption/ionization

MCE microchip electrophoresis

MEKC micellar electrokinetic chromatography

MS mass spectrometer

m/z mass-to-charge ratio

OD outer diameter

OSCE open source capillary electrophoresis

OSH open source hardware

PAGE polyacrylamide gel electrophoresis

PEEK polyether ether ketone

PMMA poly(methyl methacrylate)

PMT photomultiplier tube

Q quadrupole

QIT quadrupole ion trap

RSD relative standard deviation

SDS sodium dodecyl sulfate

SIA sequential injection analysis

SPE solid phase extraction

TIC total ion current

ToF time of flight

μTAS micro total analytical system

Part I

INTRODUCTION

1 CAPILLARY ELECTROPHORESIS

Capillary electrophoresis (CE) as an analytical separation technique allows to isolate an analyte from other compounds of a sample, detect and characterize it [1]. Charged and neutral compounds are separated based on their different mobilities in an electric field [1, 2]. As a complementary method to high performance liquid chromatography (HPLC), CE is characterised by short analysis times, high separation efficiencies and resolution [1–4]. Further advantages include minimal buffer and sample consumption, lack of organic waste production and the possibility to adjust a certain pH and temperature required to analyse rather unstable biomolecules [1, 3]. The possibility of implementing different CE methods and applying diverse detection methods, allows to separate many different analyte classes such as proteins, peptides, vitamins, nucleic acids, carbohydrates, amino acids and inorganic ions [2].

1.1 HISTORY

More than a hundred years ago Kohlrausch investigated basic theoretical principles of electrophoresis and formulated the essential equation for ion migration [5]. In 1923, Kendall and Crittenden [6] separated for the first time rare earth metals by isotachophoresis. Important pioneering work was predominantly done by Tiselius in 1930 by performing "moving boundary electrophoresis" [7]. He separated different serum proteins in plasma according to their charge by using a quartz U-tube and detecting the analytes by UV light photography [8]. For his important work, Tiselius was awarded a Nobel Prize in 1948 [4]. Subsequently, the works of Svenson [9], Longsworth [10] and Dole [11] were essential for the development of zone and displacement electrophoresis. In the early stage of CE, the method was conducted in glass tubes with large internal diameters filled with liquids and therefore leading to excessive Joule heating. As a consequence, blurred analyte zones were obtained and only low voltages could be applied [1, 8]. Later, during the development of the so-called slab gel electrophoresis (GE) in the 1950s, anticonvective media such as starch, agarose gels or paper were introduced to reduce the current [1, 2]. Gel electrophoresis as a rapid and inexpensive method is still frequently used today for preparative and analytical purposes in biochemistry enabling the separation of biomolecules such as proteins, peptides and DNA [1].

In 1967, Hjertén made an important discovery for the development of elec-

trophoresis [12]. For performing free zone electrophoresis, he coated the tubes with methyl cellulose and succeeded this way to eliminate the electroosmotic flow (EOF) [12]. High performance capillary electrophoresis was only developed in the 1980s [2]. Jorgenson and Lukacs employed in 1981 for the first time a glass capillary with a low internal diameter of 75 µm [13, 14]. The use of narrow-bore capillaries made CE popular, since the high electric resistance of the capillary reduced Joule heating [4]. Nowadays, CE is performed in miniaturized and automated systems, on field by using portable instrumentation or by using small chips (microchip capillary electrophoresis). Separation times and reproducibility have been greatly improved. Therefore, CE can be used in many areas including environmental analysis, pharmaceutical and biomedical applications, forensic sciences and industrial analysis.

1.2 BASIC PRINCIPLES AND CONCEPTS

1.2.1 *Instrumental set-up*

A typical capillary electrophoresis instrument has a relatively simple experimental set-up as shown in Figure 1. A fused silica capillary (**E**) is filled with a suitable buffer solution and dipped in two reservoirs (**A** and **G**) containing the same solution. An electrode (**B**) is attached to each reservoir, which is connected to a high voltage power supply (**D**). For sample injection, the buffer reservoir at the capillary inlet (**A**) is exchanged by a vessel containing the sample solution (**C**). After introduction of a small sample amount into the capillary, the high voltage is turned on to start the separation process. The solutes in the capillary migrate with different velocities through the capillary. Due to their difference in mobility they will separate from each other over time. A detector (**F**) connected to a data acquisition system, placed either on-column or off-column measures the separated analyte zones [3]. Signals are recorded by a data acquisition system (**H**). On a computer (**I**) the resulting data is displayed in an electropherogram with the signal intensity plotted against the migration time.

The capillary is usually made of fused silica and has an internal diameter between 10 and 100 µm [4]. The stability of the fragile glass tube is increased by a thin polyimide coating with only a few micrometer in thickness. Other materials can be used as well for the separation capillary such as borosilicate glass, fluoroethylenepropylene or tetrafluoroethylene [4]. However, fused silica is more established and can be purchased from many suppliers [4]. Larger diameter capillaries are favourable for optical detection where the optical path length is critical. Disadvantages of wide bore capillaries are higher Joule heating, which can lead to peak broadening and issues concerning sample integrity. This limits the height of voltages, which can be

applied for driving the separation without compromising the measurement. Joule heating arises due to the current passing through the conductive liquid in the applied electric field [2]. A lower internal diameter of the capillary restricts the current flow due to the higher electric resistance of the capillary [3]. Narrow bore capillaries have also the advantage to efficiently dissipate heat through the capillary wall due to the high surface area-to-volume ratio [4]. Disadvantages of narrow bore capillaries are possible difficulties in handling due to clogging issues and the possibility of increased sample adsorption at the capillary wall [3].

Electrodes made of an inert metal such as platinum or gold provide the electrical connection between the high voltage power supply and the buffer reservoirs. Usually, DC high voltages between 10 and 30 kV are applied for driving the separations. Higher voltages can result in disturbing corona discharges. In capillary electrophoresis it is important to position the two electrolyte reservoirs at the same height. Otherwise a laminar flow is arising due to siphoning effects leading to a reduced reproducibility of the measurements [3, 4]. Possible detection systems for CE are for example UV/Vis, fluorescence, refractive index, conductivity detection and mass spectrometry (see Section 1.4) [4].

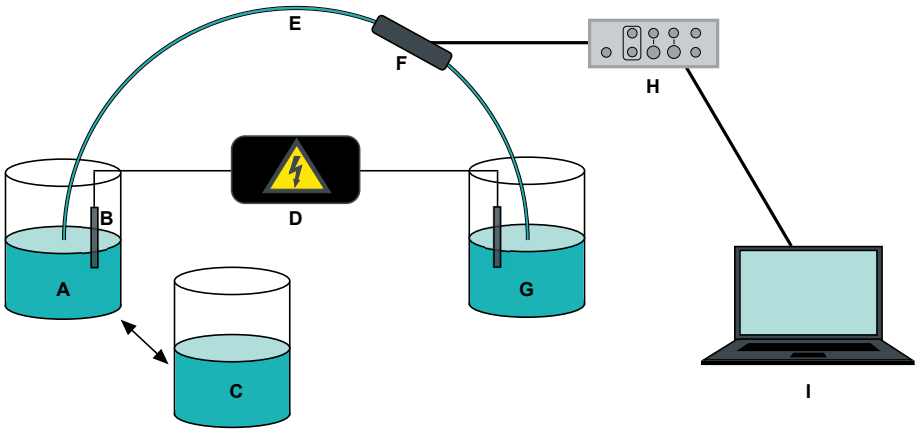

Figure 1: Set-up of a CE instrument

At the beginning of a measurement series, the capillary is usually flushed with sodium hydroxide solution [3, 4]. Due to the nature of the fused silica, the inner capillary wall consists of silanol groups (SiOH), which can be either protonated or dissociated depending on the pH of the filling solution. The conditioning step brings all silanol groups at the inner capillary wall in a well-defined state and therefore largely improves the reproducibility of the measurement [3]. For the separation, the capillary is filled with an aqueous buffer solution, normally called electrolyte or background electrolyte (BGE)

[2]. Capillary electrophoresis is very pH sensitive because of the electroosmotic flow (EOF) which largely effects the effective mobilities of the analytes (see Section 1.2.2). The electrolyte should therefore have sufficient buffering capacities in the chosen range to maintain a constant pH. Further requirements to the buffer are a low mobility to limit the current generation and a low UV absorbance when optical detection is used [3].

1.2.2 *Electroosmotic flow*

An important particularity of capillary electrophoresis is the electroosmotic flow (EOF), which leads to a bulk flow of the buffer solution through the capillary in an applied electric field [4]. This electrokinetic phenomenon is a consequence of the deprotonated silanol groups at the interior capillary wall leading to the formation of an electric double layer (see Figure 2) [4].

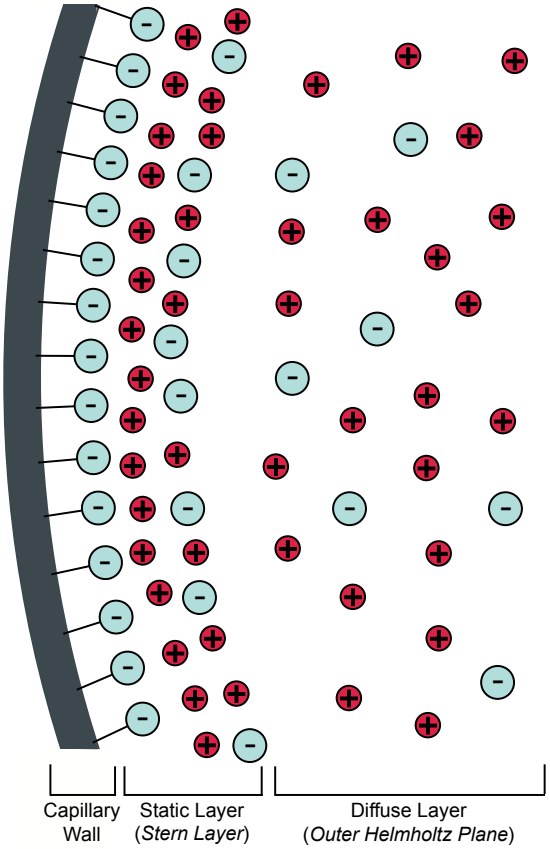

Figure 2: Scheme of the electric double layer in a fused silica capillary

Two species are accumulating in the proximity of the negative capillary surface, which are hydronium ions and oriented water dipoles from the buffer solution [4]. A double layer is formed with the first rigid layer called Stern

layer or inner Helmholtz layer [2, 15]. Next to this static layer, a more diffuse layer of mobile cations is formed, which is called outer Helmholtz layer. The diffuse layer will move towards the cathode upon application of a high voltage because the hydronium ions are less tightly attached in this region [4]. The EOF becomes significant at pH above 4 of the electrolyte solution where the silanol groups are starting to dissociate [4]. The velocity of the EOF can be calculated by using equation 1. It is proportional to the dielectric constant of the buffer (ϵ), the zeta potential (ζ), the applied electric field (E) and inversely proportional to the viscosity of the electrolyte (η) [2]. Since the zeta potential is determined by the amount and dissociation of the silanol groups of the capillary, it is generally used as a measure for the EOF strength [4].

$$\nu_{EOF} = \frac{\epsilon \zeta E}{4\pi\eta} \tag{1}$$

The EOF as a superimposing buffer flow through the capillary accelerates the separation of cations and drags neutrals and even anions towards the cathode [4]. That means that all species can be analysed in a single run. The EOF has also a significant effect on the hydrodynamic flow profile in the separation capillary. Instead of a laminar flow normally present when pumping the liquid through a capillary (Figure 3 A), the EOF leads to a plug flow profile (Figure 3 B). The flat flow appears because the pressure is not dropping along the capillary, but the driving force is evenly distributed [3]. Band broadening is therefore minimised and separation efficiency increased, which is a huge benefit of CE compared to HPLC [2, 3].

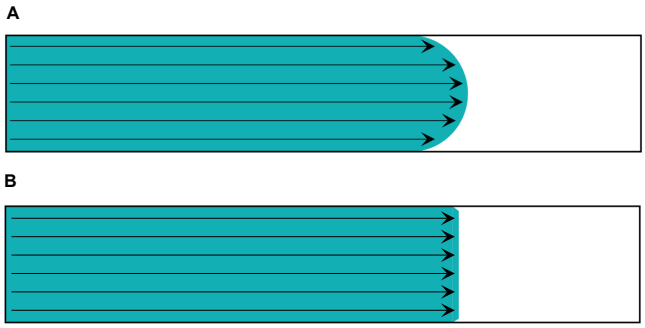

Figure 3: Flow profiles in a capillary (A) Laminar flow due to an applied pressure (B) Plug flow profile due to the EOF

Although the EOF has many advantages, it needs to be controlled. Especially when measuring at high pH values, the EOF would otherwise be too fast and therefore deteriorate the separation. Also adsorption of analytes at the negatively charged capillary wall needs to be restricted [3]. The EOF strength can be reduced by using low pH buffers, increasing the ionic strength of the electrolyte or adding organic solvents. In addition, the capillary surface property can also be changed by adding a neutral hydrophilic polymer to the buffer as a dynamic coating. The capillary wall can also be modified permanently

by a covalent coating [2, 3].
For the separation of anions, the EOF can be reversed by using buffer additives such as cetyltrimethylammoniumbromid (CTAB) or tetradecyltrimethylammonium bromide (TTAB) [4]. The inversion in the polarity of the zeta potential leads then to an EOF flow towards the anode [4, 16].

1.2.3 *Electromigration*

Capillary electrophoresis is based on the principle that electrically charged solutes migrate in a conductive liquid under an applied electric field. The electric force in the electric field accelerates the ions towards the attracting electrode. On the other hand, the frictional force in a liquid or gel opposes the movement. After reaching an equilibrium between the two forces, the ions migrate at constant velocity in the electric field. Therefore the electric force depending on the applied electric field (E) and the ion charge (q) equals the negative frictional force (equation 2). The frictional force of a spherical ion is determined by the solution viscosity (η), the ion velocity (ν) and the ion radius (r).

$$qE = 6\pi\eta\nu r \tag{2}$$

From this equation an expression for the electrophoretic velocity (ν_e) can be derived (equation 3).

$$\nu_e = \frac{qE}{6\pi\eta r} \tag{3}$$

The velocity (ν_e) is depending on the electrophoretic mobility (μ_e) and the applied electric field (E) (equation 4).

$$\nu_e = \mu_e E \tag{4}$$

By combining equations 3 and 4, an expression for the mobility of an ion in an electric field is found (equation 5). Because the viscosity is constant for a given electrolyte, the mobility only depends on the charge to size ratio of the ion [2]. Therefore highly charged and small solutes are faster than uncharged larger ones.

$$\mu_e = \frac{q}{6\pi\eta r} \tag{5}$$

Because of the superimposed electroosmotic flow (EOF), the apparent electrophoretic mobility (μ_a) of a solute is the sum of its own electrophoretic mobility (μ_e) and the electrophoretic mobility of the electroosmotic flow (μ_{EOF}) referring to equation 6.

$$\mu_a = \mu_e + \mu_{EOF} \tag{6}$$

The time needed by an analyte to migrate to the detection point is called migration time (t) and defined by the effective capillary length (L_{eff}) divided by the apparent electrophoretic velocity (ν_a) (equation 7). Although the migration time is characteristic for a given analyte, it is no absolute proof of identity.

$$t = \frac{L_{eff}}{\nu_a} = \frac{L_{eff}^2}{\mu_a V} \tag{7}$$

1.2.4 *Band broadening effects*

Broadening of zone lengths due to dispersion should be controlled in CE. Otherwise the necessary mobility difference to separate two compounds is increasing. Under ideal conditions, only longitudinal zone broadening along the capillary would be existing [3]. Therefore this factor defines the fundamental efficiency limit in CE [3]. Radial diffusion across the capillary is not relevant due to the plug flow profile of the EOF.

By application of high voltages, Joule heating becomes an important contributor to band broadening leading to a loss in resolution. The current passing through the conductive buffer leads to a temperature gradient across the capillary diameter, which destroys the plug flow profile [2]. Joule heating can be minimised by using lower conductivity buffers, applying lower voltages and decreasing the internal diameter of the capillaries. Other contributors to dispersion are the injection plug length and sample adsorption to the capillary wall causing peak tailing [3].

1.2.4.1 *Sample Injection*

Sample injection in capillary electrophoresis is challenging because only tiny sample amounts in the nanoliter to picoliter range are required. Therefore the quantity cannot be measured directly but needs to be calculated. As a rule of thumb the sample plug length should occupy less than 1 to 2 % of the effective length of the capillary. Sample overloading should be avoided because it affects the resolution and causes distortion of peaks. Various injection methods were developed for capillary electrophoresis. The most common ones are electrokinetic and hydrodynamic sample introduction. There exist also various other approaches such as split flow injection, sample gating, electric sample splitting [4].

Electrokinetic injection is based on the application of a low voltage to the capillary dipped in the sample vessel for a controlled time length [3]. The analytes move into the capillary by electrophoretic migration and EOF [3]. This injection method is simple because the high voltage module needed for the injection is already on-site. On the other hand, discrimination of analyte

ions occurs because of their differences in mobility and dependence on the sample concentration. The injected sample amount can be calculated by using equation 8. The injected sample amount in moles (Q) is dependent on the electrophoretic mobility (μ_e) of the analyte and the mobility of the EOF (μ_{EOF}) as well as on the capillary radius (r), the voltage (V), the sample concentration (C), time (t) and total capillary length (L).

$$Q = \frac{(\mu_e + \mu_{EOF})\pi r^2 VCt}{L} \tag{8}$$

Hydrodynamic injection is based on the creation of a pressure difference across the capillary. Either a pressure is applied at the inlet end or vacuum at the outlet end of the capillary [3]. Another possibility is injection by siphoning where the injection reservoir is elevated to a defined level towards the outlet end [3]. The advantage of hydrodynamic injection is that sample bias are avoided because the injection is independent of the sample matrix [3]. Therefore, hydrodynamic injection is better reproducible than electrokinetic injection [3].

The sample volume can be calculated by using the law of Hagen-Poiseuille (equation 9) [3]. The injected sample amount is a function of the pressure difference across the capillary (ΔP), the inner diameter of the capillary (d), the time length (t), the solution viscosity (η) and the capillary length (L).

$$V = \frac{\Delta P d^4 \pi t}{128 \eta L} \tag{9}$$

In the case of siphoning, the hydrostatic pressure (ΔP) is a function of the fluid density (ρ), the gravitational acceleration (g) and the height difference (Δh). ΔP can be calculated by using Pascal's law (equation 10).

$$\Delta P = \rho g \Delta h \tag{10}$$

1.3 MODES OF CAPILLARY ELECTROPHORESIS

In capillary electrophoresis, various operation modes can be applied to address different analytical tasks. The modes are based on different separation mechanisms and most of them are defined by the composition of the background electrolyte [3, 4]. The most prominent representatives are capillary zone electrophoresis (CZE), micellar electrokinetic chromatography (MEKC), capillary gel electrophoresis (CGE), capillary isoelectric focusing (cIEF) and isotachophoresis (ITP). When using CZE, MEKC and CGE, the analytes are migrating in discrete zones wherefore these are called zonal techniques [3]. CIEF on the other hand is based on focusing of the solutes and ITP is a "moving boundary" technique [3].

Capillary zone electrophoresis is the simplest operation mode with the analytes migrating in discrete zones in a capillary filled with a suitable buffer. With CZE, cations as well as anions can be separated while neutral solutes co-migrate all together with the EOF [3]. Selectivity can be controlled by the composition and the pH of the background electrolyte. Many different additives can be added to the buffer. Organic solvents for example decrease the conductivity and EOF strength because they disturb the structure of the water molecules at the capillary wall [1]. Zwitterionic salts on the other hand such as trimethylglycine or potassium sulfate improve the separation of proteins by preventing their adsorption to the capillary wall [17].

Micellar electrokinetic chromatography is an intermediate between capillary electrophoresis and chromatographic techniques [4]. A charged surfactant is added to the running buffer, for example sodium dodecyl sulfate (SDS). Above the critical micellar concentration (cmc), micelles are formed out of the negatively charged molecules leading to a dynamic stationary phase [4]. An equilibrium establishes where analytes are distributed between the electrolyte and the formed micelles [4]. The longer an analyte stays within the micelle, the slower it migrates [3]. MEKC is very useful to analyse neutral analytes, but can also be applied to charged solutes [3]. As an example, MEKC has been successfully used to analyse neutral triazine compounds in ground water [18]. Triazines are frequently used herbicides applied to the soil to increase harvest yields [18].

Analytes can also be separated on the basis of their size by using capillary gel electrophoresis, which is related to the standard slab gel electrophoresis [4]. In this method, the analytes are migrating in the electric field through a gel filled into the capillary. The gel serves at the same time as anticonvective medium to reduce the current and as sieving matrix [3]. The larger the analyte is, the more friction it will experience within the polymer network and therefore have longer migration times [4]. This method is used to separate large biological macromolecules such as proteins, nucleic acids or peptides [3, 4]. Commonly used gels are crosslinked polyacrylamide and agarose. Polyacrylamide has a smaller mesh size and is therefore more suitable for proteins while agarose with the larger mesh spacing is better for DNA [3]. CGE was applied for example to determine the form distribution of plasmids, which are small circular DNA molecules, by using a hydroxypropylmethylcellulose gel [19].

By using capillary isoelectric focusing, proteins and peptides are separated on the basis of their pI [3]. For this method, a pH gradient needs to be established across the capillary. Ampholytes are employed for this purpose, which contain an acidic and a basic moiety [3]. The method is conducted in two steps. The capillary is first filled with a mixture of ampholytes and so-

lutes. In addition, a basic solution will be placed at the cathode and an acidic one at the anode. Upon application of a voltage, the charged ampholytes and proteins migrate to the region of their pI where they become neutral. This focusing step leads to very narrow sample zones and its end is characterised by a drop in the current flow. In the following mobilising step, the zones are passed through the detector by either applying pressure or adding salt to one of the buffer containers [3]. CIEF having a very high resolution is commonly used to measure the pI of proteins and for the separation of protein isoforms [3].

Capillary isotachophoresis is a "moving boundary" technique where the separated analyte zones move all at the same velocity [3]. To achieve this, two buffer systems are used, consisting of a leading and a terminating electrolyte. In one measurement, either cations or anions can be analysed [3]. For the analysis of cations for example, the leading electrolyte contains a cation, which has a higher effective mobility than the solutes while the terminating cation has a lower mobility than the solutes. The different cations migrate then in discrete zones, but all with the same velocity. ITP is conducted in a constant current mode with the electric field varying in each zone. The method was combined with mass spectrometry to detect amyloid peptides as markers of the Alzheimer's disease by analysis of cerebrospinal fluid [20]. ITP can also be used as a preconcentration step to CZE, CGE or MEKC [3].

1.4 DETECTION METHODS

Sensitive detection in capillary electrophoresis is challenging due to the small employed dimensions. Only very small sample volumes are injected and the path lengths for optical detection are short because of the low internal diameters of the separation capillaries [4]. On the other hand, the concentration of the analyte zones at the detection end is similar to the beginning of the analysis. This is an advantage compared to HPLC, where the sample is diluted many times when arriving at the detector [4].

Many different detection techniques were developed for CE over the years. Detection can be performed on-column as well as off-column. In general, analyte detection on the capillary is favourable because dead-volumes as well as zone broadening or component mixing can be avoided [3]. Detection can either be performed by measuring the property of one solute in the mixture (UV/Vis or fluorescence detection) or by measuring a fundamental property of the whole solution (refractive index or conductivity) [4]. The recorded signals from the detector are plotted against the migration time in so-called electropherograms [2]. Detection limits can be improved by preconcentrating the sample prior to the analysis. Possible methods for concentrating the sample inside the capillary are for example isotachophoresis or sample stacking

[3]. The stacking method is based on a difference in concentration between the running electrolyte and the sample of around 10 [3]. Therefore in CE, the sample is usually not dissolved in the carrier electrolyte. Due to the lower concentration of the sample zone the electric field is higher in this region than in the buffer solution. Ions migrate therefore faster in within the sample zone until they reach the electrolyte boundary. When arriving there, they migrate slower leading to a concentrated analyte zone in this region [3].

1.4.1 *Mass Spectrometry*

Mass spectrometry (MS) as a detection method for capillary electrophoresis will be discussed in more detail in Chapter 2. It enables selective and sensitive detection and identification of small as well as large molecules on the basis of their mass-to-charge ratio (m/z) [21]. The molecular weight is determined and also structural information can be gained from the analysis [1]. Components that co-migrated in CE can easily be distinguished with MS [21, 22]. Since capillary electrophoresis and mass spectrometry are orthogonal analytical techniques, their coupling leads to a 2D separation system. In capillary electrophoresis the separation takes place in an electrolyte solution while in mass spectrometry the analytes are separated in high vacuum [1]. The interfacing between CE and MS is done in most cases via electrospray (ESI) (see Section 2.2.1.2), which is convenient to ionize polar and charged substances provided by CE [1, 21].

1.4.2 *Optical Detection*

In optical detection, the signal is usually measured on-column. Therefore, a part of the polyimide coating on the capillary has to be removed to create a detection window. In order to obtain a high resolution, the width of the detection window should be small compared to the solute zone width. Sensitivity and the linear range are dependent on the optical path length. By increasing the diameter of the separation capillary these parameters can be improved but at the cost of the resolution [3]. To overcome the maximum length of 100 µm available for separation capillaries, the optical path length can be further increased by using special designed cells such as the bubble cell or the Z-shaped cell [2].

1.4.2.1 *UV/Vis Detection*

UV/Vis absorption detection is the most commonly applied detection method to capillary electrophoresis [2, 4]. The detection is based on the absorption of light by the analyte measured at a specific wavelength. The absorption can be calculated from the ratio between the output light intensity (I) and

the initial light intensity (I_0). The so-called transmittance (T) is related to the absorption (A) on a logarithmic scale (equation 11) [4].

$$A = \log_{10} \frac{I_0}{I} \tag{11}$$

The analyte concentration can be calculated by using the Beer-Lambert's law (equation 12). The compound absorption (A) depends on its molar absorption (ϵ), the concentration (c) and the optical path length (d).

$$A = \epsilon c d \tag{12}$$

Different types of UV/Vis detectors are available. Normally a deuterium or atomic vapour lamp such as zinc, cadmium or mercury is employed as light source. The light beam is then focused onto the capillary in a detection cell. The wavelength of the emitted light is selected by using a monochromator before the signal is recorded by a photodiode or multiplier. Instead of measuring only a single or multiple wavelengths, it is also possible to use a diode-array detector (DAD) to measure the whole UV/Vis spectrum of the sample [2]. Each of the photodiodes in the DAD measures a narrow-band spectrum, which makes it easy to find quickly the optimum wavelength of all absorbing solutes [3]. Another approach is to use light-emitting diodes (LEDs) as light sources and photodiodes for detection, which make UV/Vis detection suitable for battery powered portable CE instruments due to small sizes, low power consumption and low costs [23]. As an example, a detector in the deep-UV range at 255 nm and 280 nm was developed, which is important for the analysis of various organic compounds absorbing in this region [24]. This was demonstrated by detecting 4-nitrobenzoic, 4-hydroxybenzoic and 4-aminobenzoic acid [24]. Detection limits (LOD) for UV/Vis absorption are usually in the micromolar range [21].

For analytes, which are non UV absorbing, detection can be done indirectly by adding a chromophore with a high absorption to the background electrolyte. The signals of the analytes are then observed as negative peaks [4]. However, indirect methods have a lower sensitivity than direct detection.

1.4.2.2 *Fluorescence Detection*

Fluorescence detection is very sensitive with possible detection limits in the picomolar range. Due to the rarity of fluorescent molecules, this detection method is also very selective [21, 25]. For analytes not naturally fluorescent a derivatization step can be included or indirect fluorescence detection methods be used.

The instrumental set-up of a fluorescence detector consists of an excitation

light source such as a xenon lamp. By implementation of lenses, the light is coupled to a monochromator before being focused on the capillary in the detection window. The fluorescence emission is collected in a right angle to the excitation light. An optical filter removes scattering of the excitation light before the fluorescence light is reaching the photomuliplier tube (PMT) [4]. Instead of using conventional light sources, also lasers can be used as excitation sources. Laser induced fluorescence (LIF) for capillary electrophoresis gives the lowest detection limits available in the field of separation technologies [3]. It is even possible to do analysis on a single cell level to detect for example tumor cells [26]. Laser diodes can readily be used as light source and have many advantages compared to conventional lasers concerning the smaller dimensions, lower costs and higher stability of the output [27].

1.4.3 *Electrochemical Detection*

Electrochemical detection methods include amperometry, potentiometry and conductivity [1]. Amperometric and potentiometric detection is based on the measurement of one property of the solutes while conductivity detection is a bulk detection method. Electrochemical detection techniques are especially useful for compounds which are lacking a UV or fluorescent active moiety. Such analytes can otherwise only be determined by derivatization or indirect methods, which are not very sensitive and have a limited linear range [1]. Electrochemical detection methods on the other hand have good detection limits and can more easily be miniaturized, because the optical dimensions are not an issue.

Amperometry and potentiometry are based on reactions of the analytes at the solution or electrode surface [1]. In potentiometric detection, a potential difference is created between the internal filling solution of an electrode and the sample solution [1]. This is achieved by selectively transferring ions through a membrane [1]. For miniaturization of potentiometry necessary for the coupling to capillary electrophoresis, ion-selective microelectrodes can be used [28].

Amperometric detection on the other hand is based on Faraday reactions of the analyte at a solid electrode surface upon an applied DC voltage. The resulting current is directly related to the solute concentration. Amperometry is more sensitive than conductivity detection but is limited to electroactive substances [1]. The standard amperometric detection cells rely on a three-electrode arrangement with a reference electrode, a counter electrode and a working electrode where the electrode reactions take place. With the coupling to capillary electrophoresis, even four electrodes become necessary at the detection end due to the additional required separation voltage. However, it has been demonstrated by Kappes and Hauser [29] that it is also

possible to perform CE separations with amperometric detection by employing only two electrodes. This was possible by using the electrophoretic ground electrode at the same time also as pseudo-reference and amperometric counter electrode [29, 30].

1.4.3.1 *Conductivity Detection*

In conductivity detection, an alternating potential is applied across two electrodes [1]. The resulting electric current coming from the ion movement in the solution corresponds to the conductivity of the sample [1]. The electrical conductance of the cell (G) in Siemens (S) depends on the specific conductivity of the solution (κ) in Sm^{-1}, the surface area (A) and the distance between the electrodes (l) as shown in equation 13. The cell constant is the factor l/A [31].

$$G = \kappa \frac{A}{l} \tag{13}$$

From a historical view, conductivity detectors were developed out of isotachophoresis systems, which were also operated in a constant current mode [4, 32]. The first conductivity detectors consisted of two electrodes being in direct contact with the buffer solution [1]. Because it was difficult to construct cells with the right dimension fitting the internal diameter of the separation tube, conductivity detection was not very popular in CE [33].

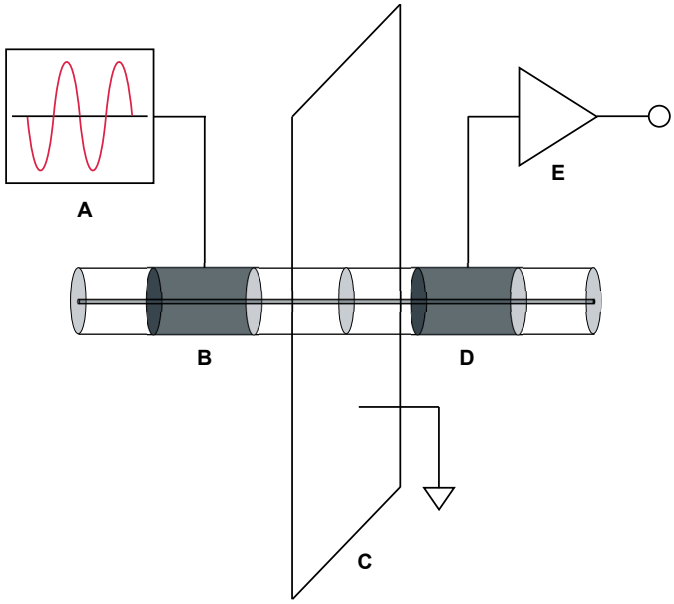

Figure 4: Schematic drawing of the C^4D detector in axial arrangement

Luckily, a contactless conductivity detector was developed in the early 1980s by Găs et al. [34]. A high-frequency signal was capacitively coupled into the electrolyte solution by mounting wires around the separation tube [33]. The

contactless arrangement of the conductivity detector solved dimensional issues as well as corrosion and fouling of the electrodes. Later in the evolution of the capacitively coupled contactless conductivity detection (C^4D), an axial cell arrangement was introduced by Zemann et al. [35] and da Silva and do Lago [36] almost at the same time. A schematic overview on the C^4D is given in Figure 4.

Two tubular electrodes are mounted on the separation column. A high-frequency alternating excitation voltage coming from a function generator (**A**) is coupled to the actuator electrode (**B**). At the pick-up electrode (**D**), the resulting AC current is measured and further processed by the detection electronics (**E**) [33]. A Faraday shield (**C**), prevents any stray capacitance between the two electrodes.

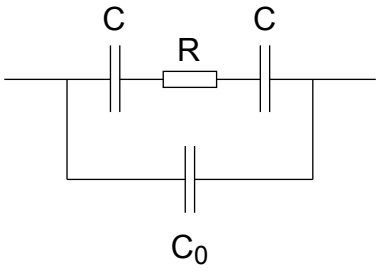

Figure 5: Equivalent electronic circuitry of a C^4D detector

An equivalent electronic circuitry helping to understand the basic behaviour is shown in Figure 5. Therefore, the detector consists of a capacitor (C), resistor (R) and a second capacitor (C) [31]. The two capacitors arise due to the electrodes while the solution between them forms a resistance [33]. The capacitive coupling between the two electrodes (C_0) is prevented by the Faraday shield [31, 33].

The detection electronics of a C^4D consists of the following stages as shown in Figure 6. The AC current received at the pick-up electrode (**A**) is transformed back into a voltage using an operational amplifier with a feedback resistor (**B**). Afterwards the signal is rectified (**C**) and the background signal subtracted with an offset (**D**). Finally the signal is amplified (**E**) and can be read out by a suitable data acquisition system.

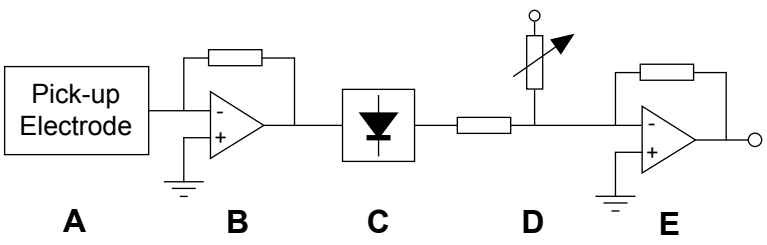

Figure 6: Detection circuitry of a C^4D detector

Instead of a DC voltage as in amperometry, alternating sinusoidal signals are applied in conductivity detection. In contact conductivity detection, the usage of alternating current prevents electrolysis reactions at the electrode surfaces while in C^4D accumulation of ions near the electrodes is avoided [33]. In addition, interferences from the detection electronics as well as polarization of the electrodes is prevented [33]. High frequencies between 1 kHz and 1 MHz have to be used to overcome the insulation layer, which is present in the contactless approach [33]. Usually, a frequency of approximately 250 kHz is applied. Best signal-to-noise ratios were observed for C^4D when using excitation voltages of several hundred volts. For example were detection limits of 0.1 to 0.2 µM for inorganic ions obtained by using an excitation voltage of 250 V [37, 38]. The gap between the two electrodes is of major importance for the resolution since it defines the detection volume and therefore the cell constant [33]. Usually it is 1 mm in size [37, 38]. The cross-sectional area is primary defined by the internal diameter of the capillary and not by the dimensions of the electrodes [31].

Compared to other detection methods such as UV/Vis detection or fluorescence, conductivity detection is universal and non-destructive for measuring charged analytes. That means that C^4D can also be combined with other detection methods such as UV/Vis to receive more information on the sample [33]. C^4D is especially useful to detect several types of inorganic ions such as alkaline, alkaline earth or heavy metals. An example is the determination of four toxic heavy metals (Cr^{3+}, Pb^{2+}, Hg^{2+}, Ni^{2+}) in different water samples with CZE-C^4D by employing a histidine/tartaric acid buffer [39]. Conductivity is also useful to measure different organic ions not containing a chromophore or fluorophore. For example mono- and disaccharides such as glucose, sucrose and fructose were analysed as anionic species in different beverages [40]. Due to its low power consumption compared to UV/Vis, C^4D is useful for the implementation in portable CE instrumentation. An application example is the analysis of pharmaceutical pollutants [41]. Different charged components such as ibuprofen, diclofenac, bezafibrate, ketoprofen and mefenamic acid, diphenhydramine, metoprolol and atenolol were determined quantitatively in waste water in Vietnam [41]. Further application areas of the C^4D include biochemistry, where DNA, amino acids, peptides and proteins can be determined [33].

2

MASS SPECTROMETRY

With mass spectrometric detection, ions in the gas phase are separated by their mass to charge ratio (m/z) and detected qualitatively and quantitatively [42, 43]. Compared to other detection methods, a large amount of information such as the molecular weight of the analyte and structural information can be received from small sample amounts [42]. Different available methods enable the ionization of the analyte prior to mass detection for example by reaction with electrons, photons and neutral atoms [42]. As a consequence various charged species are formed such as ionized atoms, molecules, fragments, or clusters [44]. A mass spectrometer works under high vacuum and consists of an ion source, a mass analyzer and a detector [42].

2.1 BASIC PRINCIPLES

2.1.1 *Mass Spectrum*

In a mass spectrum, the signal intensity representing the abundance of an analyte is plotted against the mass-to-charge ratio [21]. The physical detection unit of a mass spectrometer would be mass per electric charge (kg/C) [43]. This unit is not very convenient for handling of mass spectra because the permanent conversion of units would be necessary for interpretation. Therefore a dimensionless defined unit m/z, which is the mass-to-charge ratio was introduced [42].

Usually, a mass spectrum is normalized to its most intense peak, which is called base peak [42]. This way, comparison between different mass spectra is possible [42]. With soft ionization methods, the intact ionized molecule $M^{+\bullet}$ gives the peak with the highest intensity and is called molecular ion peak [42]. Since elements have naturally occurring isotopes, a mass spectrum of an analyte contains various isotope peaks next to the ion peak with lower intensities [45]. Depending on the ionization method, fragmentation or cluster ion peaks of the compound are obtained [42].

2.1.1.1 *Ion Chromatograms / Ion Electropherograms*

When components are separated with analytical methods, the result is obtained in form of chromatograms respectively electropherograms. The measured signal is plotted against the retention/migration time of the analytes.

Therefore, by using mass spectrometric detection for separation methods the signals are obtained in form of ion chromatograms/electropherograms, which represent the ionic abundances as a function of retention/migration time [42]. This is done by measuring the total ion current (TIC), which is obtained from a collection of consecutively acquired mass spectra over time. Therefore for each point in the chromatogram/electropherogram, a mass spectrum is obtained, which gives more information about the compounds [42].

2.2 MASS SPECTROMETER

2.2.1 *Ion sources*

In a first step of mass spectrometric analysis, the analytes have to be converted from the solid or liquid phase into ions in the gas phase because the mass analysers can only detect charged species [42, 46]. Many techniques exist to achieve this and all have their advantages and ideal application range [46]. The right choice of the ionization method has a huge impact on the qualitative and quantitative data obtained by MS [46]. Therefore, the ionization process is of great importance.

2.2.1.1 *Standard Ionization Techniques*

Ionization in mass spectrometry normally takes place inside the vacuum of the mass spectrometer [43]. The process occurs in two steps. First, the sample is volatilized from the liquid or solid phase and in a second step it gets ionized [43]. The different available techniques can be distinguished by their hardness or softness, required polarity and mass range of target analytes [42]. Hard ionization techniques lead to stronger fragmentation of the compounds, while soft ionization techniques provide predominantly the molecular ion peak. Fragment ions can be useful for structure elucidation, but make the interpretation of spectra more complicated when analysing complex mixtures or big molecules [47].

Classical ionization techniques for mass spectrometry working under high vacuum are electron impact (EI), chemical ionization (CI) and fast atom bombardment (FAB) [48]. Electron impact or electron ionization (EI) was the first ionization technique applied to mass spectrometry [47]. In a first step of the ionization process, the compounds are transferred to the gas phase by evaporation. Subsequently, the neutrals are hit by electrons with a high kinetic energy and receive a part of their energy leading to their ionization [42]. During the process molecular ions, multiply charged ions, fragment ions, rearrangement ions and ion pairs are generated [42, 49]. Multiple charging of analytes enables to analyse high molecular weight molecules by mass

spectrometers with a limited m/z range [43]. On the other hand, EI spectra are getting easily complicated for interpretation [47]. Compared to EI, chemical ionization (CI) is a soft ionization technique. Ions are generated by collision of the analyte with the ions of a reagent gas [42]. As reagent gas usually methane, ammonia or isobutane is used [42]. The gas plasma, where the ion-molecule reactions take place, consists of protons, free electrons and different ionic and radical species [42]. The method called fast atom bombardment (FAB) is based on firing particles with high kinetic energies on a surface. Ions are ejected as secondary ions from the analyte surface by the impingement with the primary ions [42]. An alternative ionization method to the previously mentioned is photoionzation (PI), where a resonance line from a lamp is used for the production of ions from the sample [47]. PI is also a soft ionization method, where fragmentation of ions is suppressed and the parent ion dominates the mass spectrum [47]. Matrix-assisted laser desorption ionization (MALDI) is a commonly used soft ionization technique for mass spectrometry [47]. The analyte is co-crystallised with a photosensitizer material, which is absorbing at the wavelength of interest. The matrix surface is irradiated with a pulsed laser beam, which leads to the release of ions [43, 50]. Normally, MALDI is performed under high vacuum where the probe consisting of sample and matrix is inserted prior to analysis [50]. In this case, the formed ions are directed towards the mass analyser in high vacuum. On the other hand can MALDI also be performed at atmospheric pressure and the formed ions transferred into the vacuum system afterwards [51]. This ionization method offers high sensitivity up to the sub-femtomole range [43].

2.2.1.2 *Ambient Ionization Techniques*

Ambient pressure ionization (API) techniques enable ionization outside the high vacuum system of the mass spectrometer [46, 52]. As first ambient ionization method, desorption electrospray ionization (DESI) was introduced in 2004 by Takáts et al. [53]. The advantage of API techniques is that only little to no sample preparation is necessary. More than 80 different ambient ionization techniques were developed since its inception, which can be roughly classified into spray, plasma and laser ionization methods [54]. The challenge with API sources is the pressure reduction along the ion pathway between the ion source and the mass analyser, which is usually solved by a multiply-staged vacuum system [48].

Electrospray (ESI) is a very soft ambient ionization method, which is based on the electrostatic spraying of the sample solution leading to a charged aerosol [43, 46, 48]. The process can be supported by a gas flow with nitrogen or a sheath-flow liquid [43]. ESI can be applied to a wide range of compounds with varying molecular weight having moderate to high polarity in the fields of forensic and environmental analysis, bioanalytics and pharma-

ceuticals [46, 55].

As shown in Figure 7, electrospray used as ionization method for mass spectrometry normally operates in the cone-jet mode [56]. For the formation of a stable spray, a buffer solution is flowing through the spray capillary at flow rates of 0.1 - 10 µL min^{-1} [57]. An electric field with voltages between 2 - 5 kV is applied to the spray capillary. This leads to the separation of charges within the liquid. Positively charged ions are accumulating at the meniscus while negatively charged ions are repelled away [22]. As soon as the critical electric field strength is reached, the initial meniscus at the capillary outlet starts to deform into a cone, which is termed Taylor cone [22, 42, 58, 59]. A jet is formed out of the cone, carrying a large excess of cations. The jet is not stable for a long time [59]. Small positively charged droplets start to take shape and overcome the cohesive forces of the liquid due to the Coulomb repulsion. They separate from the jet and move towards the counter electrode located at the mass spectrometer entrance [22, 48]. This leads to the formation of a fine spray [48, 59]. The diameter of the droplets depends on the solvent and the solutes, but are usually micrometer range. The droplets shrink on their way to the cathode because of the solvent evaporation due to the heat of the surrounding atmosphere. This leads to an increase of charges in a smaller volume within the droplets leading to Coulomb explosions at the Rayleigh limit [21]. Smaller subunits are formed out of the parent droplets [22]. After many repetitions of this process, the free ions are liberated into the gas phase [22, 42].

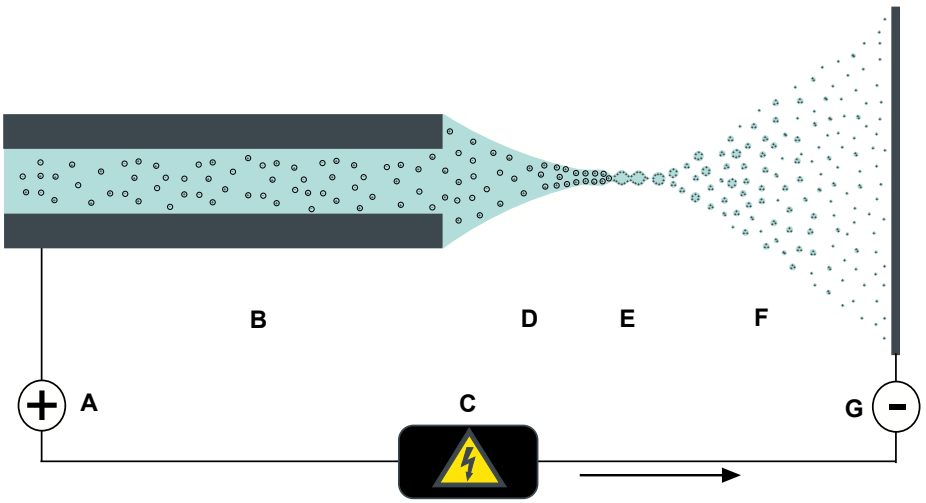

Figure 7: Schematic drawing of the ESI with the Taylor cone formation

For the ionization process, a volatile solvent is required enabling a stable electrospray. The droplet formation is hampered when solvents having a higher surface tension such as pure water are applied [48]. Electrospray is normally conducted in positive mode with applying a positive voltage to the spray capillary. Anyway, the electric field can also be reversed to gener-

ate negatively charged droplets [48].
Electrospray can be used to couple liquid separation techniques such as HPLC and CE to mass spectrometry [43]. Disadvantages of ESI are its susceptibility to ion suppression effects, which hinders the ion formation of the analyte [43, 46]. Therefore the choice of buffers for CE is limited and some samples need to be desalted prior to analysis [43]. In addition, electrospray cannot be used to ionize unpolar compounds as it relies on the liberation of already existing charged compounds [46].

In atmospheric pressure chemical ionization (APCI), the ionization process occurs due to ion/molecule reactions similar to chemical ionization but at atmospheric pressure [43]. As primary ionization source, a corona discharge from a fine needle is used to form the reactant ions. Reagent molecules are N_2, O_2, H_2O and solvent molecules present around the needle. These ions react then with the vaporized analyte and create positively and negatively charged ions [43, 48]. APCI is a complementary method to electrospray. Similar to ESI, APCI can easily be coupled to liquid separation techniques and achieves good sensitivity even at high flow rates [43]. Advantages of APCI is that the ionization technique is less prone to interferences from salts and buffers [46]. In addition, weakly polar analytes not present as ions in solution can easily be ionized [43]. On the other hand, labile compounds get thermally decomposed in the heated nebulization and the high sensitivity of APCI requires very pure solvents [43]. APCI can be applied to compounds having a moderate molecular weight and low or medium polarity [46].

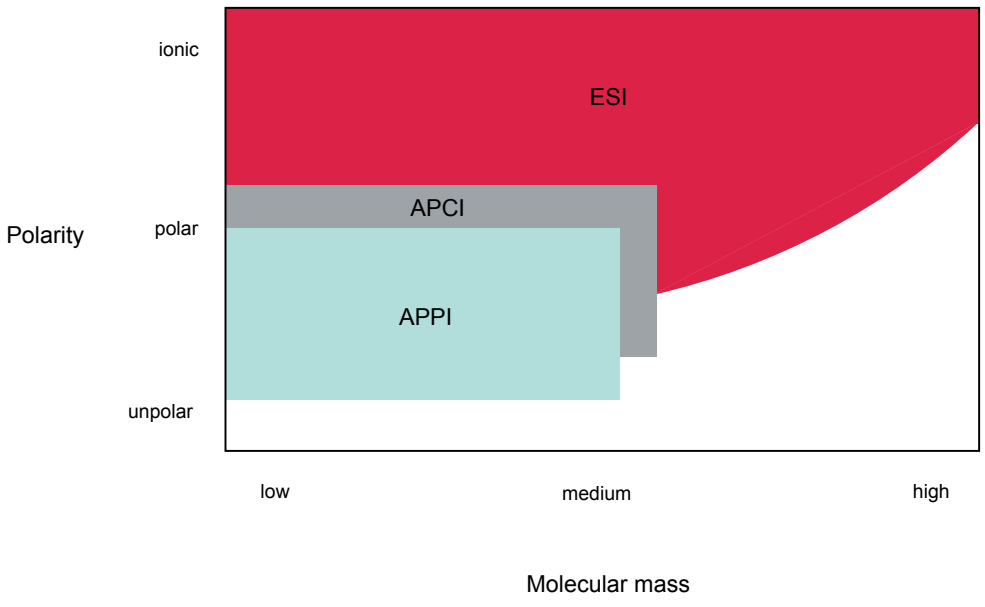

Figure 8: Application ranges of different API methods

Atmospheric pressure photo ionization (APPI) is a special case of an APCI source, where the corona discharge electrode is replaced by a photon-emitting lamp [46]. The analyte molecules in the gas phase interact with the emitted photons of a discharge lamp and form ions. APPI allows to selectively ionize the analyte by applying photons with an energy, which is higher than the ionization energy of the analyte and lower than that of the air or used solvents [46]. APPI can be applied to nonpolar compounds, which can not be ionized by ESI or APCI and is less susceptible to salt buffer effects and ion suppression than ESI and APCI [60, 61]. APPI was used for example for determine polycyclic aromatic hydrocarbons with high sensitivity by LC-MS coupling [62]. The different application fields of ESI, APCI and APPI are illustrated in Figure 8.

Desorption electrospray ionization and direct analysis in real time (DART) belong to the class of ambient desorption techniques [46]. DESI is a hybrid between desorption ionization methods and ESI [46]. Charged droplets are generated and sprayed onto the sample surface leading to a release of the analyte ions into the gas phase by chemical sputtering [42, 46]. Direct analysis in real time (DART) is related to APCI and is a dry ionization technique based on a solvent-free gas stream. Excited atoms of a noble gas are formed in a plasma discharge, which react with the atmosphere. The generated reagent ions hit the sample surface and cause the desorption and ionization of the analyte [42, 52].

2.2.2 *Mass analyser*

The separation of the generated ions in the gas phase occurs within the mass analyser based on their m/z ratio [63]. The following four mass analysers are most commonly used. A Time-of-Flight (ToF) spectrometer separates ions in a long drift tube on the basis of their velocity. ToF is quite commonly used in combination with MALDI and has a theoretically unlimited upper mass limit [43]. In addition, ToF is a high resolution and mass accuracy analyser [21]. The quadrupole mass analyser (Q) contains four parallel rods. To two rods a DC potential and to the other two an alternating frequency potential is applied [63]. This arrangement leads to an ion motion perpendicular to the dynamic electric field created in two dimensions, which is directly dependent on the m/z of the analytes [43, 63]. The quadrupole ion trap (QIT) is closely related to the quadrupole instrument with both having a similar resolution, mass accuracy and m/z range of around 4000. The resolution however is rather low for these two mass analyser types [21]. The difference of the ion trap is that it has electric fields in all three dimensions where the ions are trapped. For this reason, The QIT has an increased sensitivity in higher mass ranges compared to the linear quadrupole instrument and is

quite inexpensive wherefore it is very popular [43]. In the Fourier-transform ion cyclotron resonance (FT-ICR) instrument, magnetic field are applied to determine the m/z of an ion [43]. An FT-ICR instrument gives very high mass resolution and accuracies, but is quite expensive and has long duty cycles [21, 43].

2.2.3 *Hyphenated Methods*

For analysing complex sample mixtures a separation becomes necessary prior to the mass detection [64, 65]. The first combination of a separation method and a mass spectrometer was the hyphenation with gas chromatography (GC-MS). GC-MS is nowadays used as standard analytical technique in many fields. For example it is used for the detection of organic pollutants in the environment such as different herbicides and pesticides or for the analysis of chemical warfare agents [66]. GC-MS is also the analytical standard method of the American Society of Testing Materials (ASTM) to analyse fire debris in criminal forensic sciences [66].

Later, liquid chromatography - mass spectrometry (LC-MS) was introduced, which is a hyphenated method for the analysis of highly polar nonvolatile compounds. For LC-MS, the development of API methods such as ESI, APCI or APPI became necessary to enable sample ionization [42, 67, 68]. The separation in chromatographic methods is based on a differential partitioning of the analytes between a mobile and a stationary phase. The compound mixture is dissolved in a mobile phase, which is passed through a stationary phase. The analytes have different affinities to the stationary phase leading to their adsorption for varying time lengths and therefore to different retention times. In gas chromatography, the mobile phase is a gas and the stationary phase is a thin film bound to the separation column [42]. In liquid chromatography (LC), the mobile phase is a liquid and the stationary phase is consisting of solid particles [42]. In high performance liquid chromatography (HPLC), very high pressures in the range of 100-200 bar are applied to the separation column filled with very small packing particles to force the liquid through [42]. LC-MS is an essential tool in pharmaceutical analysis in all four stages of the development of a new drug. For example in the drug discovery step, it is the standard method for screening of new substances and in the preclinical development needed for evaluation of the drug with regard to possible impurities and identification of metabolites [69].

2.2.3.1 *Electrophoresis*

The hyphenation of CE and MS was first demonstrated in 1987 by Olivares et al. [70] who used electrospray as interface to detect quaternary ammonium

compounds. Capillary electrophoresis hyphenated to mass spectrometry requires less solvent and sample compared to chromatographic techniques and has a very high resolving power [4]. As ionization method for CE-MS, electrospray in the sheath-flow configuration is most commonly used although other methods such as MALDI or APCI are also possible [22].

Compared to a normal CE set-up, fundamental differences have to be considered when using mass spectrometry as detection method. Instead of connecting a high voltage power supply to two buffer reservoirs with the separation capillary dipped in, an open end of the capillary as interface to the mass spectrometer is required. The most important challenges in CE-MS coupling are the combination of the electric fields from the separation and electrospray voltages, the assurance of a stable electrospray due to limitations in flow rates of CE and restrictions in the electrolyte choice [21]. From an electronic view, CE-MS coupling is a three-electrode system where the ESI-MS and CE parts are two separate circuits sharing one electrode [22, 71]. The current from the capillary electrophoresis system will dominate the one of the electrospray part in terms of magnitude and therefore influence the electrochemical reactions taking place at the electrodes [22].

In CE-MS the buffer needs to fulfil the requirements of both CE and ESI part. Volatile BGE solutions are favourable with acetic acid, formic acid or ammonia being frequently used for this purpose [72]. Buffer additives on the other hand should be avoided. Although they can support the selectivity of the CE separation, ion suppression within the ESI part can occur resulting in a lower signal intensity. For positive-mode ESI it is better to use a low pH electrolyte, which supports the formation of the spray while for negative-mode ESI a high pH electrolyte is favourable [73]. Addition of organic solvents to the buffer can improve the quality of the electrospray but may deteriorate the separation.

There are two basic types of CE-MS instruments having either a sheath-flow or sheathless ESI interface [21]. One approach is to integrate a sheath liquid in the ESI interface, which supports the ionization process. In this configuration the separation capillary is surrounded by a larger diameter tube through which the sheath liquid flows [21]. The liquid usually consists of a solvent mixture such as acetonitrile, methanol, acetone or isopropanol and has a ten to hundredfold higher flow rate than the electrolyte [4]. The sheath liquid is mixed to the buffer at the ESI tip. This way, the problem of low flow rates in CE compared to LC can be circumvented and the quality of the spray is improved. The application of sheath liquid enables therefore the use of more typical electrolytes for the CE part [55]. In addition, the set-up enables an electrical contact to the exiting liquid. Therefore, the grounding of the CE circuit is simplified and the electrospray voltage can easily be applied [4, 74].

The problem with the sheath-flow approach is that the sample is diluted, which reduces the sensitivity of the measurement [4]. The other approach to CE-MS coupling is the sheathless configuration, which has a much simpler set-up and lower detection limits. The challenge is to provide an electric contact at the electrospray tip [22]. There exist different approaches to solve this problem. As an example a porous tip was designed by Moini [75] where the end of the separation capillary is etched with hydrofluoric acid enabling movement of ions and electrons to provide the electrical contact. A stainless steel tube, which is filled with BGE surrounds the separation capillary and is connected to the ESI voltage [75]. This configuration of CE-MS is now also commercially available [76]. Other sheathless CE-MS configurations are based on the insertion of a wire at the capillary tip or on a metal coating [21].

CE-MS can be applied to the fields of forensic sciences, pharmaceutical analysis and bioanalysis. It is especially useful for protein characterization in the field of biopharmaceuticals due to the highly efficient separations [21]. Other application fields include food analysis essential for maintaining safety and quality of products and control the authenticity. Of extreme importance in food and environmental analysis is the determination of pesticide residues [21]. An example is the separation of neonicotinoid insecticides by sheath-liquid ESI interface based CE-MS [77]. It was also possible to determine the broadband herbicide glyphosate and its major degradation product aminomethylphosphonic acid (AMPA) in beer [78]. Glyphosate is rather difficult to analyse with standard methods and normally requires derivatization to meet the requirements of sensitive GC or LC analysis [78].

3

PURPOSE-MADE CAPILLARY ELECTROPHORESIS SYSTEMS

3.1 INTRODUCTION

The development and commercialisation of automated CE instruments was essential for improving reproducibility and robustness of the separation technique [1, 79, 80]. CE became attractive and reliable for industrial applications where the technique was successfully implemented for diverse routine applications. On the other hand commercial CE instruments are not suitable for field, process analysis or scientific research because they are too bulky and lack in flexibility. In research, changes between method, detector and capillaries often have to be fast or completely new set-ups need to be improvised in a short amount of time [81]. As another important drawback, commercial CE instruments are very expensive leading to complications for research groups with limited funding regarding the purchase and maintenance of the equipment. Therefore over the years, many research groups built their own purpose-made CE instruments with various improvements and differentiation for specific applications. Because CE requires only minimal hardware, it is particularly suited for building self-constructed, miniaturised and portable devices [82].

One way to miniaturize electrophoresis system was enabled when a new concept of the so-called micro-total analysis system (μ-TAS) was introduced by Manz et al. [83] in 1989. The concept is also known as lab-on-a-chip (LOC) and is based on the idea that all necessary reactions for the analysis are performed on the same microfabricated system [84]. This includes all operations such as sample injection, interface flushing, reagent mixing for derivatization reactions, separation and detection [83, 84]. Microchip electrophoresis (MCE) was developed first in the scope of the μ-TAS project because CE is easy to miniaturize [84]. In microchip electrophoresis, the separations are performed in micro channels engraved on small plates made out of glass or a polymer such as polymethylmethacrylate (PMMA) [84]. The small sample and reagent volumes needed and reduced separation time due to the short separation channels lower the overall analysis costs. Other features are improvements in heat transfer allowing to apply higher voltages and better mass transfer making on-line derivatization reactions favourable [84]. An application example is the two-dimensional separation of a complex protein mixture on a PMMA microfluidic chip. This was done by combining sodium dodecyl sulfate micro capillary gel electrophoresis (SDS μ-CGE) in

the first dimension with microemulsion chromatography (μ-MEEKC) in the second dimension [85]. MCE has therefore many advantages over commercial bench-top instrumentation and a potential for portability [86]. However, the approach has some practical drawbacks since the chip fabrication procedure is cumbersome and the chips show easily siphoning effects when not straight aligned. Also detection is challenging due to geometrical constraints and flexibility is limited regarding the length of the separation channel [87]. It has also to be taken into consideration that even though the chip itself is small, also electronics and a detection system are needed.

The other approach is to work with miniaturized injection system but use standard separation capillaries. Similar separation times to MCE can be obtained when employing short conventional capillaries as shown by Rainelli and Hauser [88]. Such CE instruments have therefore the advantages of being small, flexible and low-cost. All standard detectors can be used and the instruments can also easily be built portable. For automation of the instruments, the standard injection techniques such as hydrodynamic or electrokinetic injection is less suitable. The evolution of flow injection analysis (FIA) by Růžička and Hansen [89] simplified automation of sample handling in analytics. All steps necessary for the analysis such as reagent mixing, sample pretreatment and injection are automatically carried out in a flow system [90]. FIA based manifolds can easily be combined with capillary electrophoresis and the automation of the injection procedure very simple. Since in CE only tiny sample amounts need to be injected into the separation capillary, which can not be measured directly, schemes from the sequential injection analysis (SIA) are usually employed for the injection [91]. A sample loop with a defined volume is therefore filled in a first step and the resulting sample plug afterwards moved to a split injection device [91]. Only a fraction of the initial sample amount is injected into the separation capillary by applying a controlled pressure for a fixed time length [91]. The microfluidic breadboard approach is a new concept for building miniaturised and flexible CE systems by combining different miniature off-the-shelf components on a microfluidic breadboard [87].

Due to its relatively simple experimental set-up, CE instruments can easily be built as portable version. With on-field measurements issues arising with sample transport and storage can be avoided and the lab infrastructure is not needed. This is interesting in environmental analysis, where monitoring of water quality, soil contamination and air pollution needs to be performed on-site. Analysis time is reduced and necessary decisions can be made directly on the sampling site. The first portable instrument developed enabled both potentiometric and amperometric detection in a single unit for analysis of alkali and alkaline earth metal cations [92, 93]. Since portable instruments require low power consumption, C^4D is well suited as detection method [94,

95]. One of these portable CE-C^{4}D systems was used for fast screening of nerve agents originating from chemical warfare agents (CWA) [96].

One important trend in the development of CE instruments goes towards fully automated and remote controlled CE systems [97]. The CE system can be mounted on a battery powered robotic platform. The robot drives to the given location, collects the sample, performs the analysis and sends the results to a remote station [97, 98]. Such lab-on-a-robot (LOAR) systems where introduced in 2008 [97]. For hazardous or hardly reachable places it is clearly an advantage if the analyst is not needed [97]. Under the first prototypes is an instrument based on MCE, which analysed organic acids in air samples [98]. Another application is the search of extraterrestrial life on other planets such as Mars [99]. Amino acids as the fundamental building blocks of life could be a biosignature if occurring in one predominant chiral form and are easily analysed by CE-LIF [99]. Another example is the lab-on-a-drone, which is able fly to hazardous places, collect and analyse samples in air [100]. The performance of the instrument was shown for the analysis of volatile amines and organic acids, non-volatile inorganic cations and proteins in the aerosol state in the air [100].

3.2 DESIGN OF PURPOSE-MADE MICROFLUIDIC CE INSTRUMENTS

The design of the CE instruments built in the scope of this PhD thesis was based on the concept of the microfluidic breadboard approach [87]. Different commercially available miniature parts such as small valves, vials and tubing were combined on a breadboard to build up flow based injection systems.

Pressure and flow rates in the system have to be adjusted to execute the different steps necessary for the injection procedure. Before starting building the instrument, first theoretical calculations have been performed .

The law of Hagen-Poiseuille (equation 14) allows to calculate the pressure drop over a tube, where a Newtonian and incompressible fluid is flowing through in a laminar manner. The volumetric flow rate (Q) depends on the radius of the tube (r), the pressure difference between inlet and outlet (ΔP) and inversely on the viscosity of the liquid (η) and the tube length (l). The flow rate is therefore largely determined by the inner diameter of the tubing with small changes having already a huge impact.

$$Q = \frac{dQ}{dt} = \frac{\pi r^4 \Delta P}{8 \eta l} \tag{14}$$

Further the hydraulic-electric circuit analogy can be used for the calculations, which links the Ohm's law (equation 15) to hydrodynamic properties (equation 16) [101]. The pressure difference in a fluid system (ΔP) corresponds to the voltage (U) applied to an electric circuit. The flow resistance (R_{FL}) is the analogue to the electric resistance (R) and the current (I) can be translated into the volumetric flow rate (Q).

$$U = RI \tag{15}$$

$$\Delta P = R_{FL} Q \tag{16}$$

By combining the law of Hagen-Poiseuille (equation 14) and the hydraulic-electric circuit analogy (equation 16), an expression for the flow resistance (equation 17) is found. The flow resistance (R_{FL}) is proportional to the viscosity of the liquid (η) and the length (L) and inversely proportional to the radius (r) of the tube.

$$R_{FL} = \frac{8\eta L}{\pi r^4} \tag{17}$$

Different interconnected tubes can be seen as resistors switched in series. Therefore the volumetric flow rate (Q) can be calculated from the total flow resistance (R_{FLT}) of the tubing as shown in equation 18.

$$R_{FLT} = R_{FL1} + R_{FL2} + ... + R_{FLN} \tag{18}$$

Fluid flow paths can be controlled by using valves, syringe pumps and applying different diameter tubing. Driving of liquids in tubing can either be done by implementing different types of pumps, applying pressure or vacuum on one end of the tubing. Since pumps have stepwise movements leading to uneven flow rates, different fixed pressures were included in the design of microfluidic systems for this PhD thesis. This approach leads to well controllable homogeneous fluid movements.

Sample injection based on the split injector approach (see Figure 9) requires different steps. The separation capillary coloured in brown is inserted into a Tee piece, where two tubes are connected for inflow and outflow of the liquid. The separation capillary needs to have a straight edge and should be aligned with the end of the channel within the Tee piece. In the first steps, the system interface and separation capillary need to be flushed. Then the sample loop is filled with the analyte of interest before transporting the sample plug at moderate flow rate towards the separation capillary inlet (**A**). When the sample plug is located in front of the separation capillary, the flow is stopped (**B**). Because the sample plug is diluted at the edges due to diffu-

sion processes, the concentrated middle part of the sample plug should be placed in front of the separation capillary. In the next step (**C**) a pressure is applied to the capillary inlet leading to sample injection. For a good reproducibility of the measurements, the applied pressure and injection time have to be controlled precisely. Afterwards the remaining sample in the Tee piece is flushed off (**D**) before powering up the high voltage module.

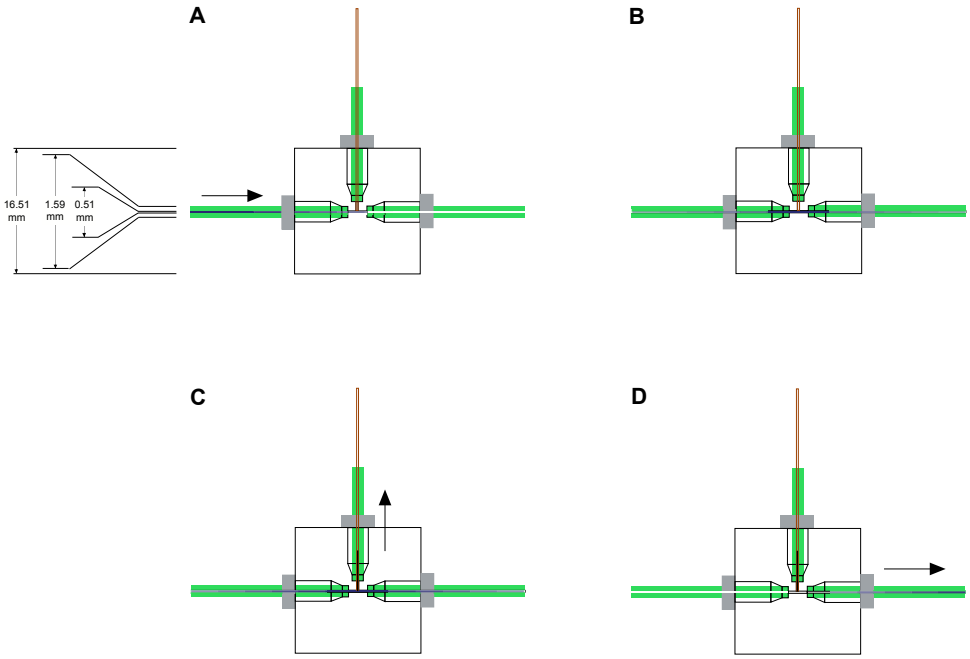

Figure 9: Schematic drawing of a split injector

As a rule of thumb around 1 - 2 % of the effective length of the separation capillary should be filled with the sample solution in order to obtain a good separation of the components. When performing fast separations, smaller sample plugs should be injected in short separation channels at the expense of loss in sensitivity [102]. Lower detection limits can be obtained by injecting longer sample plugs [102].

For the choice of the capillary diameter, the following points have to be considered. Injection and optical detection is normally easier with larger diameter capillaries. On the other hand it is much better to implement the narrowest possible capillaries in order to restrict Joule heating during the separation process. Higher voltages can be applied leading to shorter analysis time. Lower diameter capillaries are also favourable because the resolution of the separation is increased, which can be essential for compounds having similar migration times. In addition, pressure can also be applied during separations if needed for certain applications because the pressure profile

in narrow capillaries is close to a plug flow. The challenge when working with low internal diameter capillaries is that much higher pressures have to applied for an efficient flushing, but lower sample amounts have to injected. Further, it is not possible to use optical detection because the optical path length is too short, but C^4D is well suited [103].

Part II

RESULTS AND DISCUSSION

Six different projects were carried out in the scope of this doctoral thesis with the aim to further develop CE systems coupled to C^4D, fluorescence and mass spectrometry. Also two ambient ionization methods for mass spectrometry were explored. Different CE injection systems were designed and constructed, which were related to each other. Most work of this thesis was published, resulting in five articles within analytical chemistry journals. For the last project, which was still ongoing at the end of the PhD, a manuscript was written.

The single parts of the thesis will be represented with a resume of each project as well as the reprint of the corresponding article. In section 4.1 dielectric barrier discharge, which is an ambient ionization technique for mass spectrometry is described. Section 4.2 is devoted to the short project on a novel injection system for CE based on flow restrictors. The contribution to a tutorial about Forth on microcontrollers for operating analytical instruments is summarised in section 4.3. In section 4.4 the set-up of a fluorescence detector as part of a collaboration is described. Section 4.5 is dedicated to the development of an open-source capillary electrophoresis instrument. The last project dealing with the coupling of a capillary electrophoresis injection system to a mass spectrometer is summarised in section 4.6.

4

PROJECTS

4.1 A LOW-COST AMBIENT DESORPTION/IONIZATION SOURCE FOR MASS-SPECTROMETRY BASED ON A DIELECTRIC BARRIER DISCHARGE

The aim of this project was to construct a simple and low-cost ambient ionization source, which can easily be coupled to a mass spectrometer. Ambient ionization techniques for mass spectrometry have gained a lot of attention in the recent years since only little sample preparation and no high vacuum is required [54]. Dielectric barrier discharge (DBD) is rather unknown compared to DESI and DART and was introduced as ionization method for mass spectrometry in 2007 [104, 105]. Dielectric barrier discharge is based on an electric discharge between two electrodes, which are separated by an insulating dielectric barrier.

In the scope of this first project, a double-DBD ionization source in an axial arrangement was constructed based on previous published designs [106, 107]. Two isolated electrodes were axially mounted on a fused silica glass tube and the cold plasma was generated by flowing helium gas through the tube. A high voltage alternating signal provided by an electronic circuitry known as Royer oscillator was then applied to one of the electrodes [108, 109]. The ambient ionization source was characterized in terms of electronic and spectroscopic properties. The effects of variation of the supply voltage and the helium gas flow rate were evaluated systematically and the power consumption measured. Spectroscopic emission measurements were used to determine the plasma temperatures as well as for determination of the gas species present in the plasma. Different nitrogen vibrational transitions were recognised as well as emission lines of helium, hydroxide and oxygen. Nitrogen is essential in the cascade leading to the ionization of the analytes in the plasma source. Since a DBD plasma is not in its local thermal equilibrium (LTE), electronic, excitation, vibrational and rotational temperatures have different values [110]. Different methods were applied to determine the temperatures. The excitation temperature was calculated by using the Boltzmann plot while rotational and vibrational temperatures were approximated by using a modelling software. The gas temperature was also determined by using an infrared thermal imaging camera. The performance of the DBD source was demonstrated in terms of qualitative and quantitative analysis with a mass spectrometer. Different standard substances as well as flavouring substances in food samples, active substances in medications and examples of illegal drugs could be analysed directly with only little sam-

ple preparation. It was also shown that DBD is applicable to quantitative analysis by building linear calibration curves for the two model substances caffeine and nicotine.

The idea of this project was based on preliminary work of Ralf Dumler. Despite the acknowledged work of Ralf Dumler, all parts of the project including the design and construction of the DBD source, coupling to the mass spectrometer, preparation of the electronic circuitry as well as performance of all measurements were redesigned and implemented by the author. The electronic circuitry was designed by Peter C. Hauser. The project was retrospectively added to the scope of the dissertation project.

1ST PROJECT:

A low-cost ambient desorption/ionization source for mass-spectrometry based on a dielectric barrier discharge

Anal. Methods, 2018, 10, 2701-2711

Analytical Methods

PAPER

View Article Online
View Journal | View Issue

Cite this: *Anal. Methods*, 2018, **10**, 2701

A low-cost ambient desorption/ionization source for mass-spectrometry based on a dielectric barrier discharge

Jasmine S. Furter and Peter C. Hauser *

An ambient ionization source for mass-spectrometry is described. It is based on a plasma generated in helium by a dielectric barrier discharge using two external electrodes arranged axially on a fused silica tube. The plasma is created with a sinusoidal voltage source having an amplitude of 7 kilovolts and a frequency of 27 kilohertz. The plasma cell as well as the excitation circuitry were designed with simplicity in mind and both can easily be duplicated. The plasma source was characterized in terms of electronic properties and temperatures by using optical emission spectroscopy. Bands of the nitrogen second positive system at 357 nm were used for determination of the vibrational and rotational temperatures by fitting simulated to the experimental spectra with the software package Specair. With an excitation voltage of 7 kilovolts and a flow rate of 50 mL min^{-1}, a vibrational temperature of approximately 5000 K and a rotational temperature of 300 K were determined. By using the Boltzmann plot method, the excitation temperature was determined to be around 2800 K. The performance of the ionization source was demonstrated by the qualitative analysis of various standards as well as of application examples of pharmaceutical, illegal drug and food samples. Quantitative analysis of solutions is also possible. Linear calibration curves were obtained for caffeine and nicotine in the range from 1 to 1500 μM and limits of detection of 0.8 μM and 0.4 μM were determined for the two compounds respectively.

Received 28th February 2018
Accepted 24th May 2018

DOI: 10.1039/c8ay00446c

rsc.li/methods

Introduction

In recent years a number of so-called ambient ionization methods have been introduced to mass-spectrometry. Most of the devices are intended for direct analysis of the samples in solid form by exposure of their surface to the ionization device located openly in front of the inlet of the mass spectrometer. The term Ambient Desorption/Ionization (ADI) is also used to specify the process. As the direct analysis does away with the need for sample dissolution, the technique has gained significant attention. The most popular have been DESI (Desorption Electrospray Ionization) and DART (Direct Analysis in Real Time). DESI was proposed by Cooks and coworkers in 2004 and employs the impingement of an electrospray created from an appropriate solvent onto the sample for analyte desorption and ionization.[1] DART was introduced by Cody *et al.* in 2005 (ref. 2) and makes use of a high voltage DC (direct current) glow discharge at the tip of a needle to create metastables in a process gas and subsequent Penning ionization leading to charged analytes.[3] DESI and DART complement the established ionization methods for liquid samples of ESI (Electrospray Ionization) and APCI (Atmospheric Pressure Chemical Ionization) respectively. DESI works best for strongly polar analytes and is suitable for large molecules, whereas DART performs well for relatively small molecules of lower polarity.[3] DESI and DART have been commercialized and units for retrofitting to existing mass-spectrometers can be bought at a cost of several 10 000€.

A range of further ambient ionization alternatives has been described in the literature over the subsequent years. A good general overview can be gained from a monograph published in 2015 (ref. 3) and from review articles by Lebedev[4] and by Huang *et al.*[5] There have been a variety of prominent plasma based ADI sources. They differ in their construction but tend to give a performance similar to that of the DART source.[3] Hieftje and coworkers in 2008 introduced an atmospheric pressure glow discharge as an ionization source which is also based on a DC high voltage.[6] Zhang in 2007 introduced a dielectric barrier discharge (DBD) device consisting of a hollow electrode purged with He and a copper sheet electrode underneath an insulating sample bearing glass slide.[7,8] The plasma was excited with an AC (alternating current) voltage between 3500 and 4500 V at 20 kHz. The LTP (Low Temperature Plasma) probe was introduced by Cooks and coworkers in 2008 (ref. 9) and was also based on a DBD created inside a glass tube using an internal grounded needle electrode and an outer isolated concentric electrode to which an AC high voltage of typically 3 kV and 2.5 kHz was applied. Franzke and coworkers in 2009 demonstrated that a DBD plasma created with two isolated electrodes axially arranged on the same tube (double-DBD) is also suitable as an

Department of Chemistry, University of Basel, Spitalstrasse 51, 4056 Basel, Switzerland. E-mail: peter.hauser@unibas.ch; Tel: +41 61 2071003

ambient ionization source (operated at 5 kV pulsed at 35 kHz).[10] The construction of such plasma cells is inherently simpler than that of the concentric arrangements of the LTP and DART devices. The recent developments of such plasma based ionization techniques have been summarized in several review articles.[11–16]

The construction of these plasma ADI sources is relatively simple. This recently prompted Martínez-Jarquín *et al.*[17] and Upton *et al.*[18] to publish the easily duplicated designs of an LTP and a DART probe respectively, in order to make the technique available to users who have no access to the commercial products. Herein a DBD ionization (DBDI) source based on the simple axial double-DBD arrangement which is powered by a straightforward electronic circuitry is reported. The construction details are given so that it can easily be reproduced by interested readers. Its design is derived from a plasma source reported by us in 2003 for optical emission spectroscopy.[19–22]

Experimental

Instrumentation

The plasma jet was produced in a 5 cm long fused silica tube with a 2 mm OD and 1 mm ID (product no. 0955.1002, WISAG AG, Fällanden, Switzerland). This tube was placed in an electronic potting case with dimensions of 15 × 19 × 40 mm (width × height × length) into which appropriate holes had been drilled in the centres of the two narrow sides (S38 from Teko Enclosures, San Lazzaro Di Savena, Italy). The electrodes were prepared by wrapping the stripped ends of the two connecting cables around the tube and fixing them with silver epoxy conductive adhesive (product no. 186-3616, RS Components, Corby, UK). For the high voltage a special insulated cable rated for 40 kV was employed (HSW-4022-2, hivolt.de, Hamburg, Germany), whereas for the ground connection a regular insulated stranded wire was used. The assembly was sealed by filling the box with a thermally conductive, but electrically insulating epoxy glue (EPO-TEK® T7110) obtained from Epoxy Technology Inc. (Billerica, MA, USA).

The electronic circuitry consisted of the following components: 2× field effect transistors (FET) 942-IRFP250NPBF (Mouser Electronics, Mansfield, TX, USA, part number 942-IRFP250NPBF), 2× diodes UF4007 (Mouser, 512-UF4007), 2× 12 V Zener diodes 1N5349BRLG (Mouser, 863-1N5349BRLG), 2× resistors 470 Ω, 2 W (Mouser, 594-5083NW470R0J), 2× resistors 10 kΩ, 1/4 W (Mouser, 660-MF1/4DCT52R1002F), 1× foil capacitor 680 nF, 630 V (Mouser, B32654A6684J000), and 1× toroid inductor 100 μH (Mouser, 652-2300LL-101-V-RC). The flyback transformer was product no. CHT-1309A from Chirk Industry (Taoyuan, Taiwan), purchased as product no. HVT-01B from Images Scientific Instruments Inc. (Staten Island, NY, USA). The circuitry was powered by a variable voltage DC power supply (EX4210R from Thurlby Thandar Instruments, Huntingdon, UK). Please note that the high voltage generated is potentially dangerous and the circuitry was housed in a non-metallic enclosure to prevent accidental contact.

For the generation of the plasma, helium gas (99.999% purity, PanGas, Pratteln, Switzerland) was employed. The flow rate of the helium gas was adjusted by using an analog mass-flow controller with a maximum flow rate of 100 sccm (standard cubic centimetres per minute) (1159B-00100SV) obtained from MKS instruments (Andover, MA, USA). The mass flow controller was regulated from a personal laptop computer by using a purpose-made circuitry based on an Arduino Nano microcontroller board (Arduino Nano 3.0, Gravitech, Minden, NV, USA) as an interface to the computer. This model of mass flow controller is no longer for sale, but note that equivalent products, some of which may be connected directly to a computer *via* a serial bus without requiring a dedicated interface circuitry, are available from a number of manufacturers. For setting up the pneumatic part, #10–32 to 1/16″ connectors (CT2-PKG, Clippard, Cincinnati, OH, US), T-pieces and a urethane hose with a 1/8″ OD and 1/16″ ID (from Clippard) were used as well as 1/4″ nuts and ferrules (SS-400-NFSET, Swagelok, Solon, OH, USA).

Mass spectrometric detection was performed on an LCQ Deca 3D ion trap mass spectrometer (Finnigan MAT, San Jose, CA, USA) operated in full-scan positive ion mode. Data were collected using Tune Plus software vs. 2.0 (Thermo Fisher Scientific, Waltham, MA, USA). For the alignment of the plasma source in front of the mass-spectrometer, various parts from Thorlabs (Newton, NJ, USA) were used. The plasma cell was installed on an XYZ translation stage (DT12XYZ) by using a purpose-made holder made from Perspex®. The XYZ stage was placed on an optical rail (RLA150/M), which was mounted with two spacers (BA2S6/M) on an optical breadboard (MG1530/M). This also carried the mass-flow controller and the associated printed circuit board.

A 1000× high voltage probe (P6015A, Tektronix, Beaverton, OR, United States) connected to a USB-based oscilloscope (Picoscope 3204MSO, Pico Technology, Cambridgeshire, UK) was used to record voltage waveforms. Optical emission spectra in the region of 200–900 nm were recorded by using a miniature spectrometer (Flame, Ocean Optics, Dunedin, FL, USA) with a wavelength range from 200 to 1100 nm and a resolution of 2 nm. Emission spectra of the second positive system of nitrogen were acquired using an MS 260i CCD (charge-coupled device) spectrograph from Oriel (Stratford, CT, USA, spectral resolution 0.10 nm). An optical fibre (M114L01, Thorlabs) was used to couple the light to the spectrometers. Specair (http://www.specair-radiation.net/) was used for the simulation of the emission spectra to determine the rotational and vibrational temperatures. The slit function was determined using Specair by measuring the mercury emission line at 334.15 nm of a mercury argon calibration source (HG-1, Ocean Optics, Dunedin, FL, USA). For temperature measurements an infrared thermal imaging camera (Ti95) from Fluke (Everett, WA, USA) was also used.

Chemicals

Acetonitrile was purchased from Sigma-Aldrich (Buchs, Switzerland). HPLC-grade methanol was obtained from Fisher Scientific (Reinach, Switzerland). Deionized ultrapure water was produced using a Milli-Q system from Millipore (Bedford, MA,

View Article Online
Paper Analytical Methods

USA). The drug substances, scopolamine, amphetamine, THJ-2201, ethylphenidate, UR-144, 3-fluorophenmetrazine and Funky Buddha, were acquired *via* mail order from sources found on the internet. Caffeine, nicotine, vanillin and mefenamic acid were purchased from Sigma-Aldrich. Cocaine hydrochloride and opiate mixture 3 containing morphine monohydrate, codeine monohydrate and 6-acetylmorphine hydrochloride were obtained from Lipomed (Arlesheim, Switzerland). Panadol® tablets and Buderhin® nasal spray were acquired from GlaxoSmithKline AG (Münchenbuchsee, Switzerland). Claritin® tablets were obtained from Essex Chemie AG (Lucerne, Switzerland). Coffee powder, vanilla beans, cinnamon powder, pepper powder and garlic cloves were purchased from Migros (Zurich, Switzerland). Standard solutions for the qualitative analysis of scopolamine, amphetamine, mefenamic acid, methoxyphenidine, THJ-2201, UR-144, ethylphenidate, 3-fluorophenmetrazine and nicotine were prepared at 1 mg mL^{-1} concentration. Methoxyphenidine, scopolamine, nicotine, ethylphenidate, amphetamine, and 3-fluorophenmetrazine were dissolved in methanol/water (1 : 1). Mefenamic acid, UR-144 and THJ-2201 were dissolved in acetonitrile. Cocaine hydrochloride was prepared at 0.1 mg mL^{-1} concentration in methanol/water (1 : 1). The analysis was carried out on the moist substances; the composition at the time of analysis depended on the volatility of the solvent and the time elapsed. Standard solutions of caffeine and nicotine for the quantitative measurements were prepared at 1500, 1000, 500, 100, 10 and 1 μM concentrations in methanol/water (1 : 1). Food samples and pills of pharmaceuticals were measured directly without dissolution. Powders were moisturized with methanol to immobilize the substances and thus prevent a potential clogging of the inlet of the mass spectrometer.

Results and discussion

Construction

A true-to-scale schematic drawing of the plasma cell is shown in Fig. 1A. It is based on two isolated ring shaped electrodes placed axially outside a fused silica tube and thus this may be termed a double-DBD or full-DBD arrangement.[23] Most reported DBD (and LTP) cells only employ one insulated tubular electrode while the second one consists of an exposed needle electrode placed at the centre of the tube.[15] The need for the centrical alignment of an inner electrode and the resulting requirement of a sideways gas feed are not present in the double-DBD cell used here,[19,23–25] which therefore has the advantage of being easier to construct. The AC excitation voltage was applied to the electrode closer to the end of the tube, while the other was connected to the ground. This arrangement was also used by other groups[25–28] and facilitates the ignition of the plasma. In order to preclude a direct discharge between the electrodes on the outside, the fused silica tubing with the electrodes was placed in a small potting case for electronic components and embedded in an electronic grade insulating epoxy resin. This set-up has the additional advantage of preventing accidental contact with the high voltage and of providing mechanical stability. A similar plasma cell embedded in epoxy, which, however, was somewhat more complex as it was based on 3D-printed parts and two concentric fused silica tubes, was previously reported by our research group.[29]

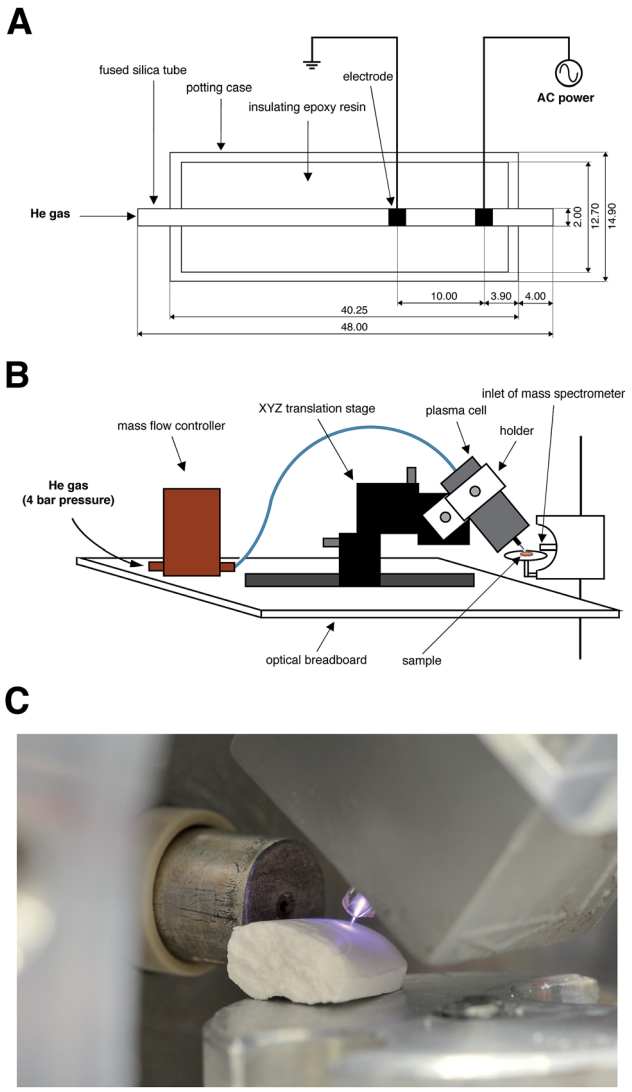

Fig. 1 (A) Schematic drawing of the DBDI plasma cell (dimensions in mm), (B) schematic drawing of the arrangement, and (C) photograph of the plasma torch.

The plasma jet was placed in front of the MS instrument according to the illustration in Fig. 1B. A purpose-made sample holder was attached directly to the instrument and features a small platform positioned slightly below the MS inlet. The plasma torch was positioned so that its tip touches the sample from the top at an approximate angle of 45°. To facilitate this alignment a small optical breadboard was mounted in front of the MS instrument. The plasma cell was attached to an XYZ translation stage, which is moved to the inlet of the MS along an optical rail mounted on top of the breadboard. The three micromanipulators of the translation stage allow a precise alignment of the plasma tip. In Fig. 1C, a picture of the plasma is given. For demonstration purposes, the beam was aligned on a pill placed on the sample holder.

The plasma was driven by a high voltage AC waveform created with an oscillator and a high voltage transformer as shown in Fig. 2. The oscillator circuitry is known as a resonant Royer oscillator.[30,31] The circuitry is freely oscillating at the resonance frequency determined largely by the inductance of the primary coils of the transformer and the capacitance of the parallel capacitor, and the transistors switch at zero volts. This arrangement makes it efficient with little power loss and the circuitry is otherwise used for applications such as driving electroluminescent lamps (which were common for back-lighting LCD displays before white LEDs were introduced) and for wireless power transfer and charging of batteries, including inductive heating and cooking. Details of the principles of the circuitry are given in Williams[30] and in Dionigi *et al.*[31] It is frequently employed for high voltage generation and many examples of this can be found on the internet by searching for "ZVS" (for "zero volt switching", but note that there are also other circuitries with this feature). The circuitry can be built from standard parts, which are readily available from distributors of electronic components. The transformer used is a so-called flyback transformer designed for creating high voltages and has a turns ratio of 1 : 260. It is rated for a power of 50 W. Similar transformers will be equally suitable. The entire circuitry was driven by a laboratory DC power supply with an adjustable voltage. Details of the high voltage AC generator have not always been given in previous publications on DBD or LTP sources for ambient ionization, but to our knowledge this is the first report on the use of the resonant Royer circuitry for this application. The cost of the mechanical parts amounted to approximately €800, the power supply to drive the oscillator costs about €450 and a suitable mass-flow controller about €1250, and so the total cost is approximately €2500. These costs should be comparable to those of purpose-built LTP and DART probes reported previously.[17,18]

Characterization

The geometry of the plasma cell given in Fig. 1A, *i.e.* using a fused silica tube with an ID of 1 mm and an OD of 2 mm and a gap of 10 mm between the electrodes, was arrived at after some experimentation. In principle, the narrower the internal diameter of the fused silica tube and the smaller the gap between the electrodes, the lower is the power needed. A low excitation voltage is also desirable considering safety issues. However a compromise has to be made for mechanical stability of the fused silica tube and narrower capillaries tended to break during handling. A shorter gap of 5 mm led to excessive heating of the plasma torch, while for a larger gap of 15 mm a higher excitation voltage was required. For the 10 mm gap an excitation voltage of 7 kV was sufficient to create a stable plasma. Note that the plasma is ignited by briefly holding a grounded cable to the orifice of the fused silica tube.

The effects of supply voltage and flow rate of the helium gas were subsequently evaluated. The high voltage AC waveform generated by the oscillating circuitry with the plasma cell attached is shown in Fig. 3A. As can be seen, the waveform is a clean sine wave oscillating at 27 kHz. However, this required an optimization of the value of the parallel capacitor in the circuitry. For a capacitance of 470 nF, instead of the 680 nF employed, a distorted waveform was observed as shown in Fig. 3B. This indicates that the plasma constitutes a reactive load to the driving circuitry. Franzke and coworkers, who studied the high voltage waveforms of a DBD as well, albeit with a pulsed supply, also presented data which show that the plasma load can lead to a distortion.[24] For supply voltages of 10, 15 and 20 V, peak-to-peak amplitudes of the output voltage of 7, 10 and 14 kV were obtained respectively. The supply current consumption was 0.25, 0.38 and 0.51 A, implying a power

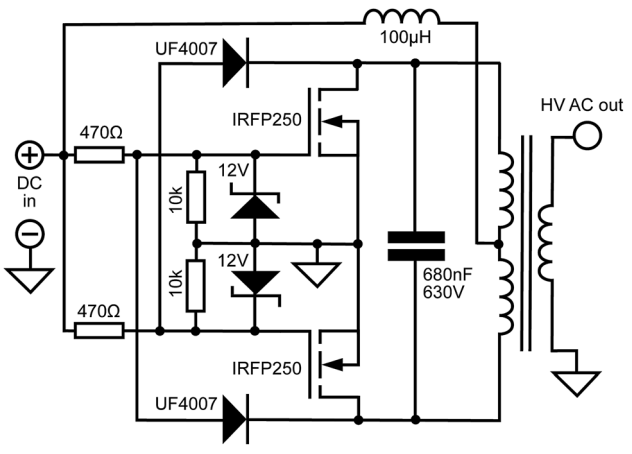

Fig. 2 Circuit diagram of the oscillator circuitry.

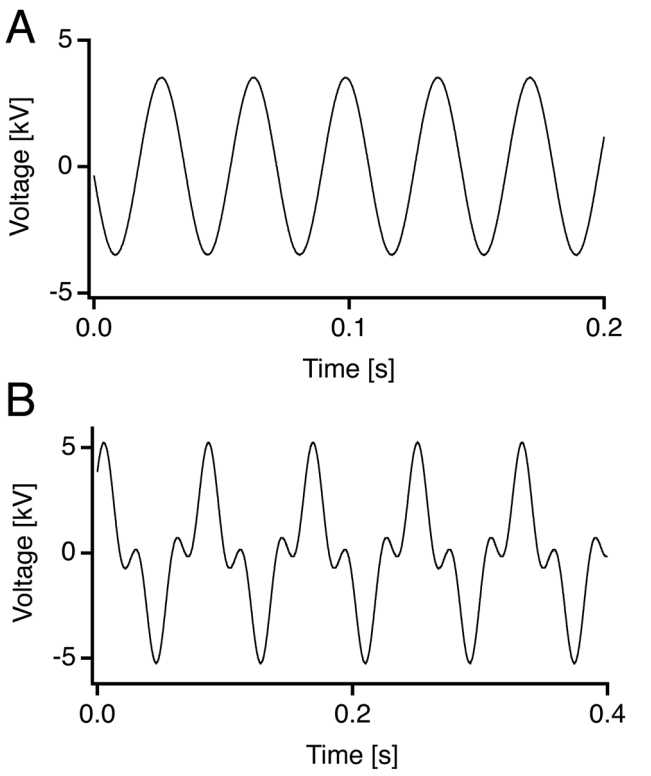

Fig. 3 Waveforms for the oscillator with the attached plasma cell obtained with a capacitor of (A) 680 nF and (B) 470 nF.

consumption of 2.5, 5.7 and 10 W respectively. The effective power coupled to the plasma, *i.e.* the efficiency of the set-up, is not known. The flow rate of helium (for the range from 10 to 100 mL min^{-1}) was found not to have any effect on the oscillation behavior or the power consumption.

Spectroscopic emission measurements were performed to specify the species generated in the plasma and for the determination of plasma temperatures. Spectra were recorded at the front of the plasma jet in an axial position due to a higher measured intensity compared to radial measurements as already reported by Guchardi.[19] In Fig. 4A and B, the emission spectrum of the plasma is shown in the range of 200 to 900 nm. The most intense bands appear due to vibrational transitions of the second positive band system of nitrogen, N_2 ($C^3\Pi_u - B^3\Pi_g$), at 316, 337, 357 and 380 nm.[32,33] Less intense emissions were observed from N_2^+ first negative system bands ($B^2\Sigma_u^+ - X^2\Sigma_g^+$) between 391 nm and 427 nm.[34] Emission lines of helium (He I) were recorded at 492, 501, 587, 667, 706 and 728 nm. A strong emission of OH at 309 nm was observed and weak emission lines of H_α at 656 nm, H_β at 486 nm and O at 777 nm could be identified. Atomic emission lines were compared to data from the NIST spectral database.[35]

Our results match the observations of Müller *et al.*,[24] who found maximum intensities of nitrogen emission lines outside the fused silica tube, while helium emission intensities decreased compared to the point of origin of the plasma. With an increasing helium flow rate (from 10 to 100 mL min^{-1}), slightly higher intensities of helium emission lines could be observed in relation to nitrogen lines. Nitrogen plays a key part in the ionization process within the plasma formed and is present as an impurity in the helium gas.[25,26,36,37] Helium metastable states generate N_2^+ ions by Penning ionization or charge transfer.[38,39] Ionized nitrogen molecules are thought to be the point of origin in a chain of reactions leading to protonated water clusters responsible for the ionization of the analytes by proton transfer, as suggested for LTP and DBD discharges by Chan *et al.*[40] and Reininger *et al.*:[41]

$$N_2^+ + 2N_2 \rightarrow N_4^+ + N_2 \quad (1)$$

$$N_4^+ + H_2O \rightarrow H_2O^+ + 2N_2 \quad (2)$$

$$H_2O^+ + (n)H_2O \rightarrow (H_2O)_nH^+ + OH \quad (3)$$

$$(H_2O)_nH^+ + M \rightarrow nH_2O + MH^+ \quad (4)$$

The temperature of a plasma is important for its characterization and can be determined by using optical emission spectroscopy. Since DBD plasmas are not in local thermal equilibrium (LTE),[42] the electronic (T_e), excitation (T_{exc}), vibrational (T_v) and rotational (T_r) temperatures are different and have to be determined separately.[43] A general rule for temperatures in non-LTE plasmas is the following: $T_e > T_v > T_r = T_g$ (T_g = gas temperature).[37] Therefore it was assumed that the rotational temperature equals approximately the gas temperature. The electronic temperature (T_e) of non-equilibrium plasmas is generally higher than the excitation temperature (T_{exc}).[44]

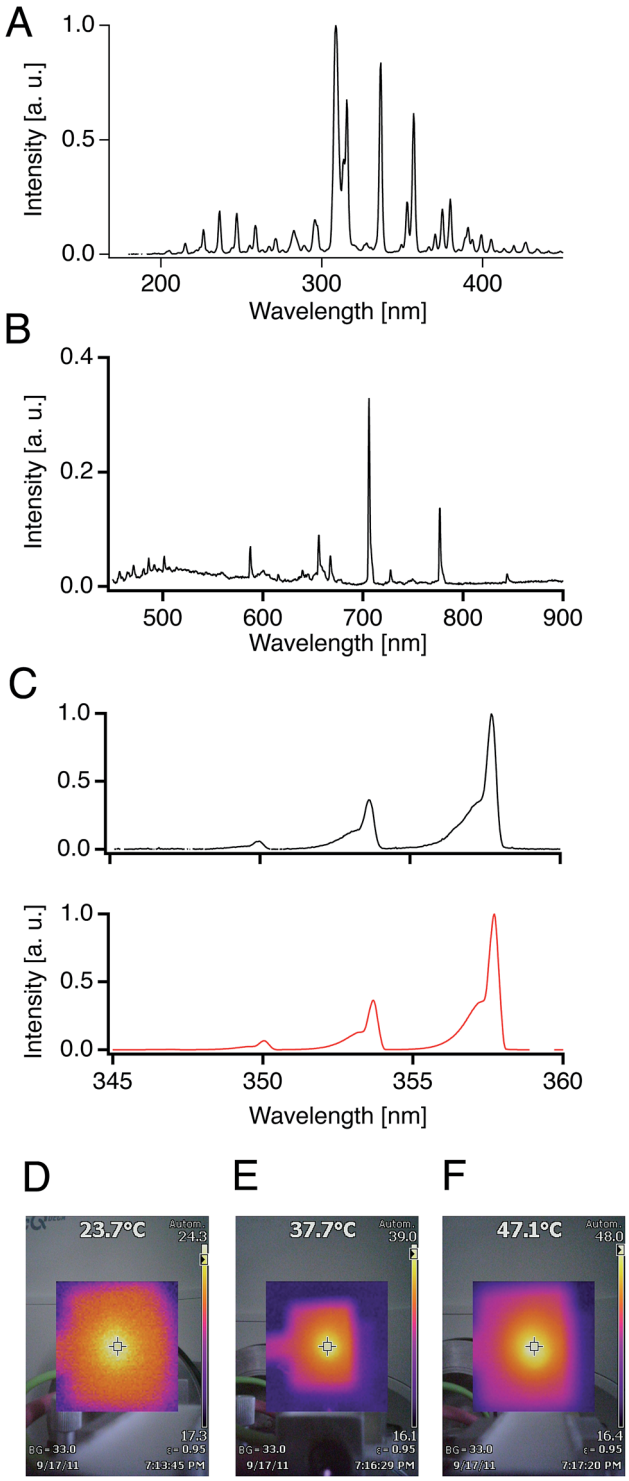

Fig. 4 Optical properties of the DBDI source. (A) Emission spectrum of the plasma source from 200 to 450 nm, (B) emission spectrum of the plasma source from 450 to 900 nm (note that different integration times were employed), and (C) experimental spectrum of the nitrogen second positive system ($\Delta\nu = 1$) rotovibrational band between 345 and 360 nm (top) and best-fitting simulated spectrum using Specair software (bottom), giving a vibrational temperature of 5000 K and a rotational temperature of 300 K. Infrared images of the DBD source for (D) 10 V, (E) 15 V and (F) 20 V supply voltage at a flow rate of 50 mL min^{-1}.

However, by using the Boltzmann plot method only the excitation temperature can be determined.[44]

The spectral modeling software package Specair was employed for the determination of the rotational and vibrational temperatures by fitting simulations to experimental spectra of the second positive system of nitrogen.[37,45,46] This approach is commonly used for the determination of temperatures in plasmas since this molecular system appears readily and is intense in different plasmas.[43,47,48] For the temperature determination, we used the N_2 rotovibrational bands ($\Delta\nu = 1$) between 340 and 360 nm.[49–52] This system was chosen since the intensity is generally much higher than that of the 380 nm system.[52] The vibrational temperature depends on the intensity ratio of the three bands between 350 and 357 nm while the rotational temperature was determined by means of the width of the emission band at 353 nm.[49] In Fig. 4C, the experimental (top) and simulated (bottom) spectra of the N_2 system are shown, acquired at a flow rate of 50 mL min^{-1} and an excitation voltage of 7 kV. Values of approximately 5000 K and 300 K were determined for the vibrational temperature and rotational temperature respectively. This means that the gas temperature of the plasma is close to room temperature, which has also been reported by other groups,[9,24,53] while the vibrational temperature is much higher. As a second approach, the gas temperature of the plasma was determined with an infrared thermal imaging camera. As shown in Fig. 4D, the measured gas temperature for an excitation voltage of 7 kV is around 297 K. By application of higher supply voltages, an increase in the gas temperature was measured. For a supply voltage of 15 V, a temperature of 311 K (Fig. 4E) and for 20 V, 320 K (Fig. 4F) was measured. The values are in good agreement with rotational temperatures obtained from the best-fit method, which are plotted in Fig. 5A. The rotational temperature increased from 300 K to 350 K following a linear behavior. When the flow rate of the helium gas was varied between 10 and 100 mL min^{-1}, no difference in the gas temperature could be observed neither by infrared measurements nor by spectroscopy.

Vibrational temperatures were determined for three different supply voltages as plotted in Fig. 5A and three different flow rates as shown in Fig. 5B. With increasing supply voltage from 10 to 20 V at a fixed helium flow rate of 50 mL min^{-1}, an increase in the vibrational temperature was measured from 5000 to 7700 K following a linear behavior. Also by increasing the helium flow rate at a fixed supply voltage of 10 V, higher vibrational temperatures were obtained varying from 4700 to 5350 K for 10 to 100 mL min^{-1}.

The excitation temperature (T_{exc}) of the plasma was obtained from a Boltzmann plot for helium emission lines (492, 501, 587, 667, 706, and 728 nm) by plotting $\ln(I_{ul}\lambda_{ul}/g_{ul}A_{ul})$ *versus* the energy E_u.[54,55] I_{ul} is the relative intensity of the transition, λ_{ul} is the transition wavelength in nm, g_{ul} the statistical weight, A_{ul} the probability emission coefficient in cm^{-1} and E_u the energy difference of the level u in eV.[56] The slope of the plot corresponds to the excitation temperature of the plasma, which was estimated to be around 2800 K for an excitation voltage of 7 kV and a helium flow rate of 50 mL min^{-1} with a correlation coefficient of 0.75. The excitation temperature did not change in the investigated flow rate range between 10 and 100 mL min^{-1} and excitation voltage range between 7 and 14 kV. For full characterization, it would be useful to also know the degree of ionization and the electron temperature (T_e); however, the determination of these parameters was not possible with the available means.

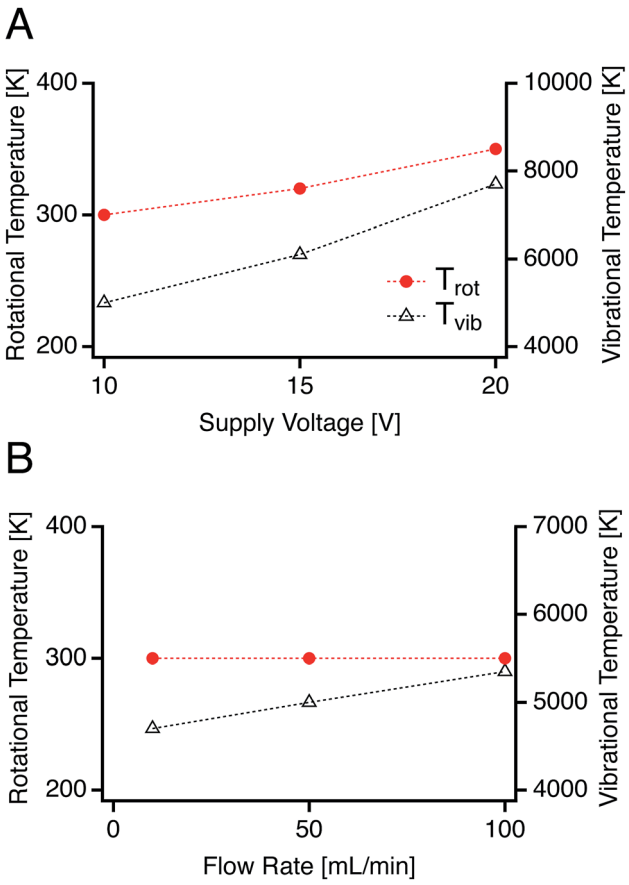

Fig. 5 Dependence of the rotational and vibrational temperatures on the (A) supply voltage between 10 and 20 V and the (B) helium flow rate between 10 and 100 mL min^{-1}.

DBD is a soft ambient ionization method, which means that a few fragments of the analytes are observed.[14] Minor fragmentation is useful to get some structural information about compounds. However high fragmentation patterns lead to a complication in the mass spectra of mixtures. We studied the application of different plasma voltages and helium flow rates to determine whether they have an effect on the fragmentation. However, it was found that the fragment intensity appears to depend more on the position of the plasma jet relative to the MS orifice and less on the applied settings.

A flow rate of 50 mL min^{-1} was chosen for the subsequent work since this was the minimum flow rate required to obtain stable MS signals. When using a lower flow rate of 10 mL min^{-1}, the absolute intensity of the signal was found to fluctuate significantly with time. Compared to other studies,[27,28] where flow rates in the range of 150 to 400 mL min^{-1} were used, the flow rate of 50 mL min^{-1} is rather low. Since no loss in performance of the DBD source was observed using this low

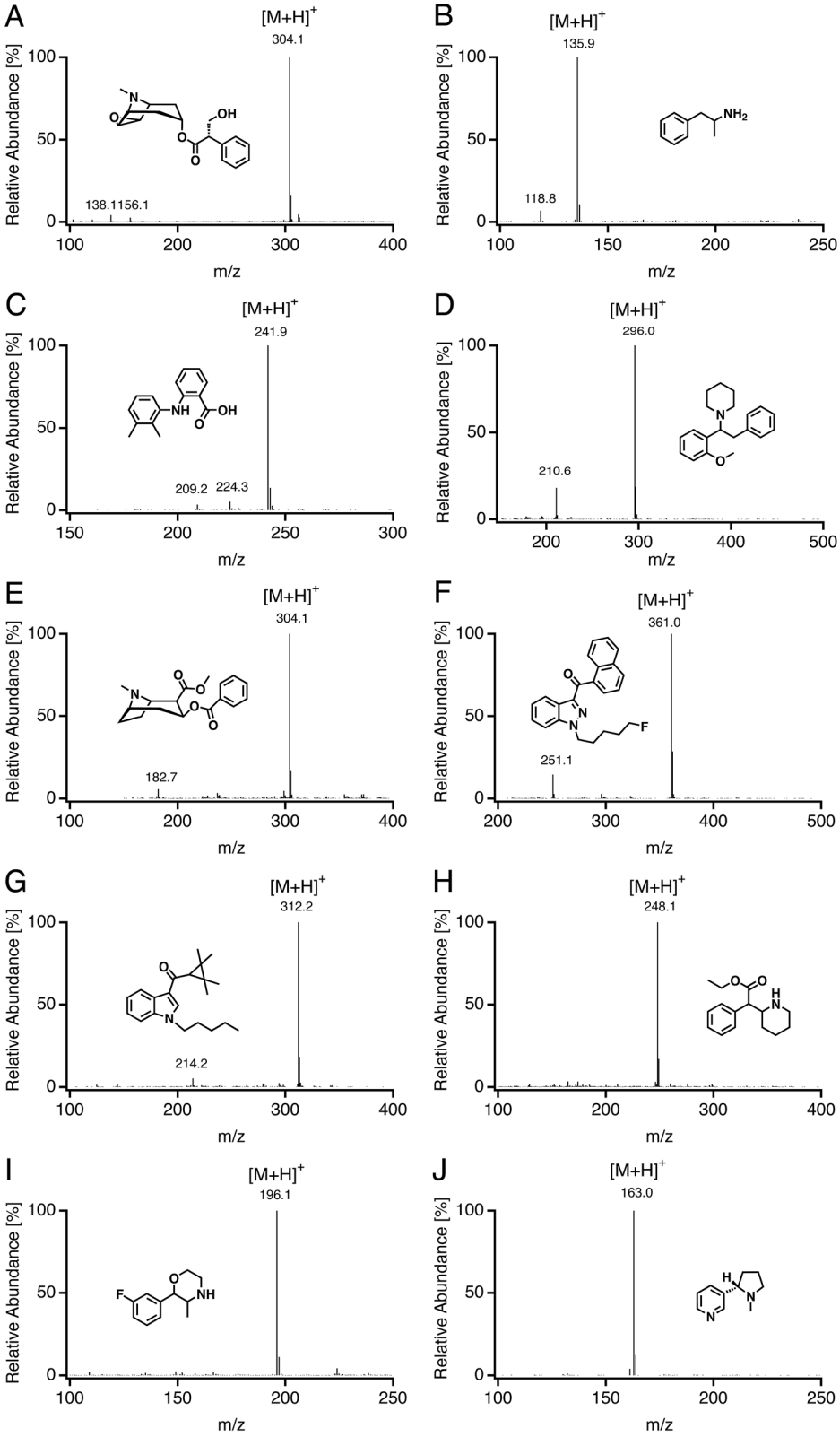

Fig. 6 DBDI-MS spectra of selected standard compounds: scopolamine (A), amphetamine (B), mefenamic acid (C), methoxyphenidine (D), cocaine (benzoylmethylecgonine) (E), THJ-2201 (1-[(5-fluoropentyl)-1*H*-indazol-3-yl](naphthalen-1-yl)methanone) (F), UR-144 (1-pentylindol-3-yl)-(2,2,3,3-tetramethylcyclopropyl)methanone (G), ethylphenidate (H), 3-fluorophenmetrazine (I), and nicotine (J).

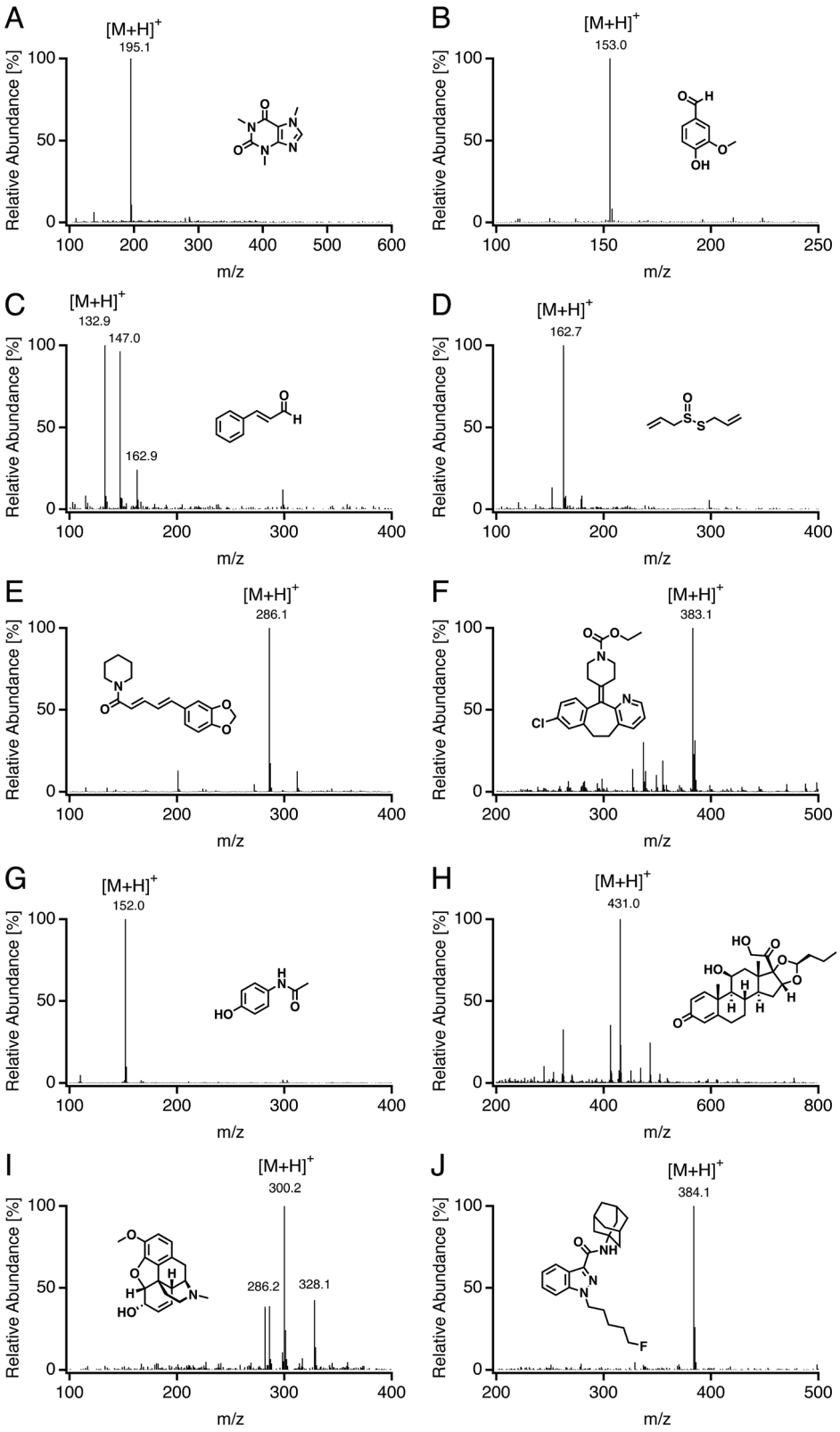

Fig. 7 DBDI-MS spectra of samples: (A) coffeine in coffee powder, (B) vanillin detected in vanilla beans, (C) cinnamaldehyde detected in cinnamon powder, (D) allicin detected in garlic cloves, (E) piperine detected in pepper powder, (F) active ingredient loratidine in Claritin® tablets, (G) active ingredient paracetamol (acetaminophen) in Panadol® tablets, (H) active ingredient budesonide in Buderhin® nasal spray, (I) opiate mixture containing 6-acetylmorphine, codeine and morphine, and (J) 5F-AKB48 (5F-APINACA) detected in Funky Buddha.

View Article Online
Paper Analytical Methods

flow rate, this setting is preferable in order to keep the consumption of helium low. The lowest possible excitation voltage of 7 kV was adopted in order to keep the heating of the cell low and minimize the possibility of any electrical arcing.

Performance

In Fig. 6, the mass spectra of a range of standard substances representing pharmaceuticals, illegal drugs, and food flavoring are given. A qualitative analysis of the moist substances was carried out after placing a small amount of the solution onto a microscope glass slide.[57] As reported by Meyer *et al.*[11] we observed that the protonated molecular ion $[M + H]^+$ was always the most abundant peak in the DBD-MS spectra with little or no fragmentation. Doubly charged ions were not detected. Examples of pharmaceutical compounds analysed are scopolamine, amphetamine and mefenamic acid. The molecular ion peak of scopolamine (Fig. 6A) was detected at 304.1 *m*/*z* with two fragment ions at 156.1 and 138.1 *m*/*z*. In Fig. 6B, amphetamine was observed as protonated molecular ion $[M + H]^+$ (*m*/*z* 135.9) with one fragment ion peak at 118.8 *m*/*z*. In Fig. 6C, the spectrum of mefenamic acid is displayed. The molecular ion peak $[M + H]^+$ was observed at 241.9 with two fragments at 224.3 and 209.2 *m*/*z*. Examples from the analysis of illegal drugs follow. In Fig. 6D, methoxyphenidine, which is a designer drug, was detected as protonated molecular ion $[M + H]^+$ at 296.0 *m*/*z*. One fragment was observed at 210.6 *m*/*z*. The molecular ion peak of cocaine (Fig. 6E) was observed at 304.1 *m*/*z*. The signal at 182.7 *m*/*z* may originate from fragmentation. THJ-2201 and UR-144 are synthetic cannabinoids, which have psychoactive effects and represent the so-called "legal highs". In Fig. 6F, THJ-2201 was detected as protonated molecular ion $[M + H]^+$ (*m*/*z* 361.0) with one fragment at 251.1 *m*/*z*. Ur-144 (Fig. 6G) was observed at 312.2 with one fragment at 214.2 *m*/z. Ethylphenidate and 3-fluorophenmetrazine are also psychostimulant compounds. Ethylphenidate (Fig. 6H) was detected at 248.1 *m*/*z* without fragmentation. In Fig. 6I, the spectrum of 3-fluorophenmetrazine is shown. The peak of the $[M + H]^+$ ion was observed at 196.1 *m*/*z*. Nicotine (Fig. 6J) was analyzed as an example of a parasympathomimetic drug, detected as protonated molecular ion $[M + H]^+$ (*m*/*z* 163.0). No fragmentation was observed.

Even though ambient ionization is not primarily intended for quantitative analysis this aspect was investigated for two model substances. Calibration curves for caffeine and nicotine for 6 concentrations in the range between 1 and 1500 μM were acquired by placing 20 μL of the standard solutions onto a microscope slide followed by immediate measurement. For each concentration, the measurements were repeated three times by averaging each time the signal height over 1 minute recording time. Linear responses over this range were found for both caffeine ($R^2 = 0.9973$) and nicotine ($R^2 = 0.9922$). The limits of detection (for peak heights corresponding to 3× the baseline noise) were determined to be 16 pmol/3.1 ng (0.8 μM) for caffeine and 8 pmol/1.3 ng (0.4 μM) for nicotine. These results are comparable to the LOD of 15 ng for TATP (triacetone triperoxide) reported by Hagenhoff *et al.*[57] for a similar set-up. Relative standard deviations (RSD) were found to be between 3 and 32%. The reason for the relatively high RSD values is thought to lie in the reproducibility of the positioning of the sample and different degrees of solvent evaporation as our system was not optimized for quantitative analysis.

In Fig. 7A–E, examples of food samples are given. Spectra were obtained by direct analysis of the respective materials without any sample preparation. Powders were moisturized using methanol. Caffeine (*m*/*z* 195.1) was detected in coffee powder (Fig. 7A) and vanillin (*m*/*z* 153.0) in vanilla beans (Fig. 7B). In Fig. 7C, the $[M + H]^+$ molecular ion peak of cinnamaldehyde in cinnamon powder is observed at 132.9 *m*/*z*. Peaks at 147.0 and 162.9 *m*/*z* may originate from coumarin and eugenol, which are further components of cinnamon. In Fig. 7D, allicin is detected as a protonated molecular ion (*m*/*z* 162.7) in fresh garlic cloves and in Fig. 7E piperine at 286.1 *m*/*z* in powdered pepper. Different pharmaceuticals were analyzed in Fig. 7F–H. Loratidine as an active component in Claritin® (Fig. 7F) was observed at 383.1 *m*/*z*, acetaminophen in Panadol® (Fig. 7G) at 152.0 *m*/*z* and budesonide in Buderhin® nasal spray (Fig. 7H) at 431.0 *m*/*z*. Two examples of illegal drugs are given. Morphine (*m*/*z* 286.2), codeine (*m*/*z* 300.2) and 6-monoacetylmorphine (*m*/*z* 328.1) could be identified in an opiate mixture (Fig. 7I). 5F-APINACA (*m*/*z* 384.1) was identified in Funky Buddha leaves, which are leaves of the marshmallow plant impregnated with the substance. 5F-APINACA is a synthetic cannabinoid. The peaks not identified in the mass spectra originate from unknown components of the sample matrix.

Conclusions

The ambient desorption/ionization source assembled in our laboratory was found to allow qualitative analysis of a variety of samples and is therefore a viable alternative to much more costly commercial aftermarket products for fitting to mass-spectrometers. The construction of the plasma cell is simple and the alignment in front of the instrument is based on commercially available micromanipulators. The construction of the high voltage oscillator circuitry is not challenging, as no surface mounted devices are needed. It is also possible to buy the entire circuitry, including the transformer, as a preassembled module for about 20€ from vendors found on the internet (eBay, AliExpress, *etc.*). Besides the qualitative analysis of solutions and solid samples, it was also found to be possible to carry out a quantitative analysis of solutions over a wide dynamic range with limits of detection of about 1 μM for two model compounds in samples with a low volume of 20 μL. The precision of this technique can possibly be improved by automation of the sampling technique.

Conflicts of interest

There are no conflicts to declare.

Acknowledgements

The authors are grateful to R. Dumler for help in obtaining some of the samples.

References

1 Z. Takats, J. M. Wiseman, B. Gologan and R. G. Cooks, *Science*, 2004, **306**, 471–473.
2 R. B. Cody, J. A. Laramee and H. D. Durst, *Anal. Chem.*, 2005, **77**, 2297–2302.
3 *Ambient Ionization Mass Spectrometry*, ed. M. Domin and R. Cody, Royal Society of Chemistry, Cambridge, 2015.
4 A. T. Lebedev, *Russ. Chem. Rev.*, 2015, **84**, 665–692.
5 M. Z. Huang, S. C. Cheng, Y. T. Cho and J. Shiea, *Anal. Chim. Acta*, 2011, **702**, 1–15.
6 F. J. Andrade, J. T. Shelley, W. C. Wetzel, M. R. Webb, G. Gamez, S. J. Ray and G. M. Hieftje, *Anal. Chem.*, 2008, **80**, 2654–2663.
7 N. Na, M. X. Zhao, S. C. Zhang, C. D. Yang and X. R. Zhang, *J. Am. Soc. Mass Spectrom.*, 2007, **18**, 1859–1862.
8 N. Na, C. Zhang, M. X. Zhao, S. C. Zhang, C. D. Yang, X. Fang and X. R. Zhang, *J. Mass Spectrom.*, 2007, **42**, 1079–1085.
9 J. D. Harper, N. A. Charipar, C. C. Mulligan, X. R. Zhang, R. G. Cooks and Z. Ouyang, *Anal. Chem.*, 2008, **80**, 9097–9104.
10 H. Hayen, A. Michels and J. Franzke, *Anal. Chem.*, 2009, **81**, 10239–10245.
11 C. Meyer, S. Müller, E. L. Gurevich and J. Franzke, *Analyst*, 2011, **136**, 2427–2440.
12 A. Albert, J. T. Shelley and C. Engelhard, *Anal. Bioanal. Chem.*, 2014, **406**, 6111–6127.
13 X. L. Ding and Y. X. Duan, *Mass Spectrom. Rev.*, 2015, **34**, 449–473.
14 C. A. Guo, F. Tang, J. Chen, X. H. Wang, S. C. Zhang and X. R. Zhang, *Anal. Bioanal. Chem.*, 2015, **407**, 2345–2364.
15 S. Brandt, F. D. Klute, A. Schütz and J. Franzke, *Anal. Chim. Acta*, 2017, **951**, 16–31.
16 S. Martínez-Jarquín and R. Winkler, *TrAC, Trends Anal. Chem.*, 2017, **89**, 133–145.
17 S. Martínez-Jarquín, A. Moreno-Pedraza, H. Guillén-Alonso and R. Winkler, *Anal. Chem.*, 2016, **88**, 6976–6980.
18 K. T. Upton, K. A. Schilling and J. L. Beauchamp, *Anal. Methods*, 2017, **9**, 5065–5074.
19 R. Guchardi and P. C. Hauser, *J. Anal. At. Spectrom.*, 2003, **18**, 1056–1059.
20 R. Guchardi and P. C. Hauser, *J. Chromatogr. A*, 2004, **1033**, 333–338.
21 R. Guchardi and P. C. Hauser, *Analyst*, 2004, **129**, 347–351.
22 R. Guchardi and P. C. Hauser, *J. Anal. At. Spectrom.*, 2004, **19**, 945–949.
23 F. D. Klute, S. Brandt, P. Vogel, B. Biskup, C. Reininger, V. Horvatic, C. Vadla, P. B. Farnsworth and J. Franzke, *Anal. Chem.*, 2017, **89**, 9368–9374.
24 S. Müller, T. Krähling, D. Veza, V. Horvatic, C. Vadla and J. Franzke, *Spectrochim. Acta, Part B*, 2013, **85**, 104–111.
25 S. B. Olenici-Craciunescu, S. Müller, A. Michels, V. Horvatic, C. Vadla and J. Franzke, *Spectrochim. Acta, Part B*, 2011, **66**, 268–273.
26 S. B. Olenici-Craciunescu, A. Michels, C. Meyer, R. Heming, S. Tombrink, W. Vautz and J. Franzke, *Spectrochim. Acta, Part B*, 2009, **64**, 1253–1258.
27 A. Michels, S. Tombrink, W. Vautz, M. Miclea and J. Franzke, *Spectrochim. Acta, Part B*, 2007, **62**, 1208–1215.
28 C.-Y. Chen, C.-H. Chiang and C.-H. Lin, *IEEE Trans. Plasma Sci.*, 2014, **42**, 3726–3731.
29 R. D. Dumler and P. C. Hauser, in *CHanalysis 2016, Conference of the Division of Analytical Sciences of the Swiss Chemical Society, November 18-19, 2016*, Beatenberg, Switzerland, 2016.
30 J. Williams, in *The Art and Science of Analog Circuit Design*, ed. J. Williams, Butterworth-Heinemann, Boston, 1998, pp. 139–193.
31 M. Dionigi, A. Costanzo, F. Mastri, M. Mongiardo and G. Monti, in *Wireless Power Transfer*, ed. J. I. Agbinya, River Publishers, Aalborg, Denmark, 2016, pp. 217–270.
32 Q. Xiong, X. Lu, J. Liu, Y. Xian, Z. Xiong, F. Zou, C. Zou, W. Gong, J. Hu, K. Chen, X. Pei, Z. Jjang and Y. Pan, *J. Appl. Phys.*, 2009, **106**, 083302.
33 D. Staack, B. Farouk, A. Gutsol and A. Fridman, *Plasma Sources Sci. Technol.*, 2005, **14**, 700–711.
34 A. Qayyum, Z. Shaista, M. A. Naveed, S. A. Ghauri, M. Zakaullah and A. Waheed, *J. Appl. Phys.*, 2005, **98**, 103303.
35 A. Kramida, Y. Ralchenko and J. Reader, *NIST Atomic Spectra Database, (ver. 5.5.2)*, National Institute of Standards and Technology, Gaithersburg, MD, 2018, January 29, https://physics.nist.gov/asd.
36 F. D. Klute, A. Michels, A. Schütz, C. Vadla, V. Horvatic and J. Franzke, *Anal. Chem.*, 2016, **88**, 4701–4705.
37 A. Ricard, in *Reactive Plasmas*, SFV, Paris, France, 1996, pp. 89–134.
38 G. C.-Y. Chan, J. T. Shelley, A. U. Jackson, J. S. Wiley, C. Engelhard, R. G. Cooks and G. M. Hieftje, *J. Anal. At. Spectrom.*, 2011, **26**, 1434–1444.
39 C. Meyer, S. Müller, B. Gilbert-López and J. Franzke, *Anal. Bioanal. Chem.*, 2013, **405**, 4729–4735.
40 G. C. Y. Chan, J. T. Shelley, J. S. Wiley, C. Engelhard, A. U. Jackson, R. G. Cooks and G. M. Hieftje, *Anal. Chem.*, 2011, **83**, 3675–3686.
41 C. Reininger, K. Woodfield, J. D. Keelor, A. Kaylor, F. M. Fernández and P. B. Farnsworth, *Spectrochim. Acta, Part B*, 2014, **100**, 98–104.
42 U. Kogelschatz, *Plasma Chem. Plasma Process.*, 2003, **23**, 1–46.
43 H. Nassar, S. Pellerin, K. Musiol, O. Martinie, N. Pellerin and J.-M. Cormier, *J. Phys. D: Appl. Phys.*, 2004, **37**, 1904–1916.
44 J. Jonkers and J. A. M. Van der Mullen, *J. Quant. Spectrosc. Radiat. Transfer*, 1999, **61**, 703–709.
45 C. O. Laux, T. G. Spence, C. H. Kruger and R. N. Zare, *Plasma Sources Sci. Technol.*, 2003, **12**, 125–138.
46 H. Khatun and A. K. Sharma, *Braz. J. Phys.*, 2010, **40**, 450–453.
47 A. Lofthus and P. H. Krupenie, *J. Phys. Chem. Ref. Data*, 1977, **6**, 113–307.
48 A. Xiao, S. M. Rowland, J. C. Whitehead and X. Tu, *IEEE Conf. Electr. Insul. Dielectr. Phenom.*, 2012, **2**, 191–194.

49 N. Masoud, K. Martus, M. Figus and K. Becker, *Contrib. Plasma Phys.*, 2005, **45**, 32–39.
50 I. Prysiazhnevych, V. Chernyak, S. Olzewski and V. Yukhymenko, *Chem. Listy*, 2008, **102**, 1403–1407.
51 J. S. Hummelt, M. A. Shapiro and R. J. Temkin, *Phys. Plasmas*, 2012, **19**, 123509.
52 A. Xiao, S. M. Rowland, X. Tu and J. C. Whitehead, *IEEE Trans. Dielectr. Electr. Insul.*, 2014, **21**, 2466–2475.
53 V. Horvatic, S. Müller, D. Veza, C. Vadla and J. Franzke, *J. Anal. At. Spectrom.*, 2014, **29**, 498–505.
54 C. Oliveira, F. M. Freitas, G. J. P. Abreu, M. P. Gomes, K. G. Grigorov, P. Getsov, I. M. Martin, R. S. Pessoa, L. V. Santos, V. W. Ribas and B. N. Sismanoglu, *J. Phys.: Condens. Matter*, 2014, **4**(3A), 19–27.
55 Z. Ouyang, V. Surla, T. S. Cho and D. N. Ruzic, *IEEE Trans. Plasma Sci.*, 2012, **40**, 3476–3481.
56 H. Park, S. J. You and W. Choe, *Phys. Plasmas*, 2010, **17**, 103501.
57 S. Hagenhoff, J. Franzke and H. Hayen, *Anal. Chem.*, 2017, **89**, 4210–4215.

4.2 INJECTION SYSTEM FOR FAST CAPILLARY ELECTROPHORESIS BASED ON PRESSURE REGULATION WITH FLOW RESTRICTORS

In capillary electrophoresis, the injection of the sample into the separation capillary is a crucial step, responsible for the quality and reproducibility of the measurement. The challenge lies in the automatic and reproducible injection of tiny amounts in the nano- or even picoliter range. Flow injection helps automating the injection process and split injection is a well-known approach for proper sample injection from initial larger amounts [89–91].

In this project, a novel injection system was developed based on the sequential injection manifold. Sample amounts in the picoliter range were injected into a short separation capillary with a small internal diameter of 10 µm. The injection process did not rely on mechanical movements of vials or syringe pumps. Rather, the injection system was based on pneumatic flow rate regulation. With one fixed pressure being applied to the buffer and sample container, only the timing of valve operations needed to be controlled. This approach made the set-up of the injection system inherently simple and reduced power consumption, which would make the system favourable for implementation in portable instrumentation.

Flow rates within the system were regulated by flow resistors, which were inserted at well-defined positions. Calculations based on the Hagen-Poiseuille law were performed in order to determine the dimensions and location of the restricting tubes. Three valves allowed to choose the flow paths as well as to fill the sample loop. One resistor reduced the initial high pressure of 6 bar to a moderate flow rate for interface flushing and sample transport steps. An additional function of this restrictor was to bring the pressure at the capillary inlet close to zero, which prevented accidental sample injection during transport. On the other hand, the full pressure was needed for an efficient flushing of the separation capillary. Although the first flow restrictor was switched in series with the capillary, the full pressure was obtained at the capillary inlet. The reason is that the ratio between the two resistor values was large. For sample injection a moderate pressure at the capillary entrance was created by switching a second resistor in parallel to the first one. With precise time control, a tiny sample amount of 0.3 pL was injected. Nine different inorganic cations could be separated in 25 s. Good repeatability within 3 % and detection limits around 5.5 µM were obtained. Mineral water was analysed quantitatively by building calibration curves for five different inorganic ions (NH_4^+, K^+, Na^+, Ca^{2+}, Mg^{2+}).

2ND PROJECT:

Injection system for fast capillary electrophoresis based on pressure regulation with flow restrictors

Electrophoresis, 2019, 40, 410-413

410 *Electrophoresis* 2019, *40*, 410–413

Jasmine S. Furter
Peter C. Hauser

Department of Chemistry, University of Basel, Basel, Switzerland

Received June 22, 2018
Revised August 21, 2018
Accepted August 22, 2018

Short Communication

Injection system for fast capillary electrophoresis based on pressure regulation with flow restrictors

A fast automated system for rapid electrophoretic separations in short conventional capillaries employing contactless conductivity detection is presented. The instrument is based on pneumatic pressurization and does not require a conventional pump. The required pressures and flow rates for the different steps of the injection and flushing processes are produced with the help of two flow restrictors. The device is implemented on a microfluidic breadboard with dimensions of ca. 13 × 20 cm and employs miniature valves. Nine inorganic cations, namely NH_4^+, K^+, Na^+, Ca^{2+}, Mg^{2+}, Mn^{2+}, Sr^{2+}, Li^+, and Ba^{2+}, could be separated in a capillary of 10 μm inner diameter and 6 cm effective length within 25 s. Following a reduction of the effective length to 4 cm, still five inorganic cations could be separated in a time span of 12 s. The repeatability of peak areas was better than 3.1 % and limits of detection between 3.5 and 5.5 μM were achieved.

Keywords:
Capillary electrophoresis / Fast separations / Fluid-handling System / Microfluidics
DOI 10.1002/elps.201800250

In capillary electrophoresis, control over the injected amount of sample is essential for obtaining good reproducibility and the best compromise between resolution, sensitivity, and analysis time. Because of diffusion effects the timing is also important. Electrokinetic injection is the simplest approach, but not suitable for quantitative analysis due to an injection bias for samples with varying background conductivities. Therefore hydrodynamic injection is preferred, but is not trivial because of the small volumes in the low nL to pL range involved. Conventional commercial capillary electrophoresis instruments rely on direct injection from a sample vial into the capillary by application of pressure or vacuum. This requires mechanical movements of vials on a sampling tray and/or of the capillary and the provision of an airtight seal while the capillary is located inside the sample vial. These movements require time and have complications with a certain tendency to failure. The conventional approach is also not suitable for automated sampling from flowing streams [1], when the separation is to be optimized by employing narrow capillaries down to 10 μm ID requiring high pressures for flushing, or when fast separations are to be carried out in short capillaries of a few centimetres in length [2–6].

For well controlled automated injection, schemes derived from the sequential injection analysis approach have been found useful. As the amount of sample which needs to be loaded into the capillary is too small to be metered directly or with a syringe pump, a larger volume is first placed into a sample loop. Subsequently, the sample is moved into a split injection device. When the sample plug is located in front of the capillary inlet, the injection of a proper sample amount is achieved by controlled pressurization for a defined length of time. Following flushing of the interface the electrophoretic separation is commenced. Finally, the capillary may also need to be flushed before the next separation. The movement of the sample plug to the capillary inlet and the flushing of the injection interface can be carried out with a displacement device such as a syringe pump, but the actual injection and flushing of the capillary must be implemented through pressurization. For simplicity all steps may then be performed by pneumatic pressurization of containers with background electrolyte solutions [7–10], which requires different pressure levels and blocking valves. The set-up reported herein has been optimized in several ways. Miniature valves with adequate holding pressure for use with capillaries of 10 μm ID (allowing a high separation efficiency) were employed and a miniature overall manifold was obtained. Only a single gas pressure level was required and all flows were set with two precisely determined fixed flow restrictors and switching valves. Furthermore, in contrast to earlier reports, the transport of sample to the split injector is carried out without pressure on the capillary inlet, which prevents spurious injection.

A schematic diagram of the instrument is shown in Fig. 1A. A constant pressure of 6 bar provided by a standard gas cylinder of nitrogen (PanGas, Pratteln, Switzerland) was applied to an airtight reservoir (LS-T116-BBRES,

Correspondence: Peter C. Hauser, Department of Chemistry, University of Basel, Klingelbergstrasse 80, 4056 Basel, Switzerland.
E-mail: peter.hauser@unibas.ch

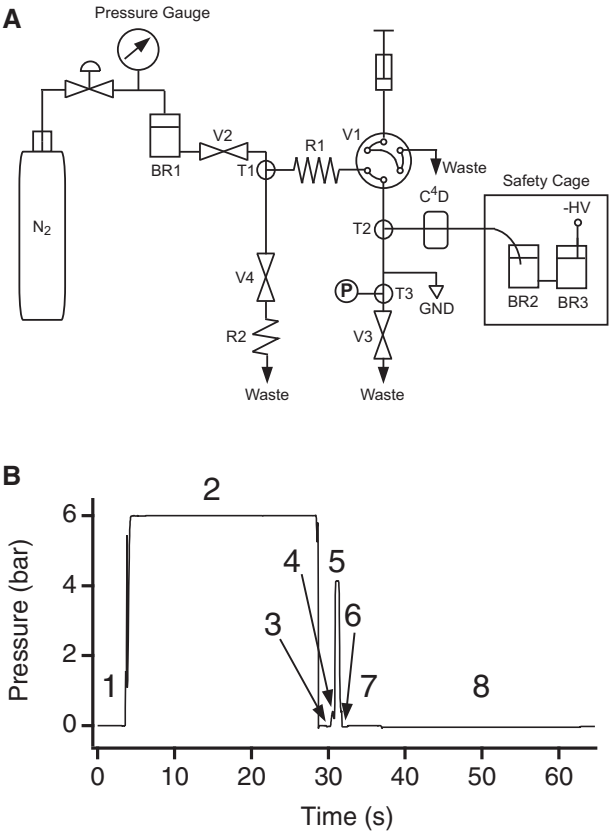

Figure 1. A) BR1-3: background electrolyte reservoirs; V1: rotary injection valve; V2-V4 blocking valves; R1 and R2: flow restrictors; T1-T3: T-pieces; P: pressure sensor; capacitively coupled contactless conductivity detector: contactless conductivity detector. B) Pressure sequence for one operation cycle. The numbers indicate the steps detailed in Table 1.

LabSmith, Livermore, CA, USA) containing BGE (BR). A six-way valve (V1) (LabSmith, LS-AV203-C360) was fitted with a sample loop with 360 μm OD, 150 μm ID, and 35 cm length (CAP360-150P, LabSmith). Samples can be loaded with a syringe, but, if desired, sample aspiration into the loop may also be automated. Valves V2, V3, and V4 (LS-AV201, LabSmith) serve to direct the flows. The two flow restrictors (R1 and R2) consisted of PEEK tubing with dimensions of 1/16" OD (1.59 mm), 0.0025" ID (63.5 μm)(1560, IDEX, Lake Forest, Illinois, USA) and 7 cm length (R1) and 1/16" OD (1.59 mm), 0.007" ID (178 μm)(IDEX, 1536) and 4 cm length (R2). A fused silica capillary with 360 μm OD, 10 μm ID and 17 cm total length (TSP-010375, Polymicro, Phoenix, AZ, USA) was employed for separation. Its high voltage end was located in a safety cage and placed in a container separate from the electrode. The voltage of –20 kilovolts was provided by a high voltage module (UM20N4/S, Spellman, Pulborough, UK). The electrophoretic ground consisted of a stainless steel tube (1/16" OD and 0.01" ID, 2.5 cm length, IDEX, U-111) as part of the manifold. Note, that due to the narrow separation capillary the electrophoretic current was a low 3 μA. Furthermore, the tubular electrode is located downstream from the injection point and regularly flushed, so that pH changes of the background electrolyte due to electrolysis or bubble formation do not affect the electrophoresis process. The miniature valves and high voltage module were linked to a notebook computer by using an Arduino microcontroller board (Arduino Nano 3.0, Gravitech, Minden, NV, USA) and a purpose made printed circuit board providing the necessary interface electronics. All devices in the system and the timing sequences were controlled with a program written in the computer language *Forth* running on the ATmega328 microcontroller of the Arduino board. Open source *AmForth*, developed for the Atmel AVR8 Atmega microcontroller family, was employed (http://amforth.sourceforge.net). User interaction with the program was achieved via a terminal emulator application (*CoolTerm*, http://freeware.the-meiers.org/) running on the notebook computer. For detection, a lab-made capacitively coupled contactless conductivity detector was used [11]. The pressure could be monitored with a sensor (LabSmith, uPS0800-T116) mounted in a T-piece (T3) just downstream from the injection point. Data acquisition for the detector and pressure sensor (the latter connected via an instrumentation amplifier, INA111, Texas Instruments, Austin, TX, USA) was carried out with an e-corder 410 with the Chart software package (eDAQ, Denistone East, NSW, Australia). All parts, except for the pressure supply, the high voltage cage and the data acquisition system, were assembled on a microfluidic breadboard with dimensions of ca. 13 × 20 cm (LabSmith) using appropriate tubings, fittings and T-pieces.

The dimensioning of the flow restrictors was carried out by considering the hydraulic-electric circuit analogy (see [12] for example) and employing the Hagen-Poiseuille law on the behavior of liquids in tubes:

$$Q = \frac{\pi r^4 \Delta P}{8\eta L} \tag{1}$$

where Q is the volumetric flow rate of the liquid, r the radius of the tube, ΔP the pressure difference between the ends of the tube, η the viscosity of the liquid and L the length of the tube. On rearrangement an expression, which is equivalent to Ohm's law, is obtained:

$$\Delta P = \frac{8\eta L}{\pi r^4} Q \approx V = R \cdot I \tag{2}$$

where V is the voltage corresponding to ΔP, R the resistance and I the current corresponding to Q.

It is thus possible to relate pressure, flow rates, and flow restrictors consisting of lengths of narrow tubing. A flow restrictor with a desired flow resistance can be fashioned from available tubing. Furthermore, as for Ohm's law, serial and parallel arrangements of flow restrictors have the corresponding effects. Volume flow rates can be transformed into flow velocities if the cross-section of the conduit is known and the requisite timing can also be deduced.

The flow restrictors were needed for two purposes. First, a reduction of the flow rate during the sample transport and interface flushing steps was achieved by implementing a relatively high flow resistance (R1) in front of the six-way valve (V1). This way, the pressure almost completely drops across

Table 1. Operation Sequence

Step	Operation	Duration (s)	Valve Setting V1	V2	V3	V4	HV[a]	Flow Rate (μL/s)	Buffer Consumption (μL)
1	Interface flushing	4	Inject	Open	Open	Closed	Off	3.4	13.6
2	Capillary flushing	25	Load	Open	Closed	Closed	Off	0.0009	0.02
3	Sample transport	1.3	Inject	Open	Open	Closed	Off	3.4	4.4
4	Pressure release	0.5	Inject	Closed	Open	Closed	Off	0	0
5	Sample injection	0.5	Inject	Open	Closed	Open	Off	325	163
6	Pressure release	0.5	Inject	Closed	Open	Closed	Off	0	0
7	Interface flushing	5	Inject	Open	Open	Closed	Off	3.4	17
8	Separation	28	Inject	Closed	Open	Closed	On	0	0

[a]HV; high voltage

this flow resistor while the liquid is still transported with a moderate flow rate of 3.4 μL/s. A backpressure through any flow restrictor at the outlet, as employed previously, is avoided in this new arrangement in order to prevent partial premature injection during the sample transfer. On the other hand, for speed, the flushing of the capillary should be carried out at maximum pressure, but due to the low flow rate imposed by the narrowness of the separation capillary the pressure drop across R1 during this step is not expected to be significant. Secondly, a reduced pressure at the capillary inlet must be obtained for controlled injection of a proper amount of sample. This was achieved by switching R2 parallel to the separation capillary through opening V4.

The typical protocol for the operation of the instrument is displayed in Table 1, showing the valve settings and the durations of the different steps as well as the resulting volumetric flow rates in the parts of the manifold concerned and the buffer volume consumed. The resulting pressure profile is given in Fig. 1B. In the first step (1), the system interface is flushed with a pressure close to zero (0.045 bar). In the second step (2) the capillary is flushed for 24 s with a pressure of 6 bar, which is not diminished by R1. During this step the sample is loaded manually into the loop of V1 by the operator. The required sample volume is around 6 μL. Subsequently, the sample plug is transported from the sample loop to the T-piece holding the separation capillary (step 3). Since the distance between sample loop and T-piece is short (3.5 cm), the transport step takes only 1.3 s. Then a defined pressure of 4.1 bar is applied to the inlet of the separation capillary for 0.5 s (step 5). Note, that it is not possible to trade a higher pressure (e.g. the full 6 bar) for a shorter injection time as the valves employed have a finite switching time which cannot be reduced. The calculated amount of sample injected is 0.3 pL (corresponding to a plug length of 4 mm). The system is again flushed for 5 s (step 7) to remove all sample residuals, followed by the turning-on of the high voltage −20 kilovolts for 28 s (step 8). Note also, the two steps (4 and 6) for releasing residual pressure. The total time for one operation sequence was 65 s.

As investigated by Tůma and co-workers [13], smaller internal diameter capillaries used in capillary electrophoresis together with capacitively coupled contactless conductivity detector require higher buffer concentrations for best sensitivity. Since 10 μm ID capillaries were used for the separation, a BGE containing 60 mM L-His, 5 mM 18-Crown-6 and 0.2 mM acetic acid providing a pH of 4 was employed for the separation of inorganic cations. In Fig. 2A the separation of nine inorganic cations (NH_4^+, K^+, Na^+, Ca^{2+}, Mg^{2+}, Mn^{2+}, Sr^{2+}, Li^+, Ba^{2+}) at 100 μM concentration is shown. Note, that under the conditions employed transient stacking is taking place leading to a sharpening of the peaks. A capillary with an effective length of 6 cm was employed and the separation was completed within 25 s. To demonstrate even faster separations for the most prominent cations, the effective length of the capillary was shortened to 4 cm and the system performance was evaluated using quantitative data. In Fig. 2B, the separation of NH_4^+, K^+, Na^+, Ca^{2+}, and Mg^{2+} in only 12 sis shown. For this separation, calibration curves based on peak areas were acquired for the range from 5 to 200 μM and correlation coefficients between 0.997 and 0.998 were obtained for the 5 cations. The reproducibilites for the peak areas (RSD values for n = 8) for the concentrations between 50 and 200 μM were found to be between 1.0 and 3.1%. The LODs were determined as 4.9 μM for NH_4^+, 4.8 μM for K^+, 5.5 μM for Na^+, 3.5 μM for Ca^{2+}, and 3.8 μM for Mg^{2+} (from the injection of solutions containing concentrations of 5 μM of the ions). Note, that one might consider the LOQ (approximately 15 μM) as the lower ends of the useful calibration ranges. Note also, that as illustrated for example by Mai et al. [10], the performance parameters, LOD, width of the linear range, and separation times, are interdependent. Lower LODs and wider linear ranges may be obtained by injection of larger amounts into longer capillaries, thus sacrificing analysis time. The instrument was tested for the analysis of a mineral water sample of Cristalp®, which was diluted 1:20. The resulting electropherogram is shown in Fig. 2C. Concentrations of 2.6 mg/L (68 μM) for K^+, 19.2 mg/L (834 μM) for Na^+, 120 mg/L (2985 μM) for Ca^{2+} and 40.0 mg/L (1647 μM) for Mg^{2+} were determined, which match very well published data of 20.0 mg/L for Na^+, 115.0 mg/L for Ca^{2+}, and 40.0 mg/L for Mg^{2+} (data for K^+ is not available) [14].

In conclusion, a compact system for CE has been developed. It has been optimized for fast analysis, which was demonstrated by the separation of nine inorganic cations

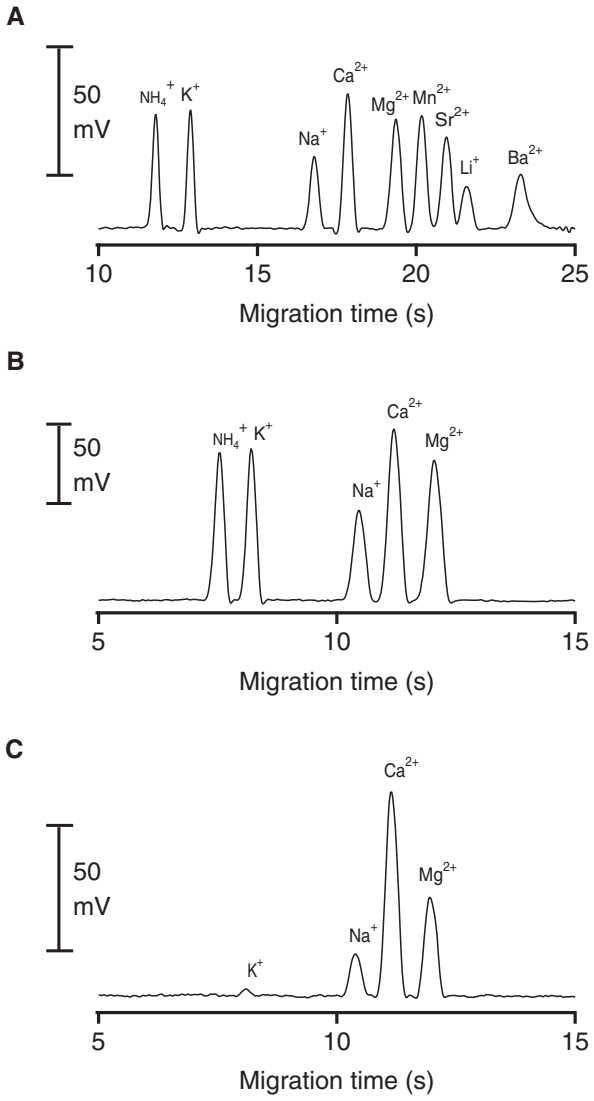

Figure 2. Analysis of inorganic cations. BGE: 60 mM L-His, 5 mM 18-Crown-6 and 0.2 mM acetic acid (pH 4). Capillary: 10 μm ID, 365 μm OD, 6 (A) and 4 (B, C) cm effective length, 17 cm total length. Injection: 0.5 s at 4.14 bars. (A) Separation of nine inorganic cations at 100 μM in 25 s, (B) separation of five inorganic anions at 200 μM in 12 s, (C) determination of cations in Cristalp® mineral water sample, diluted 1:20.

within only 25 s The system was tested successfully with a mineral water sample. It has a very flexible configuration and can easily be rearranged for other purposes, such as the determination of organic cations and anions.

The authors thank Yoel Koenka for help with the code to control the LabSmith valves and Matthias Trute for making AmForth available.

The authors have declared no conflict of interest.

References

[1] Mai, T. D., Schmid, S., Müller, B., Hauser, P. C., *Anal. Chim. Acta* 2010, *665*, 1–6.

[2] Opekar, F., Tůma, P., *J. Chromatogr. A* 2017, *1480*, 93–98.

[3] Opekar, F., Tůma, P., *J. Chromatogr. A* 2016, *1446*, 158–163.

[4] Matysik, F.-M., *Electrochem. Comm.* 2006, *8*, 1011–1015.

[5] Wuersig, A., Kubáň, P., Khaloo, S. S., Hauser, P. C., *Analyst* 2006, *131*, 944–949.

[6] Rainelli, A., Hauser, P. C., *Anal Bioanal Chem* 2005, *382*, 789–794.

[7] Mai, T. D., Le, M. D., Sáiz, J., Duong, H. A., Koenka, I. J., Pham, H. V., Hauser, P. C., *Anal. Chim. Acta* 2016, *911*, 121–128.

[8] Sáiz, J., Duc, M. T., Koenka, I. J., Martín-Alberca, C., Hauser, P. C., García-Ruiz, C., *J. Chromatogr. A* 2014, *1372*, 245–252.

[9] Pham, T. T. T., Mai, T. D., Nguyen, T. D., Sáiz, J., Pham, H. V., Hauser, P. C., *Anal. Chim. Acta* 2014, *841*, 77–83.

[10] Mai, T. D., Pham, T. T. T., Pham, H. V., Sáiz, J., Ruiz, C. G., Hauser, P. C., *Anal. Chem.* 2013, *85*, 2333–2339.

[11] Tanyanyiwa, J., Galliker, B., Schwarz, M. A., Hauser, P. C., *Analyst* 2002, *127*, 214–218.

[12] Oh, K. W., Lee, K., Ahn, B., Furlani, E. P., *Lab Chip* 2012, *12*, 515–545.

[13] Tůma, P., Samcová, E., Štulík, K., *Electroanalysis* 2011, *23*, 1870–1874.

[14] Azoulay, A., Garzon, P., Eisenberg, M. J., *J. Gen. Intern. Med.* 2001, *16*, 168–175.

4.3 INTERACTIVE CONTROL OF PURPOSE BUILT ANALYTICAL INSTRUMENTS WITH FORTH ON MICROCONTROLLERS

In scientific research in the field of instrumental analytics it is important to quickly automate new set-ups. Different components of such purpose made instruments, for example valves, syringe pumps and high voltage modules have to be linked and connected to a personal laptop computer. Nowadays, this is even mandatory because most devices can only be controlled electronically. This challenges from the field of automation technology need to be handled by analytical scientists, who are no experts in electronics or programming. One approach to solve this issue is to use the commercial available software LabVIEW, which can be used for instrument control and data acquisition. It is a visual programming language package, which allows to flexibly customize a graphical user interface (GUI). The drawbacks of LabVIEW are that programming skills are needed for setting up the software environment and that it is quite expensive. With the appearance of inexpensive microcontroller platforms such as the Arduino, it became easier to control different parts of an instrumental set-up [111]. Without having many competences in electronics or programming, parts can be connected and operated by using the integrated development environment (IDE) of the platform on the computer. Many libraries are provided and a variety of examples available in the internet. The standard C-based software for the Arduino needs to be compiled and uploaded to the microcontroller. Afterwards, it is running independently, which makes it ideal for standalone operations. However, during the development of new experimental set-ups in analytics, different parameters need to changed frequently. Therefore an interactive communication with the microcontroller is better.

For this application field, the interpreted programming language Forth is ideal because it allows an interactive execution of commands and is also more efficient than C [112, 113]. Forth can be complied to various processors, including the ATmega328 microcontroller of the Arduino. In Forth, commands are carried out in small subroutines, which are called Words. These small Words first can be tested interactively and independently from each other and then easily be combined to larger structures. This way, the control software is developed by a simple bottom up approach.

My participation to the publication was to demonstrate the experimental set-up of a capillary electrophoresis instrument and analysis examples, which was solely controlled with the Forth programming language by using the AMForth package. By reverse engineering the I^2C communication protocol of commercially available valves was found out and a Forth code written for controlling them. Another contribution to the publication was the development of a graphical user interface (GUI). Although Forth has many

advantages as programming language, some things are missing when controlling the instrument solely from a command prompt. For example it is difficult to stop a running process or to follow analogue values. In addition, it may be useful to store the values in a text file or display them in a real time chart. If an experimental set-up is used for a longer time, it can also be desirable to increase the user friendliness for other users working on the instrument. Java was used as the language to program the GUI and communicating with the microcontroller running Forth code. For this work, a simple GUI was programmed, which gathered the voltage values from an alcohol sensor where the conductivity was changing with the breath alcohol content. The measurement could be started and stopped with the GUI and values saved in a text file. A real time plot allowed to follow the breath alcohol over time. Code extracts showing the basic communication between microcontroller and graphical user interface can be found in the appendix (see Part v). This initial simple GUI was further developed during the PhD.

3RD PROJECT:

Interactive control of purpose built analytical instruments with Forth on microcontrollers - A tutorial

ACA, 2019, 1058, 18-28

Analytica Chimica Acta 1058 (2019) 18–28

Contents lists available at ScienceDirect

Analytica Chimica Acta

journal homepage: www.elsevier.com/locate/aca

Tutorial

Interactive control of purpose built analytical instruments with Forth on microcontrollers - A tutorial

Jasmine S. Furter, Peter C. Hauser*

University of Basel, Department of Chemistry, Klingelbergstrasse 80, 4056, Basel, Switzerland

HIGHLIGHTS

- The computer language Forth is available for many popular microcontroller platforms.
- Forth is an interpreted language and allows direct interactive control of instruments.
- It greatly augments the usefulness of platforms such as the Arduinos in laboratory applications.

GRAPHICAL ABSTRACT

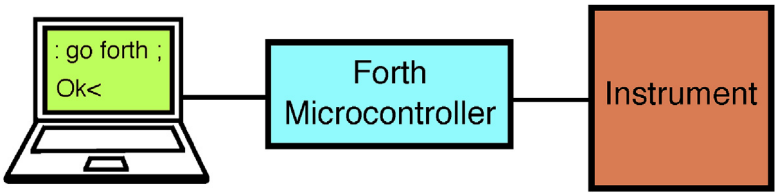

ARTICLE INFO

Article history:
Received 27 August 2018
Received in revised form
30 October 2018
Accepted 31 October 2018
Available online 5 November 2018

Keywords:
Forth
Microcontroller
Personal computer
Experimental systems
Interactiv control
Valve
Mass-flow controller
Capillary eletrophoresis
Sensor

ABSTRACT

The use of the computer language Forth for controlling experimental analytical instruments built in laboratories is described. Forth runs on a microcontroller and as it is an interpreted language the user can directly communicate with it by employing a terminal emulator program running on a personal computer. Thus the user can test attached hardware, such as pumps, valves, electronic pressure regulators, detectors and chemical sensors, directly from the keyboard. This overcomes the lack of interactivity, a significant shortcoming, of the computer languages C and C++, the default on such microcontroller platforms as the Arduinos, which have become very popular in recent years for laboratory applications. Common examples of purpose built experimental analytical laboratory instruments are sequential injection analysis systems, microfluidic devices, or automated sample extraction systems. Application examples from our laboratory are given, namely the regulation of mass-flow controllers for gases, the sequencing of an experimental capillary electrophoresis instrument and the acquisition of a signal from an alcohol sensor.

Contents

1. Introduction 19
2. Forth 19
3. Forth on microcontrollers 20
4. Analog mass flow controllers 23

Abbreviations: PC, personal computer; OSHW, open source hardware; IDE, integrated development environment; RPN, reverse Polish notation; REPL, read evaluate print loop; GPIO, general purpose input/output; TTL, transistor transistor logic; IC, integrated circuit; ADC, analog-to-digital conversion; DAC, digital-to-analog conversion; SPI, serial peripheral interface bus; I^2C, Inter-integrated circuit; UART, universal asynchronous receiver-transmitter; USB, universal serial bus; IC, integrated circuit; GUI, graphical user interface.

* Corresponding author.
E-mail address: Peter.Hauser@unibas.ch (P.C. Hauser).

https://doi.org/10.1016/j.aca.2018.10.071
0003-2670/

5. Purpose built capillary-electrophoresis instrument 23
6. Embedded assembly code 24
7. Graphical user interface and data storage 25
8. Conclusions 26
Supplementary data 27
References 27

1. Introduction

In our research group in analytical chemistry we often have the need to build experimental systems or small instruments not available commercially. In the early days of personal computers (PCs) electronic hardware could often be connected directly to the computer (*e.g.* through its parallel port) and controlled with software running on the PC. It used to be fairly common for analytical chemists in research laboratories to assemble such purpose made systems. However, as PCs have become more powerful they also have become more complex, as have the available interfaces. The LabVIEW graphical development platform from National Instruments (Austin, Texas, US) is an effort to address this situation, but is relatively costly. While the software is elegant, it also still requires a significant effort in mastering it. On the other hand the introduction of electronic open source hardware (OSHW), such as the Arduino microcontroller platform [1], has made it possible again for researchers in analytical laboratories, without being experts in electronic engineering, to build increasingly sophisticated systems based on programming microcontrollers to access hardware devices and sequence operations. This may include such devices as electronically controlled high voltage power supplies, different kinds of pneumatic and hydraulic valves, pressure and flow rate controllers for gases, pumps, function generators, or physical and chemical sensors. Indeed the Arduino platform has gained popularity as a tool in research laboratories and enabled projects otherwise not easily possible, see for instance these references [2–13], as well as examples from our laboratory [14–20]. Urban gives a more comprehensive list of applications of the Arduino and similar platforms specifically by researchers in analytical chemistry [21] and Dryden et al. have provided a more general review on the trend to open-source hardware (not just electronic circuitry) in this discipline [22]. The Arduino platform owes its success not only to the standardized and inexpensive hardware, but also to a large extent to its integrated development environment (IDE) running on a PC for developing the microcontroller software. This hides most of the underlying complexity of the development cycle of the C-based software and renders the programming of the microcontroller much more accessible to non-experts. However, while it undoubtedly is a highly useful development, we found the Arduino IDE limited for our purposes in that it was designed for producing devices which operate with a fixed software program in a stand-alone fashion independent of the personal computer employed for its development. This does not address well the common situation in the research laboratory, where frequent changes to experimental arrangements and parameters are necessary and an interactive control of the experimental set-up is needed. The programming language Forth is an alternative to C/C++, which is better suited for such purposes.

2. Forth

Forth was developed by Charles H. Moore in the 1970s (*i.e.* at about the same time as C), because of his frustration with the then prevalent Fortran and Cobol. In the early days Forth was used mainly for interactive operation of radiotelescopes [23–25]. This early set-up is illustrated in Fig. 1. To control the instrumentation the user would type commands in the Forth language on the terminal. The computer would then directly interpret the input strings and immediately act on them to carry out the different operations required, such as positioning the telescope, setting up the receiver as well as collecting and processing its signals for graphical representation. Forth gained popularity during the 1980s and also found uses in analytical laboratories [26–34]. The PC software package Asyst, once popular in the laboratory for instrument control and data processing, was based on Forth [35]. Moore is an advocate of keeping things simple [25], and during the conception of Forth, microprocessor hardware and memory was expensive, thus Forth is lean and efficient. While for programming modern PCs it may be desirable to use a computer language with advanced powerful built-in features, Forth is still of interest for programming small microcontrollers, such as those used for the Arduino platform. Indeed commercial versions are available for many current microcontrollers from at least two active vendors, namely Forth Inc [36]. and MPE [37], and there is a range of open source implementations. The websites of Forth Inc. and MPE list a number of commercial applications of Forth. It has, for example, been employed by NASA for the software on many space probes [38], including the recently concluded Cassini-Huygens mission to Saturn [39], as well as by the European Space Agency on the Rosetta mission to the comet 67P/Churyumov-Gerasimenko [40].

Forth is an interpreted language (such as Basic or Python), so that commands can be executed interactively. However, it also includes a compiler, which is entered from the interpreter, and allows the compilation of subroutines, called Words in the Forth environment. The Words are actual extensions of the Forth language and can then be invoked via the interpreter and also be used in the

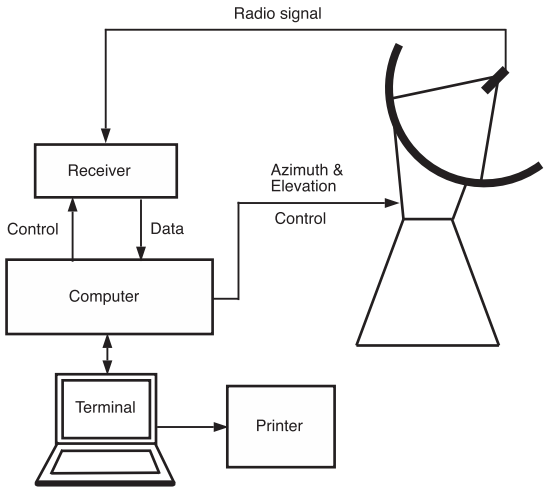

Fig. 1. Simplified representation of the original application of Forth for the control of radiotelescopes. Adapted from Ref. [23].

compilation of new Words. Forth thus builds on modules, which can be interactively and independently tested and when satisfied combined to larger functions. Memory locations in the microcontroller as well as peripheral hardware items connected to the ports of the microcontroller can be examined directly from the keyboard when developing the software. This process allows for an efficient bottom up approach for developing control software. Such an approach is not possible with conventional compiled languages, such as the C/C++ used by the Arduino IDE, where even small programs have to go through the development cycle consisting of writing the source code, compilation of the entire program, uploading to the microcontroller and execution for testing. While this process is much faster for modern microcontrollers than it used to be, the lack of interactivity of C/C++ still does not facilitate the incremental building of the software that is possible with Forth. Forth makes use of a stack to pass parameters from one Word to another, but the use of global variables is also possible. A so-called postfix approach is employed which corresponds to the algebraic Reverse Polish Notation (RPN) (as used in some pocket calculators). Thus the Forth language has a syntax which is close to the way a microprocessor or microcontroller operates. Forth can be considered a lower level language than C, being close to assembly, but due to its extensibility it can also be an abstract high level language.

A brief session with the open source GForth running on a PC is shown in Fig. 2 for illustration. Following the start up of the program in a terminal window the Forth interpreter is available. The interactive nature of Forth allows its use as a calculator by placing first 2 and then 3 on the stack followed by the multiplication (*) and the printing (.) of the result on the screen. When the execution is completed, the Forth interpreter indicates its readiness for further user input with the 'ok' prompt. The product of this calculation is the factorial of 3. The next line shows the definition of a Forth Word for the calculation of factorials. The colon (:) instructs the interpreter to enter the compiler mode. The first statement ('factorial') is the name of the new Forth Word being defined. After a stack manipulation a loop is entered in which the loop index is the multiplier. The compilation mode is exited with the semicolon (;). The new word can then be tested immediately and used as shown in the example by the calculation of the factorials of 3 and 4. It is also directly available for incorporation in the next higher level definition, in this case for the calculation of superfactorials (products of the factorials).

Experienced programmers tend to find Forth somewhat strange as some of its concepts are quite different from the more common computer languages. On the other hand, its syntax is very simple and for new programmers without a bias the essentials of Forth are easy to learn. It has also often been stated that programming in Forth is much more efficient than in C [25], the language currently used predominantly for microcontroller programming. One of the reasons for this must be the lack of interactivity of compiled languages which does not allow the immediate and incremental testing of subroutines/functions as illustrated in Fig. 2 for Forth.

```
Last login: Mon Apr 23 17:23:58 on ttys019
AnC:~ peterhauser$ gforth
Gforth 0.7.3, Copyright (C) 1995-2008 Free Software Foundation, Inc.
Type `bye' to exit
ok
2 3 * . 6  ok
: factorial 1 swap 1 + 1 do I * loop ;  ok
3 factorial . 6  ok
4 factorial . 24  ok
: superfactorial 1 swap 1 + 1 do I factorial * loop ;  ok
3 superfactorial . 12  ok
4 superfactorial . 288  ok
bye
ac19:~ peterhauser$
```

Fig. 2. A short Forth session in the terminal window on a PC. The user input has been coloured red. See the text for details. (For interpretation of the references to colour in this figure legend, the reader is referred to the Web version of this article.)

Although programming has been dominated by compiled languages, such as C and languages derived from it, the interpreted language Python has in recent years gained a strong following. Even for compiled languages the so-called REPL concept has become popular. REPL stands for “Read Evaluate Print Loop” and refers to the possibility of interactive testing and execution of program snippets. Compiled languages now often have a REPL tool. Another feature that has always been available in Forth is the possibility to tailor the compiler to create different versions of Words, a form of object oriented programming [41].

A good introduction to Forth is the book “Starting Forth”, which is out of print, but available from the internet as pdf-file [42]. Forth may be explored using a web-based emulator [43,44] and free trial versions for PCs are available from the two major commercial vendors of Forth. The open source GForth is available for the three main versions of operating systems for PCs (*i.e.* Windows, Linux and Mac OS) [45]. A modern, fully featured, freeware Forth for the Macintosh is available under the name of iMops [46].

3. Forth on microcontrollers

Different versions of Forth are available for the major microcontroller families and are listed in Table 1. The commercial products are advanced versions which are optimized to create efficient code and come with the usual support while the open source versions are not quite a polished. The choice of microcontroller depends on different criteria. The devices with the narrower busses (8, 16 bit) are generally less powerful than the 32 bit devices in terms of processing speed and available memory, and also tend to have fewer ports for connecting peripherals. On the other hand, it requires less effort to learn to use the simpler devices. Prior familiarity may also play a role. Other criteria may be the operating voltage (*e.g.* 5 V or 3.3 V) for compatibility with connected devices,

Table 1
The main available versions of forth for some of the major microcontroller families.

Microcontroller Family	Architecture	Forth Versions
AVR	8 bit	AmForth[a] FlashForth[b] SwiftX[c] Forth 7[d] 328eForth[e]
PIC	8/16 bit	FlashForth[b]
MSP430	16 bit	AmForth[a] Mecrisp[f] NoForth[g] SwiftX[c] Forth 7[d] 430eForth[e] 4E4th[h]
ARM	32 bit	Mecrisp-Stellaris[e] SwiftX[c] Forth 7[d] STM32eForth720[e]

[a] http://amforth.sourceforge.net, open source.
[b] http://flashforth.com, open source.
[c] https://www.forth.com, commercial.
[d] http://www.mpeforth.com, commercial.
[e] https://sites.google.com/offete23.com/eforth/home, commercial.
[f] http://mecrisp.sourceforge.net, open source.
[g] http://home.hccnet.nl/anij/nof/noforth.html, open source.
[h] http://www.4e4th-ide.org, open source.

the type(s) of interfaces needed, or if the microcontroller is available in a conventional through-hole package or only as a surface mount device. The microcontrollers usually also require some peripheral circuitry such as a quartz oscillator or a power regulator. In the wake of the success of the Arduino the manufacturers of microcontrollers have produced a large variety of evaluation kits for their products which are available at low cost (some for less than € 10) and may be used directly in a research environment so that it is generally not necessary to produce microcontroller boards in the lab. The simpler microcontrollers have about the same processing power and memory space as the early PCs, so that Forth, which was developed for resource restrained platforms, is a good match for these devices. The development of the open source Forth packages for these popular microcontrollers and inexpensive boards constitutes a small revival of Forth.

The installation of Forth in the flash memory of the microcontroller needs to be carried out with the help of a dedicated device programmer (a piece of hardware attached to a PC) available from the manufacturers of the controllers or as inexpensive third party devices. The microcontrollers on the Arduino boards come preloaded with a bootloader program which works hand-in-hand with the Arduino IDE and allows installation of user programs written in C/C++ via a serial interface to the PC and a device programmer is not needed. Thus to get started with Forth on a microcontroller requires a bit more effort than when using the Arduino IDE platform, which may be considered a disadvantage, but this is not a significant hurdle as the suppliers strive to make the downloading of programs into their devices as simple as possible. Many recent development boards include a programmer on the board itself (*e.g.* the MSP430 Launchpads from Texas Instruments and the ARM based Nucleo and Discovery boards from STMicroelectronics). Note, that an Arduino board can still be used with Forth, but the bootloader cannot be employed and is overwritten when Forth is burnt onto the device.

The PC-linked approach for controlling experiments proposed here is illustrated in Fig. 3. The devices which are to be controlled or read during an experiment are connected to the microcontroller via its ports, namely GPIO (general purpose input/output, logic signals for turning devices on and off and testing the status of signals), ADC (analog-to-digital convertor for measuring signals), DAC (digital-to-analog convertor for control signals), SPI, I^2C, UART (3 different serial peripheral interfaces for communication with devices) *etc.* as appropriate. Often also interface electronics to provide power and for voltage level shifting are needed. The microcontroller itself is attached to a PC via a USB port of the latter. As most microcontrollers do not have a built-in USB port a bridging device is needed to translate between USB and serial TTL signals at 5 or 3.3 V compatible with its UART. Many development boards come fitted with an appropriate module but it is also possible to use an inexpensive USB-to-TTL serial cable with built in convertor IC. Superficially the connection of an Arduino to a personal computer running the Arduino IDE looks identical. However, with the Arduino IDE the program is cross-compiled on the PC before download for subsequent execution on the microcontroller. With a PC-linked Forth-microcontroller the approach is significantly different. The Forth environment runs directly on the microcontroller and constitutes its own basic operating system. The PC acts as a dumb terminal, running a terminal emulator program. This resembles very much the approach taken by Moore for interactive control of radiotelescopes, except that it is now done with modern much more compact and less expensive computing hardware and in our case the attached devices are not heavy machinery but small valves, sensors etc. One of the simplest possible arrangements is shown in the photo of Fig. 4. A MSP430G2553 microcontroller running Mecrisp Forth is fitted on a breadboard for demonstration, and connected to a computer with a USB-TTL bridge cable. The microcontroller is powered through the USB port of the computer (a voltage regulator is needed to bring the 5 V of the port to the required 3.3 V), and is used to control a valve with its own power supply via an optocoupler. While the switching of a valve alone does not, of course, require a microcontroller this is needed for automated timing. Communication with attached devices is carried out via writing and reading to and from registers on the microcontroller. Ports generally have to be set up by configuring control registers. The interactive nature of Forth allows setting and reading back of these registers from the keyboard, which is an excellent way of learning to work with microcontrollers and to debug the software. Attached devices can then be controlled directly and

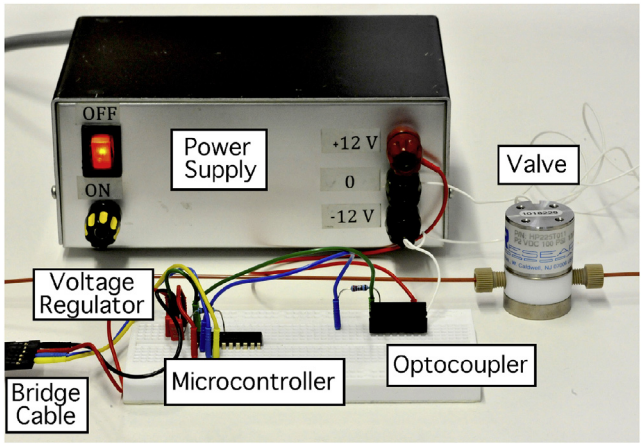

Fig. 4. Photo of a minimal arrangement with a MSP430 microcontroller and an optocoupler on a breadboard to switch a solenoid valve. The power supply is only needed to drive the valve, the microcontroller is powered through the USB port of the PC via the USB-TTL-bridge cable.

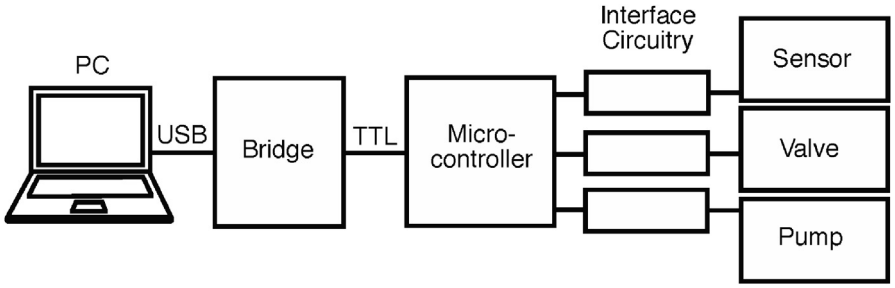

Fig. 3. Hardware configuration for the interactive control of sensor and actuator devices based on a microcontroller linked to a PC. The interfaces to the hardware make use of the different I/O-ports of the controller.

tested by issuing short commands from the keyboard. For the switching of the valve via the MSP430G2553 microcontroller first the pin to which the valve is connected has to be configured as a logical signal output with the following command sequence:

```
1 p1dir cbis!
```

"1" stands for a so-called mask indicating that it is bit 0 (portpin 1.0) which needs to be configured. This value is put on the stack first. "p1dir" is a constant which holds the address of the register which configures port 1. When the constant is executed the address is also placed on the stack. "cbis!" sets the bit designated by the mask in the register to a logic high, *i.e.* in this case configures the pin as an output. The valve can then be turned on and off similarly by writing to the output register (whose address is held by the constant "p1out"), and a timing sequence, *e.g.* for flushing a manifold for 1 s by opening the valve, may be programmed as follows:

```
: valve-on 1 p1out cbis! ;

: valve-off 1 p1out cbic! ;

: flush valve-on 1000 ms valve-off ;
```

"cbis!" in this case sets the bit in the output register, so that a logic high, or 3.3 V, appears on the pin, which turns on the opto-coupler driving the valve. "cbic!" clears the bit in the register, *i.e.* turns it to a logic low or 0 V, switching the valve off.

For more complex set-ups each operation can be developed and tested in this fashion until all steps function satisfactorily. ADCs, DACs, as well as devices connected to the microcontroller via the SPI, I^2C, or UART ports can be operated similarly by reading and writing to the registers of the microcontrollers. For the more complex operations involving the serial ports libraries of Forth Words, with their source code, are available from the suppliers of the package employed. On consultation of the data book for the microcontroller the interaction of software and hardware can be fully understood without too much effort. In contrast, the Arduino IDE tends to hide underlying details from the user. This makes it simple to use, but it is also restricting. The programmer using Forth can reach a deeper understanding and closer control than when working with the Arduino IDE. For the microcontroller of the basic Arduino boards we found the book by Williams on AVR programming to be very helpful [47] (The examples in the book are given in C, but can easily be translated into Forth. Incidentally, while the author clearly is fluent in C, he is also a proponent of Forth [48].) In the development of Forth software, hardware specific details, concerning the microcontroller used or the attached devices, should be contained and abstracted in low level Words. This allows their easy reuse for new applications, or if some hardware components are changed in an experimental system only the relevant basic "driver" Words need to be rewritten.

For running complete experiments or measurement protocols different options are possible. The user may enter commands sequentially to carry out the desired operations. If a higher degree of automation is desired, all individual commands may be compiled into a single final Forth Word. A further possibility is to write a menu based program on the microcontroller. This consists of a Forth routine which sends a prompt to the user who then issues a keyboard command according to the desired operation. It is also possible to write a script, *i.e.* the sequence of Forth Words to be carried out is contained in a text file which is downloaded to the microcontroller using the terminal emulator. The Forth interpreter on the microcontroller acts on this as if the commands were entered directly on the keyboard.

This flexible and interactive approach is not directly possible with a microcontroller progammed in C/C++ and not intended with the Arduino IDE as this has been designed for programming embedded devices. However, several approaches to tie Arduinos to PCs for control of attached electronic hardware have been reported. Koenka [49], Desai [50], Pratt [51] and Steinsberger [14] have described the use of the open source language Python running on a PC to interact with Arduinos. In each of these cases a dedicated slave program written in C/C++ was installed on the microcontroller using the Arduino IDE. This firmware on the Arduino waits for commands sent from the PC, carries out the command and then returns to the listening status. The commercial software packages LabVIEW [52] and MATLAB [53] similarly can be extended to tie in Arduinos and other microcontroller platforms by making use of special communication firmware on the microcontrollers. These approaches may be the shortest paths to working systems if the user is already fluent in the language employed on the PC and in dependance on its nature, this software might allow a degree of

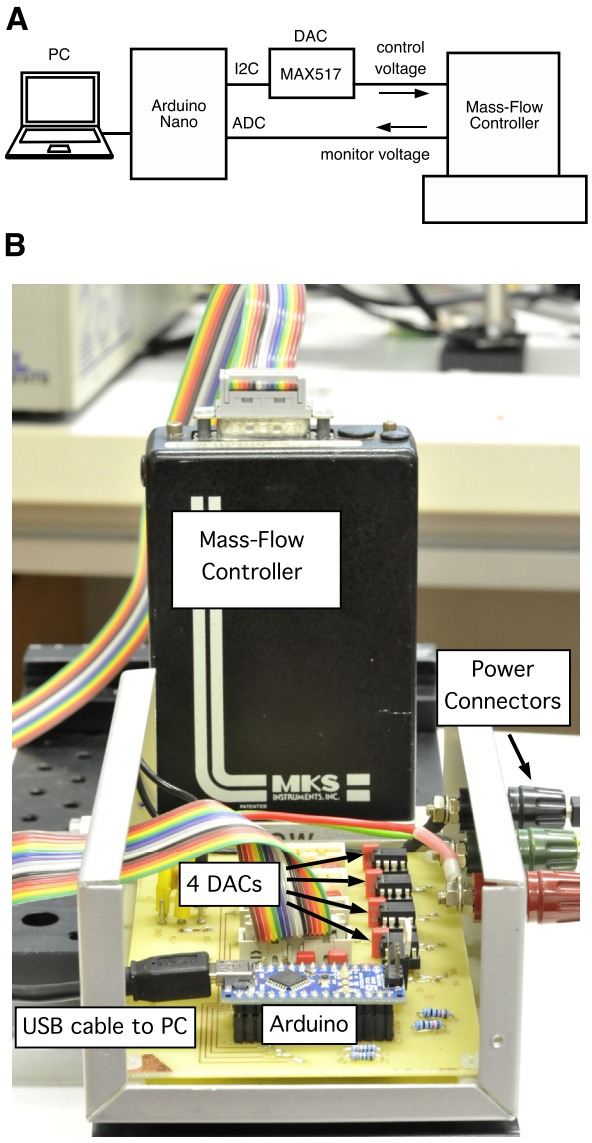

Fig. 5. A) Simplified circuit diagram for the connection of analog mass-flow controllers for gases (only one out of 4 possible channels is shown). B) Photograph of the set-up with a single mass-flow controller.

interactivity. However, in comparison to the direct use of Forth on the microcontroller this is a rather convoluted approach and there are limitations. A slave program in C/C++ running on a microcontroller can only carry out operations which have been predefined. In particular, we found the Firmata package [54] employed by Desai [50], and, to our knowledge, for tying the Arduinos to MATLAB [53], to be limited. In Forth, the interpreter automatically listens to incoming commands and the entire vocabulary of Forth Words is always available by default. If the C/C++ firmware provided is not adequate for a task at hand then this has to be first extended by the user. In this case two separate software environments (Python, LabVIEW or MATLAB, as well as C/C++) have to be mastered. Furthermore, the development of the C/C++ routine would be more complicated than writing Forth on the microcontroller as interactive testing of the code is then not possible.

4. Analog mass flow controllers

A common application in our laboratory is the setting of mass-flow controllers for adjustment of flow rates of gases. These mass-flow controllers require an analog control voltage and the traditional approach is to use for each gas stream a separate potentiometer with a multiturn dial to manually set the voltage and a panel meter to monitor the actual flow rate. Note, that other types of mass-flow controllers are also available which are interfaced digitally. The circuitry employed for up to four analog mass-flow controllers is shown in a simplified version in Fig. 5 as well as the printed circuit board in its case. The Arduino Nano board employed as microcontroller platform can be plugged onto the main printed circuit board, which was produced in our laboratory. As the microcontroller on the Arduino Nano does not have any built-in digital-to-analog convertors (DAC), external integrated circuits (MAX517), which are connected to the Arduino via an I^2C serial bus, are used to generate the necessary analog control voltages between 0 and 5 V. The Forth Word to send the numerical value to be converted to the MAX517 is very simple (any text following a backslash is a comment):

```
: Max517    \ defining the name of the new Word
        i2c.start    \ joining the I2C bus
        44 2 * i2c.tx    \ beginning transmission to the MAX517 with the address 44
        0 i2c.tx    \ transmitting a command byte (0) required by the MAX517
        i2c.tx    \ transmitting the number for conversion
i2c.stop ;    \ stopping the transmission
```

The i2c routines (i2c.start, i2c.tx and i2c.stop) are part of the AmForth package for the Arduino. The multiplication of the I^2C device address by two (in the 3rd line) is required by the I^2C standard. The user can than simply put the number representing the voltage to be passed to the mass-flow controller on the stack and type “Max517” followed by a carriage return in order to set the gas flow rate. Note, that the code is very similar to the corresponding native C/C++ Arduino code [55], but the latter cannot be used interactively in the manner described.

Instead of working with raw voltages to set the mass-flow controllers, the code can be expanded to account for the range of the mass-flow controller and calibration for different types of gases so that the flow rate can be set directly. It is therefore possible to build up a flexible and automated system quite easily. The monitor output of the mass-flow controllers, indicating the actual flow-rate (also a voltage between 0 and 5 V), can be measured directly with the analog-to-digital convertors (ADC) contained in the microcontroller. Compared to the traditional control set-up with potentiometers and panel meters this arrangement not only is much more powerful and versatile, but is also significantly less expensive (unless, of course, a computer needs to be purchased solely for this application).

5. Purpose built capillary-electrophoresis instrument

A more complex set up, an experimental capillary electrophoresis instrument is schematically shown in Fig. 6A. It runs on a pressurized buffer container and is intended for fast analysis, which requires rapid and well reproducible hydrodynamic operations and hence computer control. It incorporates a high voltage module and several valves for controlling different injection and flushing operations. The valves are miniature rotary valves from LabSmith (www.labsmith.com), which have the additional advantages of high holding pressure, low internal volume and of needing to be powered only during the switching operation. These were designed as part of an ecosystem for microfluidic devices and are normally operated with a dedicated software from the company which is running on a PC via two special interfaces from LabSmith. The first one of these (EIB200 uProcess Interface) translates the USB signals from the PC to I^2C signals and the second one (4VM01 Valve Manifold) the I^2C signals to dedicated control signals for the valves. In order to incorporate the valves into the system of Fig. 6 these were linked to the Arduino via the I^2C port and the so-called Valve Manifold. In Fig. 6B the electronic arrangement employing an Arduino Nano running AMForth for precise timing of the different required fluid transfer operations is shown (flushing, sample transfer to the capillary inlet, partial injection of the sample plug). A fast electropherogram acquired with the system is illustrated in Fig. 6C. Note that the Forth system was only used for control of the hardware, the signal was measured with a commercial data acquisition system. The annotated Forth code developed for this instrument is available in the supporting information.

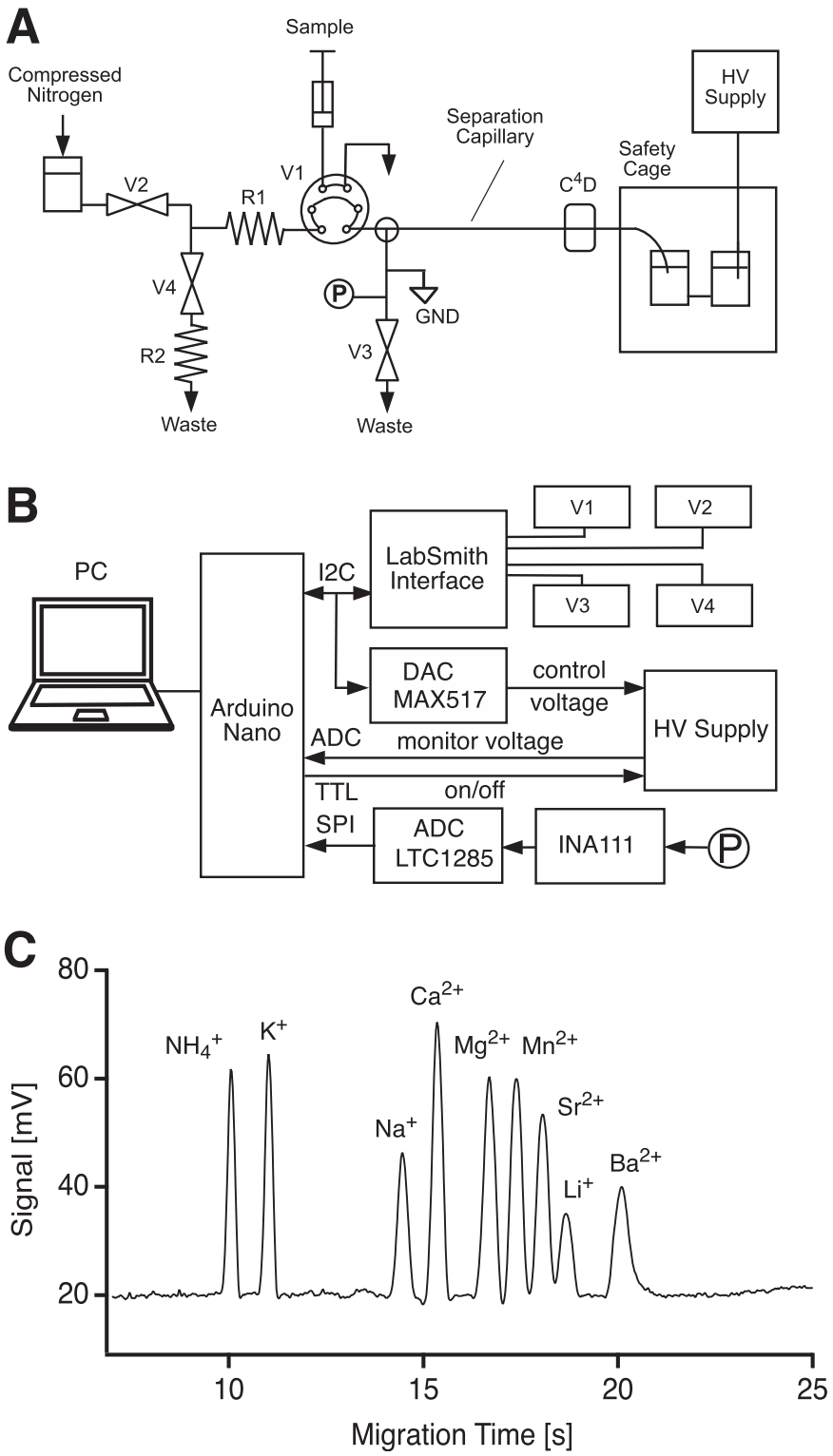

Fig. 6. A) Schematic diagram of the experimental electrophoresis system for fast separations in short capillaries. V1: rotary valve; V2-4: on/off valves, R1 and R2: flow restrictors; P: pressure sensor; C^4D contactless conductivity detector; HV: high voltage. B) Block diagram of the electronic control, not showing the power supplies. The pressure sensor (uPS, LabSmith) is connected via an instrumentation amplifier (INA111) and a 12 bit ADC (LTC1285). The analog control voltage for the high voltage supply is produced with an external DAC as not available with the microcontroller of the Arduino Nano. C) Fast separations of a standard mixture of cations.

6. Embedded assembly code

Many versions of Forth also include an assembler, *i.e.* it is possible to write individual Words written in the assembly language rather than in Forth. This may have a significant effect on the execution speed of the code as illustrated in the oscilloscope trace given in Fig. 7. Using AmForth an output pin of an Arduino Uno was first toggled high once with a Word written in Forth as fast

as it allows and then 5 times using a routine witten in assembly. The code is given below. Note that “ddrb”, “portb” and “portb-io"are constants which hold the hardware addresses of the registers associated with port b of the microcontroller on the Arduino Uno (ATmega328). “$20” and "$00” are the numbers in the hexadecimal format to be placed into the registers by executing “c!".

As can be seen, the assembly code executed significantly faster. The Forth routine required approximately 7 μs to execute while the assembler routine only required about 160 ns. Thus for highly speed sensitive operations the inclusion of assembly routines may be useful. Please note however, that some versions of Forth include special methods for optimizing compilation so that the difference may not always be as pronounced as in this example.

```
: initPB5    \ setting up pin 5 of port b
  $20 ddrb c!    \ setting pin as output
  $00 portb c!    \ setting the output pin to a logic low (off)
\ toggling in Forth
:  blink-forth
    $20 portb c! $00 portb c!  ;    \ one toggle, on and off
\ toggling in assembly code
code blink-asm    \ starting the definition of a Word in assembly
    portb-io #5 sbi,  portb-io #5 cbi,    \ one toggle, on and off
    portb-io #5 sbi,  portb-io #5 cbi,
    portb-io #5 sbi,  portb-io #5 cbi,
    portb-io #5 sbi,  portb-io #5 cbi,
    portb-io #5 sbi,  portb-io #5 cbi,
end-code
: blink-both  initPB5  blink-forth  blink-asm  ;
```

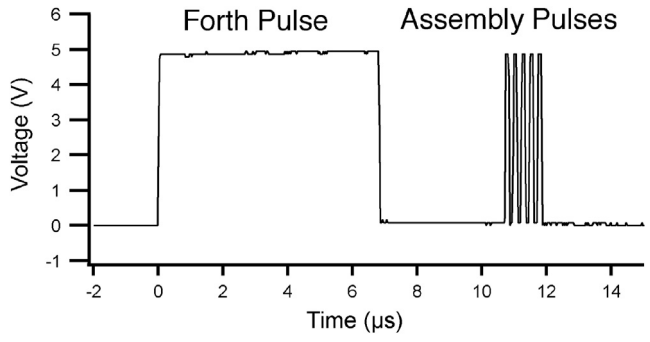

Fig. 7. Oscilloscope trace for toggling an output pin of an Arduino without delay programmed in Forth (the first pulse) and assembler (5 pulses).

7. Graphical user interface and data storage

In the laboratory it is often required to follow a measurement over time and have a graphical represention of the data. Furthermore data might need to be stored for future use. Commercial data logging systems based on hardware connected to a PC are available for this purpose and, as in the capillary electrophoresis set-up described above, the combination of such a ready made package with a Forth based microcontroller for running an experimental system is often the easiest solution. However, in order to obtain a lean arrangement one might want to utilize the microcontroller attached to the PC also for data acquisition. If a set-up is to be used for an extended time it may also be desirable to control it via a graphical user interface (GUI) on the PC, *e.g.* to facilitate its

availability to other users. These features can be obtained by employing a language on the PC which allows the programming of a GUI and communicates with the attached microcontroller as discussed above. The programming effort is then considerably larger but may be warranted by the benefits. However, the use of a Forth based microcontroller as proposed here, instead of one programmed in C/C++, has the advantage of not having to write special routines for communication to run on the controller, and therefore requires less effort. The Forth interpreter is already designed to constantly listen to incoming commands and to execute them. It is possible to develop the routines in Forth in the usual way, and then design the software running on the PC to send instructions identical to commands that would be typed directly into the serial terminal emulator program or downloaded to the microcontroller as text file. The implementation of button presses or setting of parameters via a GUI is relatively straightforward. Slightly more challenging is the handling of strings sent back by the Forth interpreter as this might not just contain numbers representing measurements but also the usual prompt (in the minimum an "OK"), codes for linefeeds etc. and the program on the PC has to handle this correctly.

An example of such a GUI application is shown in Figs. 8 and 9. An alcohol sensor is connected to an Arduino Nano which is running AmForth (Fig. 8). The sensor ("Alcohol click" from MikroElektronika, purchased from Mouser, Mansfield, TX, USA, as product No. 932-MIKROE-1586) is a tin oxide based device which changes its conductivity when exposed to alcohol vapour. The signal is converted to a variable voltage by connecting the sensor to a voltage source in series with a resistor. The GUI windows on the attached PC containing the controls to run the experiment as well as a display of a graph of the reading are shown in Fig. 9A and B. In this example a peak due to exhalation of breath alcohol is shown. The program to accomplish the interaction was written in Java, and also allows saving of the acquired data in a file whose name can be chosen by the user. The code running on the PC essentially has to carry out the following operations: 1) setting up the graphical windows on the computer display, 2) establishing the communication to the Arduino via USB, 3) sending down the Forth code to initiate readings from the sensor via the ADC built into the microcontroller (e. g. "A0 analog–read."), 4) parsing the string returned (to remove the "OK"), 5) converting the remaining character to a number, and 6) saving the readings in a file and displaying the values. To our knowledge, the tethering of a microcontroller running Forth to a master program on a PC in such a way has not been reported previously.

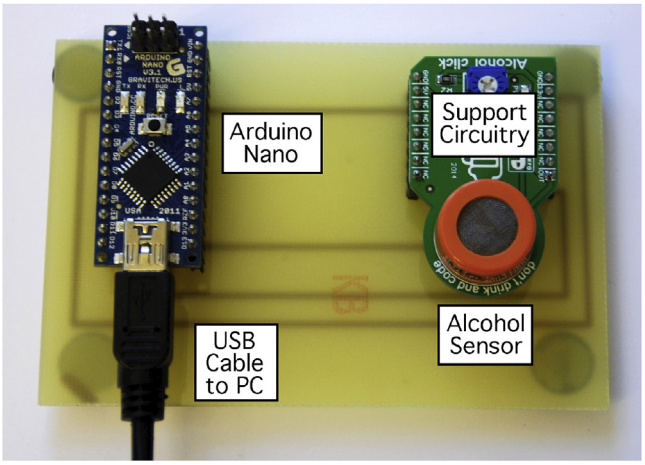

Fig. 8. An alcohol sensor placed on a printed circuit board together with an Arduino Nano for acquiring the signal to a PC.

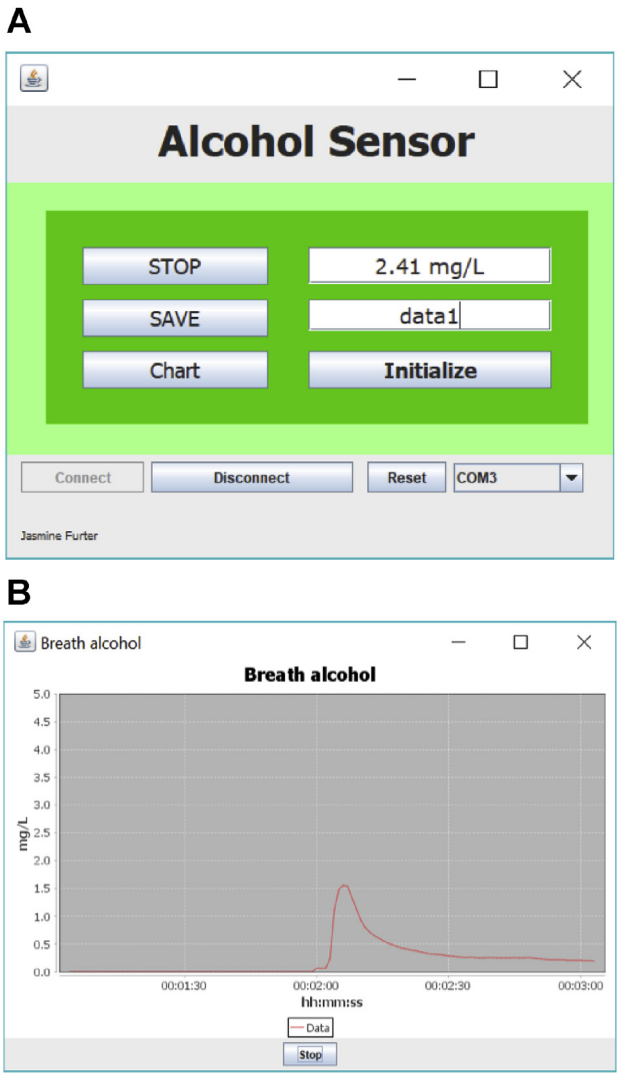

Fig. 9. A) Screenshot of the graphical user interface (GUI) with the alcohol signal displayed in mg/L, the Connect/Disconnect button to start communication with the Arduino via the USB interface, the START/STOP button for reading out values from analog port A0 of the Arduino and the SAVE/STOP button for saving data to an external. txt file using the name from the text field (data1). The Chart button opens a new window displaying the signal in a real-time chart. The Initialize button is used to send initializing Words to the Arduino establishing the analog input communication. B) Real-time chart with a breath alcohol signal measured 10 min after an intake of 10 mL of whisky (40 vol %, Cardhu, single malt Scotch whisky). Data points were collected at a time interval of 1 s (1 point/second).

The user is free to choose the programming language for the PC according to preference; a currently popular language is Python which is also well suited and it is, of course, also possible to use Forth on the computer as well. Note, that systems which are based on a master program running on a PC may also include hardware not tied to the microcontroller. Many electronic instruments are provided with drivers for different programming languages running on PCs, so that these devices may then be connected to the computer (via USB) and controlled directly by the master program rather than via the Forth running on the microcontroller. A mixed approach may be the best option for more complex tasks.

8. Conclusions

Forth deserves more attention as an enabling tool for building

microcontroller based (analytical) instrumentation. Open source initiatives on electronic hardware have made big strides to put the power of microcontrollers in the hands of researchers, and we believe Forth is a further important empowering tool. Besides the Arduinos, similar low cost microcontroller boards are available from manufacturers in the form of evaluation kits, which may even be cheaper and are perfectly suited for experimental systems. Forth further increases the utility of these electronic hardware platforms, allowing interactive applications not readily possible with the C-based programming environments that have become the de-facto standard. While the articles on the use of Forth in the analytical laboratory cited above date back a few years, the advantages and features of Forth still hold today and can now be transferred to the modern microcontroller platforms. The adoption of Forth breaks down barriers built up over the years through the increasing complexity of personal computers, not by adding, but removing, layers of abstraction. In the spirit of KISS (Keep It Simple and Straightforward) this approach can thus play an important role in the development of open laboratory hardware.

Some readers may already be familiar with programming languages such as C, C++ or Python and it may be argued that it would be better to adhere to those languages. Others, who have not programmed before, may feel that it would be a better investment of their time if they learnt one of those more popular languages. However, C and C++ as compiled languages cannot run interactively and the interpreter language Python does not generally fit into the limited memory space of microcontrollers (with the exception of MicroPython [56], which, however, requires the most powerful 32 bit controllers). While some of the concepts of Forth (the stack, the RPN notation) are somewhat unusual and perhaps some users find them difficult, the basic concepts (loops, decision constructs, masking, subroutines/functions etc.) are shared with other languages, so that the extra effort in learning Forth is limited and not much has to thrown overboard if subsequently switching to the use of an other language. Furthermore, even in the research and teaching environment productivity can be an important factor. Our research involves the building of computer controlled instruments by postgraduate students. Forth is simple and not burdened by advanced programming concepts which are not needed for our tasks. It can thus be learnt very quickly and it has been our experience that it could be easily mastered and employed productively even during short projects when there was not sufficient time to learn LabVIEW or Python. Forth thus allows researchers, who are not experts in programming, to build systems which are otherwise beyond their reach.

Appendix A. Supplementary data

Supplementary data to this article can be found online at https://doi.org/10.1016/j.aca.2018.10.071.

References

[1] https://www.arduino.cc/, 1.10.2018.
[2] J.R. Lake, K.C. Heyde, W.C. Ruder, Low-cost feedback-controlled syringe pressure pumps for microfluidics applications, PLoS One 12 (2017) e.0175089.
[3] A. Nemiroski, D.C. Christodouleas, J.W. Hennek, A.A. Kumar, E.J. Maxwell, M.T. Fernandez-Abedul, G.M. Whitesides, Universal mobile electrochemical detector designed for use in resource-limited applications, Proc. Natl. Acad. Sci. U. S. A 111 (2014) 11984–11989.
[4] A.D. Mazzeo, W.B. Kalb, L. Chan, M.G. Killian, J.F. Bloch, B.A. Mazzeo, G.M. Whitesides, Paper-based, capacitive touch pads, Adv. Mater. 24 (2012) 2850–2856.
[5] T.R. Rosa, F.S. Betim, R.D. Ferreira, Development and application of a labmade apparatus using open-source "arduino" hardware for the electrochemical pretreatment of boron-doped diamond electrodes, Electrochim. Acta 231 (2017) 185–189.
[6] P.H. Liu, P.L. Urban, Plug-volume-modulated dilution generator for flask-free chemistry, Anal. Chem. 88 (2016) 11663–11669.
[7] D.S. Silva, B.F. Reis, Evaluation of the schlieren effect employing a LED-based photometer with a long-pathlength flow cell for reagentless photometric determination of ethanol in distilled ethanolic beverages, Microchem. J. 129 (2016) 325–331.
[8] S.H. Chiu, P.L. Urban, Robotics-assisted mass spectrometry assay platform enabled by open-source electronics, Biosens. Bioelectron. 64 (2015) 260–268.
[9] C.D.M. de Morais, J.C. Carvalho, C. Sant'Anna, M. Eugenio, L.H.S. Gasparotto, K.M.G. Lima, A low-cost microcontrolled photometer with one color recognition sensor for selective detection of Pb2+ using gold nanoparticles, Anal. Methods 7 (2015) 7917–7922.
[10] T. Jarvinen, G.S. Lorite, A.R. Rautio, K.L. Juhasz, A. Kukovecz, Z. Konya, K. Kordas, G. Toth, Portable cyber-physical system for indoor and outdoor gas sensing, Sensor. Actuator. B Chem. 252 (2017) 983–990.
[11] C.L. Chen, T.R. Chen, S.H. Chiu, P.L. Urban, Dual robotic arm "production line" mass spectrometry assay guided by multiple Arduino-type microcontrollers, Sensor. Actuator. B Chem. 239 (2017) 608–616.
[12] R.N. Gillanders, I.D.W. Samuel, G.A. Turnbull, A low-cost, portable optical explosive-vapour sensor, Sensor. Actuator. B Chem. 245 (2017) 334–340.
[13] S. Kanaparthi, S. Badhulika, Low cost, flexible and biodegradable touch sensor fabricated by solvent-free processing of graphite on cellulose paper, Sensor. Actuator. B Chem. 242 (2017) 857–864.
[14] T. Steinsberger, P. Kathriner, P. Meier, A. Mistretta, P.C. Hauser, B. Müller, A portable low cost coulometric micro-titrator for the determination of alkalinity in lake and sediment porewaters, Sensor. Actuator. B Chem. 255 (2018) 3558–3563.
[15] D.A. Bui, P.C. Hauser, A deep-UV light-emitting diode-based absorption detector for benzene, toluene, ethylbenzene, and the xylene compounds, Sensor. Actuator. B Chem. 235 (2016) 622–626.
[16] I.J. Koenka, N. Küng, P. Kubáň, T. Chwalek, G. Furrer, B. Wehrli, B. Müller, P.C. Hauser, Thermostatted dual-channel portable capillary electrophoresis instrument, Electrophoresis 37 (2016) 2368–2375.
[17] T.D. Mai, M.D. Le, J. Sáiz, H.A. Duong, I.J. Koenka, H.V. Pham, P.C. Hauser, Triple-channel portable capillary electrophoresis instrument with individual background electrolytes for the concurrent separations of anionic and cationic species, Anal. Chim. Acta 911 (2016) 121–128.
[18] J. Sáiz, I.J. Koenka, C. García-Ruiz, B. Müller, T. Chwalek, P.C. Hauser, Micro-injector for capillary electrophoresis, Electrophoresis 36 (2015) 1941–1944.
[19] H.H. See, P. Hauser, Automated electric-field-driven membrane extraction system coupled to liquid chromatography-mass spectrometry, Anal. Chem. 86 (2014) 8665–8670.
[20] T.D. Mai, T.T.T. Pham, H.V. Pham, J. Sáiz, C. Garcia Ruiz, P.C. Hauser, Portable capillary electrophoresis instrument with automated injector and contactless conductivity detection, Anal. Chem. 85 (2013) 2333–2339.
[21] P.L. Urban, Universal electronics for miniature and automated chemical assays, Analyst 140 (2015) 963–975.
[22] M.D.M. Dryden, A.R. Wheeler, DStat: a versatile, open-source potentiostat for electroanalysis and integration, PLoS ONE 10 (2015) 17.
[23] C.H. Moore, E.D. Rather, The FORTH program for spectral line obersvering, Proc. IEEE 61 (1973) 1346–1349.
[24] C.H. Moore, Forth, A new way to program a mini-computer, Astron. AstroPhys. Suppl. 15 (1974) 497–511.
[25] E.D. Rather, D.R. Colburn, C.H. Moore, in: T. J. j. Bergin, R. G. j. Gibson (Eds.), History of Programming Languages II, ACM Press, New York, 1996, pp. 625–670.
[26] J.V. Petersen, Languages for the laboratory: Part II, Anal. Chem. 55 (1983) 756A–766A.
[27] D.P. Zollinger, M. Bos, FORTH - a good programming environment for laboratory automation? 1. Introduction to the language, Trends Anal. Chem. 4 (1985) 60–61.
[28] D.P. Zollinger, M. Bos, FORTH - a good programming environment for laboratory automation? 2. An example from the laboratory, Trends Anal. Chem. 4 (1985) 112–114.
[29] F.T.M. Dohmen, P.C. Thijssen, FORTH - a programming environment for online instrumentation. 1. UV-vis spectrophotometer, Trends Anal. Chem. 4 (1985) 167–169.
[30] P.C. Thijssen, F.T.M. Dohmen, FORTH - a programming environment for online instrumentation. 2. Floating point matrix package, Trends Anal. Chem. 4 (1985) 218–219.
[31] F.T.M. Dohmen, P.C. Thijssen, A forth package for computer-controlled flow-injection analysis, Talanta 33 (1986) 107–110.
[32] T.J. Cardwell, R.W. Cattrall, P.C. Hauser, I.C. Hamilton, A multi-ion sensor cell and data-acquisition system for flow injection analysis, Anal. Chim. Acta 214 (1988) 359–366.
[33] P.C. Hauser, S.S. Tan, T.J. Cardwell, R.W. Cattrall, I.C. Hamilton, Versatile manifold for the simultaneous determination of ions in flow injection analysis, Analyst 113 (1988) 1551–1555.
[34] P.C. Hauser, T.J. Cardwell, R.W. Cattrall, S.S. Tan, Measurement of pH by flow injection over a wide dynamic range with PVC/neutral Carrier electrodes, Anal. Chim. Acta 221 (1989) 139–146.
[35] K.L. Ratzlaff, ASYST-2.1, J. Chem. Inf. Comput. Sci. 29 (1989) 128–129.
[36] www.forth.com, 1.10.2018.
[37] www.mpeforth.com, 1.10.2018.
[38] https://web.archive.org/web/20101024223709/http://forth.gsfc.nasa.gov/, 1.10.2018..

[39] H. Malcom, H.K. Utterback, Flight software in the space department: a look at the past and a view toward the future, Johns Hopkins APL Tech. Dig. 20 (1999) 522–532.
[40] http://www.mpeforth.com/wp/wp-content/uploads/2015/12/MPE_PR_From_Telescope_to_Comet_2014_11_13.pdf, 1.10.2018..
[41] D. Pountain, Object-oriented Forth, Implementation of Data Structures, Academic Press, London, 1987.
[42] http://www.exemark.com/FORTH/StartingFORTHfromForthWebsitev9_2013_12_24.pdf, 1.10.2018..
[43] https://skilldrick.github.io/easyforth/, 1.10.2018.
[44] https://brendanator.github.io/jsForth/, 1.10.2018.
[45] https://www.gnu.org/software/gforth/gforth.html, 1.10.2018..
[46] http://powermops.org/, 1.10.2018.
[47] E. Williams, Make: AVR Programming, Maker Media, Sebastopol, 2014.
[48] https://hackaday.com/2017/01/27/forth-the-hackers-language/, 1.10.2018..
[49] I.J. Koenka, J. Sáiz, P.C. Hauser, Instrumentino: an open-source modular Python framework for controlling Arduino based experimental instruments, Comput. Phys. Commun. 185 (2014) 2724–2729.
[50] P. Desai, Python Programming for Arduino, Packt, Birmingham, 2015.
[51] A. Pratt, Python 3, Programming and GUIs, Elektor, London, 2017.
[52] https://www.labviewmakerhub.com/, 1.10.2018.
[53] https://ch.mathworks.com/hardware-support/arduino-matlab.html?s_tid=srchtitle, 1.10.2018..
[54] https://github.com/firmata/arduino, 1.10.2018..
[55] https://www.chemie.unibas.ch/~hauser/open-source-lab/Arduino-DAC/Arduino-DAC.html, 1.10.2018..
[56] http://micropython.org/, 30.10.2018.

Jasmine S. Furter carried out her undergraduate studies at the University of Basel and obtained her MSc in 2017. She is currently carrying out her PhD studies on analytical instrumentation. Her main field of research is the development of new methods for capillary electrophoresis with contactless conductivity detection and mass spectrometry using microfluidics for the miniaturization of experimental setups. She very much enjoys the multidisciplinary nature of her projects.

Peter C. Hauser carried out his undergraduate studies in Switzerland and then obtained an MSc at the University of British Columbia (UBC) under Prof. M. W. Blades (1985), followed by a PhD at LaTrobe University (Melbourne, Australia) under Prof. R. W. Cattrall (1988). Following a lectureship at Auckland University (New Zealand) in 1996 he took up his current position as Associate Professor at the University of Basel. His research interests in the analytical sciences have always included electronic aspects and he has been designing electronic analytical devices since the 1980s.

4.4 MODULAR INSTRUMENTATION FOR CAPILLARY ELECTROPHORESIS WITH LASER INDUCED FLUORESCENCE DETECTION USING PLUG-AND-PLAY MICROFLUIDIC, ELECTROPHORETIC AND OPTIC MODULES

Commercial CE equipment is often not accessible in academia due to limited financial means. In-house built CE instruments on the other hand offer an affordable alternative enabling to develop portable CE versions for on-site measurements and more flexible set-ups regarding different CE configurations. Laser induced fluorescence (LIF) is a very attractive detection method as it offers highly sensitive and selective results but its use is hindered by high purchase costs. Affordable purpose-build fluorescent detectors are now available but require special equipment such as 3D printers [114–116]. The wider establishment of such purpose made devices is therefore hindered due to the implementation of customized parts prepared by workshop facilities of universities and require in addition mechanical and electronic skills of the researchers.

Within this project a CE-LIF instrument was developed, which is low-cost and requires no mechanical or electronic skills of the analyst. Rather, a Lego toy based concept offers a simple approach for building analytical platforms with a high degree of standardization. Different optical, electronic and microfluidic modules containing commercially available parts can easily be plugged together. My contribution to this project was building a laser induced fluorescence detector. The excitation light at 488 nm was focused on an optical fibre by using optical lenses. The optical window of the separation capillary was positioned in a cross. The excitation light was coupled to the capillary and the fluorescent light picked up in a right angle by using optical fibres. The light was then passed through an optical band-pass filter to cut off the remaining excitation light. Subsequently, the light was converted to an electric current by implementing a photomultiplier tube. A transimpedance amplifier enabled the conversion of the current into a voltage signal, which could then be recorded by using a data acquisition system connected to a computer. The performance of the system was evaluated by separating gluocose-oligosaccharides labelled with APTS (8-aminopyrene-1,3,6-trisulfonic acid). Oligosaccharide ladders are important as reference for the quality control of therapeutic glycoproteins [117, 118]. A new background electrolyte was developed enabling stacking of the labelled analytes. The best buffer capacity was obtained by using zwitterionic beta-alanine/MES electrolyte. Detection limits of the Lego detector were compared to a commercial LIF detector resulting in obtained values of 14 nM compared to 1.2 nM of the commercial one. At the same time the overall costs of the CE-LIF could be reduced to around 30 % of a commercial set-up with the fluorescence detector available for around 5000 Euros.

4TH PROJECT:

Modular instrumentation for capillary electrophoresis with laser induced fluorescence detection using plug-and-play microfluidic, electrophoretic and optic modules

ACA, 2020, 1135, 47-54

Analytica Chimica Acta 1135 (2020) 47–54

Contents lists available at ScienceDirect

Analytica Chimica Acta

journal homepage: www.elsevier.com/locate/aca

Modular instrumentation for capillary electrophoresis with laser induced fluorescence detection using plug-and-play microfluidic, electrophoretic and optic modules

Théo Liénard–Mayor [a], Jasmine S. Furter [b], Myriam Taverna [a, c], Hung Viet Pham [d], Peter C. Hauser [b, **], Thanh Duc Mai [a, *]

[a] Université Paris-Saclay, CNRS, Institut Galien Paris-Saclay, 92296, Châtenay-Malabry, France
[b] University of Basel, Department of Chemistry, Klingelbergstrasse 80, 4056, Basel, Switzerland
[c] Institut Universitaire de France (IUF), France
[d] VNU Key Laboratory of Analytical Technology for Environmental Quality and Food Safety Control (KLATEFOS), VNU University of Science, Vietnam National University, Hanoi (VNU), Nguyen Trai Street 334, Hanoi, Viet Nam

HIGHLIGHTS

- A novel instrumental design inspired by the Lego-toy concept was developed.
- A Lego-CE instrument was constructed from off-the-shelf microfluidic and electrophoretic components.
- A Lego-LIF detector was developed from a USB-powered laser source, ready-to-use microfluidic and optic parts.
- A new background electrolyte was developed for improvement of CE-LIF performance.
- Different modes of pressure-assisted electrophoresis was demonstrated with the Lego-CE-LIF system.

GRAPHICAL ABSTRACT

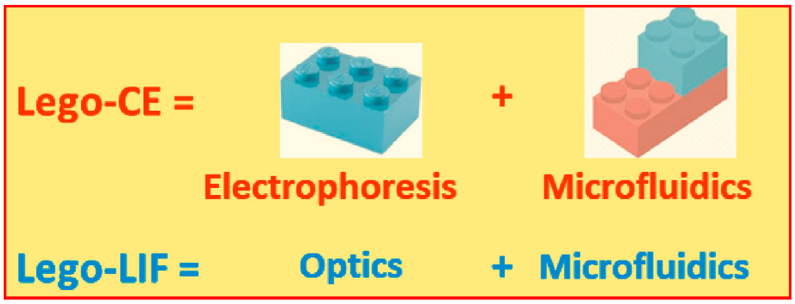

ARTICLE INFO

Article history:
Received 22 June 2020
Received in revised form
7 August 2020
Accepted 14 August 2020
Available online 25 August 2020

Keywords:
Lego instrumentation
Capillary electrophoresis
Microfluidics

ABSTRACT

This study reports on the development of a novel instrument for capillary electrophoresis (CE) coupled with laser induced fluorescence (LIF) detection that is inspired by the Lego-toy concept. The Lego CE-LIF design is an evolution of purpose-made CE instrumentation, allowing the users to construct their own analytical device with a high degree of standardization (*i.e.* a "standard" setup) without requirement of mechanical and electronic workshop facilities. To allow instrument reproduction outside the original fabrication laboratory, which is not trivial for in-house-built CE systems, the new design is based on unprecedent 'plugging' hyphenation of various off-the-shelf parts available for microfluidics, optics and electrophoresis. To render the operation with Lego CE-LIF optimal, we developed a new background electrolyte (BGE), using for the first time extremely high concentrations of zwitterionic and large weakly charged species for much improvement of detection sensitivity. The Lego CE-LIF was demonstrated for separation and detection of oligosaccharides labelled with 8-aminopyrene-1,3,6-trisulfonic acid (APTS).

* Corresponding author.
** Corresponding author.
E-mail addresses: peter.hauser@unibas.ch (P.C. Hauser), thanh-duc.mai@u-psud.fr (T.D. Mai).

https://doi.org/10.1016/j.aca.2020.08.025

LIF detection
Oligosaccharides

The new gel-free BGE for oligosaccharide analysis also allowed simplification of the conventional CE-LIF protocol used with commercial instruments while keeping satisfactory separation performances. Furthermore, the new BGE is fully compatible with a non-thermostatted Lego CE instrument thanks to low current and therefore low heat generation under application of a high voltage.

1. Introduction

After almost 40 years of development and instrument commercialization, capillary electrophoresis (CE) is now among established analytical techniques and becomes the method of choice for several classes of analytes, notably DNA, glycans, therapeutic proteins, chiral molecules, and inorganic ions [1]. The majority of the works on CE have been carried out using bench-top commercial instruments. While such systems offer robustness with a high degree of automation and standardization, their high prices render them often not accessible to researchers in academia, especially to laboratories with limited budget and modest infrastructure. In this context, in-house built CE instrumentation has appeared as an affordable alternative to satisfy the urgent need for inexpensive and simple analytical devices for versatile applications. Indeed, such purpose-made instruments are not only much less expensive than commercial systems but can also be constructed as portable versions [2–4] or with flexible configurations adapted to different needs [5]. Over 10 years, our groups have demonstrated the use of purpose-made CE devices for various analytical screening applications, notably quality control of antibiotics [6,7], environmental monitoring [8–10], food control [11,12], forensics [13] and clinical analyses [14]. With the aim to open further the access to CE instrumentation, Kuban et al. have recently presented a review detailing all steps required to construct an open-source CE system [15]. This is indeed part of the action plan of the European network promoting portable, affordable and simple analytical platforms [16]. Nevertheless, a mechanical and electronic workshop, even modestly equipped, is often required for construction of purpose-made and open-source CE systems. Exception can be found only for the simplest CE setup with syphoning injection in which an operator only needs a ready-to-use high voltage (HV) module, one capillary and different small vials to carry out electrophoretic separations. Nevertheless, this mode of injection which is the least reproducible, together with manual capillary flushing with a plastic syringe is not fully appreciated by users due to a high risk of contamination during operation and from the air [6]. Construction of more elaborated versions avoiding the syphoning injection normally require some electronic and mechanical skills that are not always available in analytical laboratories with routine operations. This hinders the wider adoption of in-house built CE instrumentation.

With the goal to drastically improve the CE popularity as a simple and affordable approach to the population, we present herein a Lego CE concept to facilitate technology/methodology transfer between different laboratories and eliminate the workshop facility requirement. This design is inspired by the Lego toy concept, in which the users with no mechanical and electronic competences can easily assemble a CE system from different commercially available ready-to-use electrophoretic and microfluidic modules. This new CE instrument was coupled with a laser induced fluorescence (LIF) detector that was also constructed with the Lego design, using off-the-shelf optical, electronic and microfluidic parts. The performance of Lego CE-LIF was evaluated in terms of injection reproducibility and detection sensitivity. A demonstration of the Lego CE-LIF system was made with separation and detection of oligosaccharides labelled with 8-aminopyrene-1,3,6-trisulfonic acid (APTS). Such analyses are commonly carried out on commercial bench-top CE instruments using conventional buffers containing inorganic ions that may not be optimal for CE-LIF. To significantly improve the CE-LIF detection performance, a new background electrolyte (BGE) was therefore developed using for the first time zwitterionic and large weakly charged species at very high concentrations to allow excellent stacking of fluorescently labelled oligosaccharides. The new BGE for CE-LIF is inspired from low-conductivity buffers for CE coupled with capacitively coupled contactless conductivity detection (C^4D) [17,18] and electrolytes buffered with an isoelectric ampholyte for CE with indirect photometric detection [19]. Comparison was made with a conventional BGE used for this purpose to highlight the advantageous features of our new buffer for CE-LIF. This optimization was inspired by our recent work on reinvestigation of CE-LIF conditions for proteins and peptides analyses [20]. Finally, different modes of pressure-assisted electrophoresis was demonstrated with the Lego-CE-LIF instrument, using the new BGE for CE-LIF, for the optimized separations of labelled oligosaccharides.

2. Experimental

2.1. Chemicals and reagents

All chemicals for preparation of buffers were of analytical or reagent grade and purchased from Sigma-Aldrich (Lyon, France). Glucose oligosaccharides (dextran ladder) and fluorescent reagents (APTS and fluorescein isothiocyanate FITC) were bought from Sciex (Villebon sur Yvette, France). β-Alanine, 2-(*N*-morpholino)ethanesulfonic acid (MES), acetic acid, lithium hydroxide monohydrate, tris(hydroxymethyl)aminomethane (Tris) and 2-(Cyclohexylamino) ethanesulfonic acid (CHES) were used for preparation of background electrolyte (BGE) solutions.

2.2. Apparatus and material

Method development for establishment of new BGEs for CE-LIF was performed with a Beckman Coulter PA800+ system (Sciex Separation, Brea, CA) coupled with a LIF detector ($\lambda_{excitation}$: 488 nm, $\lambda_{emission}$: 520 nm). Instrument control was carried out using Karat 8.0 software (Sciex Separation). A standalone LED induced fluorescence (LEDIF) detector was purchased from Adelis (Zetalif, Picometrics, Toulouse, France). Data acquisition (for Zetalif or Lego LIF detector) was done with a Mini-corder ER181 data acquisition system (eDAQ Europe, Warszawa, Poland) connected to the USB-port of a personal computer. Polyimide coated fused silica capillaries of 50 μm id and 375 μm od (TSP050375, Polymicro, CM Scientific, Silsden, UK) or UV transparent coated fused silica capillaries of 50 μm id and 375 μm od (TSH050375, CM Scientific, Silsden, UK) were used for all CE experiments. Deionized water was purified using a Direct-Q3 UV purification system (Millipore, Milford, MA, USA). pH values of buffer solutions and samples were acquired with a SevenCompact pH meter (Mettler Toledo,

Schwerzenbach, Switzerland). Selection of BGE compositions and buffer ionic strength (IS) calculations were based on simulations with the computer program PhoeBus (Analis, Suarlée, Belgium).

For Lego CE instrumentation, all fluid connections were made with 0.02 in. inner diameter (id) and 1/16 in. outer diameter (od) Teflon tubing from Upchurch Scientific (Oak Harbor, WA, USA). The electrophoresis module was based on a dual polarity high voltage power supply with ±30 kV maximum output (HVPS for CZE, Villa Labeco, Slovakia). The high voltage safety cage is a regular Perspex box purchased from Amazon. The microfluidic manifold is composed of different modules purchased from Fluigent (Paris, France), including an ElectroWell (or FluiWell 4C) setup and a pressure controller (Flow EZ). Capillary flushing and sample injection were done with a device to generate either vacuum (MZ 2NT, Vacuubrand, Wertheim, Germany) or compressed air (FLPG Plus, Fluigent).

For modular LIF setup, the current amplifier (DC-100kHz, AMP120), the fiber patch cables (1000 μm, M35L01 and 600 μm, M53L01), an optical breadboard (MBH4545/M), spacers (BA2S7/M), the in-line fiber optic filter mount (FOFMS/M – UV) and cover (FOFM-CV), the 488 nm notch filter (NF488-15) and the FITC emission filter (MF530-43) were purchased from ThorLabs (Maisons-Laffitte, France). The photosensor module with PMT tube (H10721-210), the fiber adapter (E5776-51) was purchased from Hamamatsu Photonics (Massy, France). A microfluidic manifold Assy 5 port (P-154, Upchurch) was used for optical cell setup. The 488 nm laser module (488L-14A, Integrated Optics) was purchased from Acal Bfi (Evry, France).

2.3. Methods

2.3.1. Preparation and storage of fluorescently labelled oligosaccharides

The preparation of fluorescently labelled glucose oligosaccharides was performed according to the protocol of Reider et al. [21]. Briefly, 2 mg of dextran ladder was added in a 200 μL PCR tube, followed by addition of 4 μL of 40 mM APTS in 20% acetic acid (AcOH), 4 μL of 20% AcOH, 2 μL of 1 M sodium cyanoborohydride (NaBH3CN) in tetrahydrofuran (THF). The mixture was incubated at 70 °C for 30 min with open vial cap. After the reaction the samples were diluted in 100 μL deionized water, aliquoted and stored at −20 °C. Further dilution of this stock solution was carried out before CE-LIF analysis.

2.3.2. CE-LIF of oligosaccharides

Analyses of APTS-labelled oligosaccharides were carried out with a BGE composed of either 858 mM β-Alanine and 822 mM MES (IS = 50 mM, pH 5.04) (BGE 1); 364 mM Beta-Alanine and 538 mM MES (IS = 25 mM, pH = 4.75) (BGE 2); or 25 mM LiOH and 47 mM acetic acid (IS = 25 mM, pH = 4.75) (BGE 3). The optimized BGE (BGE 1) was adopted for the rest of the study. CE separations with the Lego-CE-LIF system were implemented using fused-silica capillaries with ID of 50 μm, the total length of 45 cm and effective length of 23 cm under a separation voltage of −25 kV. The fused silica capillaries were preconditioned with 1 M NaOH for 5 min, water for 5 min, 1 M HCl for 5 min, water for 5 min, and the BGE 1 for 15 min prior to use. Between runs the capillary was rinsed with the BGE for 5 min.

3. Results and discussion

3.1. System design and performance

3.1.1. Lego CE

Our Lego concept is essentially an evolution of in-house-made compact CE whose first version was introduced by Hauser et al. in 1998 [22] and open-source CE introduced by Kuban et al. in 2019 [15]. The Lego CE setup is a balance between costly bench-top commercial CE instruments and low-cost in-house-built devices that are hardly reproduced from one laboratory to another. The logic behind the Lego CE concept is demonstrated in Fig. S1 in the electronic supplementary information (ESI). For construction of in-house-built and open-source CE instruments, people normally have to rely on technical drawings that are either provided by the host laboratories (for the in-house-built ones) or available on-line and free-of-charge (for the open-source ones) to reproduce the electronical, mechanical and fluidic modules. To understand and follow these technical drawings, specific knowledge and skills are normally required, which are unfortunately not always available in the majority of analytical laboratories. These challenges could on the other hand overcome with our Lego CE design with a high degree of standardization, and without recourse to any technical drawings for construction of plug-and-play modules. The Lego CE design we developed here is based on unprecedented hyphenation (specifically for CE instrumentation) of various off-the-shelf parts available for microfluidics and electrophoresis. More concretely, we used a high-accuracy miniature pressure controller setup, a high voltage generator for CE, a device for gas compression or vacuum generation and a fluidic interface dedicated to microfluidic operation to build the CE system. A simplified schematic drawing of the Lego CE system is shown in Fig. 1. Compressed air generated from an air compressor or a gas tank is driven to a stand-alone pressure controller (*i.e.* Flow EZ 1000 mbar, Fluigent) to provide precise pressure for hydrodynamic injection (generally from 30 to 100 mbar) and capillary flushing (1000 mbar). Alternatively, similar operations could be carried out from the opposite side of the capillary, using a vacuum generator and a pressure controller (*i.e.* Flow EZ -800 mbar, Fluigent) providing negative pressures for injection (−30 mbar to −100 mbar) and capillary flushing (−800 mbar). If both negative and positive pressures are desired, a Flow EZ push-pull module can be used for pressure manipulation in the range of −800 mbar to +1000 mbar. This offers setup flexibility to users. Note that any pressure in the range from 0 to 1000 mbar (or from 0 to - 800 mbar) can be set and monitored for injection or capillary flushing purposes either with physical knob and a digital screen integrated on the pressure controller or with a computer-linked control program (see Fig. S2). In addition, pressure assistance during electrophoresis, which is not trivial in in-house-made CE instruments, can also be applied to accelerate the analysis time or improve the separation resolution, as pressure can be precisely controlled and monitored during application of high voltages (see section below). In in-house made CE instruments [6,9,13,23–27], a desired pressure value sometimes can not be precisely set and monitored. Thus, optimization of hydrodynamic injection in these cases is generally done with injection time variation rather than pressure adjustment. Both optimization modes (time and pressure) are now available in our Lego CE version. Solutions to be injected in the capillary (i.e. sample, BGE or other generating solutions) can be easily changed by plugging the corresponding vial to the fluiwell or electrowell interface (Fig. S2A and B in ESI for their setup). In our case with the electrowell (Fig. S2C), a platinum electrode is already integrated in this interface so a ground connection can be made easily without any further module modification. If the fluiwell interface is used instead on the GND side, a steel tubing commonly used for HPLC can be employed for ground connection. In this case the capillary end is centered and extruded from the GND steel electrode so that they are both in contact with the working solution (Fig. 1). For high voltage generation, a commercial module containing a ±30 kV Spellman unit with an integrated digital display was employed, allowing control and monitoring of the voltage and

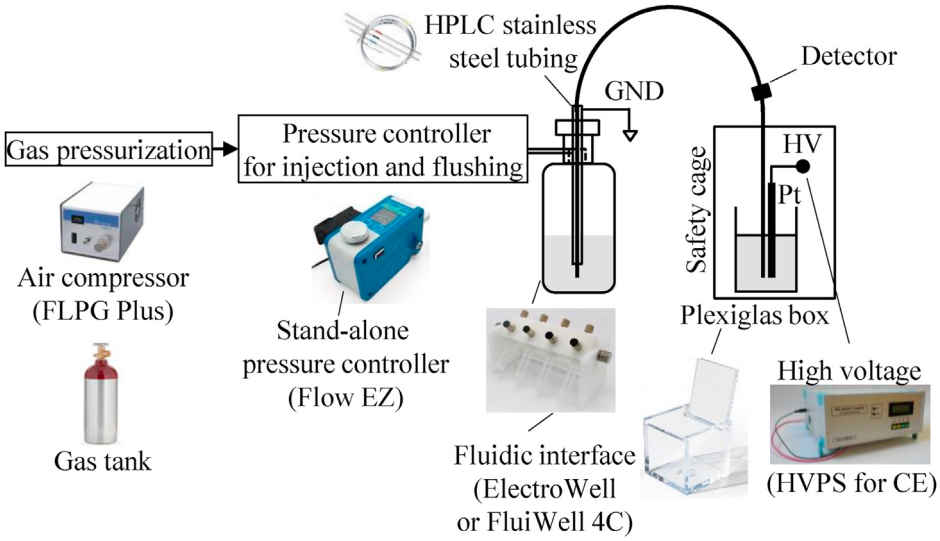

Fig. 1. Schematic drawing of Lego CE design. GND: Ground electrode.

current during electrophoresis. The high voltage side was isolated using a Perspex box for cosmetic or arrangement purposes that can be purchased online. Alternatively, any cage made from electrically isolating materials (e.g. poly (methyl methacrylate), mica, polyvinyl chloride (PVC)) could be used [28]. The total cost for construction of this Lego CE system from these off-the-shelf components is estimated to be 5000 Euros.

3.1.2. Lego LIF

The detection module is one of the most critical parts of the whole CE instrument. Among all detection types commonly employed for CE, fluorescence detection, or laser-induced fluorescence (LIF) detection in particular, is often used to improve significantly the detection sensitivity, especially for determination of biomolecules such as proteins and peptides. The popularity of fluorescence detection in CE however is often hindered (at least partially) by very high purchase costs of commercial LIF or LED-induced-fluorescence (LEDIF) detectors. Efforts to produce purpose-made fluorescence detectors adapted to modest budgets and infrastructure were already communicated [29–31], but normally require electronic and mechanical skills and workshop, with 3D-printing facilities in some cases [29,31]. For teaching purpose, Thompson et al. introduced a low-cost CE-LEDIF device for testing some fluorophore standards [32]. As part of the Lego-CE instrument, we developed a new Lego LIF detector. The Lego-LIF design exploits off-the-shelf components commonly used in microfluidics and optics in order to minimize (or eventually eliminate) the need for workshop and skills that are not always available in laboratories with routine analyses. The schematic design of Lego LIF detector is demonstrated in Fig. 2 whereas a photo of the system can be seen in Fig. S3 in ESI. A miniature LIF module from Integrated Optics, powered with a USB cable from a personal computer, was used for the first time in CE-LIF to provide the excitation wavelength of 488 nm which is most commonly used for fluorescence detection of biomolecules. The incident excitation light was set perpendicular to the optical window of the separation capillary using a black microfluidic interface. This interface plays the role of an optical cell, allowing excellent light alignment. The emission light was collected from an outlet of the interface situated perpendicular to both incident light and the capillary (Fig. 2). The emission light was then passed through an optical band-pass filter (or FITC 530 nm emission filter). A notch filter for 488 nm can be optionally added to block any residual excitation light. The filtered light was then diverted to a photomultiplier tube (photo sensor) to convert incident photons into electric current signals. These were subsequently converted into voltage signals and amplified using a *trans*-impedance amplifier, prior to analog-to-digital conversion and data acquisition into a computer. All these optical, microfluidic and electronic components are ready-to-use modules and can be plugged together using the adaptors provided by the suppliers. Users can choose different laser/LED types for the light source from various suppliers, depending on the budget available and the target applications. In our particular case where cost-effectiveness and miniaturization are the two most important criteria, a miniature USB-powered high-performing laser module was chosen. The overall cost for such Lego LIF detector was estimated to be 5000 euros, which is much cheaper (less than 25%) than the purchase cost of a commercial fluorescence detector for CE.

3.1.3. Performance evaluation

To evaluate the injection function of the new Lego CE, a series of tests were implemented with injection of a standard FITC solution at different pressures and injection times conventionally used in commercial CE systems. The reproducibility data for peak areas obtained at different injection pressures and times are shown in Table 1. Good injection reproducibility was achieved at any injection pressure and time, except for the case of 30 mbar over 5 s. The poorest reproducibility under this condition could be probably due to the too short time for pressure manipulation at a relatively low pressure range. The reproducibility for migration time was excellent (RSD % < 0.5%) under a delivery pressure of 400 mbar, proving again the added value of this system, exhibiting precise pressurization. For evaluation of detection signals, the performance of Lego LIF detector was compared to that of a commercial LEDIF detector, using the same separation capillary and CE conditions. Electropherograms for analysis of FITC at 110 nM that were obtained with both detectors are shown in Fig. 3, whereas comparison data are presented in Table 2. Very good linearity (R^2 better than 0.997) was acquired, whether the calibrations were made with peak areas or peak heights, proving a very good response of the Lego LIF to the variation of FITC concentrations. The detection sensitivity was approximately 10 times better for the commercial LEDIF (see Table 2). This can be explained by the fact that no focusing lens or special optical setups were employed for the Lego LIF as otherwise

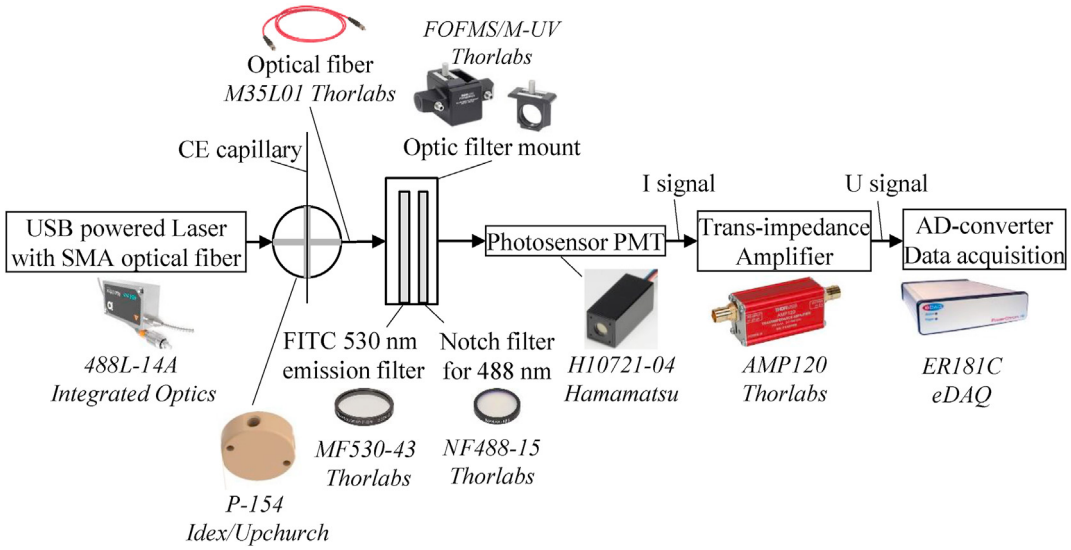

Fig. 2. Schematic drawing of Lego LIF design.

required for a costly commercial fluorescence detector. In addition, the photosensor module with PMT tube used for Lego LIF is a miniaturized and inexpensive version, which might perform less efficiently than the one used for the commercial counterpart. In the former one, no electronic filtering was included in the photomultiplier tube or *trans*-impedance amplifier module, whereas this feature was already integrated in the latter one. This explains the more noisy background for the raw signal of Lego LIF (see Fig. 3A), which was not the case for the commercial detector (no signal difference between Fig. 3C and D). The lack of electronic filtering in the Lego LIF was therefore compensated by digital filtering function offered by the data acquisition module, allowing significant reduction of background noise and improvement of detection sensitivity (Fig. 3B). The LOD values presented in Table 2 were achieved for the filtered signals.

3.2. Separation and detection of fluorescently labelled oligosaccharides with lego CE-LIF

Glucose-oligosaccharides are often used as the ladder reference for analyzing N-glycans released from glycoproteins, serving for quality control of therapeutic glycoproteins and diagnostic purposes [33,34]. For oligosaccharides and glycans labeling, APTS is the most frequently used fluorescent agent whereas BGEs containing inorganic ions are often used for CE-LIF separation of labelled oligosaccharides and glycans [35,36]. The electroosmotic flow (EOF) is normally suppressed so that the negatively charged APTS-tagged oligosaccharides (and glycans) can migrate against the EOF to

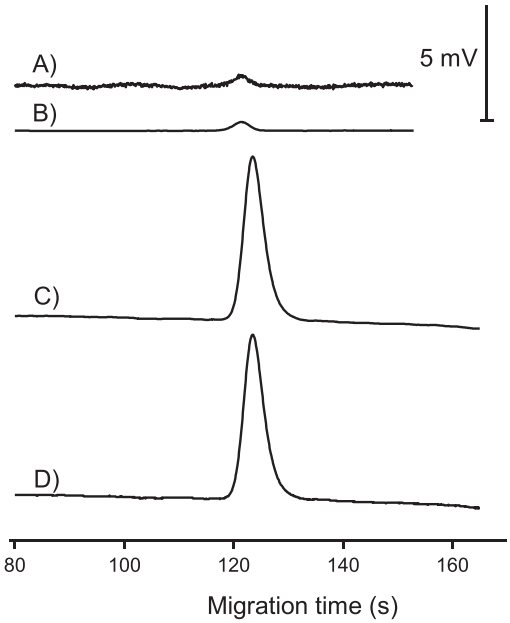

Fig. 3. Electropherograms for CE-LIF separation of FITC 1 μM using A) Lego LIF detector without digital filter; B) Lego LIF detector with digital filter; C) commercial LEDIF detector without digital filter; and D) commercial LEDIF detector with digital filter. CE conditions: BGE composed of Tris/CHES (IS of 20 mM, pH 8.4); silica capillary with L_{eff} of 25 cm and L_{tot} of 45 cm; high voltage of 25 kV with normal polarity; hydrodynamic injection at 50 mbar over 10s.

Table 1
Salient performance data for the test on injection reproducibility realized with the Lego CE system. Analyte: FITC 1 μM; delivery pressure: 400 mbar; silica capillary with l_{eff} of 35 cm and L_{tot} of 60 cm.

Injection pressure	Injection time	Peak area (mV·s) (mean value)	RSD % (n = 4) Peak area
30 mbar	5 s	0.66	10.8
	10 s	1.06	2.37
	20 s	2.03	3.00
50 mbar	05 s	0.97	1.26
	10 s	1.68	4.08
	20 s	3.10	1.51
100 mbar	5 s	1.70	5.88
	10 s	3.33	1.85
	20 s	6.13	1.49

Table 2
Data on comparison on LOD and linearity between 2 LIF detectors.

Detector	Calibration range (nM)	Linearity (R^2) with peak area	Linearity (R^2) with peak height	LOD (nM)
Lego LIF	30–1000	0.999	0.997	14
Commercial LIF (ZetaLIF)	3–1000	0.999	0.999	1.2

Analyte: FITC 1 μM. CE conditions: BGE composed of Tris/CHES (IS 20 mM, pH 8.4), silica capillary with l_{eff} of 25 cm and L_{tot} of 45 cm; high voltage of 25 kV with normal polarity; hydrodynamic injection at 50 mbar over 10s.

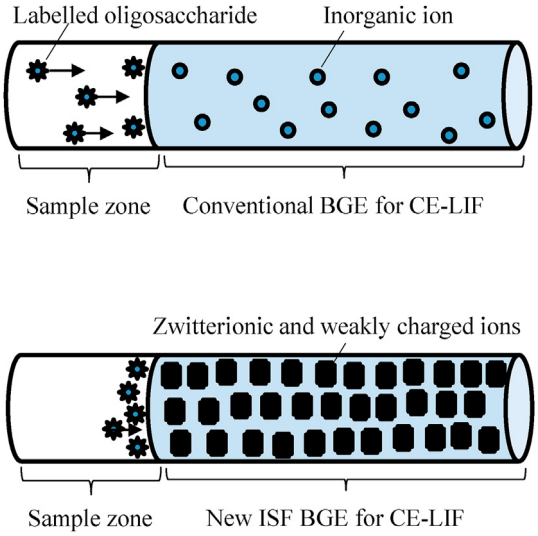

Fig. 4. Principle of our new BGE optimization strategy for CE-LIF of labelled oligosaccharides.

arrive at the LIF detector for detection. All BGE compositions reported so far for CE-LIF analysis in general, and CE-LIF for such purpose in particular contain inorganic ions (*e.g.* phosphate, borate etc.) and/or use inorganic acid and base (typically NaOH and HCl) for pH adjustment. These BGEs with low UV absorbing feature, while being well adapted to UV detection, may not be optimal for LIF detection. We have recently demonstrated that a much-improved performance for CE-LIF detection of proteins and peptides could be achieved with our new BGEs for CE-LIF thanks to a better stacking effect and lower current generation [20]. With a similar rationality, we optimized the BGE composition for CE-LIF of labelled oligosaccharides this time. The principle behind this strategy is illustrated in Fig. 4. By using a very dense zone of zwitterionic and large weakly charged ions in the BGE to block the sample zone, the target analytes will be well stacked in the sample-BGE boundary. While this stacking phenomenon can be observed using conventional BGE containing inorganic ions, this effect is expected to be pushed up to the maximum with our new BGE composition. The use of extremely high BGE concentrations, while not readily possible with inorganic ions due to high current generation, is now feasible thanks to the very low electrophoretic movement of the large and/or zwitterionic molecules constituting the BGE. Via simulation with the Phoebus program, we compared the properties of different new BGEs for CE-LIF at pH 4.75 that have never been used before for such purpose (Table 3). The lithium acetate buffer at the same pH, frequently employed by different groups for CE-LIF of oligosaccharides and glycans [35,36], was used as a reference for these comparisons. Among these new BGEs, beta-alanine/MES exhibits the best buffer capacity and was expected to provide the best stacking effect due to the highest components' concentrations (364 mM beta alanine et 538 mM MES). Another BGE composed of Naphtyl-1-amine and MES, which is thought to offer equivalent performance to that of beta-alanine/MES, is not considered due to the presence of a carcinogenic agent. Separation performance for CE-LIF of APTS-labelled oligosaccharides was thus compared between LiOH/Acetic acid and beta-alanine/MES BGEs, using first a commercial instrument (Fig. 5A and B). At IS of 25 mM, the signals of oligosaccharides obtained with beta-alanine/MES were two times higher than those obtained with LiOH/acetic acid buffer. With equivalent background noises observed, this confirms a much better LIF sensitivity with the new beta-alanine/MES BGE. The electroosmotic flow mobility was found a bit higher for beta-alanine/MES buffers, which explains the longer migration times of oligosaccharide peaks. To further improve the stacking effect, the IS of beta-alanine/MES was doubled and the electropherogram for these conditions is shown in Fig. 5C. Conveniently, with beta-alanine/MES BGE, an increase in IS from 25 to 50 mM only leads to a tolerable increase in the generated current (from 13 to 25 μA under 30 kV). The beta-alanine/MES BGE (IS 50 mM) led to much higher peak signals (almost 3 times) than the conventional LiOH/Acetic acid buffer for the first 5 peaks. For slower-migrating ones (due to the presence of a higher EOF magnitude with our new BGE), the peaks were more broadened, leading to a less performance in detection sensitivity. Compared to previously communicated CE-LIF conditions for this purpose [35,36], our new BGE offered higher signals. Noted also that low current generation (leading to low Joule heating) was achieved and no bubble formation was observed when working with our non-thermostatted system.

The Lego CE-LIF was then used with this buffer for separations of APTS-labelled oligosaccharides. The CE-LIF electropherogram obtained is shown in Fig. 6A. Excellent peak shapes and separation resolutions were achieved for glucose units GU1 till GU6. To compensate for the peak retardation when using beta-alanine/MES BGE, pressure assistance could be applied during electrophoresis, which is not a complication when using the Flow EZ pressure controller. As can be seen in Fig. 6B, the peaks arrived faster to the detector and more glucose units could be visualized under the pressure assistance at 30 mbar. The pressure-assisted electrophoresis can even be finely tuned by using a pressure gradient. By applying a pressure of 30 mbar at 0s and then 20 mbar at 5 min, the fast arrival of the first four peaks could be maintained, whereas separation resolution for the slower ones, which could correspond to the sizes of large N-glycans of glycoproteins, was improved (see Fig. 6C). Note that the unit displayed for LIF signals in Fig. 5 was RFU as the electropherograms were obtained with a LIF detector from Sciex, whereas that in Figs. 3 and 6 was in a mV scale as the signals were converted with an external data acquisition module. With this demonstration, we expect to open a door for various applications exploiting both hydrodynamic and electrokinetic principles with Lego CE-LIF. We also provide here a tool that could be tuned to get it adapted for any kind of prospective glycan analysis. Indeed by playing on voltages and pressures we would achieve the best separation performances whatever the kind of glycans to be analyzed (i.e. *N*- or O-glycans, smaller or longer ones or even a mixture of these types).

Table 3
Inorganic-species-free BGE compositions at IS of 25 mM and pH of 4.75, simulated with Phoebus program.

BGE compositions	I (μA) at 30 kV 50 μm 65 cm	buffer capacity (mmol/l.pH)	Expected quality	Remark
LiOH 25 mM + Acetic acid 47 mM	16	28	Reference	
Acetic acid 47 mM + His 26 mM	14	30		similar to LiOH/Acetic acid
Pyridine 32 mM + MES 538 mM	16	71	+	carcinogenic
TRIS 25 mM + MES 538 mM	11	59	+	
Beta-alanine 364 mM + Anisic Acid 36 mM	13	70	+	
Beta-alanine 364 mM + Sorbic Acid 48 mM	14	79	+	
Beta-alanine 358 mM + Phenylphosphonic acid 24 mM	7	53	+	
Beta-alanine 364 mM + Furoic Acid 26 mM	13	54	+	
Beta-alanine 364 mM + methanesulfonic acid 25 mM	17	53	+	
Naphtyl-1-Amine 170 mM + MES 538 mM	9	105	++	carcinogenic
Beta-alanine 364 mM + MES 538 mM	13	109	+++	

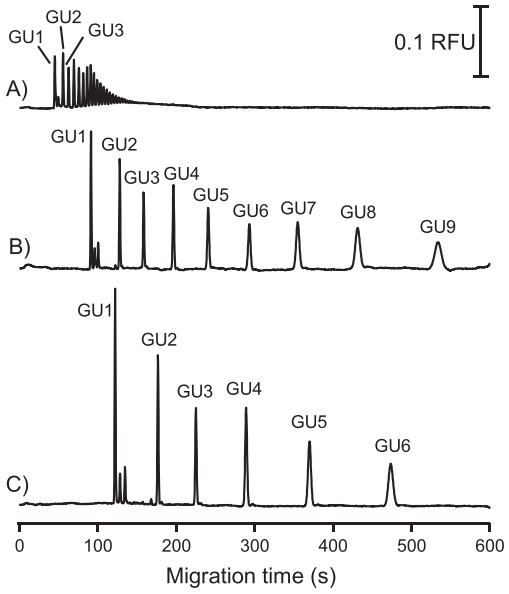

Fig. 5. Electropherograms for CE-LIF separations of oligosaccharide ladders carried out with a commercial PA800+ system, using A) conventional LiOH/Acetic acid BGE (IS 25 mM, pH 4.75); B) beta-alanine/MES BGE (IS 25 mM, pH 4.75); and C) beta-alanine/MES BGE (IS 50 mM, pH 5.04). CE conditions: HV -25 kV; capillary of 50 μm ID with total length of 30 cm and effective length of 20 cm; hydrodynamic injection at 50 mbar over 10s.

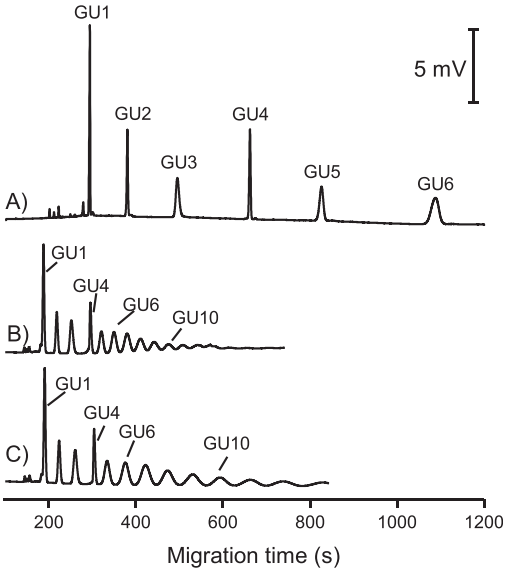

Fig. 6. Electropherograms for CE-LIF separations of oligosaccharide ladders using the Lego CE-LIF instrument. CE conditions: BGE composed of beta-alanine/MES with IS of 50 mM and pH 5.04; HV -25 kV; fused silica capillary with L_{tot} of 45 cm and L_{eff} of 23 cm; hydrodynamic injection at 50 mbar over 10s. A) Without pressure assistance; B) With pressure assistance at 30 mbar from t = 0s; C) With pressure gradient: 30 mbar at t = 0s, then 20 mbar at t = 5 min.

4. Conclusions

We successfully developed a new Lego CE-LIF instrument that can be constructed from off-the-shelf modules. Recourse to mechanical and electronic workshops can therefore be avoided. A high degree of standardization with an affordable construction cost can be achieved with this Lego CE-LIF design. The Lego design would allow the users to setup their own analytical devices at a cost at least 70% cheaper than the purchase price of a commercial system while keeping a high degree of standardization (*i.e.* a 'standard' setup) and facilitation of technology transfer that are not offered by in-house-made versions. This design was demonstrated for separation of fluorescently labelled oligosaccharides that serve as a reference for glycoprotein-derived glycan analysis. We also successfully developed a new BGE based on large weakly charged and zwitterionic molecules at very high concentrations for such analyses. This new BGE matches well to the Lego CE-LIF operation in terms of low current generation (to avoid Joule heating in a non-thermostatted system), and high stacking effect for improved LIF detection sensitivity. Various applications of Lego CE-LIF are envisaged in different domains in order to increase the popularity of such design as an interesting alternative to in-house-built hardly standardizable CE instrumentation.

CRediT authorship contribution statement

Théo Liénard–Mayor: Methodology, Validation, Investigation, Writing - original draft. **Jasmine S. Furter:** Methodology, Validation. **Myriam Taverna:** Writing - review & editing. **Hung Viet Pham:** Resources, Methodology. **Peter C. Hauser:** Resources, Supervision, Writing - review & editing. **Thanh Duc Mai:** Project administration, Funding acquisition, Supervision, Writing - original draft, Writing - review & editing.

Declaration of competing interest

The authors declare that they have no known competing financial interests or personal relationships that could have appeared to influence the work reported in this paper.

Acknowledgements

The authors are grateful for the financial support by the Agence

Nationale de la Recherche (ANR, France) with the grant no. ANR-18-CE29-0005-01. The VNU Key Laboratory of Analytical Technology for Environmental Quality and Food Safety Control (KLATEFOS) is also acknowledged for some instrumental support. We thank Dr. Thuy Tran-Maignan and Ms. Bin Yang (Institut Galien Paris Sud) for useful discussions and their help in sample preparation, as well as Mr. Jean-Jacques Vachon (Institut Galien Paris Sud) for his help in instrumental setup.

Appendix A. Supplementary data

Supplementary data to this article can be found online at https://doi.org/10.1016/j.aca.2020.08.025.

References

[1] R.L.C. Voeten, I.K. Ventouri, R. Haselberg, G.W. Somsen, Capillary electrophoresis: trends and recent advances, Anal. Chem. 90 (2018) 1464–1481.
[2] M. Zhang, S.C. Phung, P. Smejkal, R.M. Guijt, M.C. Breadmore, Recent trends in capillary and micro-chip electrophoretic instrumentation for field-analysis, Trends Environ. Anal. Chem. 18 (2018) 1–10.
[3] A.V. Schepdael, Recent advances in portable Analytical electromigration devices, Chromatography (2016) 3, https://doi.org/10.3390/chromatography3010002.
[4] A.P. Lewis, A. Cranny, N.R. Harris, N.G. Green, J.A. Wharton, R.J.K. Wood, K.R. Stokes, Review on the development of truly portable and in-situ capillary electrophoresis systems, Meas. Sci. Technol. 24 (2013).
[5] P. Paul, C. Sanger-van de Griend, E. Adams, A. Van Schepdael, Recent advances in the capillary electrophoresis analysis of antibiotics with capacitively coupled contactless conductivity detection, J. Pharmaceut. Biomed. Anal. 158 (2018) 405–415.
[6] T.A.H. Nguyen, T.N.M. Pham, T.B. Le, D.C. Le, T.T.P. Tran, T.Q.H. Nguyen, T.K.T. Nguyen, P.C. Hauser, T.D. Mai, Cost-effective capillary electrophoresis with contactless conductivity detection for quality control of beta-lactam antibiotics, J. Chromatogr. A 1605 (2019), 360356, https://doi.org/10.1016/j.chroma.2019.07.010.
[7] T.N.M. Pham, T.B. Le, D.D. Le, T.H. Ha, N.S. Nguyen, T.D. Pham, P.C. Hauser, T.A.H. Nguyen, T.D. Mai, Determination of carbapenem antibiotics using a purpose-made capillary electrophoresis instrument with contactless conductivity detection, J. Pharmaceut. Biomed. Anal. (2019) 112906.
[8] P. Kubáň, H.T.A. Nguyen, M. Macka, P.R. Haddad, P.C. Hauser, New fully portable instrument for the versatile determination of cations and anions by capillary electrophoresis with contactless conductivity detection, Electroanalysis 19 (2007) 2059–2065.
[9] M.D. Le, H.A. Duong, M.H. Nguyen, J. Saiz, H.V. Pham, T.D. Mai, Screening determination of pharmaceutical pollutants in different water matrices using dual-channel capillary electrophoresis coupled with contactless conductivity detection, Talanta 160 (2016) 512–520.
[10] H.A. Duong, M.D. Le, K.D.M. Nguyen, H.C. Peter, H.V. Pham, T.D. Mai, In-house-made capillary electrophoresis instruments coupled with contactless conductivity detection as a simple and inexpensive solution for water analysis: a case study in Vietnam, Environ. Sci. Process Impacts 17 (2015) 1941–1951.
[11] T.D. Nguyen, M.H. Nguyen, M.T. Vu, H.A. Duong, H.V. Pham, T.D. Mai, Dual-channeled capillary electrophoresis coupled with contactless conductivity detection for rapid determination of choline and taurine in energy drinks and dietary supplements, Talanta 193 (2018) 168–175.
[12] T.H.H. Le, T.Q.H. Nguyen, C.S. Tran, T.T. Vu, T.L. Nguyen, V.H. Cao, T.T. Ta, T.N.M. Pham, T.A.H. Nguyen, T.D. Mai, Screening determination of food additives using capillary electrophoresis coupled with contactless conductivity detection: a case study in Vietnam, Food Contr. 77 (2017) 281–289.
[13] T.A.H. Nguyen, T.N.M. Pham, T.T. Ta, X.T. Nguyen, T.L. Nguyen, T.H.H. Le, I.J. Koenka, J. Saiz, P.C. Hauser, T.D. Mai, Screening determination of four amphetamine-type drugs in street-grade illegal tablets and urine samples by portable capillary electrophoresis with contactless conductivity detection, Sci. Justice 55 (2015) 481–486.
[14] A.P. Vu, T.N. Nguyen, T.T. Do, T.H. Doan, T.H. Ha, T.T. Ta, H.L. Nguyen, P.C. Hauser, T.A.H. Nguyen, T.D. Mai, Clinical screening of paraquat in plasma samples using capillary electrophoresis with contactless conductivity detection: towards rapid diagnosis and therapeutic treatment of acute paraquat poisoning in Vietnam, J. Chromatogr. B 1060 (2017) 111–117.
[15] P. Kuban, F. Foret, G. Erny, Open source capillary electrophoresis, Electrophoresis 40 (2019) 65–78.
[16] E.C.i.S.a. Technology, PortASAP - European Network for the Promotion of Portable, Affordable and Simple Analytical Platform, 2019. http://portasap.eu/.
[17] T.D. Mai, P.C. Hauser, Contactless conductivity detection for electrophoretic microseparation techniques, Chem. Rec. 12 (2012) 106–113.
[18] P. Kubáň, P.C. Hauser, 20th anniversary of axial capacitively coupled contactless conductivity detection in capillary electrophoresis, TrAC Trends Anal. Chem. (Reference Ed.) 102 (2018) 311–321.
[19] C. Johns, M. Macka, P.R. Haddad, Indirect photomeric detection of anions in capillary electrophoresis using dyes as probes and electrolytes buffered with an isoelectric ampholyte, Electrophoresis 21 (2000) 1312–1319.
[20] M. Morani, M. Taverna, T.D. Mai, A fresh look into background electrolyte selection for capillary electrophoresis-laser induced fluorescence of peptides and proteins, Electrophoresis (2019), https://doi.org/10.1002/elps.201900084.
[21] B. Reider, M. Szigeti, A. Guttman, Evaporative fluorophore labeling of carbohydrates via reductive amination, Talanta 185 (2018) 365–369.
[22] T. Kappes, P.C. Hauser, Portable capillary electrophoresis instrument with potentiometric detection, Anal. Commun. 35 (1998) 325–329.
[23] T.D. Mai, M.D. Le, J. Saiz, H.A. Duong, I.J. Koenka, H.V. Pham, P.C. Hauser, Triple-channel portable capillary electrophoresis instrument with individual background electrolytes for the concurrent separations of anionic and cationic species, Anal. Chim. Acta 911 (2016) 121–128.
[24] T.T.T. Pham, T.D. Mai, T.D. Nguyen, J. Sáiz, H.V. Pham, P.C. Hauser, Automated dual capillary electrophoresis system with hydrodynamic injection for the concurrent determination of cations and anions and application to the monitoring of biological ammonium removal from contaminated ground water, Anal. Chim. Acta 841 (2014) 77–83.
[25] T.A.H. Nguyen, T.N.M. Pham, T.T. Doan, T.T. Ta, J. Sáiz, T.Q.H. Nguyen, P.C. Hauser, T.D. Mai, Simple semi-automated portable capillary electrophoresis instrument with contactless conductivity detection for the determination of beta-agonists in pharmaceutical and pig-feed samples, J. Chromatogr. A 1360 (2014) 305–311.
[26] T.D. Mai, T.T.T. Pham, J. Sáiz, P.C. Hauser, Portable capillary electrophoresis instrument with automated injector and contactless conductivity detection, Anal. Chem. 85 (2013) 2333–2339.
[27] T.D. Mai, S. Schmid, B. Müller, P.C. Hauser, Capillary electrophoresis with contactless conductivity detection coupled to a sequential injection analysis manifold for extended automated monitoring applications, Anal. Chim. Acta 665 (2010) 1–6.
[28] T.A.H. Nguyen, V.R. Nguyen, D.D. Le, T.T.B. Nguyen, V.H. Cao, T.K.D. Nguyen, J. Saiz, P.C. Hauser, T.D. Mai, Simultaneous determination of rare earth elements in ore and anti-corrosion coating samples using a portable capillary electrophoresis instrument with contactless conductivity detection, J. Chromatogr. A 1457 (2016) 151–158.
[29] L.D. Casto, K.B. Do, C.A. Baker, A miniature 3D printed LED-induced fluorescence detector for capillary electrophoresis and dual-detector taylor dispersion analysis, Anal. Chem. 91 (2019) 9451–9457.
[30] M. Ryvolova, J. Preisler, F. Foret, P.C. Hauser, P. Krasensky, B. Paull, M. Macka, Combined contactless conductometric, photometric, and fluorimetric single point detector for capillary separation methods, Anal. Chem. 82 (2010) 129–135.
[31] J. Prikryl, F. Foret, Fluorescence detector for capillary separations fabricated by 3D printing, Anal. Chem. 86 (2014) 11951–11956.
[32] J.E. Thompson, K. Shurrush, G. Anderson, An inexpensive device for capillary electrophoresis with fluorescence detection, J. Chem. Educ. 83 (2006) 1677.
[33] P. Zhang, S. Woen, T. Wang, B. Liau, S. Zhao, C. Chen, Y. Yang, Z. Song, M.R. Wormald, C. Yu, P.M. Rudd, Challenges of glycosylation analysis and control: an integrated approach to producing optimal and consistent therapeutic drugs, Drug Discov. Today 21 (2016) 740–765.
[34] M. Hu, Y. Lan, A. Lu, X. Ma, L. Zhang, Chapter One - glycan-based biomarkers for diagnosis of cancers and other diseases: past, present, and future, in: L. Zhang (Ed.) Prog. Mol. Biol. Transl. Sci., Academic Press2019, pp. 1-24..
[35] G. Lu, C.L. Crihfield, S. Gattu, L.M. Veltri, L.A. Holland, Capillary electrophoresis separations of glycans, Chem. Rev. 118 (2018) 7867–7885.
[36] L.R. Ruhaak, G. Zauner, C. Huhn, C. Bruggink, A.M. Deelder, M. Wuhrer, Glycan labeling strategies and their use in identification and quantification, Anal. Bioanal. Chem. 397 (2010) 3457–3481.

4.5 LOW-COST AUTOMATED CAPILLARY ELECTROPHORESIS INSTRUMENT ASSEMBLED FROM COMMERCIALLY AVAILABLE PARTS

In the scope of this project, an automated, flexible and low-cost CE instrument was developed. Commercial CE equipment is now commonly used in industry for routine applications. However, for research group the instruments are too rigid in the set-up and are quite expensive regarding the purchase and maintenance. Although many research groups subsequently published purpose made CE instruments for specific tasks, often customized parts are contained in the set-up complicating their duplication. The open source development, which has gained a lot of popularity in the recent years, could be a contribution for sharing knowledge. It is already known for a long time that software code is being shared free of charge [119]. More recently, the principle was applied to physical problems as open source hardware (OSH) [120]. People are encouraged to rebuild most diverse products such as machines, instruments or other physical objects. The development has now also been extended to scientific instrumentation [81, 121, 122]. But as highlighted by Bonvoisin et al. [120] it is more complex to share hardware than software, since a lot of details on the construction have to be given. On the other hand, there are many advantages of OSH as this trend offers people to rebuild cheap alternatives to commercial equipment, while allowing the user to modify parts of the instrument and customize it for a specific purpose. As a further benefit, people gain a deeper understanding on the principles of the instrument they are using and on demand parts can easily be repaired or exchanged. Kubáň et al. [123] have discussed different parts needed for the construction of CE instruments from an OSH perspective and summarised relevant publications.

Within this research project, a compact capillary electrophoresis instrument was built based on the microfluidic breadboard approach [87]. The set-up of the instrument contained a microfluidic, a pneumatic and an electric part, which were implemented in three boxed and could easily be stacked. A commercially available C^4D detector was included in the set-up. The instrument was operated from a personal laptop computer by using the graphical user interface described above. Only commercially available miniature components were used, which simplifies the duplication of the system. The complete costs were around 6500 Euro. The instrument performance was tested by separating alkaline and alkaline earth metals (Cs^+, Rb^+, K^+, Ca^{2+}, Na^+, Mg^{2+}, Sr^{2+}, Li^+, Ba^{2+}) as well as different heavy metals (Mn^{2+}, Fe^{3+}, Cd^{2+}, Pb^{2+}, Zn^{2+}, Co^{2+}, Cu^{2+}, Ni^{2+}). In addition, nine inorganic cations relevant for honey quality were chosen and quantitatively analysed in four different honey samples. Relative standard deviations were around 2.5 % with 6.8 % for iron due to precipitation. Detection limits were between 5 and 20 µM.

More details on the construction of the instrument can be found in the appendix (see Part v).

5TH PROJECT:

Low-cost automated capillary electrophoresis instrument assembled from commercially available parts

Electrophoresis, 2020, 41, 2075-2082

ISSN 0173-0835 · ELCTDN 41 (24) 2020 · Vol. 41 · No. 24 · December 2020

ELECTROPHORESIS

Electrokinetics ⋮ Fluidics ⋮ Proteomics 24 ⋮ 20

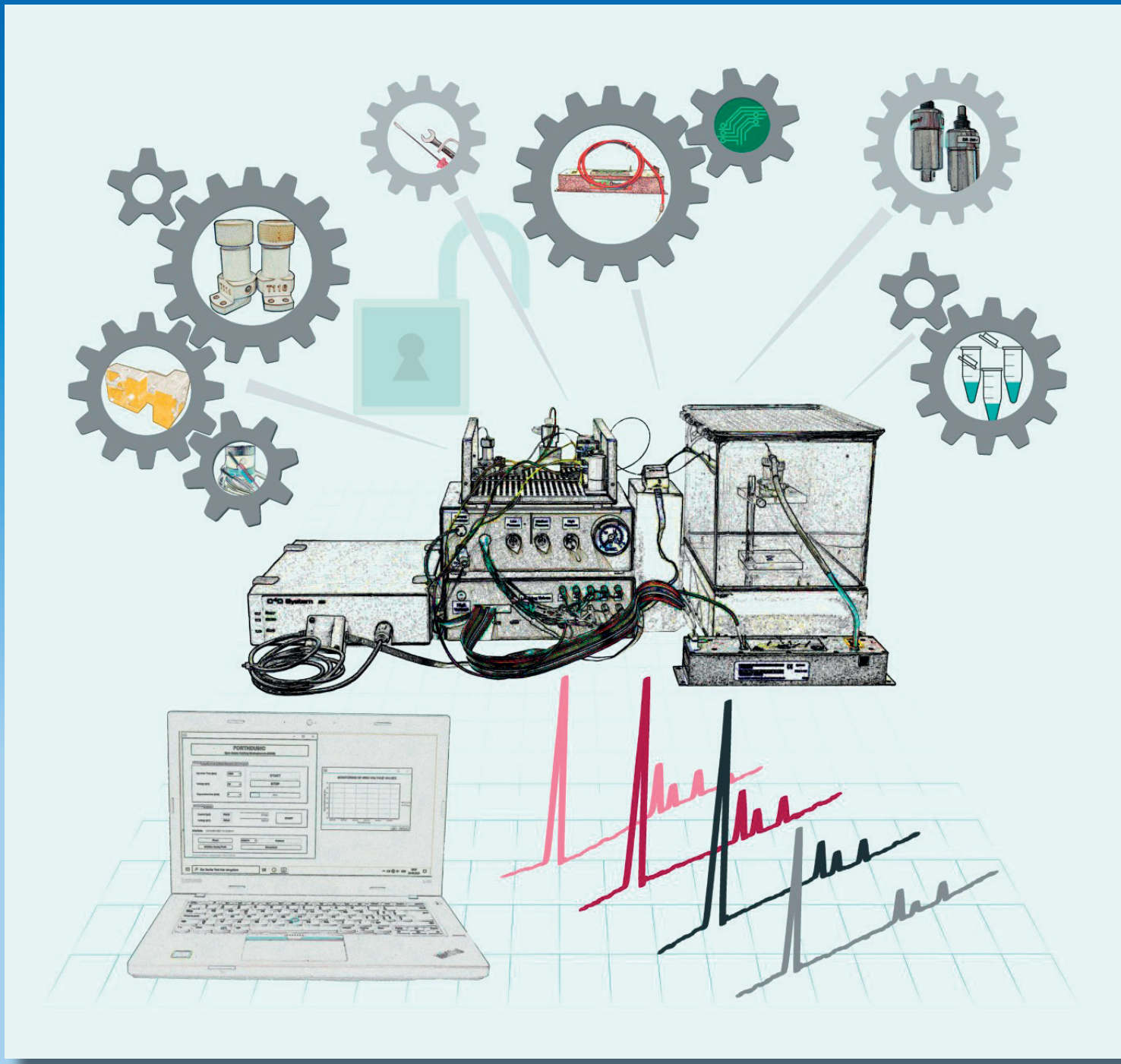

www.electrophoresis-journal.com

WILEY-VCH

Electrophoresis 2020, *41*, 2075–2082

Jasmine S. Furter
Marc-Aurèle Boillat
Peter C. Hauser

Department of Chemistry, University of Basel, Basel, Switzerland

Received July 24, 2020
Revised August 25, 2020
Accepted August 26, 2020

Research Article

Low-cost automated capillary electrophoresis instrument assembled from commercially available parts

A CE instrument that can be assembled from commercially available components with minimal construction effort is described. Except for the electronic control circuitry no specially made parts are required. It is based on a flexible design of microfluidic, electropneumatic, and electronic sections and different configurations can easily be implemented. Automated injection into the capillary is performed hydrodynamically by the application of a pressure for a controlled length of time. The performance of the device was tested with a contactless conductivity detector by separating different metal ions. In addition, nine metal cations related to the quality of honey were separated in 2.3 min and four honey samples were analysed quantitatively to demonstrate the applicability of the method.

Keywords:
Arduino / Capillary electrophoresis / Conductivity detection / Microfluidic breadboard approach / Microfluidics / Open source hardware
DOI 10.1002/elps.202000211

Additional supporting information may be found online in the Supporting Information section at the end of the article.

1 Introduction

CE is a very versatile separation technique addressing different analytical tasks ranging from high-molecular-weight proteins to small inorganic analytes [1,2]. Compared to HPLC, CE is inherently much simpler because high pressures are not required and the separation is carried out in simple capillaries. It is also more environmentally friendly because only small amounts of buffer and sample are required [3,4]. However, commercially available CE instruments are quite costly, which limits the wider adoption of the technique. Commercial instruments were also mainly developed for routine applications in the laboratory and are therefore not suited for field or process analysis and also lack the flexibility often needed in scientific research.

Since CE requires only relatively little hardware, it is particularly well suited for in-house building and several research groups have reported purpose made instruments for different purposes (see, e.g., [5–27]). Portable instruments feature prominently and the developments up to 2010 were reviewed by Macka and co-workers [28]. An important aspect of these devices is the sample injection and flushing of the capillary. The simplest approach is electrokinetic injection [7,10], but this allows quantification only if the background conductivity of sample and standards are matched. Hydrodynamic injection is therefore preferred. This may be achieved by manual syphoning (raising the inlet end of the capillary after placing it into the sample vial)[29]. While very simple such instruments can be built, manual injection procedures are highly dependent on the skill of the operator and are prone to cross-contamination. Different approaches to at least partly automate this process for purpose built instruments have therefore been described [15–19,23,24,26]. A further important aspect of the instruments is the detector, and this is easily the most complicated part. Due to its relative simplicity, universality in comparison to optical detection, and low power consumption, contactless conductivity detection (C^4D) has frequently been employed with these instruments.

The sharing of the designs of general electronic hardware and of instruments, which has become known under the designation of Open Source Hardware (OSH; https://www.oshwa.org/) [30–33], enables users to build inexpensive alternatives to commercial equipment, while allowing customization for specific purposes. As a further benefit, a deeper understanding of the working of the instruments is gained and

Correspondence: Professor Dr. Peter Hauser, Department of Chemistry, University of Basel, Klingelbergstrasse 80, 4056 Basel, Switzerland.
E-mail: peter.hauser@unibas.ch

Abbreviations: **BR**, buffer reservoir; **FIA**, flow injection analysis; **HV**, high voltage; **OSH**, open source hardware

Color online: See article online to view Figs. 1 and 5 in color.

also enables repairs, which for commercial analytical instruments is very costly and often requires a qualified service technician sent by the supplier. Kubáň et al. have discussed the construction of CE instruments and relevant publications from an OSH perspective [34]. Many research groups have indeed invested a significant effort in developing dedicated CE instruments. However, with the exception of the simple instrument with fluorescence detection reported by Anderson [8], the designs contain customized parts, which were usually manufactured by internal workshops of universities. Thus potential users who do not have access to mechanical construction facilities do not benefit.

The instrument described herein was designed to be assembled from commercially available components and can thus easily be duplicated. It is based on the microfluidic breadboard approach with different miniature components being used for the microfluidic system [35]. The setup was kept as simple and straight-forward as possible, while featuring automated sample injection and capillary flushing. Note that, to accomplish this, the construction of a small dedicated electronic interface circuitry cannot be avoided. However, this was also made simple by employing a ready made Arduino microcontroller board and driver modules available for the hydrodynamic valves. Also, for ease of construction, a commercially available C^4D was employed for detection.

2 Materials and methods

2.1 Instrumentation

The three cases (product no. 384.18) to contain the microfluidic, pneumatic, and electronic parts were obtained from Teko (Bologna, Italy). The microfluidic breadboards (LS-LS-BB600) and the fluid containers (LS-BBRES-1ML and LS-BBRES-5ML) were purchased from LabSmith (Livermore, CA, USA). Samples are contained in disposable 1.5 mL Eppendorf® tubes and a microfluidic reservoir holder (XS, Elveflow, Paris, France) is used for injection. The separation capillary with 365 μm OD and 25 μm ID (TSP-025375, Molex-Polymicro, Phoenix, AZ, USA) is inserted into a T-piece (T116-203, LabSmith) by using a tubing sleeve (U360-SLV, IDEX, Lake Forest, IL, USA) next to a grounded metal tube (U-101, IDEX). The separation voltage is provided by a high voltage module (UM30N4/S, Spellman, Pulborough, UK). The high voltage part is enclosed in a Perspex case (sold as food container; 02428MDK, Amazon, Seattle, WA, USA) equipped with a microswitch to interrupt the high voltage on opening for safety. Liquid streams are controlled by using two check valves (CV-3315, IDEX) and two 2-way, normally open, solenoid valves (HP225T021, NResearch, West Caldwell, NJ, USA). For most connections 1/16“ OD and 0.02” ID PEEK tubing (1532L, IDEX) is used. The sample loop is made out of 1/16“ OD and 0.01” ID PEEK tubing (1531L, IDEX). Optional pressure sensors for the hydraulic section (uPS0800-T116) were obtained from LabSmith. Signals are detected by using a C^4D system from eDAQ (Denistone East, NSW, Australia), consisting of a head stage (ET120-317), a C^4D data acquisition system (ER225), and the associated software (PowerChrom). Electropherograms were acquired at a sampling rate of 10 points per by second applying the following settings: 100 kHz frequency, 100% peak amplitude, and head stage gain (HG) on.

The pneumatic part is operated with compressed nitrogen from a standard gas cylinder. The pressure is first reduced with a high-pressure gas regulator followed by a two-stage piston regulator (PR2-7NX-1NH-3V, Beswick, Greenland, NH, USA), which delivers a highly stable outlet pressure even on decreasing source pressures. Read-out of delivery pressures is enabled with a pressure gauge (K8-16-40, SMC, Chiyoda, Tokio, Japan), and optionally with electronic pressure sensors (PSE530-M5-L, SMC). The remaining pneumatic parts were purchased from Clippard (Cincinnati, OH, USA). A second pressure regulator PR2 (DR-2NR-5) allows to set precisely a pressure between 0.07 and 3.4 bar. Gas pressures are applied with the help of two-way (E2L10C-7W012) and three-way latching valves (E3L10C-7W012) mounted on single-station (E10M-01) and two-station manifolds (E10M-02) and two check valves (MCV-1BB). The pneumatic connections are made using a tubing with 1/8" OD and 1/16" ID (URH1-0402), hose connectors (CT2-PKG), and T-pieces (T22-2).

For electronic control, an Arduino microcontroller board (Arduino Nano 3.0, Gravitech, Minden, NV, USA) is connected to a notebook computer. A purpose-made printed circuit board (PCB) provides the necessary electronic interface to the system. The digital-to-analog converter (MAX517) is a product from Maxim Integrated (San Jose, CA, USA). The H-bridge drivers (BD6220F-E2) to operate the latching pneumatic valves are products of Rohm (Kyoto, Japan). Two valve drivers (225D1 × 75R, NResearch, West Caldwell, NJ, USA) are required for control of the hydraulic solenoid valves. The graphical user interface (GUI) program running on a personal computer was written in Java by using the Java development kit (JDK 8.0.91) and Netbeans 8.1. The software routines running on the ATmega328 microcontroller of the Arduino were written in Forth with the open source *AmForth* interpreter (http://amforth.sourceforge.net/). The serial terminal emulator used was *CoolTerm* (http://freeware.the-meiers.org/).

2.2 Reagents and methods

All chemicals were of analytical grade and deionized ultrapure water was used for preparing solutions by using a Milli-Q system from Millipore (Bedford, MA, USA). The following salts were used for preparation of the standard solutions. Potassium chloride, lithium chloride, rubidium chloride, strontium chloride, manganese(II) chloride, iron(III) nitrate, lead(II) chloride, copper(II) chloride, and nickel(II) chloride were purchased from Merck (Zug, Switzerland). Sodium chloride, magnesium chloride, barium chloride, and cobalt(II) chloride were obtained from Fluka (Buchs, Switzerland). Cesium chloride, cadmium(II) chloride, iron(II)

chloride, and zinc(II) chloride were acquired from Sigma–Aldrich (Buchs, Switzerland). Calcium chloride was obtained from VWR (Dietikon, Switzerland). Stock solutions at 10 mM concentration of each salt were prepared and diluted on purpose to the required concentration. For the preparation of the BGEs, the following chemicals were used. L-Histidine (His), 18-crown-6, and α-hydroxyisobutyric acid (HIBA) were purchased from Sigma–Aldrich. Acetic acid (HAc) glacial was obtained from VWR and 2-morpholinoethanesulfonic acid monohydrate (MES) was purchased from Fluka. Stock solutions of 200 mM of these substances were made, except for acetic acid, which was diluted to a 1 M stock solution. The BGEs were prepared daily from these stock solutions, filtered through 0.45 μm membrane filters (4654, Pall Corporation, NY, USA), and degassed. The capillary was conditioned by flushing for 10 min with 1 M sodium hydroxide solution prepared from sodium hydroxide pellets (Thermo Fisher, Waltham, MD, USA), afterward with deionized water for 10 min and finally with the running buffer until the baseline was stable. Three brands of honey were purchased from a local supermarket (Coop, Basel, Switzerland), while one sample was received directly from a beekeeper (Kiel, Germany). The samples were dissolved in deionized water, filtered, and analyzed without further pretreatment after calibrating the CE instrument. All measurements were carried out in a thermostatted laboratory with a temperature of about 22°C.

3 Results and discussion

3.1 Instrument design

Commercial instruments typically rely on a rotary sample tray, mechanical motions to move vials and the capillary end as well as pressurization of vials with air for injection and capillary flushing. This imparts a high degree of automation, but such an instrument cannot easily be built in-house. On the other hand, as discussed in the introduction, fully manual operation is cumbersome. Electrokinetic injection would simplify the procedure, but hydrodynamic injections should be employed to avoid a sampling bias. A possible approach to avoid direct manipulation of the capillary is to place its inlet end into a commercially available T-piece, as described, for example, by Furter [36]. The sample is first transported into this device and then part of the plug is injected hydrodynamically into the capillary. The transport of liquids may be achieved by conventional pumping with syringe- or peristaltic pumps, but as the sample volumes to be injected into the capillary are in the picolitre range direct metering of the volume is not possible. The actual injection into the capillary must therefore be achieved by application of pressure, following the closure of the exit end of the T-piece. By careful control of the applied pressure and automated timing high precision can thus be attained without having to rely on the skill of the operator. Pressurization is best done with a pneumatic pressure source. This, for simplicity, may then also be employed for pumping of solutions, including the flushing of the capillary with background electrolyte (BGE). It also improves precision as stepwise movements of pumps are avoided.

Besides the fluidic part of the manifold surrounding the separation capillary such a scheme requires a pneumatic manifold as well as an electronic circuitry for controlling of valves to sequence the operations. A photograph of the instrument is shown in Fig. 1. The different functions are contained in separate cases (with dimensions of 203 × 160 × 69.5 mm), which were stacked to obtain a compact benchtop CE instrument. The capillary extends to the high voltage section, which is enclosed in a Perspex cage for safety. The detector cell sits between the injector and the high voltage compartment.

The hydraulic part of the instrument is based on the microfluidic breadboard approach [35]. The miniature fluidic components are fixed onto a commercially available breadboard. Similar to lab-on-chip devices, compact analytical systems are obtained, which allow fast separations, but the setup is much less rigid and in particular the length of the separation capillary can be easily adjusted for optimisation of the resolution. A further advantage compared to lab-on-chip devices is the improved detection possible on standard capillaries. The particular set-up used is illustrated in Fig. 2, but other configurations may also readily be implemented. Please note that, for simplicity, no temperature control was implemented. The T-piece that holds the injection end of the capillary is connected to the sample delivery manifold. The sample is inserted into the sample loop (R), located between two further T-pieces, by pressurization of the sample vial (a 1.5 mL Eppendorf tube). This is achieved with a special device that caps the vial. It has two ports, one for the sample entry via a tube extending into the vial, the other for pneumatic pressurization. The BGE is placed in container BR1. Both liquids are transported by pneumatic pressurization as detailed below. Two check valves (CV1 and CV2) avoid crosswise backflow of each liquid into the respective other container. Two active solenoid valves (V1 and V2) guide liquids to either one of the two waste containers or to the separation capillary. The required pressures, tubing diameters and lengths, as well as the timings for the different steps of the procedures, were optimized for the system by calculations based on the Hagen-Poiseuille law and the hydraulic-electric circuit analogy. Details on these procedures can be found in our previous publication [36]. Verification of the pressure profiles is possible by placing miniature hydraulic pressure sensors (available from LabSmith) at different positions in the manifold, but is not necessary for routine use. The lowest possible pressure that can be applied to the containers is 0.3 bar as the cracking pressure due to the spring tension of the check valves has to be overcome. In order to further reduce the pressure to 0.009 bar at the capillary inlet, the sample loop was implemented as a flow restrictor R. This serves to minimize partial injection into the capillary during the transport of the sample plug. For an efficient flushing of the capillary and injection of the sample, a higher pressure of around 2 bar is used resulting in around 4.3 nL/s liquid flow. The separation capillary with an internal diameter of 25 μm, an effective length of 30 cm, and a total length of 45 cm was inserted in T-piece T3. Note, that

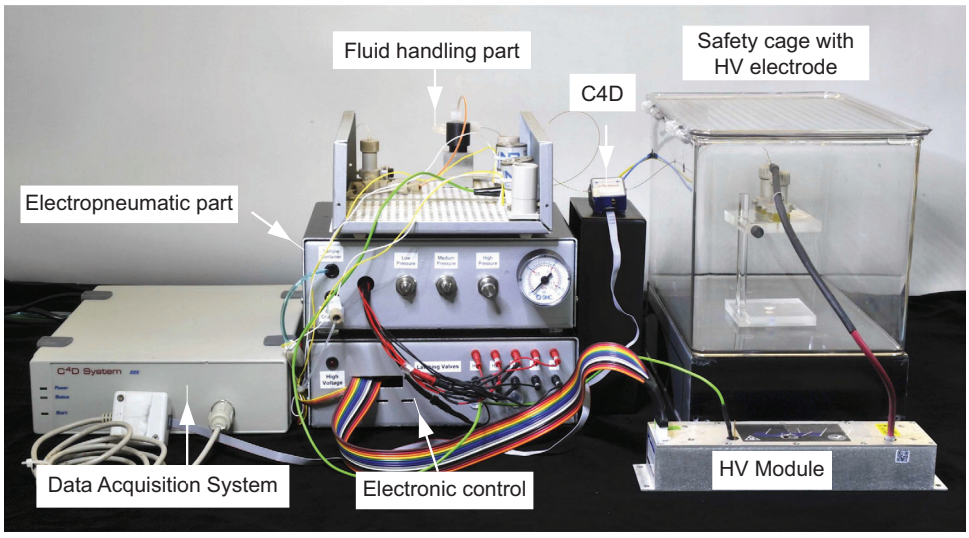

Figure 1. Photograph of the instrument.

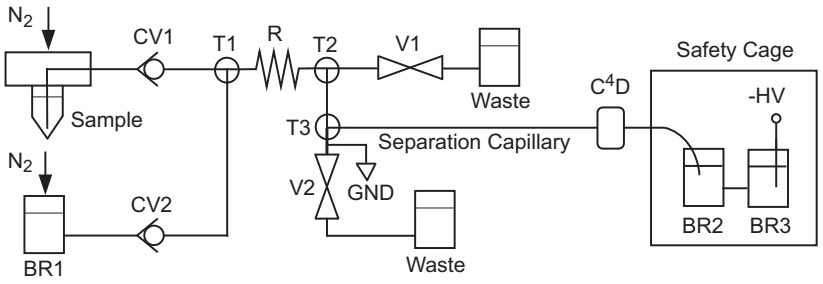

Figure 2. Microfluidic part. BR1-3: background electrolyte reservoirs; CV1 and CV2: check valves; T1-T3: T-pieces; R: flow restricting tube; V1 and V2: solenoid valves; C^4D: capacitively coupled contactless conductivity detector.

the diameter of 25 μm gives better resolution than the larger diameters employed for optical detection but is well compatible with contactless conductivity detection [37,38]. A stainless steel tube (OD: 1/16"; ID: 0.5 mm; length: 3.3 cm) next to T3 in downstream direction is connected to ground, while the high voltage is applied to the outlet end of the capillary. With this arrangement, bubbles formed by electrolysis were prevented from entering the capillary. The high voltage is applied at the detector end of the capillary to allow the placement of valves and so on. at the grounded injection end. This is not a problem with the contactless conductivity detector. The capillary outlet and the high voltage electrode (Pt-wire) are contained in two separate reservoirs joined by a short tube of 2.3 cm length and an ID of 250 μm. This forms a diffusion barrier and delays the entry of electrolysis products into the separation capillary [39].

A scheme of the electropneumatic part is shown in Fig. 3. Pressure originates from a standard compressed nitrogen gas source and is reduced to 2 bar with pressure regulator PR1 and read out with a pressure gauge (M). By using T-piece T1 the pressure pathway is split, with one tube being connected to the second pressure regulator (PR2), which further reduces the pressure to 0.3 bar. The sample container requires pressurization at 0.3 bar only, while the buffer reservoir requires pressurization at both levels depending on the step in the operation, which is achieved by actuation of one of the valves

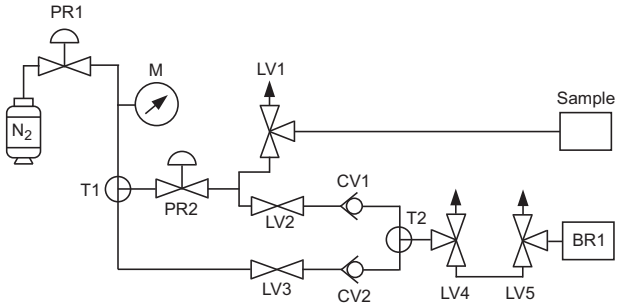

Figure 3. Electropneumatic part. N_2: nitrogen gas cylinder; PR1 and PR2: pressure regulators; M: pressure gauge; CV1 and CV2: check valves; LV1-LV5: latching valves; T4 and T5: T-pieces.

LV1 to LV3. To prevent backflow of the gas, two check valves are inserted. Valves LV4 and LV5 enable the release of pressure from the upstream manifold and the buffer container, respectively. The pneumatic pressures may also optionally be monitored by attaching electronic pressure sensors.

The electronically controlled components cannot be connected directly to the Arduino microcontroller board. In particular, the 12 V power to drive the solenoids of the valves is not available. The construction of an interface circuitry is therefore necessary. A schematic representation is shown in Fig. 4. The two hydraulic valves are connected to the Arduino

Electrophoresis 2020, *41*, 2075–2082

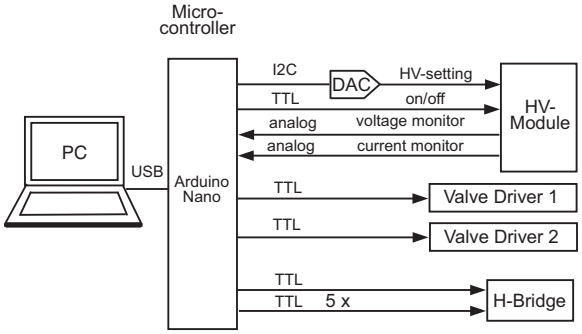

Figure 4. Electronic circuitry with the Arduino Nano to control the device. I2C = inter-integrated circuit, a serial communication bus. DAC = digital-to-analog convertor. TTL = transistor transistor logic, on/off-control signals.

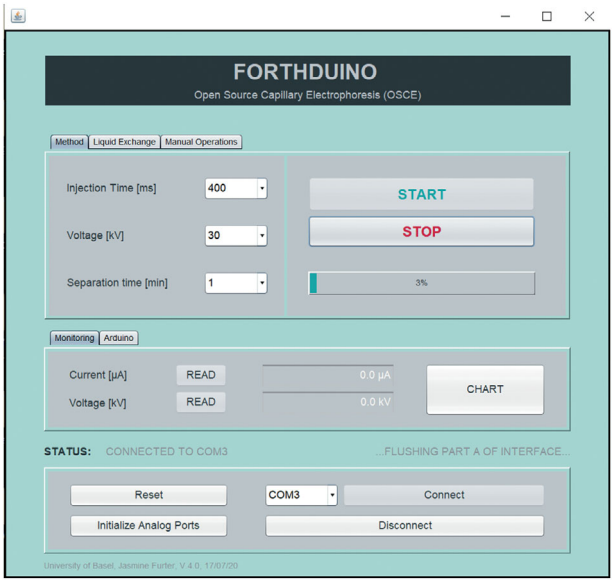

Figure 5. Screenshot of the graphical user interface (GUI) to operate the instrument. The CONNECT and DISCONNECT buttons are used to establish communication with the Arduino via USB interface. Parameters regarding separation and injection time as well as applied voltage can be chosen in the window. START/STOP buttons are used for starting or interrupting the operation cycle. The applied high voltage and the resulting current through the capillary can be monitored in the window below.

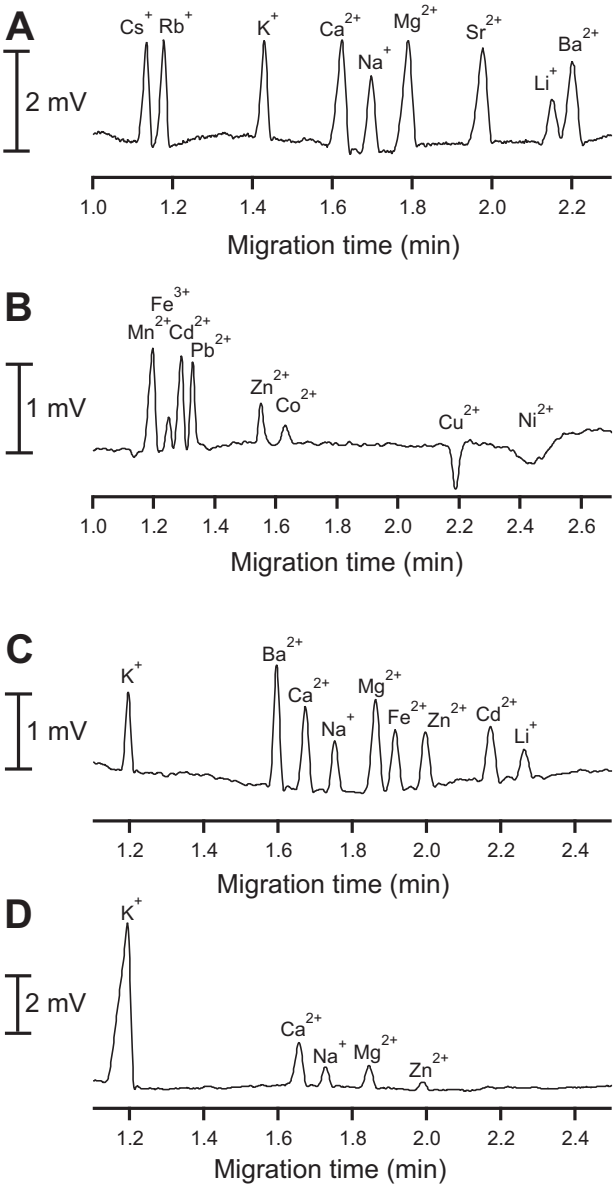

Figure 6. (A) Separation of nine alkaline and alkaline earth metals in 2.2 min. BGE: 15 mM L-His, 50 mM HAc, 4 mM 18-crown-6. (B) Separation of eight common heavy metal cations in 2.6 min: BGE: 5 mM MES/L-His, 3 mM HIBA. (C) Separation of different metals related to the quality of honey in 2.3 min. BGE: 15 mM L-His, 50 mM HAc. (D) Analysis of a honey sample with K^+ as the predominant ion, Ca^{2+}, Na^+, and Mg^{2+} in lower quantities, Zn^{2+} as trace element. Capillary: 25 µM ID, 365 µM OD, 30 cm effective length, 45 cm total length. Injection: 0.4 s at 2 bar. Measurements conducted with −30 kV applied to the capillary outlet end.

via individual valve driver circuitries provided by the valve manufacturer. The latching pneumatic valves are operated via H-bridge switches in integrated circuit form which allow reversal of the voltage, which is necessary for the switching between the two positions. The high voltage module is turned on and off with a control signal from the Arduino and the voltage is set via a digital-to-analog (DAC) convertor IC. It is a negative polarity module with a maximum output voltage of −30 kV. The particular module was chosen as it is a regulated supply (giving precise control over the output voltage) and allows the monitoring of both, the actual voltage and current at the high voltage output, via test signals given out by the module. This is deemed important, in particular current monitoring will indicate bubbles or blockage in the capillary. These signals can be acquired via the analog-to-digital convertor built into the microcontroller of the Arduino. If anions are to be determined a positive HV module at the detector end can be used.

To allow direct control of the instrument, the original Arduino software on the microcontroller was replaced with a *Forth* interpreter. This enables interactive software

development and control of the attached hardware with commands sent to the microcontroller from the attached notebook computer via a USB (universal serial bus) cable. For details on this tethered microcontroller arrangement see our previous publication [40]. In the development of the instrument, a serial terminal program was employed for text based interaction, but in its application a graphical user interface (GUI) as shown in Fig. 5 is used. The GUI was written in Java, and communicates with the *Forth* software running on the microcontroller. The user can adjust different settings such as injection time and separation voltage, and then start and also interrupt the measurement. Data acquisition is carried out separately with the software provided by the manufacturer of the detector.

3.2 Procedures

Each analysis starts by flushing of the different sections with background electrolyte. The sample loop is first flushed with 0.3 bar applied pressure by opening V1 while V2 is closed. The injection T-piece is then rinsed, again with 0.3 bar applied pressure, by closing V1 and opening V2. Subsequently, both valves V1 and V2 are closed for flushing the separation capillary with 2 bar applied pressure. The sample loop is then filled with the analyte solution by opening V1 and closing V2 while 0.3 bar is applied to the sample container by opening LV1. Subsequently the sample plug is transported to the injection T-piece using the same arrangement as for the flushing of the interface. The sample is then injected by application of a pressure pulse of 2 bar for 400 ms by closing V1 and V2, leading to a sample plug of 1.73 nL (3.52 mm length, 1.2% occupancy) in the capillary. Following another flush to remove extra sample the separation is carried out by turning on the high voltage. The content of the buffer container (1.1 mL) was found to be sufficient for about eight measurements and one complete analysis procedure takes about 80 s. A table with the operating details and diagrams detailing the pneumatic and hydraulic flow paths can be found in the Supporting Information. Note, that the capillary was conditioned by flushing with sodium hydroxide solution at the beginning of each working day followed by a rinse with water. For this the content of container BR1 was replaced with the appropriate solution, and the capillary end was temporarily removed from the high voltage container (BR2).

3.3 Performance

In Fig. 6A, the electropherogram for a standard solution containing nine alkaline and alkaline earth metals (Cs^+, Rb^+, K^+, Ca^{2+}, Na^+, Mg^{2+}, Sr^{2+}, Li^+, Ba^{2+}) at 200 μM concentration is shown where the ions were separated within 2.2 min. The BGE consisted of 15 mM L-His, 50 mM HAc (pH 4), and 4 mM 18-crown-6, which is a commonly used buffer for the separation of inorganic cations by CE-C^4D [9]. The separation of a standard solution of eight common heavy metal ions (Mn^{2+}, Fe^{3+}, Cd^{2+}, Pb^{2+}, Zn^{2+}, Co^{2+}, Cu^{2+}, Ni^{2+}) at 150 μM is shown in Fig. 6B. The BGE was optimized for best separation of these ions and consisted of 5 mM MES/L-His and 3 mM HIBA (pH 5) [41].

Subsequently, different metal ions relevant for the quality of honey were separated. The composition of the mineral content in honey is directly influenced by the geographical environment and may therefore serve as an indicator of its origin [42]. Honey analysis also allows conclusions on environmental pollution on the basis of the heavy metal content [42–48]. As predominant ion, potassium is present and in lower quantities calcium, sodium, and magnesium as well as many different trace elements [48,49].

Besides the four main mineral cations in honey (K^+, Ca^{2+}, Na^+, Mg^{2+}), five additional metals were determined (Fe^{2+}, Zn^{2+}, Ba^{2+}, Cd^{2+}, Li^+). The BGE, consisting of 15 mM L-His and 50 mM HAc (pH 4), was derived from a similar buffer described in a previous publication on the analysis of inorganic ions in honey by CE [47]. In Fig. 6C the electropherogram of the standard solution (K^+, Ba^{2+}, Ca^{2+}, Na^+, Mg^{2+}, Fe^{2+}, Zn^{2+}, Cd^{2+}, Li^+) at 100 μM concentration is shown. Calibration curves based on peak areas were acquired in the range of 100 and 500 μM, except for magnesium and iron(II), which were only separable between 100 and 250 μM. Good correlation coefficients between 0.9991 and 0.9999 were obtained. Reproducibilities for the peak areas were observed between 0.3 and 2.5% RSD for five subsequent measurements. Iron has a lower reproducibility (RSD = 6.8%) because it is slowly precipitating in aqueous solution exposed to air. For this reason, the measurements were conducted as fast as possible once dilutions were prepared. Limits of detection (LODs) were found to be between 5 and 20 μM, corresponding to 0.63 to 2.6 mg/kg in the honey samples. Note, that if lower detection limits are required this could be achieved by increasing the injected amount, but at the cost of lengthened analysis times [9,35].

After calibrating the system, four different honey samples were analysed. An example electropherogram is shown in Fig. 6D. Results from the honey analysis can be found in Table 1. In agreement to previous published results, potassium was found to be present as the most abundant cation, varying between 357 (sample 4) and 760 mg/kg (sample 3). The highest value for calcium was found in sample 1 with 80.7 mg/kg while the lowest value was found in sample 4 with 43.2 mg/kg. Concentrations for sodium were in the range between 19.3 and 34.9 mg/kg and for magnesium between 15.1 and 23.4 mg/kg. Zinc was found to be present at a low quantity in sample 1 with 56.3 mg/kg. These results are in good agreement with previous published values [44,48,49].

4 Concluding remarks

The open source instrument assembled from commercially available parts was found to allow fast separations with good reproducibility. The design files for the electronic circuitry are available as Supporting Information to this article, and may

Table 1. Inorganic cations in honey samples

Sample	K^+ (mg/kg)	Ca^{2+} (mg/kg)	Na^+ (mg/kg)	Mg^{2+} (mg/kg)	Zn^{2+} (mg/kg)
1	597 ± 25	80.7 ± 5.7	34.9 ± 1.4	23.4 ± 0.5	56.3 ± 5.6
2	685 ± 26	73.8 ± 3.8	32.7 ± 1.7	22.3 ± 1.5	–
3	760 ± 73	50.0 ± 3.0	28.8 ± 2.6	18.0 ± 1.6	–
4	357 ± 10	43.2 ± 3.9	19.3 ± 3.1	15.1 ± 1.2	–

The errors are confidence intervals at the 95% confidence level ($n = 4$).

be used to order the board from a PCB manufacturing service. It was kept simple, and while some skills in electronic construction techniques are required, completion of the circuitry is not overly demanding. On the other hand, the reader may want to make modifications, for example, to implement two channels for the concurrent determination of anions and cations [23,35], or to also more fully automate capillary conditioning with sodium hydroxide solution. A low cost, nonregulated high voltage module without monitoring outputs may be employed for cost savings. The instrument is relatively compact, and may be built in a field portable version. If best stability in baseline, peak areas, and migration times is important, or the instrument is to be used in an environment with strongly fluctuating temperatures, thermostatting may be desired. As described by Koenka et al. [23], this is also relatively easily implemented. The use of a cylinder of compressed gas may not always be convenient, and a small air pump may be employed instead. The cost of the complete instrument is approximately €6500, of which about €3500 is for the contactless conductivity detector. To save money, such a detector could also be built in-house (see, e.g., [50–55]), but this is a bit more demanding than the construction of the instrument itself. Note that do Lago has made the design of an open source C^4D available on the GitHub repository (https://github.com/claudimir-lago/openC4D).

We thank Rene Furter for his support with the Java programming and Johannes Abraham for valuable help with the latching valves.

The authors have declared no conflict of interest.

5 References

[1] Voeten, R. L. C., Ventouri, I. K., Haselberg, R., Somsen, G. W., *Anal. Chem.* 2018, *90*, 1464–1481.

[2] Weinberger, R., *Practical Capillary Electrophoresis*, Academic Press, Chappaqua 1993.

[3] Li, S. F. Y., *Capillary Electrophoresis - Principles, Practice and Applications*, Elsevier, Amsterdam 1993.

[4] Landers, J. P., *Handbook of Capillary Electrophoresis*, CRC Press, Boca Raton 1997.

[5] Kappes, T., Hauser, P. C., *Anal. Commun.* 1998, *35*, 325–329.

[6] Kappes, T., Schnierle, P., Hauser, P. C., *Anal. Chim. Acta* 1999, *393*, 77–82.

[7] Kappes, T., Galliker, B., Schwarz, M. A., Hauser, P. C., *TrAC Trends Anal. Chem.* 2001, *20*, 133–139.

[8] Anderson, G., Thompson, J. E., Shurrush, K., *J. Chem. Educ.* 2006, *83*, 1677–1680.

[9] Mai, T. D., Schmid, S., Müller, B., Hauser, P. C., *Anal. Chim. Acta* 2010, *665*, 1–6.

[10] Lee, M., Cho, K., Yoon, D., Yoo, D. J., Kang, S. H., *Electrophoresis* 2010, *31*, 2787–2795.

[11] Marini, R. D., Rozet, E., Montes, M. L., Rohrbasser, C., Roht, S., Rhème, D., Bonnabry, P., Schappler, J., Veuthey, J.-L., Hubert, P., Rudaz, S., *J. Pharm. Biomed. Anal.* 2010, *53*, 1278–1287.

[12] Kubáň, P., Seiman, A., Makarotseva, N., Vaher, M., Kaljurand, M., *J. Chromatogr. A* 2011, *1218*, 2618–2625.

[13] da Costa, E. T., Neves, C. A., Hotta, G. M., Vidal, D. T., Barros, M. F., Ayon, A. A., Garcia, C. D., do Lago, C. L., *Electrophoresis* 2012, *33*, 2650–2659.

[14] Segato, T. P., Bhakta, S. A., Gordon, M. T., Carrilho, E., Willis, P. A., Jiao, H., Garcia, C. D., *Anal. Methods* 2013, *5*, 1652–1657.

[15] Mai, T. D., Pham, T. T., Pham, H. V., Saiz, J., Ruiz, C. G., Hauser, P. C., *Anal. Chem.* 2013, *85*, 2333–2339.

[16] Saiz, J., Mai, T. D., Hauser, P. C., Garcia-Ruiz, C., *Electrophoresis* 2013, *34*, 2078–2084.

[17] Kobrin, E. G., Lees, H., Fomitsenko, M., Kubáň, P., Kaljurand, M., *Electrophoresis* 2014, *35*, 1165–1172.

[18] Saiz, J., Duc, M. T., Koenka, I. J., Martin-Alberca, C., Hauser, P. C., Garcia-Ruiz, C., *J. Chromatogr. A* 2014, *1372C*, 245–252.

[19] Nguyen, T. A., Pham, T. N., Doan, T. T., Ta, T. T., Saiz, J., Nguyen, T. Q., Hauser, P. C., Mai, T. D., *J. Chromatogr. A* 2014, *1360*, 305–311.

[20] Cabot, J. M., Fuguet, E., Roses, M., Smejkal, P., Breadmore, M. C., *Anal. Chem.* 2015, *87*, 6165–6172.

[21] Willis, P. A., Creamer, J. S., Mora, M. F., *Anal. Bioanal. Chem.* 2015, *407*, 6939–6963.

[22] Evans, E., Costrino, C., do Lago, C. L., Garcia, C. D., Roux, C., Blanes, L., *J. Forensic Sci.* 2016, *61*, 1610–1614.

[23] Koenka, I. J., Küng, N., Kubáň, P., Chwalek, T., Furrer, G., Wehrli, B., Müller, B., Hauser, P. C., *Electrophoresis* 2016, *37*, 2368–2375.

[24] Greguš, M., Foret, F., Kubáň, P., *J. Chromatogr. A* 2016, *1427*, 177–185.

[25] Saar-Reismaa, P., Erme, E., Vaher, M., Kulp, M., Kaljurand, M., Mazina-Sinkar, J., *Anal. Chem.* 2018, *90*, 6253–6258.

[26] Pan, J. Z., Fang, P., Fang, X. X., Hu, T. T., Fang, J., Fang, Q., *Sci. Rep.* 2018, *8*, 1791.

[27] Fuiko, R., Saracevic, E., Koenka, I. J., Hauser, P. C., Krampe, J., *Talanta* 2019, *195*, 366–371.

[28] Ryvolová, M., Preisler, J., Brabazon, D., Macka, M., *TrAC Trends Anal. Chem.* 2010, *29*, 339–353.

[29] Torres, N. T., Och, L. M., Hauser, P. C., Furrer, G., Brandl, H., Vologina, E., Sturm, M., Bürgmann, H., Müller, B., *Environ. Sci. Process Impacts* 2014, *16*, 879–889.

[30] Bonvoisin, J., Mies, R., Boujut, J.-F., Stark, R., *J. Open Hardware* 2017, *5*, 1–18.

[31] da Costa, E. T., Mora, M. F., Willis, P. A., do Lago, C. L., Jiao, H., Garcia, C. D., *Electrophoresis* 2014, *35*, 2370–2377.

[32] Pearce, J. M., *Science* 2012, *337*, 1303–1304.

[33] Fisher, D. K., Gould, P. J., *Mod. Instrum.* 2012, *1*, 8–20.

[34] Kubáň, P., Foret, F., Erny, G., *Electrophoresis* 2019, *40*, 65–78.

[35] Koenka, I. J., Sáiz, J., Rempel, P., Hauser, P. C., *Anal. Chem.* 2016, *88*, 3761–3767.

[36] Furter, J. S., Hauser, P. C., *Electrophoresis* 2019, *40*, 410–413.

[37] Mai, T. D., Hauser, P. C., *Talanta* 2011, *84*, 1228–1233.

[38] Mai, T. D., Hauser, P. C., *Electrophoresis* 2013, *34*, 1796–1803.

[39] Saito, R. M., Brito-Neto, J. G. A., Lopes, F. S., Blanes, L., da Costa, E. T., Vidal, D. T. R., Hotta, G. M., do Lago, C. L., *Anal. Methods* 2010, *2*, 164–170.

[40] Furter, J. S., Hauser, P. C., *Anal. Chim. Acta* 2019, *1058*, 18–28.

[41] Tanyanyiwa, J., Hauser, P. C., *Electrophoresis* 2002, *23*, 3781–3786.

[42] Anklam, E., *Food Chem.* 1998, *63*, 549–562.

[43] Buldini, P. L., Cavalli, S., Mevoli, A., Sharma, J. L., *Food Chem.* 2001, *73*, 487–495.

[44] Maria Rizelio, V., Gonzaga, L. V., Borges Gda, S., Maltez, H. F., Costa, A. C., Fett, R., *Talanta* 2012, *99*, 450–456.

[45] Pascual-Maté, A., Osés, S. M., Fernández-Muiño, M. A., Sancho, M. T., *J. Apic. Res.* 2018, *57*, 38–74.

[46] Sajtos, Z., Andrasi, M., Gaspar, A., *J. Chromatogr. B* 2020, *1142*.

[47] Shi, M., Gao, Q., Feng, J., Lu, Y., *J. Chromatogr. Sci.* 2012, *50*, 547–552.

[48] Suarez-Luque, S., Mato, I., Huidobro, J. F., Simal-Lozano, J., *J. Chromatogr. A* 2005, *1083*, 193–198.

[49] Pisani, A., Protano, G., Riccobono, F., *Food Chem.* 2008, *107*, 1553–1560.

[50] Drevinskas, T., Kaljurand, M., Maruška, A., *Electrophoresis* 2014, *35*, 2401–2407.

[51] Zhang, M., Stamos, B. N., Dasgupta, P. K., *Anal. Chem.* 2014, *86*, 11547–11553.

[52] Stojkovic, M., Schlensky, B., Hauser, P. C., *Electroanalysis* 2013, *25*, 2645–2650.

[53] Francisco, K. J. M., do Lago, C. L., *Electrophoresis* 2009, *30*, 3458–3464.

[54] Takeuchi, M., Li, Q. Y., Yang, B. C., Dasgupta, P. K., Wilde, V. E., *Talanta* 2008, *76*, 617–620.

[55] Tanyanyiwa, J., Galliker, B., Schwarz, M. A., Hauser, P. C., *Analyst* 2002, *127*, 214–218.

4.6 NEW AUTOMATED INJECTION SYSTEM FOR CAPILLARY ELECTROPHORESIS MASS SPECTROMETRY BASED ON PNEUMATIC CONTROL

The powerful combination between capillary electrophoresis and mass spectrometry unites the advantages of both analytical techniques. CE requires small buffer and sample amounts and provides high resolution and very efficient separations. Mass spectrometry on the other hand enables high sensitivity and selectivity of measurements. In addition, information on molecular masses as well as structures of the compounds can be obtained. Electrospray is the most commonly used ionization source for the coupling. Sheathless as well as sheath flow interfaces of the electrospray approaches exist. The advantage of the sheathless ESI interface is that the sample is not diluted and therefore higher intensities are reached. In addition, the experimental set-up is less complicated. Týčová and Foret [124] demonstrated in 2015 an interface-free set-up for the coupling of CE and MS where the electrophoretic capillary was used at the same time as separation column and electrospray emitter [125, 126]. The capillary outlet had a conus shape and was covered with a hydrophobic coating. One high voltage was used at the same time for driving the separation and the electrospray. No physical electric contact was required at the capillary outlet end. This "interface-free" sheathless nanoelectrospray was adopted in this work for coupling CE and MS.

In the scope of this project, a compact automated capillary electrophoresis was developed for coupling to mass spectrometry. Injection systems for CE are often based on flow injection analysis, which simplifies automation by controlling flows with small pumps and valves. However, it's difficult to couple such injection systems with mass spectrometry [127]. The reason is that for the coupling, the high voltage has to be applied to the injection end while the mass spectrometer inlet is grounded. To avoid failure of electronic devices at the injection end due to the high voltage applied, only air operated valves and different pressures were used for regulating flow rates and flow paths within the system. The whole instrument consists of three different modules including a microfluidic, pneumatic and an electronic part. The fluid handling system is based on the microfluidic breadbard approach [87]. A conductivity detector was added to the set-up. Regarding the buffer, a compromise had to made in the buffer composition to satisfy the requirements of both electrophoretic separations and electrospray. Since a volatile buffer is required for the electrospray, the obtained baseline of the C^4D was rather unstable. However, the approach allowed to control the separation process better. In case of clogging of the capillary or incorrect injection, the separation could be quickly stopped. The electronic properties of the electrospray in terms of voltage and current were determined for different buffer systems. Current values were found to be between 56 and 1666 nA and voltage values between 1.1 and 3.7 kV in the range of 1.5 and 20 kV applied

voltage. The effect of flow rate in the range of 28 and 57 nL/min and a voltage between 1.5 and 20 kV on the signal intensity was investigated in order to find the optimal settings for the electrospray. Qualitative separations of three benzalkonium homologues and quantitative separation of four different pesticides were performed. Good detection limits between 0.4 and 0.8 µM and reproducibilities between 5.2 and 6.6 % could be obtained. In addition, pesticides in spiked grape juice were extracted by using an SPE column and analysed.

Compact automated capillary electrophoresis instrument for coupling with mass spectrometry by using sheathless electrospray

Jasmine S. Furter, Peter C. Hauser*

Department of Chemistry, University of Basel, Klingelbergstrasse 80, 4056 Basel, Switzerland.

*Corresponding author.

E-mail address: peter.hauser@unibas.ch

Phone: + 41 61 207 10 03

Abbreviations: APCI: atmospheric pressure chemical ionization; BAC: benzalkonium chloride; BGE: background electrolyte; BR: buffer reservoir; CE: capillary electrophoresis; C^4D: capacitively coupled contactless conductivity detection; ESI: electrospray; FIA: flow injection analysis; HV: high voltage; MALDI: matrix assisted laser desorption ionization; MS: mass spectrometry; nanoESI: nanoelectrospray

Keywords: Arduino Nano, Capillary Electrophoresis, Conductivity Detection, Microfluidics, Microfluidic Breadboard Approach, Nanoelectrospray, Sheathless Interface

Abstract

A compact automated capillary electrophoresis instrument for coupling with electrospray mass spectrometry is described. To avoid malfunction of electronic devices at the injection end due to the applied high voltage, no electronic devices were included. Instead, pneumatic valves and different pressures were applied for regulating flow rates and controlling flow paths within the system. The flexible set-up of the instrument based on the microfluidic breadboard approach allows the user to make easy amendments in capillary length, inner diameter, applied pressure and voltage values. On demand, a second detector can easily be installed in front of the mass spectrometer as demonstrated with a conductivity detector. The coupling to the mass spectrometer is based on a sheathless nanoelectrospray in an "interface-free" configuration. The separation capillary was therefore used as the electrophoretic column and as electrospray tip. The effect of the flow rate and applied voltage on the signal intensity and the electronic properties of the electrospray was determined in order to find the best settings. The instrument performance was tested by analysing four pesticides quantitatively as well as separating three benzalkonium chloride homologues qualitatively by employing volatile acetic acid based buffers.

1 Introduction

CE as a versatile separation technique provides fast, efficient and high-resolution separations while requiring only small sample and buffer amounts. Mass spectrometry on the other hand is characterised by high sensitivity and selectivity and provides information on molecular masses as well as on structures of unknown substances [1, 2]. The hyphenation is therefore powerful because it unites the advantages of both techniques. CE-MS has become quite popular [3, 4] since its inception in 1987 by Olivares et al. [5]. Electrospray is the most commonly used ionization source for the hyphenation [5-7]. Atmospheric chemical ionization (APCI) [8, 9] and matrix assisted laser desorption ionization (MALDI) [10, 11] are also possible but less often utilised. Coupling of CE and MS is not straight forward compared to other hyphenated techniques. The conventional CE set-up cannot be maintained since mass spectrometry is an off-column detection technique. Therefore, an open end of the capillary is necessary for the interface. At the same time a stable electric contact with the buffer solution is required at the capillary outlet for the CE as well as for the electrospray process [12]. Another difficulty are non-volatile salts usually contained in the buffer for CE not compatible with electrospray ionization [13].

Most ESI interface constructions can be categorized in two types, which are either a sheath-flow or sheathless interface. In the sheath liquid configuration, the separation capillary is surrounded by a tube with larger diameter. The sheath liquid consisting of a conductive volatile solvent is flowing through the tube and mixed to the buffer at the capillary outlet while being connected to the high voltage power supply [14]. In this set-up, the electrospray quality is improved due to the changed buffer composition and stabilised flow rates. On the other hand, the sensitivity of the electrospray is lowered due to dilution of the analyte and the experimental set-up is more complicated. In addition, a laminar flow is established, which counteracts the advantages of a CE separation [15].

When following a sheathless approach, the ionization efficiency and sensitivity are increased, but establishment of an electric contact at the capillary end is challenging [10, 16-18]. Moini et al. [19, 20] described an interface based on a porous capillary tip etched with hydrofluoric acid for enabling ion movements. Other approaches depend on a sub-micrometre fracture in the capillary wall for mounting an electric contact [21, 22] or on a conductive coating such as a gold [16] or graphite [23]. On the other hand, it has been demonstrated that the physical electric contact between capillary outlet and ground-state electrode is not necessarily required for driving the electrospray [24-26]. One high voltage module can enable at the same time driving of the electrophoretic separation and electrospray. The electric circuitry is closed by buffer ions, which cross the gap between capillary outlet and mass spectrometer inlet [25]. These "interface-free" designs relied on fine electrospray tips, which were pulled in flames. More recently in 2015, Týčová et al. [27] demonstrated a similar "interface-free" set-up based on a conus shaped capillary end covered by a hydrophobic coating for stabilising the electrospray [28, 29].

While interfaces requiring minimal instrumental efforts are available, only few automated instruments for the coupling of CE and MS have been reported. Some groups make use of the autosampler and power supply of a commercially available CE instrument and employ a second high voltage power supply for improvising the interface to the mass spectrometer [30, 31]. Grundmann and Matysik [15] described a device based on capillary batch injection (CBI), which was optimized for dealing with very small sample amounts. For the analysis of monoclonal antibodies, an automated off-line CE/MALDI-MS instrument was built by Biacchi et al. [32] enabling additional UV detection. In addition, different microfluidic capillary electrophoresis platform (MCE) were used to automate the CE-MS operation [33, 34]. In microchip electrophoresis, the separation is taking place in small channels engraved on a substrate made of glass or polymer providing minimal buffer and sample consumption, small dimensions and fast separations. Although MCE enables fast separations, low reagent consumption and improved mass transfer [35] the approach has some disadvantages such as the

cumbersome fabrication procedure, challenging detection and rigidity in the set-up especially for the separation length and diameter. On the other hand, similar operation performance can be reached by using miniaturized injection systems with short standard capillaries having a low internal diameter [36]. Consumption of buffer and sample is low while the set-up offers much more flexibility [37].

Here we describe an automated CE-MS instrument following the microfluidic breadboard approach [37]. Different miniature components were used to build the injection system while the interface to the mass spectrometer is based on an interface-free sheathless nanoelectrospray. The compact device enables fully automated operation and the whole set-up as well as the interface are kept simple allowing an easy installation in front of the mass spectrometer. Following a dual detection approach, a capacitively coupled contactless conductivity detector (C^4D) was added to the set-up.

2 Materials and methods

2.1 Instrumentation

The microfluidic part was implemented in a purpose-made Perspex® cage with dimensions of 28.6 x 25.6 x 14.6 cm equipped with a microswitch for interrupting the high voltage on opening. The fluid handling part was built upon a microfluidic breadboard made of Perspex® with dimensions of 24.8 x 22.8 x 0.8 cm. Box and microfluidic breadboard were built by the internal workshop of the university. A microfluidic reservoir holder (XS, Elveflow, Paris, France) enabled pressurization of disposable 1.5 mL Eppendorf® tubes, which contained the sample solution. The vials containing the buffer and waste solutions (LS-BBRES-1ML and LS-BBRES-5ML) were purchased from LabSmith (Livermore, CA, USA). The separation capillary with 363 µm OD and 15 µm ID (TSP-015375, Molex-Polymicro, Phoenix, AZ, USA) was inserted into a Tee piece (T116-203, LabSmith) by using a tubing sleeve (U360-SLV, IDEX, Lake Forest, IL, USA). The separation voltage was provided by a high voltage module

(UM20P4/S, Spellman, Pulborough, UK) and applied to the injection end by using a Platinum electrode inserted into a Tee piece. Liquid streams were controlled by using two check valves (CV-3315, IDEX) and two 2-way, normally closed, air operated valves (PMDP-2R-1/4UG, Takasago Electric, Nagoya, Japan). For most connections 1/16" OD and 0.02" ID PEEK tubing (211607-10, BGB) was used. The flow resistors were made out of 1/16" OD and 0.005" ID PEEK tubing (211604-5, BGB). Pressure sensors for following pressure in the hydraulic section (uPS0800-T116) were obtained from LabSmith. The interface to the mass spectrometer was mounted on an in-house built optical breadboard with dimensions 29.9 x 7.0 x 1.0 cm. The capillary outlet was positioned in front of the mass spectrometer by fixing it on a purpose-made Perspex® holder. A XYZ translation stage (DT12XYZ) placed on an optical rail (RLA150/M) from Thorlabs (Newton, NJ, USA) allowed precise adjustment of the capillary position by using micromanipulators.

As pressure source for the pneumatic part compressed nitrogen from a standard gas cylinder was used. The following pneumatic parts were purchased from Clippard (Cincinnati, OH, USA). The pressure was first reduced with a two-stage gas regulator to 5.5 bar followed by a precision gas regulator (DR-2NR) allowing to set the pressure between 0.1 and 6.9 bar. A second precision pressure regulator (DR-2-5) enables further pressure reduction between 0.07 and 3.4 bar. Read-out of the pressure values was enabled with a pressure gauge (K8-16-40, SMC, Chiyoda, Tokio, Japan) and two electronic pressure sensors (PSE530-M5-L, SMC Gas pressures were applied to the microfluidic part by using 2-way (E2L10C-7W012) and 3-way latching valves (E3L10C-7W012) mounted on single-station (E10M-01), 2-station manifolds (E10M-02) and 4-station manifolds (E10M-04). Two check valves (MCV-1BB) prevented gas backflow. For the connection between the pneumatic parts, 1/8" OD and 1/16" ID (URH1-0402) tubing, hose connectors (CT2-PKG) and T-pieces (T22-2) were used. Stainless steel mufflers (15070) attached to the pneumatic manifolds reduced the noise produced by the latching valves.

For electronic control, a purpose made-printed circuit board (PCB) containing an Arduino microcontroller board (Arduino Nano 3.0, Gravitech, Minden, NV, USA) was connected to a notebook computer. The board provided the necessary copper tracks for connecting the different electronic parts of the instrument. The digital-to-analog converter (MAX517) for regulating the high voltage output was a product from Maxim Integrated (San Jose, CA, USA). The H-bridge drivers (BD6220F-E2) needed for operating the latching pneumatic valves were products of Rohm (Kyoto, Japan). The miniature pressure sensors were connected to instrumentation amplifiers (INA111AP, Burr-Brown, Tucson, AZ, USA) used in voltage adder configuration each with a resistance of 2.2 kΩ. Pressure values from the sensors were read out using the e-corder. The graphical user interface (GUI) program running on a personal computer was written in *Java* by using the *Java* development kit (JDK 8.0.91) and *Netbeans* 8.1. The software routines running on the ATmega328 microcontroller of the Arduino were written in Forth with the open source *AmForth* interpreter (http://amforth.sourceforge.net/).

The solution conductivity was detected by using a lab-made capacitively coupled contactless conductivity detector connected to an e-corder 410 (eDAQ, Denistone East, NSW, Australia) for data acquisition.

Mass spectrometric detection was performed on a LCQ Deca 3D ion trap mass spectrometer 2.0 (Finnigan MAT, San Jose, CA, USA). Data was acquired in turbo scan (55000 amu/sec) and selective ion monitoring (SIM) mode. Injection time into the mass spectrometer was 200 ms and 2 microscans were collected. Data was acquired and processed by using the XCalibur 2.0.7 (Thermo Fisher Scientific, Waltham, MA, US).

2.2 Reagents and methods

Deionized ultrapure water was used for preparing solutions by using a Milli-Q system from Millipore (Bedford, MA, USA). All solvents were of HPLC grade. Dichloromethane (DCM) was obtained from Honeywell (Muskegon, MC, USA), methanol and acetonitrile from VWR

(Dietikon, Switzerland). The following salts of analytical grade were used for the preparation of the standard solutions. Pyrifenox, pyrimethanil, pirimicarb, cyprodinil, benzyldimethyldodecylammonium chloride, benzyldimethyltetradecylammonium chloride and benzyldimethylhexadecylammonium chloride were obtained from Merck (Darmstadt, Germany). 2-amino-1-butanol was obtained from Alfa Aesar (Ward Hill, USA). Stock solution of the pesticides and 2-amino-1-butanol were prepared in methanol at 10 mM concentration and diluted to the required concentration on demand. Stock solution of the benzalkonium chloride homologues were prepared in a concentration of 10 mM in a mixture of water and acetonitrile (1:4). Acetic acid glacial and ammonia were obtained from VWR. Formic acid 98% was obtained from J. T. Baker (Phillipsburg, NJ, USA). Stock solutions of formic acid and ammonia in concentrations of 5 M respectively 1 M were stored in the fridge and used for preparing the BGE fresh on demand. The prepared electrolytes were filtered through 0.45 μm membrane filters (SF1303-2, BGB) and degassed. The capillary was conditioned by flushing for 30 min with 0.1 M sodium hydroxide solution prepared from sodium hydroxide pellets (Thermo Fisher, Waltham, MD, USA), afterwards with deionized water for 10 min and finally with the running buffer until the baseline was stable. Grape juice was purchased from a local supermarket (Coop, Basel, Switzerland). For solid phase extraction C18 cartridges (12102052, Agilent, Santa Clara, CA, USA) were used. The cartridges were conditioned with 4 mL methanol followed by 4 mL water. Afterwards 2 mL of the analyte solution was passed through. The cartridges were dried in a nitrogen stream and the absorbed pesticides eluted by flushing with 10 mL dichloromethane. The solvent was evaporated in a nitrogen gas stream and the residue redissolved in 1 mL methanol.

2.4 Fabrication of the capillary tip

For the preparation of the capillary tips, the procedure described by Týčová et al. [29] was followed. The capillary was ground in a 5 degree angle with sandpaper in two different grit

sizes (600, 2500). For the grinding process, the capillary was inserted on an in-house made device enabling rotation of the sandpaper with a Dremel (300, Mt. Prospect, IL). Afterwards the tip was dipped in a mixture of polytetrafluoroethylene preparation, 60 wt % dispersion in H_2O obtained from Sigma Aldrich (St. Louis, MO, USA) and nail polish (Néonail hard top UV gel polish, Cosmo group, Poznari, Poland) (4:1). The tip was dried, heated with the heat gun for 3 minutes and exposed to a UV lamp for 5 minutes. The quality of the resulting capillary tip was controlled by using a USB microscope camera (AD7013MZT, Dino-Lite, Torrance, CA, USA).

3 Results and Discussion

3.1 Instrument Design

3.1.1 CE part

Miniaturized injection systems for capillary electrophoresis are often based on flow injection analysis employing microfluidic channels [38, 39]. Automation is simple because no mechanical movements of the capillary are required compared to commercial instrumentation and sample and buffer amounts can kept small [40-42]. As highlighted by Grundmann et al. [15] it's difficult to couple FIA systems with MS. The challenge is that the high voltage has to be applied to the injection end due to the grounded inlet of the mass spectrometer. Consequently, no electronic devices can be used for controlling the injection procedure.

The injection system described herein was solely operated by timed pressure application. Flow rates were adjusted by inserting tubing with suitable internal diameters and employing passive check valves and air operated valves for controlling flow pathways. As in the previously reported design [43], the described instrument is based on three modules, including a microfluidic, pneumatic and an electronic part. In the microfluidic section, the actual sample injection into the separation capillary is carried out. High precision is reached by pneumatic pressurization of the liquids since stepwise movements of pumps are avoided. The required

pressures are provided by pressure regulators and latching valves enclosed in a pneumatic section. An electronic part connects the high voltage module as well as the latching valves to a microcontroller allowing the automated operation of the pneumatic valves as well as tuning of the high voltage. The instrument was installed on a board with dimensions of 53 x 35 x 38 cm, which can easily be fixed in front of the mass spectrometer. A technical drawing of the set-up is shown in Fig. 1A with a photograph of the instrument in Fig. 1B and the set-up of the capillary end coupled to the mass spectrometer in Fig. 1C.

The fluid handling part of the instrument is based on the microfluidic breadboard approach [37]. By combining different miniature commercially available microfluidic components on a breadboard, a simple injection system was created. A schematic overview on the entire hydraulic part is shown in Fig. 2. The separation capillary with an internal diameter of 15 µm and a total length of 80 cm was connected to the injection manifold by insertion in a Tee piece (T3) with a tubing sleeve while the other end was left open for the interfacing with the mass spectrometer. It's favorable to use narrow-bore capillaries to drive the separations in CE because Joule heating is lowered enabling the application of higher separation voltages and the use of higher conductivity electrolytes while lower sample amounts are required [44, 45]. The high voltage for driving both separation and electrospray was connected next to the separation capillary downstream through another Tee piece (T4) while the MS inlet was grounded. The whole module was enclosed in a Perspex cage for safety reasons. The sample loop located between T1 and T2 was filled with the analyte solution by pressurizing the sample vial with a specifically designed airtight cap. The BGE was filled in the buffer container (BR) required for interface and capillary flushing steps. Two check valves (CV1 and CV2) avoided the respective cross-over of sample and buffer solution. The only active elements within the injection system were two normally closed on/off valves, which were opened on pressure application. These valves channeled the fluids either to one of the waste containers or the separation capillary.

Similar to previous publications [43, 46], calculations were performed during the design process by using the law of Hagen-Poiseuille and the hydraulic-electric circuit analogy [47].

The electropneumatic part is schematically shown in Fig. 3. The pressure provided by a standard nitrogen gas cylinder was reduced by a first pressure regulator PR1 to 3 bar. The pressure pathway was split in Tee piece T2. One tube was connected to a second pressure regulator PR2, which reduced the pressure further to 0.9 bar. Pressurization of the sample vial was achieved by actuating latching valve LV1. Pressures of 0.9 and 3 bar were applied to the buffer vial with the valves LV2 and LV3. Because two different pressures were united in one tube, two check valves CV1 and CV2 prevented backflow of the gas into respectively other direction. The three-way valves LV6 and LV7 enabled pressure release from the system. LV4 and LV5 were responsible for the actuation of the air-operated on/off valves in the system. Please note that a pressure between 3 and 6 bar has to be applied for opening the hydrodynamic valves. Monitoring of the pressure was done by attaching two electronic pressure sensors after the first and the second pressure regulator through the Tee pieces T1 and T5.

The set-up of the electronic part is relatively simple as shown in Fig. 4 since no electronic valves or syringes were needed. The latching valves and the high voltage module were connected to an interface circuitry containing an Arduino microcontroller board. A TTL signal from the Arduino allowed switching the high voltage module on and off while the output was regulated via the digital-to-analog converter Max517. The maximum output voltage was +20 kV. Output voltage and current were monitored through analog input pins of the Arduino, which were internally connected to an analog-to-digital converter. The latching valves were actuated via H-bridge switches. Basic actions of the injection system were programmed by using Forth commands [48] and the previously described GUI enabled a comfortable operation of the instrument [43]. As an online detection method, the C^4D could easily be added between CE and MS part. Data acquisition of the conductivity signal was carried out separately with the eDAQ chart software.

3.1.1 Electrospray interface

For coupling of the compact capillary electrophoresis instrument to the mass spectrometer, a sheath less interface-free design described by Týčová et al. [27-29] was employed. Only one high voltage power supply was needed for both separation and electrospray. In addition, the preparation of the electrospray tip was simple requiring only grinding and coating with a hydrophobic Teflon film. As a challenge, the quality of the electrospray relies fully on the shape of the capillary end and therefore a careful preparation of the tip was necessary. Once prepared, the tip could be used for several measurement days. The tip was positioned in a distance of 2 mm in front of the MS inlet for achieving a stable electrospray.

In order to find the optimal settings for the electrospray, the effect of the applied voltage and the flow rate were evaluated in terms of electronic properties and signal intensity.

The electronic properties of the electrospray were determined by applying different voltages at the injection end. Since the separation capillary and the gap between capillary end and mass inlet are arranged in sequence, they can be seen as two resistors switched in series (equation 1).

$$R_t = R_{CE} + R_{ESI} \qquad 1$$

$$I_{ESI} = I_{CE}\left(1 - \frac{V_{ESI}}{V_{app}}\right) \qquad 2$$

In consequence, the current is the same for both parts under electrospray conditions. The current for the electrophoretic separation can be measured in an additional experiment by dipping the capillary end in a vial filled with electrolyte. By knowing all these parameters, the voltage for the electrospray can be calculated following equation 2. Since the current depends on the conductivity of the solution, the experiments were conducted with three different buffer solutions. In Fig. 5A the measured electrospray current is plotted against the applied voltage while in Fig. 5B the calculated electrospray voltage is shown in dependence of the applied voltage. No variation in the electronic properties could be observed when varying the flow rate of the electrospray. The electrospray current increased almost linearly with the applied electric

field in the range of 1.5 and 10 kV as well as with conductivity of the solution. When using a buffer containing 0.05 M acetic acid adjusted to pH 4 with ammonia, current values between 56 and 1108 nA were obtained. Currents increased when going to higher conductivity buffer solutions. For a buffer system with 0.2 M acetic acid/ammonia at pH 4, currents between 61 and 1406 nA were measured and for 1 M formic acid values between 59 and 1666 nA. For all buffer solutions, a sharp increase was observed in the range of 15 and 20 kV. The resulting electrospray voltage increased also in a linear fashion between 1.5 and 7 kV applied voltage and reached a plateau after 10 kV following a sigmoid function. Calculated values were between 1.1 and 3.1 kV for the lowest conductivity (0.05 M HAc pH 4) and between 1.1 and 2.7 kV for the highest conductivity (1 M formic acid). In the range of 1.5 kV and 7 kV, the electronic properties of the different buffer solutions are in a similar range. On the other hand the values drift apart when measuring applying voltages between 10 and 20 kV.

The electronic properties were compared to the results obtained from the measurements. In order to find the optimal conditions for the electrospray, a solution containing pyrimethanil as a modeling substance was injected into the separation capillary in a concentration of 50 µM. 0.2 M acetic acid adjusted to pH 4 was used as electrolyte. The sample plug was pumped through the capillary under electrospray conditions and the resulting peak area plotted against the applied voltage as shown in Fig. 6A. The maximum signal was obtained when applying 3 kV to the separation capillary corresponding to 1.7 kV and 120 nA for the electrospray. At 5 kV applied pressure, the signal already decreased rapidly and after 10 kV no signal could be obtained anymore. This observation corresponds to the plateau region in the electrospray current measurement. It can therefore be assumed that corona discharges or an electrospray multi jet mode start to prevail at these voltages and as a consequence the analyte signal decreases rapidly [27]. In order to avoid corona discharges at the capillary tip, the electrospray voltage should remain below approximately 2.3 kV [25, 49]. For the further measurements, a voltage of 4 kV corresponding to an electrospray voltage of 2.0 kV and 148 nA current was

used. Even though 3 kV gives a higher signal, the electrospray is much more stable at 4 kV with an acceptable signal intensity. In Fig. 6B signal intensity depending on variation of the flow rate is plotted. Due to restricted range of possible pressures for operating the pneumatic valves, only flow rates between 28 nL/min (3 bar) and 57 nL/min (6 bar) were tested. The observed relation between flow rate and signal intensity was not linear although a decrease in signal intensity was seen when going from the 28 to 57 nL/min. This observation corresponds to the reported higher ionization degree of the analyte at low flow rates [50, 51]. For the following measurements, the lowest possible flow rate of 28 nL/min was applied due higher obtained signal intensities and a limited resolution of the mass spectrometer.

In order to obtain an acceptable resolution of the electropherograms, the electronic conditions were changed in the middle of the measurements. First, 20 kV were applied under no flow conditions enabling the separation of the analyte in the electric field. The time length of this first step was adjusted to the migration time of the analytes by performing test runs. When the analytes were close to the capillary outlet in separated zones, the conditions were changed. The solution was pumped to the outlet with 3 bar applied pressure and 4 kV for enabling optimal electrospray conditions. The whole sequence was programmed and needed no attention of the operator.

The effect of the different steps within the operation sequence on the electrospray properties were further investigated and the results displayed in Fig. 7. 2-amino-1-butanol was added in a concentration of 100 µM to the buffer serving as electrospray marker. The above described protocol was followed with switching the conditions after 14 minutes. As can be seen from the electropherogram, no electrospray was obtained during the separation step. Only when reducing the voltage and applying pressure, the signal of 2-amino-1-butanol can be seen. This observation is consistent with the above described assumption that at a voltage of 20 kV and no flow conditions, corona discharges predominate and consequently the analyte is not ionized.

3.2 Procedures

In flow injection analysis, different steps are necessary for proper sample injection following a defined operation sequence. Pressure profiles as shown in Fig. 8 were measured by placing miniature hydraulic pressure sensors at the buffer container and T3 during instrument set-up. Note that the pressure sensors were removed during the measurements due to the high voltage applied to this part. The different steps of the operation sequence are detailed in Table 1 with the corresponding valve positions, duration and volumetric flow rates.

The injection process starts by flushing both parts of the interface with the background electrolyte (BGE) by opening first V1 and closing V2 and afterwards reversing the valve position (**1**+**2**). For interface flushing and sample transport a pressure of 0.9 bar was applied to the buffer container resulting in a flow rate of 6.8 µL/s. Due to the inserted flow resistor R, the pressure at the capillary inlet was reduced to 0.01 bar. For capillary flushing, sample injection and electrospray a pressure of 3 bar was used resulting in a flow rate of 28.3 nL/min. The low flow rate is not problematic since a stable electrospray can also be maintained in the nL min^{-1} range [52, 53]. At the same time a nano electrospray (nano-ESI) increases ionization efficiency as well as tolerance towards ion suppression and solvent composition [50, 51]. Following to the flushing of the capillary (**3**), the sample loop located between T1 and T2 was filled with the analyte (**4**) by opening V1 and closing V2. The sample plug was then transported to the separation capillary inlet located in the Tee piece (**5**) with the same configuration as for the interface flushing. The injection occurred by closing V1 and V2 and applying a pressure of 3 bar to the capillary inlet for 1.2 s (**6**) leading to a sample plug of 0.57 nL (3.23 µm, 0.4% occupancy). Afterwards, the interface was flushed to remove all sample residues (**7**+**8**) and the high voltage turned on to 20 kV for performing the separation (**9**). After separating the analytes, the configuration was changed for enabling a stable electrospray (**10**). One filling of the buffer container (1.1 mL) was sufficient for performing five measurements while the content of the

sample container content (1.0 mL) lasted for around 14 measurements. The injection process takes around 180 s.

3.3 Performance

For conductivity detection, a background electrolyte with a high ionic strength, but low conductivity is required to give a good S/N ratio [54]. On the other hand, for electrospray, the BGE should be volatile and buffer components such as ammonium acetate/formate, formic or acetic acid are best suited [54]. Non-volatile buffers on the other hand cause dirt at the orifice of the mass spectrometer. When combining both detection techniques, a compromise in the buffer composition has to be made for the benefit of the electrospray quality. The advantage of installing the second detector, is that the separation process can be controlled better when observing the conductivity. For example clogging of the separation capillary can quickly be detected as well as if the sample was injected correctly. Consequently the separation process can be interrupted quickly on demand. On the other hand, the sensitivity of the conductivity detection with these buffers is quite low and the baseline is unstable. Therefore the conductivity is not useful for quantitative detection.

In Fig. 9, the obtained electropherograms when separating three different benzalkonium chloride (BAC) homologues (benzyldimethyldodecylammonium chloride, benzyldimethyltetradecylammonium chloride and benzyldimethylhexadecylammonium chloride) at 50 µM concentration are displayed [55]. A volatile buffer containing 0.05 M acetic acid adjusted to pH 4 with ammonia was employed. The voltage was switched from 20 kV to electrospray conditions after 10.5 min. In Fig. 9A the ion electropherogram obtained with the mass spectrometric detection is shown while in Fig. 9B the signals obtained with the conductivity detector are displayed.

Subsequently, four different pesticides in a standard solution at 50 µM concentration were separated and the resulting electropherograms displayed in Fig. 10. A buffer containing 0.2 M

acetic acid adjusted to pH 4 with ammonia was used [56]. The conditions were switched after 14 minutes to an electrospray friendly level. The ion electropherogram was collected with the mass spectrometer within 15.3 minutes and is shown in Fig. 10A. Conductivity signals were measured after 10.8 minutes as shown in Fig. 10B. Grape juice spiked with the pesticides at a concentration of 10 μM and extracted with SPE was analysed with the calibrated system and the resulting electropherogram shown in Fig. 10C.

Calibration curves based on peak areas of the analytes were acquired for the four pesticides in the range of 10 and 50 μM with the mass spectrometer as shown in Table 2. Correlation coefficients between 0.9944 and 0.9970 were obtained. Reproducibilities of the peak areas were between 5.2 and 6.6% RSD for four subsequent measurements. RSD values for the migration times were between 0.2 and 0.4%. Detection limits (LODs) were found to be between 0.36 and 0.76 μM.

4 Concluding Remarks

A compact automated CE injection system enabling coupling to a mass spectrometer was developed. The injection system is solely operated by pressure application and employs an interface free sheathless electrospray. The instrument has a flexible set-up enabling easy amendments in capillary dimensions and method. In addition, a second detector can easily be added as demonstrated with a capacitively coupled contactless conductivity detector. Good reproducibilities and detection limits were obtained when analyzing four pesticides quantitatively.

5 References

[1] C.W. Klampfl, CE with MS detection: A rapidly developing hyphenated technique, ELECTROPHORESIS 30(S1) (2009) S83-S91. https://doi.org/https://doi.org/10.1002/elps.200900088.
[2] J. Schappler, J.-L. Veuthey, S. Rudaz, 18 Coupling CE and microchip-based devices with mass spectrometry, in: S. Ahuja, M.I. Jimidar (Eds.), Separation Science and Technology, Academic Press2008, pp. 477-521. https://doi.org/https://doi.org/10.1016/S0149-6395(07)00018-9.
[3] R. Ramautar, O.A. Mayboroda, G.W. Somsen, G.J. de Jong, CE-MS for metabolomics: Developments and applications in the period 2008–2010, ELECTROPHORESIS 32(1) (2011) 52-65. https://doi.org/https://doi.org/10.1002/elps.201000378.
[4] R. Haselberg, G.J. de Jong, G.W. Somsen, Capillary electrophoresis–mass spectrometry for the analysis of intact proteins 2007–2010, ELECTROPHORESIS 32(1) (2011) 66-82. https://doi.org/https://doi.org/10.1002/elps.201000364.
[5] J.A. Olivares, N.T. Nguyen, C.R. Yonker, R.D. Smith, On Line Mass Spectrometric Detection for Capillary Zone Electrophoresis, Analytical chemistry 59 (1987) 1230-1232.
[6] R.D. Smith, J.A. Olivares, N.T. Nguyen, H.R. Udseth, Capillary Zone Electrophoresis Mass-Spectrometry Using an Electrospray Ionization Interface, Analytical Chemistry 60(5) (1988) 436-441. https://doi.org/DOI 10.1021/ac00156a013.
[7] R.D. Smith, H.R. Udseth, C.J. Barinaga, C.G. Edmonds, Instrumentation for High-Performance Capillary Electrophoresis Mass-Spectrometry, Journal of Chromatography 559(1-2) (1991) 197-208. https://doi.org/Doi 10.1016/0021-9673(91)80070-W.
[8] Y. Takada, M. Sakairi, H. Koizumi, Atmospheric Pressure Chemical Ionization Interface for Capillary Electrophoresis/Mass Spectrometry, Anal. Chem. 67 (1995) 1474-1476.
[9] Y. Tanaka, K. Otsuka, S. Terabe, Evaluation of an atmospheric pressure chemical ionization interface for capillary electrophoresis–mass spectrometry, Journal of Pharmaceutical and Biomedical Analysis 30(6) (2003) 1889-1895. https://doi.org/https://doi.org/10.1016/S0731-7085(02)00532-0.
[10] G. Bonvin, J. Schappler, S. Rudaz, Capillary electrophoresis–electrospray ionization-mass spectrometry interfaces: Fundamental concepts and technical developments, Journal of Chromatography A 1267 (2012) 17-31. https://doi.org/https://doi.org/10.1016/j.chroma.2012.07.019.
[11] H. Zhang, R.M. Caprioli, Capillary Electrophoresis Combined with Matrix-Assisted Laser Desorption/Ionization Mass Spectrometry; Continuous Sample Deposition on a Matrix-precoated Membrane Target, Journal of Mass Spectrometry 31(9) (1996) 1039-1046. https://doi.org/https://doi.org/10.1002/(SICI)1096-9888(199609)31:9<1039::AID-JMS398>3.0.CO;2-F.
[12] E.J. Maxwell, D.D.Y. Chen, Twenty years of interface development for capillary electrophoresis–electrospray ionization–mass spectrometry, Analytica Chimica Acta 627(1) (2008) 25-33. https://doi.org/https://doi.org/10.1016/j.aca.2008.06.034.
[13] G. de Jong, Capillary Electrophoresis–Mass Spectrometry (CE-MS) Principles and Applications, Wiley-VCH, Weinheim, Germany, 2016.
[14] R.D. Smith, C.J. Barinaga, H.R. Udseth, Improved electrospray ionization interface for capillary zone electrophoresis-mass spectrometry, Analytical Chemistry 60(18) (1988) 1948-1952. https://doi.org/10.1021/ac00169a022.
[15] M. Grundmann, F.M. Matysik, Analyzing small samples with high efficiency: capillary batch injection-capillary electrophoresis-mass spectrometry, Anal Bioanal Chem 404(6-7) (2012) 1713-21. https://doi.org/10.1007/s00216-012-6282-2.

[16] Z. Kele, G. Ferenc, E. Klement, G.K. Toth, T. Janaky, Design and performance of a sheathless capillary electrophoresis/mass spectrometry interface by combining fused-silica capillaries with gold-coated nanoelectrospray tips, Rapid Commun Mass Spectrom 19(7) (2005) 881-5. https://doi.org/10.1002/rcm.1866.
[17] K. Klepárník, Recent advances in combination of capillary electrophoresis with mass spectrometry: Methodology and theory, ELECTROPHORESIS 36(1) (2015) 159-178. https://doi.org/https://doi.org/10.1002/elps.201400392.
[18] R. Ramautar, J.-M. Busnel, A.M. Deelder, O.A. Mayboroda, Enhancing the Coverage of the Urinary Metabolome by Sheathless Capillary Electrophoresis-Mass Spectrometry, Analytical Chemistry 84(2) (2012) 885-892. https://doi.org/10.1021/ac202407v.
[19] M. Moini, Simplifying CE-MS operation. 2. Interfacing low-flow separation techniques to mass spectrometry using a porous tip, Anal Chem 79(11) (2007) 4241-6. https://doi.org/10.1021/ac0704560.
[20] M. Moini, C.M. Rollman, Compatibility of highly sulfated cyclodextrin with electrospray ionization at low nanoliter/minute flow rates and its application to capillary electrophoresis/electrospray ionization mass spectrometric analysis of cathinone derivatives and their optical isomers, Rapid Communications in Mass Spectrometry 29(3) (2015) 304-310. https://doi.org/https://doi.org/10.1002/rcm.7106.
[21] A. Hirayama, H. Abe, N. Yamaguchi, S. Tabata, M. Tomita, T. Soga, Development of a sheathless CE-ESI-MS interface, ELECTROPHORESIS 39(11) (2018) 1382-1389. https://doi.org/https://doi.org/10.1002/elps.201800017.
[22] T.T.T.N. Nguyen, N.J. Petersen, K.D. Rand, A simple sheathless CE-MS interface with a sub-micrometer electrical contact fracture for sensitive analysis of peptide and protein samples, Analytica Chimica Acta 936 (2016) 157-167. https://doi.org/https://doi.org/10.1016/j.aca.2016.07.002.
[23] Y.Z. Chang, G.R. Her, Sheathless Capillary Electrophoresis/Electrospray Mass Spectrometry Using a Carbon-Coated Fused-Silica Capillary, Analytical Chemistry 72(3) (2000) 626-630. https://doi.org/10.1021/ac990535e.
[24] M. Mazereeuw, A.J.P. Hofte, U.R. Tjaden, J. Van Der Greef, A novel sheathless and electrodeless microelectrospray interface for the on-line coupling of capillary zone electrophoresis to mass spectrometry, Rapid Communications in Mass Spectrometry 11(9) (1997) 981-986. https://doi.org/10.1002/(sici)1097-0231(19970615)11:9<981::aid-rcm901>3.0.co;2-s.
[25] E.X. Vrouwe, J. Gysler, U.R. Tjaden, J. van der Greef, Chip-based capillary electrophoresis with an electrodeless nanospray interface, Rapid Communications in Mass Spectrometry 14(18) (2000) 1682-1688. https://doi.org/https://doi.org/10.1002/1097-0231(20000930)14:18<1682::AID-RCM78>3.0.CO;2-E.
[26] L. Goodwin, J.R. Startin, B.J. Keely, D.M. Goodall, Analysis of glyphosate and glufosinate by capillary electrophoresis–mass spectrometry utilising a sheathless microelectrospray interface, Journal of Chromatography A 1004(1) (2003) 107-119. https://doi.org/https://doi.org/10.1016/S0021-9673(03)00572-7.
[27] A. Tycova, F. Foret, Capillary electrophoresis in an extended nanospray tip–electrospray as an electrophoretic column, Journal of Chromatography A 1388 (2015) 274-279. https://doi.org/https://doi.org/10.1016/j.chroma.2015.02.042.
[28] A. Týčová, J. Prikryl, F. Foret, Reproducible preparation of nanospray tips for capillary electrophoresis coupled to mass spectrometry using 3D printed grinding device, Electrophoresis 37(7-8) (2016) 924-30. https://doi.org/10.1002/elps.201500467.
[29] A. Týčová, M. Vido, P. Kovarikova, F. Foret, Interface-free capillary electrophoresis-mass spectrometry system with nanospray ionization-Analysis of dexrazoxane in blood plasma, J Chromatogr A 1466 (2016) 173-9. https://doi.org/10.1016/j.chroma.2016.08.042.

[30] G. Zhu, L. Sun, T. Linkous, D. Kernaghan, J.B. McGivney IV, N.J. Dovichi, Absolute quantitation of host cell proteins in recombinant human monoclonal antibodies with an automated CZE-ESI-MS/MS system, ELECTROPHORESIS 35(10) (2014) 1448-1452. https://doi.org/https://doi.org/10.1002/elps.201300545.
[31] G. Zhu, L. Sun, J. Heidbrink-Thompson, S. Kuntumalla, H.-y. Lin, C.J. Larkin, J.B. McGivney IV, N.J. Dovichi, Capillary zone electrophoresis tandem mass spectrometry detects low concentration host cell impurities in monoclonal antibodies, ELECTROPHORESIS 37(4) (2016) 616-622. https://doi.org/https://doi.org/10.1002/elps.201500301.
[32] M. Biacchi, R. Bhajun, N. Saïd, A. Beck, Y.N. François, E. Leize-Wagner, Analysis of monoclonal antibody by a novel CE-UV/MALDI-MS interface, ELECTROPHORESIS 35(20) (2014) 2986-2995. https://doi.org/https://doi.org/10.1002/elps.201400276.
[33] X. Li, S. Zhao, H. Hu, Y.-M. Liu, A microchip electrophoresis-mass spectrometric platform with double cell lysis nano-electrodes for automated single cell analysis, Journal of Chromatography A 1451 (2016) 156-163. https://doi.org/https://doi.org/10.1016/j.chroma.2016.05.015.
[34] J.S. Mellors, K. Jorabchi, L.M. Smith, J.M. Ramsey, Integrated Microfluidic Device for Automated Single Cell Analysis Using Electrophoretic Separation and Electrospray Ionization Mass Spectrometry, Analytical Chemistry 82(3) (2010) 967-973. https://doi.org/10.1021/ac902218y.
[35] E.R. Castro, A. Manz, Present state of microchip electrophoresis: State of the art and routine applications, Journal of Chromatography A 1382 (2015) 66-85. https://doi.org/https://doi.org/10.1016/j.chroma.2014.11.034.
[36] A. Rainelli, P.C. Hauser, Fast electrophoresis in conventional capillaries by employing a rapid injection device and contactless conductivity detection, Analytical and Bioanalytical Chemistry 382(3) (2005) 789-794. https://doi.org/10.1007/s00216-005-3063-1.
[37] I.J. Koenka, J. Sáiz, P. Rempel, P.C. Hauser, Microfluidic Breadboard Approach to Capillary Electrophoresis, Analytical Chemistry 88(7) (2016) 3761-3767. https://doi.org/10.1021/acs.analchem.5b04666.
[38] P. Kuban, R. Pirmohammadi, B. Karlberg, Flow injection analysis–capillary electrophoresis system with hydrodynamic injection, Analytica Chimica Acta 378(1) (1999) 55-62. https://doi.org/https://doi.org/10.1016/S0003-2670(98)00631-X.
[39] T.D. Mai, S. Schmid, B. Müller, P.C. Hauser, Capillary electrophoresis with contactless conductivity detection coupled to a sequential injection analysis manifold for extended automated monitoring applications, Analytica Chimica Acta 665(1) (2010) 1-6. https://doi.org/https://doi.org/10.1016/j.aca.2010.03.014.
[40] P. Kuban, A. Engström, J.C. Olsson, G. Thorsén, R. Tryzell, B. Karlberg, New interface for coupling flow-injection and capillary electrophoresis, Analytica Chimica Acta 337(2) (1997) 117-124. https://doi.org/https://doi.org/10.1016/S0003-2670(96)00339-X.
[41] P. Tůma, F. Opekar, I. Jelínek, Split-flow injector for capillary zone electrophoresis, Journal of Chromatography A 883(1) (2000) 223-230. https://doi.org/https://doi.org/10.1016/S0021-9673(00)00446-5.
[42] F. Opekar, P. Coufal, K. Štulík, Rapid Capillary Zone Electrophoresis Along Short Separation Pathways and Its Use in Some Hyphenated Systems: A Critical Review, Chemical Reviews 109(9) (2009) 4487-4499. https://doi.org/10.1021/cr900018r.
[43] J.S. Furter, M.-A. Boillat, P.C. Hauser, Low-cost automated capillary electrophoresis instrument assembled from commercially available parts, ELECTROPHORESIS 41(24) (2020) 2075-2082. https://doi.org/https://doi.org/10.1002/elps.202000211.
[44] T.D. Mai, P.C. Hauser, Study on the interrelated effects of capillary diameter, background electrolyte concentration, and flow rate in pressure assisted capillary electrophoresis with contactless conductivity detection, ELECTROPHORESIS 34(12) (2013) 1796-1803. https://doi.org/https://doi.org/10.1002/elps.201200586.

[45] T.D. Mai, P.C. Hauser, Pressure-assisted capillary electrophoresis for cation separations using a sequential injection analysis manifold and contactless conductivity detection, Talanta 84(5) (2011) 1228-1233. https://doi.org/https://doi.org/10.1016/j.talanta.2010.12.023.
[46] J.S. Furter, P.C. Hauser, Injection system for fast capillary electrophoresis based on pressure regulation with flow restrictors, ELECTROPHORESIS 40(3) (2019) 410-413. https://doi.org/https://doi.org/10.1002/elps.201800250.
[47] K.W. Oh, K. Lee, B. Ahn, E.P. Furlani, Design of pressure-driven microfluidic networks using electric circuit analogy, Lab Chip 12(3) (2012) 515-45. https://doi.org/10.1039/c2lc20799k.
[48] J.S. Furter, P.C. Hauser, Interactive control of purpose built analytical instruments with Forth on microcontrollers - A tutorial, Analytica Chimica Acta 1058 (2019) 18-28. https://doi.org/https://doi.org/10.1016/j.aca.2018.10.071.
[49] Y.P. Raizer, Gas Discharge Physics, Springer-Verlag, Heidelberg, 1991.
[50] R. Juraschek, T. Dulcks, M. Karas, Nanoelectrospray--more than just a minimized-flow electrospray ionization source, J Am Soc Mass Spectrom 10(4) (1999) 300-8. https://doi.org/10.1016/S1044-0305(98)00157-3.
[51] I. Marginean, K. Tang, R.D. Smith, R.T. Kelly, Picoelectrospray ionization mass spectrometry using narrow-bore chemically etched emitters, J Am Soc Mass Spectrom 25(1) (2014) 30-6. https://doi.org/10.1007/s13361-013-0749-z.
[52] M.S. Wilm, M. Mann, Electrospray and Taylor-Cone theory, Dole's beam of macromolecules at last?, International Journal of Mass Spectrometry and Ion Processes 136(2) (1994) 167-180. https://doi.org/https://doi.org/10.1016/0168-1176(94)04024-9.
[53] M. Wilm, M. Mann, Analytical Properties of the Nanoelectrospray Ion Source, Analytical Chemistry 68(1) (1996) 1-8. https://doi.org/10.1021/ac9509519.
[54] A. Beutner, R.R. Cunha, E.M. Richter, F.M. Matysik, Combining C(4) D and MS as a dual detection approach for capillary electrophoresis, Electrophoresis 37(7-8) (2016) 931-5. https://doi.org/10.1002/elps.201500512.
[55] B.V. Para, O. Núñez, E. Moyano, M.T. Galceran, Analysis of benzalkonium chloride by capillary electrophoresis-tandem mass spectrometry, ELECTROPHORESIS 27(11) (2006) 2225-2232. https://doi.org/https://doi.org/10.1002/elps.200500716.
[56] J. Hernández-Borges, M.Á. Rodríguez-Delgado, F.J. García-Montelongo, A. Cifuentes, Highly sensitive analysis of multiple pesticides in foods combining solid-phase microextraction, capillary electrophoresis-mass spectrometry, and chemometrics, ELECTROPHORESIS 25(13) (2004) 2065-2076. https://doi.org/https://doi.org/10.1002/elps.200405938.

Table 1 Operation sequence

Step	Operation	Duration	Flow Rate	Buffer Amount	Sample Amount	V1	V2
		(s)	(µL s^{-1})	(µL)	(µL)		
1	Interface flushing (P1)	2	6.8	14	-	Open	Closed
2	Interface flushing (P2)	3.5	6.8	24	-	Closed	Open
3	Capillary flushing	120	4.7E-04	5.7E-02	-	Closed	Closed
4	Filling sample loop	10	6.8	-	76	Open	Closed
5	Sample transport	2.5	6.8	16.9	-	Closed	Open
6	Sample Injection	1.2	4.7E-04	5.7E-04	-	Closed	Closed
7	Interface flushing (P1)	10	6.8	68	-	Open	Closed
8	Interface flushing (P2)	12	6.8	81	-	Closed	Open
9	High voltage on	variable	0	-	-	Open	Closed
10	Electrospray	variable	2.8E-02	variable	-	Closed	Closed

Table 2 Validation data for the determination of four pesticides

Ion	Migration time	Range	Correlation coefficient	LOD	LOQ	Precision of migration time (n=4)	Precision of peak area (n=4)
	(s)	(μM)	r^2	(μM)	(μM)	(% RSD)	(% RSD)
Pyrifenox	15.27	10-50	0.9958	0.44	1.45	0.2	5.2
Cyprodinil	15.41	10-50	0.9970	0.76	2.54	0.3	3.2
Pirimicarb	15.55	10-50	0.9944	0.36	1.20	0.3	6.6
Pyrimethanil	15.78	10-50	0.9952	0.47	1.56	0.4	6.1

Figure Captions

Fig. 1 (A) Schematic overview of the CE-MS set-up with the different modules. Injection takes place in the fluid handling part consisting of a microfluidic flow injection manifold. Flow rates and flow paths are controlled by pressures provided by a pneumatic part. An electronic part including a microcontroller enables automated operation of the set-up with a personal computer. The separation capillary is interfaced to the mass spectrometer inlet by positioning the ground and coated tip at the XYZ translation stage in a distance of 2 mm to the mass spectrometer inlet. (B) Photograph of the capillary electrophoresis instrument coupled to the mass spectrometer. (C) Photograph of the capillary outlet as electrospray emitter positioned in front of the mass spectrometer.

Fig. 2 Microfluidic part. N_2: nitrogen gas; BR: buffer reservoir; CV1 and CV2: check valves; R: flow resistance; T1-T4: Tee pieces; V1 and V2: pressure operated two-way valves; C^4D: capacitively coupled contactless conductivity detector; HV: high voltage; MS: mass spectrometer; GND: ground.

Fig. 3 Electropneumatic part. N_2: nitrogen gas cylinder; PR1 and PR2: pressure regulators; M1 and M2: electronic pressure sensors; LV1-LV7: latching valves; T1-T7: Tee pieces; CV1 and CV2: pneumatic check valves.

Fig. 4 Electronic part including an Arduino Nano as microcontroller for interface to the computer. I2C: inter-integrated circuit, DAC: digital-to-analog converter; TTL: transistor-transistor-logic; HV-Module: high voltage module.

Fig. 5 Electronic properties of the electrospray for the buffer solutions 1 M formic acid, 0.2 M acetic acid adjusted to pH 4 with ammonia and 0.05 M acetic acid adjusted to pH 4 with ammonia. (A) Electrospray current in dependence of the applied voltage. (B) Calculated electrospray voltage in dependence of the applied voltage.

Fig. 6 Variation of voltage and pressure for finding optimal conditions for the electrospray.

Buffer: 0.2 M HAc pH 4 with NH3, Injection: 3 bar for 1.5 s, Capillary: 15 µM, 80 cm length, Analyte: 50 µM pyrimethanil. (A) Dependence of the peak area on the applied voltage in the range of 1.5 and 10 kV and (B) the applied flow rate in the range of 20 and 60 nL/min.

Fig. 7 Electrospray marker 2-amino-1-butanol added to the buffer 0.2 M HAc adjusted to pH4 with NH_3 in a concentration of 100 µM in red. A blank sample containing only the buffer is shown in black. (A) Mass spectrum and (B) ion electropherogram with an applied voltage of 20 kV and subsequent switching to electrospray friendly conditions with a flow rate of 28 nL/min and a voltage of 4 kV.

Fig. 8 Pressure profile of one operation cycle measured at the (A) buffer reservoir (BR) and (B) at the Tee piece (T3) with the separation capillary inlet. The different steps with the numbers are listed in Table 1.

Fig. 9 Qualitative separation of three benzalkonium chloride homologues at a concentration of 50 µM within 11.3 min. BGE: 0.05 M HAc pH 4 adjusted with ammonia with (A) mass spectrometric detection (B) C^4D detection. (**1**) benzyldimethyldodecylammonium chloride, (**2**) benzyldimethyltetradecylammonium chloride and (**3**) benzyldimethylhexadecylammonium chloride.

Fig. 10 Separation of four different pesticides at a concentration of 50 µM within 16 min. BGE: 0.2 M HAc adjusted to pH 4 with ammonia with (A) mass spectrometric detection (B) C^4D detection. (**1**) pyrifenox, (**2**) pirimicarb, (**3**) cyprodinil, (**4**) pyrimethanil. (C) mass spectrometric detection of grape juice spiked with 10 µM pesticides extracted with SPE. (**1**) pyrifenox, (**2**) pirimicarb, (**3**) cyprodinil, (**4**) pyrimethanil.

A

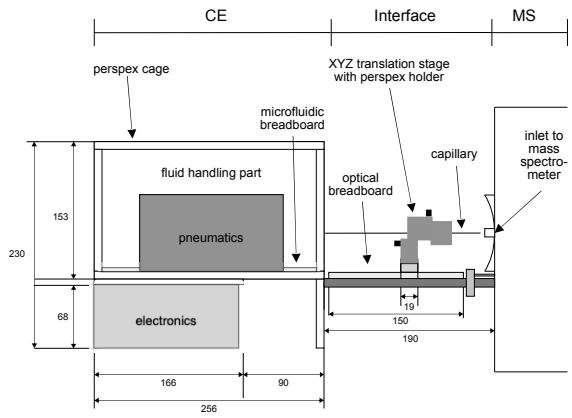
CE
Interface
MS
perspex cage
XYZ translation stage with perspex holder
microfluidic breadboard
capillary
inlet to mass spectro-meter
fluid handling part
optical breadboard
pneumatics
153
230
68
electronics
19
150
190
166
90
256

B

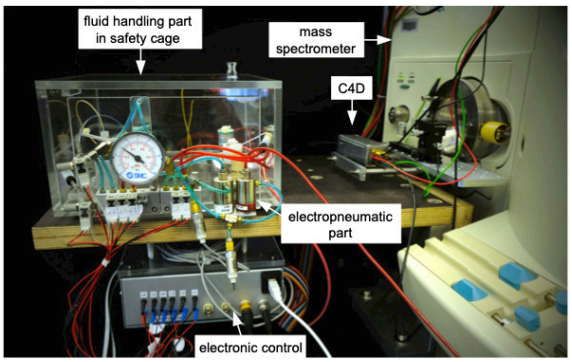
fluid handling part in safety cage
mass spectrometer
C4D
electropneumatic part
electronic control

C

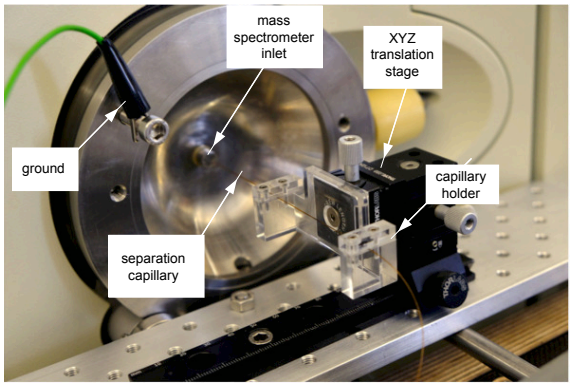
mass spectrometer inlet
XYZ translation stage
ground
capillary holder
separation capillary

Figure 1

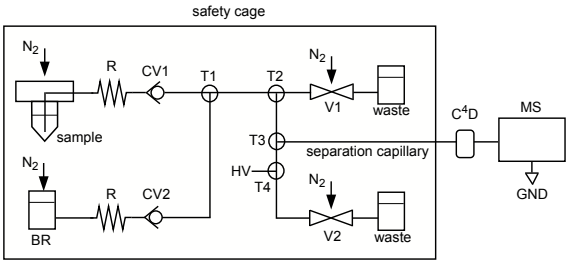
safety cage
N2
R
CV1
T1
T2
N2
V1
waste
C4D
MS
sample
T3
separation capillary
N2
HV
T4
R
CV2
N2
BR
V2
waste
GND

Figure 2

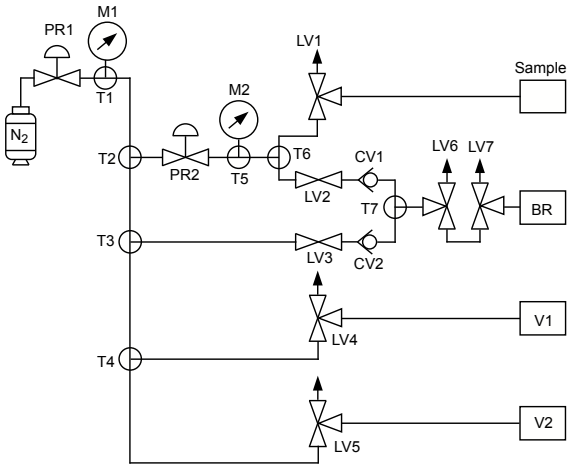
M1
PR1
T1
N2
T2
PR2
M2
T5
T6
LV1
Sample
LV2
CV1
T7
LV6
LV7
BR
T3
LV3
CV2
V1
LV4
T4
V2
LV5

Figure 3

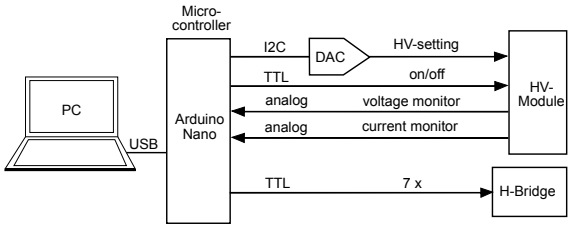
Micro-
controller
I2C
DAC
HV-setting
TTL
on/off
HV-
Module
PC
Arduino
Nano
analog
voltage monitor
analog
current monitor
USB
TTL
7 x
H-Bridge

Figure 4

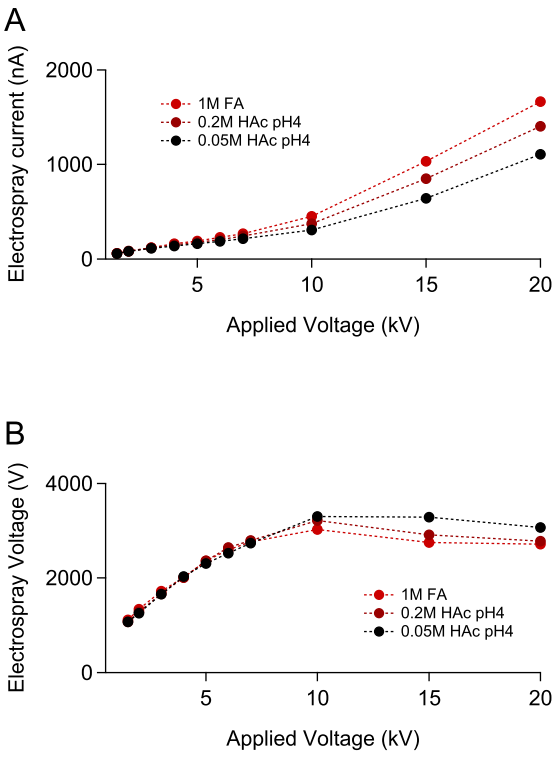
A
Electrospray current (nA)
2000
1000
0
1M FA
0.2M HAc pH4
0.05M HAc pH4
5
10
15
20
Applied Voltage (kV)
B
Electrospray Voltage (V)
4000
2000
0
1M FA
0.2M HAc pH4
0.05M HAc pH4
5
10
15
20
Applied Voltage (kV)

Figure 5

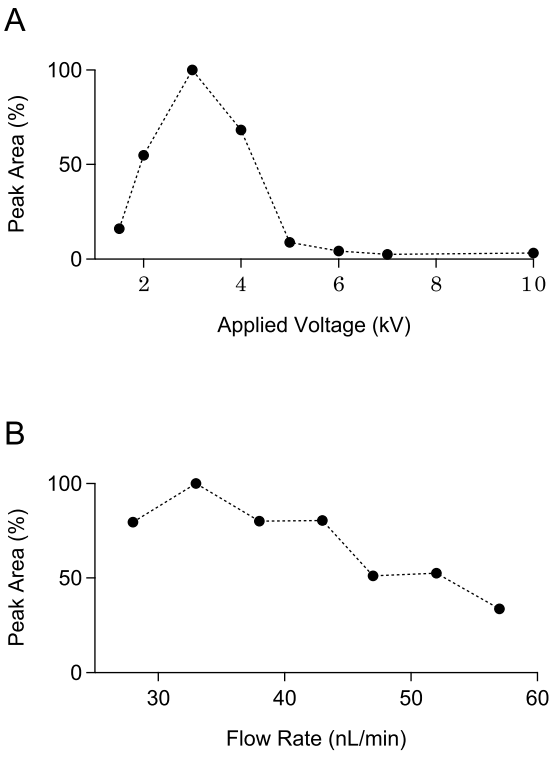
A
100
50
0
Peak Area (%)
2
4
6
8
10
Applied Voltage (kV)
B
100
50
0
Peak Area (%)
30
40
50
60
Flow Rate (nL/min)

Figure 6

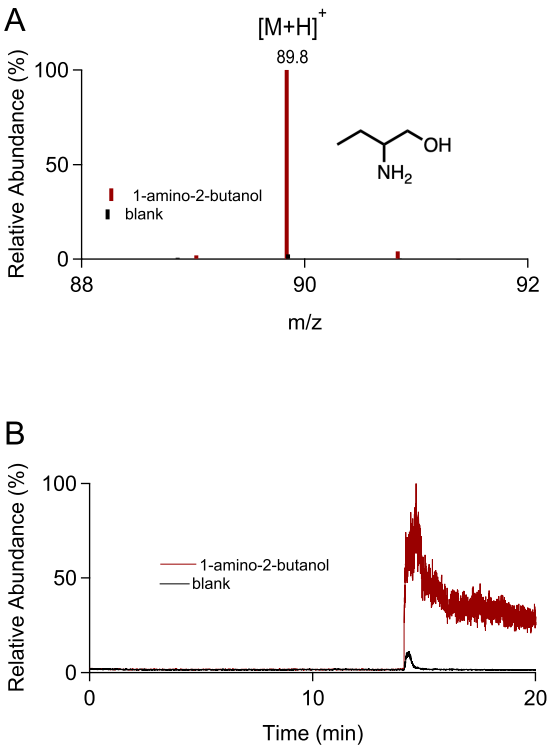
A
[M+H]+
89.8
Relative Abundance (%)
100
50
0
1-amino-2-butanol
blank
OH
NH2
88
90
92
m/z
B
Relative Abundance (%)
100
50
0
1-amino-2-butanol
blank
0
10
20
Time (min)

Figure 7

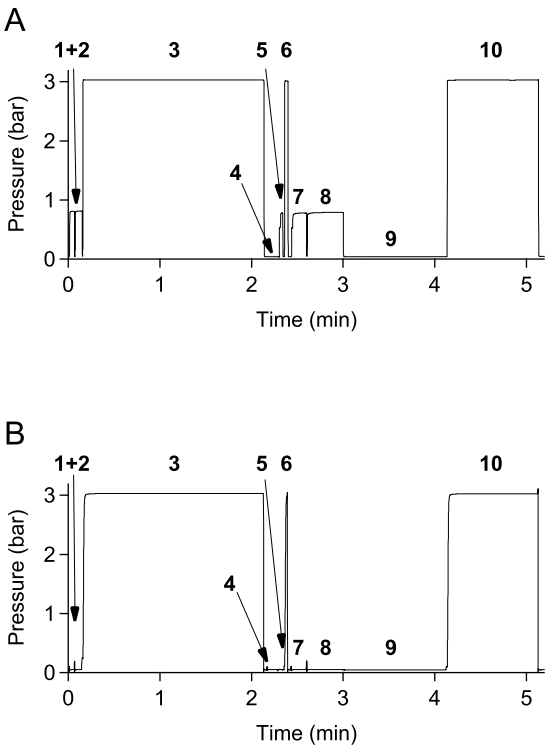
A
1+2
3
5
6
10
4
7
8
9
Pressure (bar)
Time (min)
B
1+2
3
5
6
10
4
7
8
9
Pressure (bar)
Time (min)

Figure 8

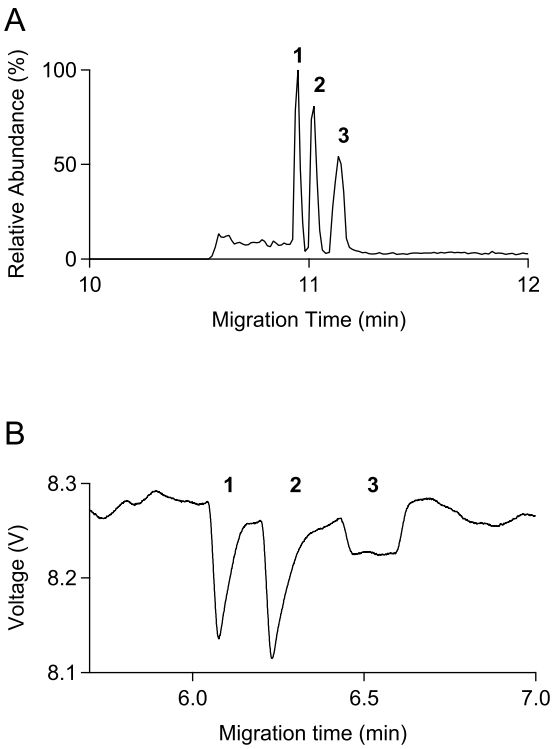
A
Relative Abundance (%)
100
50
0
1
2
3
10
11
12
Migration Time (min)
B
Voltage (V)
8.3
8.2
8.1
1
2
3
6.0
6.5
7.0
Migration time (min)

Figure 9

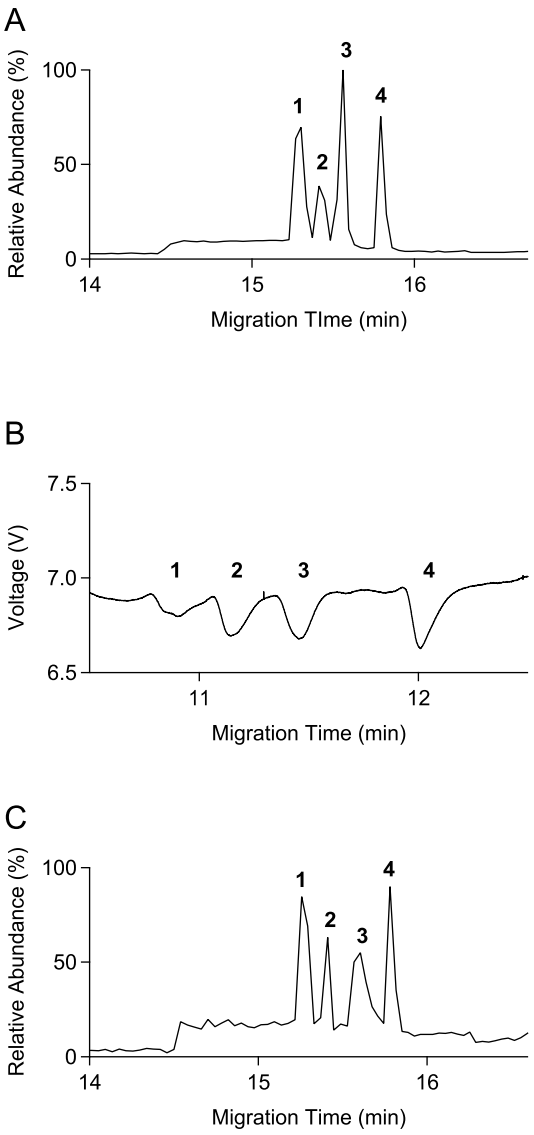
A
Relative Abundance (%)
100
50
0
14
15
16
Migration TIme (min)
1
2
3
4
B
Voltage (V)
7.5
7.0
6.5
11
12
Migration Time (min)
1
2
3
4
C
Relative Abundance (%)
100
50
0
14
15
16
Migration Time (min)
1
2
3
4

Figure 10

Part III

REFERENCES

BIBLIOGRAPHY

(1) Landers, J. P., *Handbook of Capillary Electrophoresis*, 2nd ed.; CRC Press: Boca Raton, 1997.

(2) Manz, A; Dittrich, P. S.; Pamme, N.; Iossifidis, D., *Bioanalytical Chemistry*, 2nd ed.; Imperial College Press: London, 2015.

(3) Heiger, D., *High Performance Capillary Electrophoresis*; Agilent Technologies: Germany, 2000.

(4) Jandik, P.; Bonn, G., *Capillary Electrophoresis of Small Molecules and Ions*; Wiley-VCH: Weinheim, 1993.

(5) Kohlrausch, F. *Wiedemanns Ann.* **1897**, *62*, 209.

(6) Kendall, J.; Crittenden, E. D. *Proc. Natl. Acad. Sci. U.S.A.* **1923**, *9*, 75–78.

(7) Tiselius, A. *Nova Acta Regiae Soc. Sci. Upsal.* **1930**, *7*, 1–107.

(8) Vesterberg, O. *J. Chromatogr. A* **1989**, *480*, 3–19.

(9) Svensson, H. *Kolloid-Z.* **1939**, *87*, 181–186.

(10) Longsworth, L. G. *J. Am. Chem. Soc.* **1945**, *67*, 1109–1119.

(11) Dole, V. P. *J. Am. Chem. Soc.* **1945**, *67*, 1119–1126.

(12) Hjertén, S. *Arkiv Kemi* **1958**, *13*, 151–152.

(13) Jorgenson, J. W.; Lukacs, K. D. *Anal. Chem.* **1981**, *53*, 1298–1302.

(14) Flanagan, R. J.; Taylor, A. A.; Watson, I. D.; Whelpton, R., *Fundamentals of Analytical Toxicology*, 2nd ed.; Wiley-VCH: West Sussex, 2007.

(15) Stevens, T. S.; Cortes, H. J. *Anal. Chem.* **1983**, *55*, 1365–1370.

(16) Huang, X.; Luckey, J. A.; Gordon, M. J.; Zare, R. N. *Anal. Chem.* **1989**, *61*, 766–770.

(17) Bushey, M. M.; Jorgenson, J. W. *J. Chromatogr.* **1989**, *480*, 301–310.

(18) Frías, S; Sánchez, M. J.; Rodríguez, M. A. *Anal. Chim. Acta* **2004**, *503*, 271–278.

(19) Schmidt, T.; Friehs, K.; Schleef, M.; Voss, C.; Flaschel, E. *Anal. Biochem.* **1999**, *274*, 235–240.

(20) De Lassichère, C. C.; Mai, T. D.; Taverna, M. *J. Chromatogr. A* **2019**, *1601*, 350–356.

(21) De Jong, G., *Capillary Electrophoresis–Mass Spectrometry (CE-MS): Principles and Applications*; Wiley-VCH: Weinheim, 2016.

(22) Bonvin, G.; Schappler, J.; Rudaz, S. *J. Chromatogr. A* **2012**, *1267*, 17–31.

(23) Krčmová, L.; Stjernlof, A.; Mehlen, S.; Hauser, P. C.; Abele, S.; Paull, B.; Macka, M. *Analyst* **2009**, *134*, 2394–2396.

(24) Bui, D. A.; Hauser, P. C. *J. Chromatogr. A* **2015**, *1421*, 203–208.

(25) Wu, S.; Dovichi, N. J. *J. Chromatogr. A* **1989**, *480*, 141–155.

(26) Keithley, R. B.; Weaver, E. M.; Rosado, A. M.; Metzinger, M. P.; Hummon, A. B.; Dovichi, N. J. *Anal. Chem.* **2013**, *85*, 8910–8918.

(27) Melanson, J. E.; Lucy, C. A. *Analyst* **2000**, *125*, 1049–1052.

(28) Walker, J. L. *Anal. Chem.* **1971**, *43*, 89A–93A.

(29) Kappes, T.; Hauser, P. C. *Analyst* **1999**, *124*, 1035–1039.

(30) Schwarz, M. A.; Galliker, B.; Fluri, K.; Kappes, T.; Hauser, P. C. *Analyst* **2001**, *126*, 147–151.

(31) Kubáň, P.; Hauser, P. C. *Electrophoresis* **2004**, *25*, 3387–3397.

(32) Mikkers, F. E. P.; Everaerts, F. M.; Verheggen, T. P. E. M. *J. Chromatogr. A* **1979**, *169*, 11–20.

(33) Kubáň, P.; Hauser, P. C. *Anal. Chim. Acta* **2008**, *607*, 15–29.

(34) Găs, B.; Demjaněnko, M.; Vacík, J. *J. Chromatogr. A* **1980**, *192*, 253–257.

(35) Zemann, A. J.; Schnell, E.; Volgger, D.; Bonn, G. K. *Anal. Chem.* **1998**, *70*, 563–567.

(36) Da Silva, J. A. F.; do Lago, C. L. *Anal. Chem.* **1998**, *70*, 4339–4343.

(37) Tanyanyiwa, J.; Galliker, B.; Schwarz, M. A.; Hauser, P. C. *Analyst* **2002**, *127*, 214–218.

(38) Kubáň, P.; Hauser, P. C. *Electrophoresis* **2004**, *25*, 3398–3405.

(39) Lau, H. F.; Quek, N. M.; Law, W. S.; Zhao, J. H.; Hauser, P. C.; Li, S. F. Y. *Electrophoresis* **2011**, *32*, 1190–1194.

(40) Carvalho, A. Z.; da Silva, J. A. F.; do Lago, C. L. *Electrophoresis* **2003**, *24*, 2138–2143.

(41) Le, M. D.; Duong, H. A.; Nguyen, M. H.; Sáiz, J.; Pham, H. V.; Mai, T. D. *Talanta* **2016**, *160*, 512–520.

(42) Gross, J. H., *Mass Spectrometry*, 3rd ed.; Springer: Cham, 2017.

(43) Glish, G. L.; Vachet, R. W. *Nat. Rev. Drug Discov.* **2003**, *2*, 140–150.

(44) Kienitz, H., *Massenspektrometrie*, 3rd ed.; Chemie: Weinheim, 1968.

(45) Todd, J. F. J. *Int. J. Mass Spectrom. Ion Processes* **1995**, *142*, 209–240.

(46) Awad, H.; Khamis, M. M.; El-Aneed, A. *Appl. Spectrosc. Rev.* **2015**, *50*, 158–175.

(47) Hiraoka, K., *Fundamentals of Mass Spectrometry*, 3rd ed.; Springer: New York, 2013.

(48) Bruins, A. P. *Trends Anal. Chem.* **1994**, *13*, 37–43.

(49) Märk, T. D. *Int. J. Mass Spectrom. Ion Phys.* **1982**, *45*, 125–145.

(50) Karas, M.; Bachmann, D.; Bahr, U.; Hillenkamp, F. *Int. J. Mass Spectrom. Ion Processes* **1987**, *78*, 53–68.

(51) Laiko, V. V.; Baldwin, M. A.; Burlingame, A. L. *Anal. Chem.* **2000**, *72*, 652–657.

(52) Weston, D. J. *Analyst* **2010**, *135*, 661–668.

(53) Takáts, Z.; Wiseman, J. M.; Gologan, B.; Cooks, R. G. *Science* **2004**, *306*, 471–473.

(54) Javanshad, R.; Venter, A. R. *Anal. Methods* **2017**, *9*, 4896–4907.

(55) Schmitt-Kopplin, P.; Frommberger, M. *Electrophoresis* **2003**, *24*, 3837–3867.

(56) Dole, R. B., *Electrospray Ionization Mass Spectrometry - Fundamentals, Instrumentation and Applications*; Wiley-VCH: Chichester, 1997.

(57) Cech, N. B.; Enke, C. G. *Mass Spectrom. Rev.* **2001**, *20*, 362–387.

(58) Taylor, G. I. *Proc. R. Soc. Lond. A* **1964**, *280*, 383–397.

(59) Wilm, M. S.; Mann, M. *Int. J. Mass Spectrom. Ion Processes* **1994**, *136*, 167–180.

(60) Smoker, M.; Tran, K.; Smith, R. E. *J. Agric. Food Chem.* **2010**, *58*, 12101–12104.

(61) Hanold, K. A.; Fischer, S. M.; Cormia, P. H.; Miller, C. E.; Syage, J. A. *Anal. Chem.* **2004**, *76*, 2842–2851.

(62) Robb, D. B.; Covey, T. R.; Bruins, A. P. *Anal. Chem.* **2000**, *72*, 3653–3659.

(63) El-Aneed, A.; Cohen, A.; Banoub, J. *Appl. Spectrosc. Rev.* **2009**, *44*, 210–230.

(64) Williams, J. D.; Burinsky, D. J. *Int. J. Mass. Spectrom.* **2001**, *212*, 111–133.

(65) Kondrat, R. W. *Int. J. Mass. Spectrom.* **2001**, *212*, 89–95.

(66) Chauhan, A.; Chauhan, P. *J. Anal. Bioanal. Tech.* **2014**, *5*, 1–5.

(67) Ardrey, R. E., *Liquid Chromatography-Mass Spectrometry: An Introduction*; Wiley-VCH: Chichester, 2003.

(68) Vestal, M. L. *Science* **1984**, *226*, 275–281.

(69) Lee, M. S.; Kerns, E. H. *Mass Spectrom. Rev.* **1999**, *18*, 187–279.

(70) Olivares, J. A.; Nguyen, N. T.; Yonker, C. L. R.; Smith, R. D. *Anal. Chem.* **1987**, *59*, 1230–1232.

(71) Smith, A. D.; Moini, M. *Anal. Chem.* **2001**, *73*, 240–246.

(72) Hommerson, P.; Khan, A. M.; de Jong, G. J.; Somsen, G. W. *Mass Spectrom. Rev.* **2011**, *30*, 1096–1120.

(73) Ramautar, R.; Somsen, G. W.; de Jong, G. J., *The Role of CE-MS in Metabolomics, Metabolomics in Practice*; Lämmerhofer, M., Weckwert, W., Eds.; Wiley-VCH: Boston, 2013, pp 177–208.

(74) Smith, R. D.; Loo, J. A.; Barinaga, C. J.; Edmonds, C. G.; Udseth, H. R. *J. Chromatogr. A* **1989**, *480*, 211–232.

(75) Moini, M. *Anal. Chem.* **2007**, *79*, 4241–4246.

(76) Lindenburg, P. W.; Haselberg, R.; Rozing, G.; Ramautar, R. *Chromatographia* **2015**, *78*, 367–377.

(77) Sánchez-Hernández, L.; Hernández-Domínguez, D.; Bernal, J.; Neusüss, C.; Martín, M. T.; Bernal, J. L. *J. Chromatogr. A* **2014**, *1359*, 317–324.

(78) Wimmer, B.; Pattky, M.; Zada, L. G.; Meixner, M.; Haderlein, S. B.; Zimmermann, H.-P.; Huhn, C. *Anal. Bioanal. Chem.* **2020**, *412*, 4967–4983.

(79) Li, S. F. Y., *Capillary Electrophoresis - Principles, Practice and Applications*, 3rd ed.; Elsevier Science: Amsterdam, 1993.

(80) Toraño, J. S.; Ramautar, R.; de Jong, G. *J. Chromatogr. B.* **2019**, *1118–1119*, 116–136.

(81) Fisher, D. K.; Gould, P. J. *Modern Instrumentation* **2012**, *1*, 8–20.

(82) Ryvolová, M.; Preisler, J.; Brabazon, D.; Macka, M. *Trends Anal. Chem.* **2010**, *29*, 339–353.

(83) Manz, A.; Graber, N.; Widmer, H. M. *Sens. Actuators B. Chem.* **1990**, *B1*, 244–248.

(84) Castro, E. R.; Manz, A. *J. Chromatogr. A* **2015**, *1382*, 66–85.

(85) Osiri, J. K.; Shadpour, H.; Soper, S. A. *Anal. Bioanal. Chem.* **2010**, *398*, 489–498.

(86) Segato, T. P.; Bhakta, S. A.; Gordon, M. T.; Carrilho, E.; Willis, P. A.; Jiao, H.; Garcia, C. D. *Anal. Methods* **2013**, *5*, 1652–1657.

(87) Koenka, I. J.; Sáiz, J.; Rempel, P.; Hauser, P. C. *Anal. Chem.* **2016**, *88*, 3761–3767.

(88) Rainelli, A.; Hauser, P. C. *Anal Bioanal Chem* **2005**, *382*, 789–794.

(89) Růžička, J.; Hansen, E. H. *Anal. Chim. Acta* **1975**, *78*, 145–157.

(90) Kubáň, P.; Karlberg, B. *Anal. Chim. Acta* **2009**, *648*, 129–145.

(91) Mai, T. D.; Schmid, S.; Müller, B.; Hauser, P. C. *Anal. Chim. Acta* **2010**, *665*, 1–6.

(92) Kappes, T.; Hauser, P. C. *Anal. Commun.* **1998**, *35*, 325–329.

(93) Kappes, T.; Schnierle, P.; Hauser, P. C. *Anal. Chim. Acta* **1999**, *393*, 77–82.

(94) Kappes, T.; Galliker, B.; Schwarz, M. A.; Hauser, P. C. *Trends Anal. Chem.* **2001**, *20*, 133–139.

(95) Kubáň, P.; Nguyen, H. T. A.; Macka, M.; Haddad, P. R.; Hauser, P. C. *Electroanalysis* **2007**, *19*, 2059–2065.

(96) Kubáň, P.; Seiman, A.; Makarotseva, N.; Vaher, M.; Kaljurand, M. *J. Chromatogr. A* **2011**, *1218*, 2618–2625.

(97) Berg, C.; Valdez, D. C.; Bergeron, P.; Mora, M. F.; Garcia, C. D.; Ayon, A. *Electrophoresis* **2008**, *29*, 4914–4921.

(98) Da Costa, E. T.; Neves, C. A.; Hotta, G. M.; Vidal, D. T. R.; Barros, M. F.; Ayon, A. A.; Garcia, C. D.; do Lago, C. L. *Electrophoresis* **2012**, *33*, 2650–2659.

(99) Creamer, J. S.; Mora, M. F.; Willis, P. A. *Anal. Chem.* **2017**, *89*, 1329–1337.

(100) Drevinskas, T.; Maruška, A.; Girdauskas, V.; Dūda, G.; Gorbatsova, J.; Kaljurand, M. *Anal. Methods* **2020**, *12*, 4977–4986.

(101) Oh, K. W.; Lee, K.; Ahn, B.; Furlani, E. P. *Lab Chip* **2012**, *12*, 515–545.

(102) Mai, T. D.; Pham, T. T. T.; Pham, H. V.; Sáiz, J.; Ruiz, C. G.; Hauser, P. C. *Anal. Chem.* **2013**, *85*, 2333–2339.

(103) Mayrhofer, K.; Zemann, A. J.; Schnell, E.; Bonn, G. K. *Anal. Chem.* **1999**, *71*, 3828–3833.

(104) Na, N.; Zhang, C.; Zhao, M.; Zhang, S.; Yang, C.; Fang, X.; Zhang, X. *J. Mass Spectrom.* **2007**, *42*, 1079–1085.

(105) Na, N.; Zhao, M.; Zhang, S.; Yang, C.; Zhang, X. *J Am Soc Mass Spectrom* **2007**, *18*, 1859–1862.

(106) Harper, J. D.; Charipar, N. A.; Mulligan, C. C.; Zhang, X.; Cooks, R. G.; Ouyang, Z. *Anal. Chem.* **2008**, *80*, 9097–9104.

(107) Hayen, H.; Michels, A.; Franzke, J. *Anal. Chem.* **2009**, *81*, 10239–10245.

(108) Williams, J., *The Art and Science of Analog Circuit Design*; Williams, J., Ed.; Butterworth-Heinemann: Boston, 1998, pp 139–193.

(109) Dionigi, M.; Costanzo, A.; Mastri, F.; Mongiardo, M.; Monti, G., *Wireless Power Transfer*; Agbinya, J. I., Ed.; River Publishers: Aalborg, 2016, pp 217–270.

(110) Kogelschatz, U. *Plasma Chem. Plasma Process.* **2003**, *23*, 1–46.

(111) Urban, P. L. *Analyst* **2015**, *140*, 963–975.

(112) Zollinger, D. P.; Bos, M. *Trends Anal. Chem.* **1985**, *4*, 60–61.

(113) Rather, E. D.; Colburn, D. R.; Moore, C. H., *History of Programming Languages II*; Bergin T, J., Gibson, R. G., Eds.; ACM Press: New York, 1996, pp 625–670.

(114) Casto, L. D.; Do, K. B.; Baker, C. A. *Anal. Chem.* **2019**, *91*, 9451–9457.

(115) Ryvolová, M.; Preisler, J.; Foret, F.; Hauser, P. C.; Krásenský, P.; Paull, B.; Macka, M. *Anal. Chem.* **2010**, *82*, 129–135.

(116) Prikryl, J.; Foret, F. *Anal. Chem.* **2014**, *86*, 11951–11956.

(117) Zhang, P. et al. *Drug Discov. Today* **2016**, *21*, 740–765.

(118) Hu, M.; Lan, Y.; Lu, A.; Ma, X.; Zhang, L. *Prog. Mol. Biol. Transl. Sci.* **2019**, *162*, 1–24.

(119) Bonaccorsi, A.; Rossi, C. *Res. Policy* **2003**, *32*, 1243–1258.

(120) Bonvoisin, J.; Mies, R.; Boujut, J.-F.; Stark, R. *J. Open Hardw.* **2017**, *5*, 1–18.

(121) Pearce, J. M. *Science* **2012**, *337*, 1303–1304.

(122) Da Costa, E. T.; Mora, M. F.; Willis, P. A.; do Lago, C. L.; Jiao, H.; Garcia, C. D. *Electrophoresis* **2014**, *35*, 2370–2377.

(123) Kubáň, P.; Foret, F.; Erny, G. *Electrophoresis* **2019**, *40*, 65–78.

(124) Týčová, A.; Foret, F. *J. Chromatogr. A* **2015**, *1388*, 274–279.

(125) Týčová, A.; Prikryl, J.; Foret, F. *Electrophoresis* **2016**, *37*, 924–930.

(126) Týčová, A.; Vido, M.; Kovarikova, P.; Foret, F. *J. Chromatogr. A* **2016**, *1466*, 173–179.

(127) Grundmann, M.; Matysik, F. M. *Anal. Bioanal. Chem.* **2012**, *404*, 1713–1721.

Part IV

LIST OF PUBLICATIONS AND POSTERS

PUBLICATIONS AND POSTERS

1. Jasmine S. Furter, Peter C. Hauser
   A low-cost ambient desorption/ionization source for mass-spectrometry based on a dielectric barrier discharge.
   Analytical Methods, 2018, 10, 2701–2711.

2. Jasmine S. Furter, Peter C. Hauser
   Injection system for fast capillary electrophoresis based on pressure regulation with flow restrictors.
   Electrophoresis, 2019, 40, 410–413.

3. Jasmine S. Furter, Peter C. Hauser
   Interactive control of purpose built analytical instruments with Forth on microcontrollers - A tutorial.
   Analytica Chimica Acta, 2019, 1058, 18–28.

4. Théo Liénard–Mayor, Jasmine S. Furter, Myriam Taverna, Hung Viet Pham, Peter C. Hauser, Thanh Duc Mai
   Modular instrumentation for capillary electrophoresis with laser induced fluorescence detection using plug-and-play microfluidic, electrophoretic and optic modules.
   Analytica Chimica Acta, 2020, 1135, 47–54.

5. Jasmine S. Furter, Marc-Aurèle Boillat, Peter C. Hauser
   Low-cost automated capillary electrophoresis instrument assembled from commercially available parts.
   Electrophoresis, 2020, 41, 2075–2082.

6. Jasmine S. Furter, Johannes Abraham, Peter C. Hauser
   Versatile capillary electrophoresis instruments based on the microfluidic breadboard approach.
   26th International Symposium on Electroseparation and Liquid Phase-Separation Techniques, Toulouse, France, September 2019.

Part V

APPENDIX

SUPPLEMENTARY INFORMATION TO THE 3RD PROJECT

Code extracts from the graphical user interface written in Java showing the basic communication protocol between the GUI and the Arduino microcontroller

Code extract showing how communication with RS232 interface is established

```
private void butConnectActionPerformed(java.awt.event.ActionEvent evt) {
        if (portInStream == null){
            Enumeration en = CommPortIdentifier.getPortIdentifiers();
            while (en.hasMoreElements()) {
                CommPortIdentifier cpi = (CommPortIdentifier)en.nextElement();
                if (cpi.getPortType() == CommPortIdentifier.PORT_SERIAL) {
                    if (cpi.getName().equals(selectedPort)) {
                        try {
                        com = (SerialPort)cpi.open("RS232Test",1000);
                              if (debug) System.out.println
                              ("CONNECT> "+selectedPort+" found and opened.");
                        com.setSerialPortParams (BAUD, DATABITS, STOPBITS,
                        PARITY_NONE);
                        portInStream = new InputStreamReader(com.getInputStream());
                        portInBuffReader = new BufferedReader (portInStream);
                        portOutStream = new PrintStream (com.getOutputStream());
                              if (debug) System.out.println ("CONNECT> InputStream is
                              now open and I try to read.");
                        butConnect.setEnabled(false);
                        butDisconnect.setEnabled(true);
                              } catch (PortInUseException | IOException |
                              UnsupportedCommOperationException e) {
                            System.err.println(e.toString());
                            System.exit(1);
                        }
                    }
                }
            }
        }
    }
```

Sources:

- http://www.kuligowski.pl/java/rs232-in-java-for-windows,1
- https://blog.henrypoon.com/blog/2011/01/01/serial-communication-in-java-with-example-program/
- https://gist.github.com/tkojitu/1924274

Code showing how a command is send to the Arduino as string

```
private int SendCommandToArduino (String cmd, String functionName){
        try{
                if (debug){
                        System.out.println (functionName+"> Sending ["+cmd+"]");
                }
                if (portOutStream != null){
                        portOutStream.println(cmd);
                }else{
                        System.err.println("SendCommandToArduino> ERROR: portOutStream
                        not valid")
                }
        }
        catch (Exception e) {
                System.err.println("SendCommandToArduino> ERROR: "+e.toString());
                return (-1);
        }
        return (0);
        }
```

Sources:

- **http://forum.arduino.cc/index.php?topic=438956.0**

Code showing how data is read (part of the main routine)

```
while (true) {
        try {
                if (analogread){
                        gui.SendCommandToArduino ("A0 analog_read .", "Endlessloop");
                        Thread.sleep(500);
                        gui.jCheckBox2.setText("STOP");
                }
                else{
                        Thread.sleep(1000);
                        gui.jCheckBox2.setText("START");
                }

                line1=portInBuffReader.readLine();
                line2=portInBuffReader.readLine();
                line3=portInBuffReader.readLine();
                line4=portInBuffReader.readLine();

                if (line2!=null){

                        String g1 = line2;
                        String sub1 = g1.substring(0);
                        String [] foo = sub1.split("ok");
                        for (String token : foo){
                                guimain.x = (int) Double.parseDouble(token);
                                guimain.val = (( guimain.x * 4 ) / 1023);
                                guimain.val2 = Math.round(guimain.val * 100) / 100.0;
                                value = String.valueOf(guimain.val2);
                                gui.resolution.setText(value + " " + "mg/L");
                        }
                }
        }
}
```

Sources:

- http://www.drdobbs.com/jvm/control-an-arduino-from-java/240163864
- https://stackoverflow.com/questions/15996345/java-arduino-read-data-from-the-serial-port

Code displayed in console during communication with Arduino

```
run:
MAIN> scanning ports..
DEBUG> found port COM3
DEBUG> selected port COM3
CONNECT> COM3 found and opened.
CONNECT> InputStream ist now open and I try to read.
butResetActionPerformed> Sending [-analoginput2]
butResetActionPerformed> Sending [marker -analoginput2]
butResetActionPerformed> Sending [PORTC 0 portpin: A0]
butResetActionPerformed> Sending [adc.init]
Endlessloop> Sending [A0 analog_read .]
Endlessloop> Sending [A0 analog_read .]
Endlessloop> Sending [A0 analog_read .]
Endlessloop> Sending [A0 analog_read .]
Endlessloop> Sending [A0 analog_read .]
BUILD SUCCESSFUL (total time: 20 seconds)
```

SUPPLEMENTARY INFORMATION TO THE 5TH PROJECT

Flow paths and the operating sequence of the microfluidic part, calculation of the overall costs, electronic circuitry and pictures of each part

Flow Paths

Electropneumatic part

Microfluidic part

Interface flushing (Part 1) & Sample transport

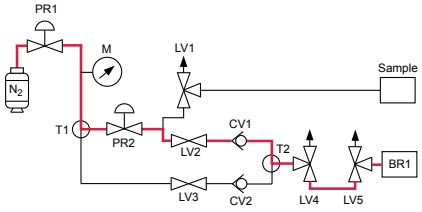

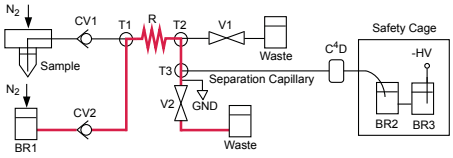

Interface flushing (Part 2)

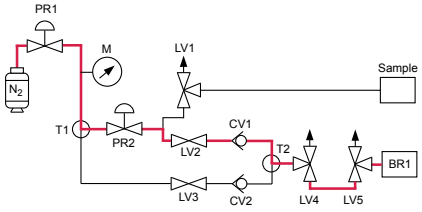

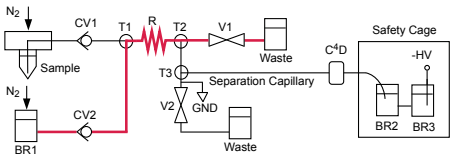

Capillary flushing & Injection

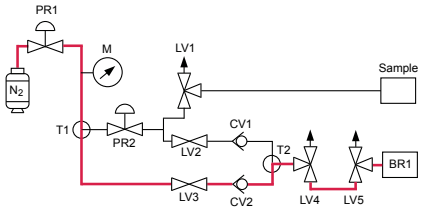

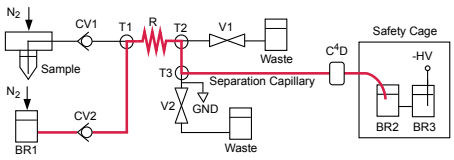

Filling sample loop

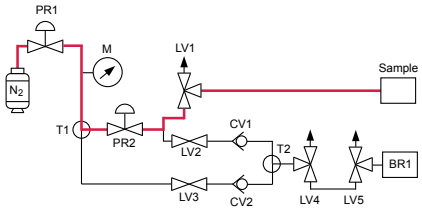

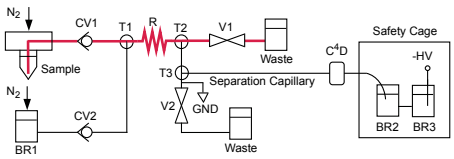

Parts for CE device						
Name	Designation in figures	Supplier	Product number	Amount	Cost in Euro	Total Cost in Euro
Microfluidic Part						
One-Piece Fitting		LabSmith	LS-100	12	11.63	139.56
One-Piece Plug		LabSmith	LS-101	10	9.61	96.10
Interconnect Tee	T1-3	LabSmith	LS-203	3	20.23	60.69
Breadboard Reservoir 5 mL	Waste	LabSmith	LS-BBRES-5ML	2	60.68	121.36
Breadboard Reservoir 1.1 mL	BR1-3	LabSmith	LS-BBRES-1ML	3	80.91	242.73
Breadboard		LabSmith	LS-LS-BB600	2	46.52	93.04
uPS Pressure Sensor		LabSmith	LS-uPS	2	151.71	303.42
Solenoid Valves	V1-2	NResearch	HP225T021	2	79.45	158.91
Tubing Sleeves, 1/16" OD, 390 µm ID		Idex	U360-SLV	1	37.00	37.00
Check Valve Inlet Assembly 3 psi 1/4-28 .020	CV1-2	Idex	CV-3315	2	95.41	190.83
Flangeless Ferrules		Idex	P-200N	10	1.26	12.64
Flangeless Nut		Idex	P-218	10	1.90	18.95
Y Assembly		Idex	P-512	1	30.89	30.89
PEEK Tubing 1/16" OD x .010" ID		Idex	1531L	1	163.57	163.57
PEEK Tubing 1/16" OD x .020" ID		Idex	1532L	1	163.57	163.57
Perspex Box		Amazon	1283MDTEU	1	14.99	14.99
Case 203x160x69.5mm Aluminium		Teko	384.18	3	23.48	70.44
Microfluidic Reservoir for 1.5 mL Eppendorf® - XS	Sample	DARWIN microfluidics	-	1	126.00	126.00
Bel-Art™ SP Scienceware™ Conical Tube Holder		Bel-Art™	F187960000	1	19.65	19.65
TSP Standard FS Tubing, 25µm ID, 363µm OD, 10 m		BGB	TSP-025375	1	100.69	100.69
Pneumatic Part						
2-Stage Piston Regulator	PR1	Beswick Engineering	PR2-7NX-1NH-3V	1	149.99	149.99
Precision Regulator	PR2	Clippard	DR-2NR-5	1	37.62	37.62
2-Way Latching Valves	LV2, LV3	Clippard	E2L10C-7W012	2	40.44	80.87
3-Way Latching Valves	LV1, LV4, LV5	Clippard	E3L10C-7W012	3	38.11	114.32
Single-Station Manifold		Clippard	E10M-01	3	10.68	32.04
2-Station Manifold		Clippard	E10M-02	1	13.38	13.38
Male to Single Barb Connectors		Clippard	CT2-PKG	14	3.78	52.95
1/16 ID Hose T Fitting		Clippard	T22-2-PKG	3	10.10	30.30
Check Valve	CV1-2	Clippard	MCV-1BB	2	5.68	11.36
Angled Push-In Fitting		Clippard	PQ-FEO4P-PKG	1	19.25	19.25
Urethane Hose 1/8"		Clippard	URH1-0402-BLT-050	1	12.68	12.68
Pressure Switch		SMC	PSE530-M5	2	52.18	104.36
Pressure Gauge	M	SMC	K8-16-40	1	7.97	7.97
Electronic Part						
High Voltage Module	HV-Module	Spellman	UM30N4/S	1	458.00	458.00
Arduino Nano 3.0	Arduino Nano	Arduino	A000005	1	16.87	16.87

Digital to Analog Converter	DAC	Maxim	MAX517BEPA+	1	4.78	4.78
H Bridge	H-Bridge	ROHM Semiconductor	BD6220F-E2	5	2.19	10.95
Valve Driver	Valve Driver 1-2	NResearch	225D1X75R	2	16.88	33.75
Circuit Board Epoxy Base 16/10th - 35 microns - 2 sides		C.I.F.	AB16	1	8.46	8.46
Voltage Regulator		Texas Instruments	LM340T5	1	1.39	1.39
Power Supply		MEAN WELL	GST60A12-P1J	1	15.30	15.30
Instrumentation Amplifier		Texas Instruments	INA111AP	2	10.50	21.00
Pin Header Male 13		Molex	22-27-2131	1	0.56	0.56
Socket		WURTH ELEKTRONIK	61300411821	1	0.35	0.35
Crimp Housing 1x13P		Molex	22-01-2135	2	0.47	0.93
Female Connector		WURTH ELEKTRONIK	61300911821	2	0.34	0.69
15-PIN Female Header		Gravitech	15Fx1-254mm	2	1.06	2.12
USB Connector		Neutrik	NAUSB-W	1	5.35	5.35
Capacitor 100 nF		Wima	MKS2C031001A00KSSD	13	0.34	4.48
Capacitor 10 µF		AVX	TAP106M035CCS	1	1.47	1.47
Resistor 4.7k		MULTICOMP PRO	MF25 4K7	2	0.04	0.08
Resistor 270		MULTICOMP PRO	MF25 270R	1	0.04	0.04
C4D headstage		EDAQ	ET120-317	1	428.42	428.42
C4D data acquisition		EDAQ	ER225	1	2985.98	2985.98
Total						6833
Note, that some additional small parts are required, such as wires for electrical connections etc.						

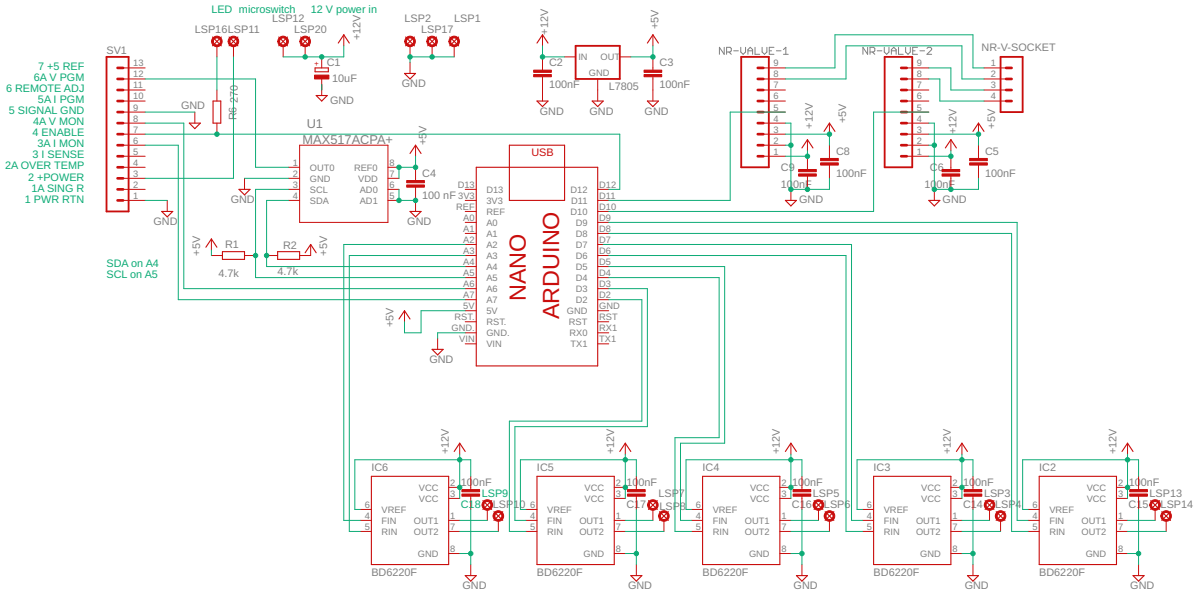
LED microswitch
12 V power in
7 +5 REF
6A V PGM
6 REMOTE ADJ
5A I PGM
5 SIGNAL GND
4A V MON
4 ENABLE
3A I MON
3 I SENSE
2A OVER TEMP
2 +POWER
1A SING R
1 PWR RTN
SDA on A4
SCL on A5
MAX517ACPA+
NANO
ARDUINO
USB
L7805
NR-VALUE-1
NR-VALUE-2
NR-V-SOCKET
BD6220F
IC6
IC5
IC4
IC3
IC2
GND
+5V
+12V

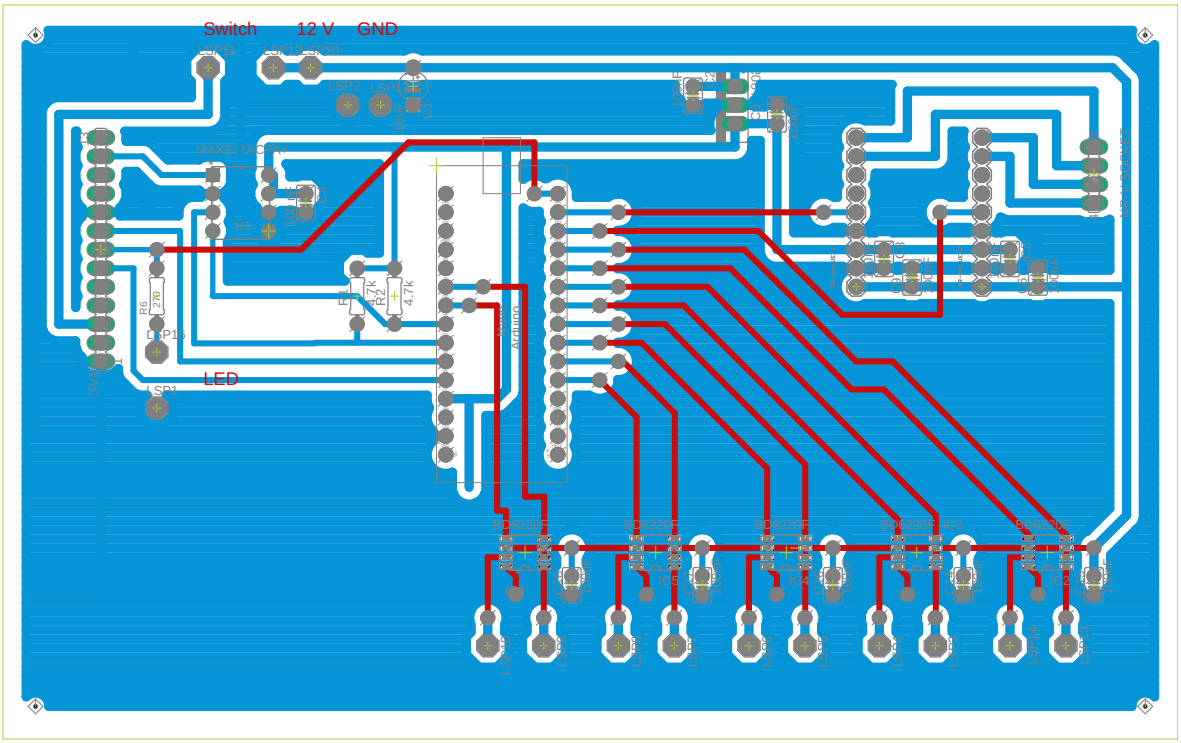
Switch
12 V
GND
LED
MAX517ACPA+
NANO
ARDUINO
BD6220F

Operating sequence

Step	Operation	Duration	Flow Rate	Buffer Amount	Sample Amount	V1	V2
		(s)	(μL s^{-1})	(μL)	(μL)		
1	Interface flushing (P1)	0.5	15	7.4	-	Open	Closed
2	Interface flushing (P2)	1.0	15	15	-	Closed	Open
3	Capillary flushing	60	4.3E-03	0.26	-	Closed	Closed
4	Pressure release	0.5	0	-	-	Open	Open
5	Filling sample loop	8	15	-	118	Open	Closed
6	Pressure release	1.5	0	-	-	Open	Closed
7	Sample transport	0.6	15	8.9	-	Closed	Open
8	Sample Injection	0.4	4.3E-03	1.73	-	Closed	Closed
9	Pressure release	1.0	0	-	-	Open	Closed
10	Interface flushing (P1)	1.5	15	22	-	Open	Closed
11	Interface flushing (P2)	5.0	15	74	-	Closed	Open
12	Pressure release	0.5	0	-	-	Open	Open
13	High voltage on	variable	0	-	-	Open	Closed

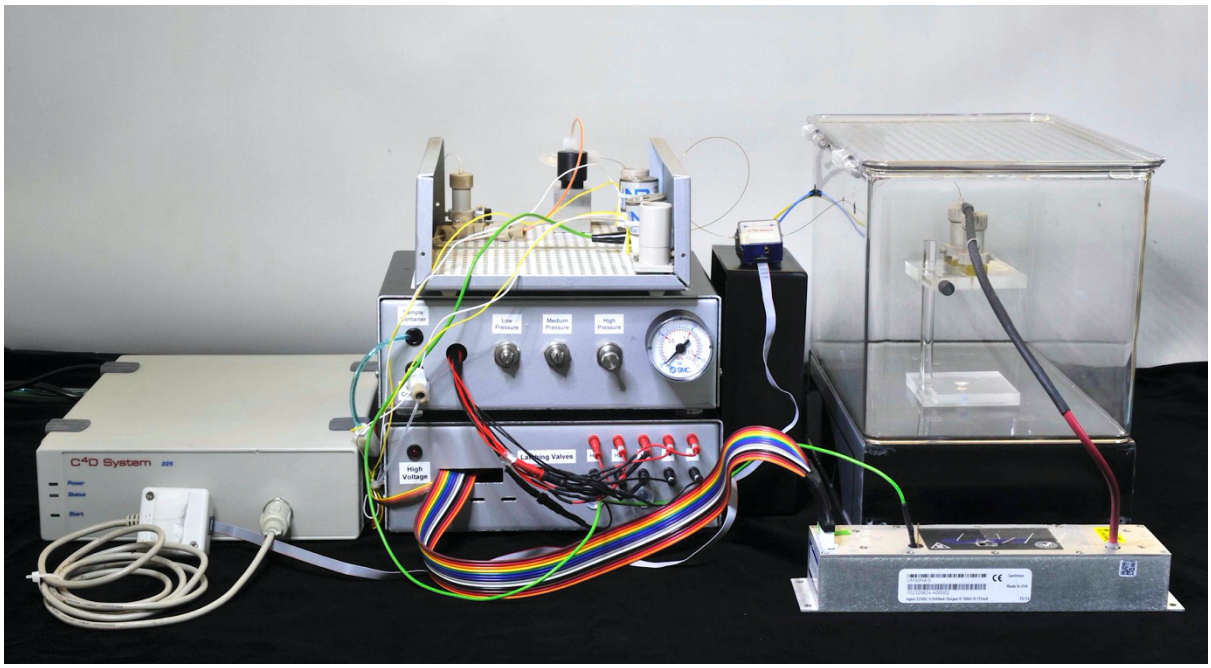
C4D System
Low Pressure
Medium Pressure
High Pressure
High Voltage

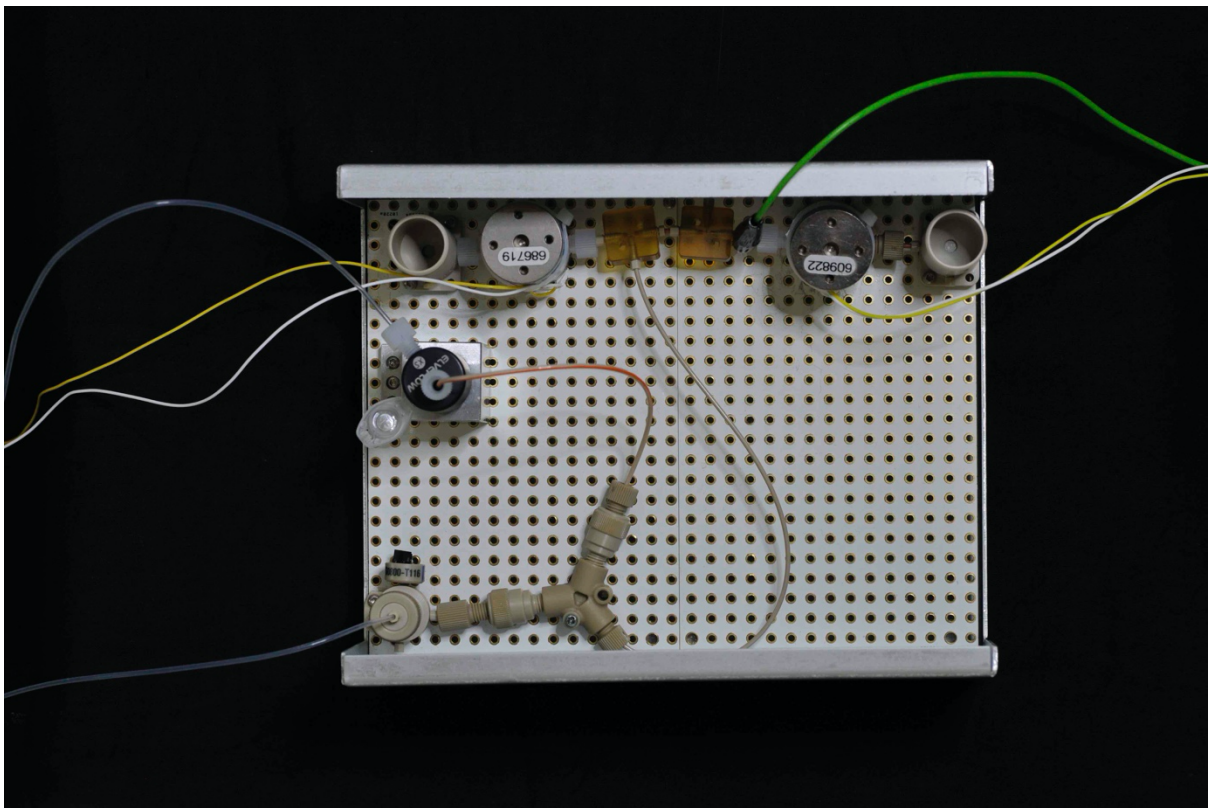
686719
609822

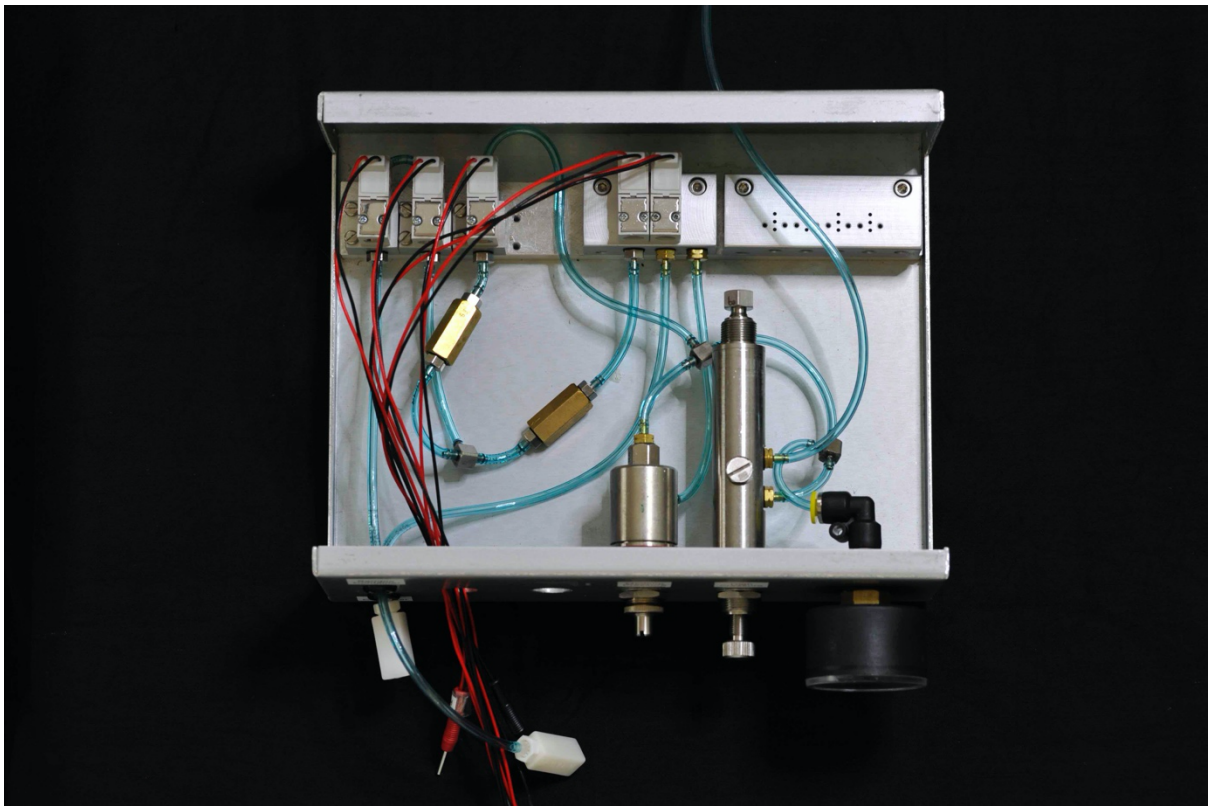

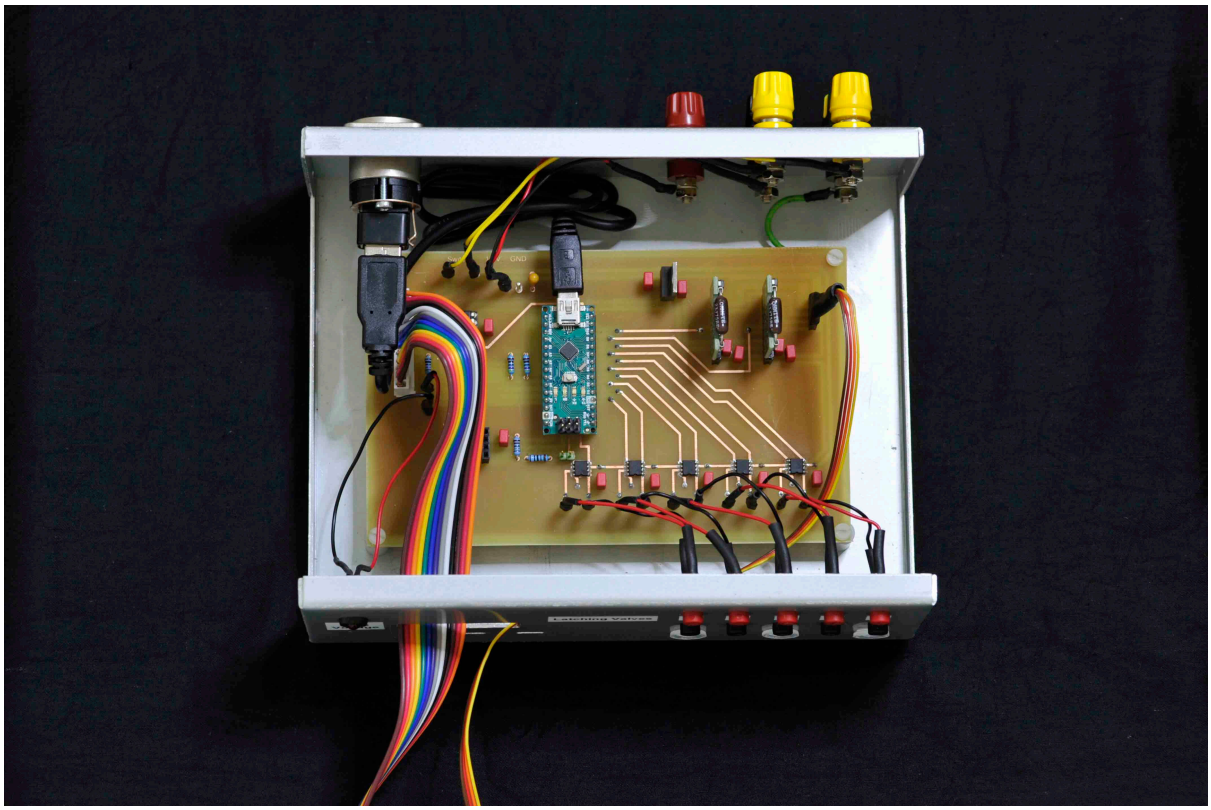

VERSATILE CAPILLARY ELECTROPHORESIS INSTRUMENTS BASED ON THE MICROFLUIDIC BREADBOARD APPROACH

Poster presented at the 26th International Symposium on Electroseparation and Liquid Phase-Separation Techniques in Toulouse, France, September 2019.

VERSATILE CAPILLARY ELECTROPHORESIS INSTRUMENTS BASED ON THE MICROFLUIDIC BREADBOARD APPROACH

Jasmine S. Furter, Johannes Abraham, and Peter C. Hauser

Departement of Chemistry, University of Basel, Klingelbergstrasse 80, 4057 Basel, Switzerland

j.furter@unibas.ch

University of Basel

I. INTRODUCTION

Capillary electrophoresis (CE) as a very versatile separation technique is nowadays frequently used in industrial and environmental areas addressing different analytical tasks ranging from high-molecular-weight proteins, peptide analyses, DNA sequencing to small inorganic analytes.[1] Automation was an essential step in the development of CE instruments leading to an enhancement in reproducibility and robustness of the separation technique.[2] Today, commercial CE instruments are often used for one specific application as benchtop instruments, but lack in flexibility for scientific research or field applications. The microfluidic breadboard approach [3] to CE instruments is based on different miniature components as a modular system for building microfluidic injection systems on breadboards. Similar to lab-on-chip devices, buffer and sample amounts are reduced, but the setup is much less rigid. Easy amendments in capillary length, inner diameter, applied voltage, injected sample amount and detection method can be made. Injection processes are automated by using a microcontroller and operated with a software in the programming language *Forth*. As examples the instruments can be used for measuring biogenic amines in food and inorganic ions in water.

II. SET-UP OF THE INSTRUMENT

Commercially available miniature components, which are suitable for withstanding high pressures while consuming low power, allow building microfluidic channels on compact breadboards.

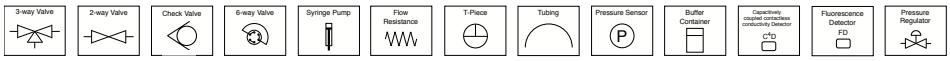

One previously published configuration of a CE instrument is shown, using flow resistors to control flow rates within the system.[4] The instrument was optimized for fast analysis of inorganic cations.

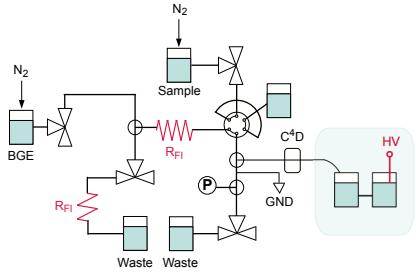

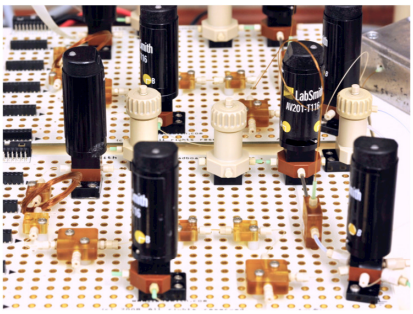

III. DETECTION

For the analysis of inorganic ions, a lab-made capacitively coupled conductivity detector (C4D) was used.

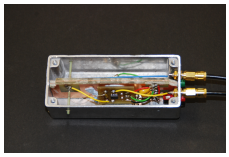

Analytes at low concentrations were detected by laser induced fluorescence (LIF). For this purpose, a fluorescence detector was built by using a laser diode with an excitation wavelength at 637 nm.

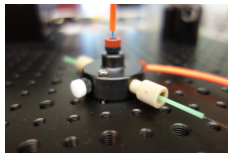

IV. RESULTS

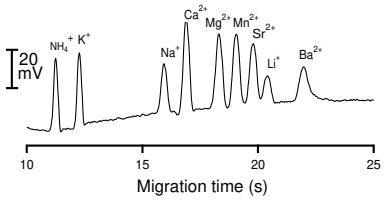

Analysis of inorganic ions at 80 µM, BGE: 60 mM L-His, 5 mM 18-Crown-6 and 0.2 mM acetic acid (pH 4), capillary 10 µm ID, 365 µm OD, 6 cm effective length, 17 cm total length, Injection: 0.5 s at 4.14 bars.

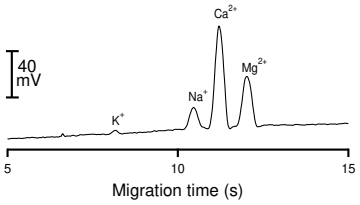

Determination of inorganic cations in mineral water (Cristalp®) (1:20 dil.), BGE: 60 mM L-His, 5 mM 18-Crown-6 and 0.2 mM acetic acid (pH 4), capillary 10 µm ID, 365 µm OD, 4 cm effective length, 17 cm total length, Injection: 0.5 s at 4.14 bars.

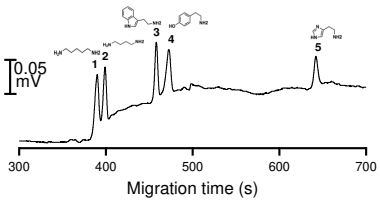

Analysis of biogenic amines at 400 nM, derivatized with Cy5. 1: Cadaverine, 2: Putrescine, 3: Tryptamine, 4: Tyramine, 5: Histamine. BGE: 60 mM sodium tetraborate, 10 % 2-propanol (pH 10), capillary 50 µm ID, 365 µm OD, 60 cm effecive length, 65 cm total length, Injection: 0.4 s at 1.35 bars. Chemical structures of the underivatized biogenic amines are shown.

V. PNEUMATICS

A constant pressure delivered by a nitrogen gas cylinder is used to drive liquids in the microfluidic channels. Miniature pressure regulators provide the required pressures needed for the different steps in the injection sequence.

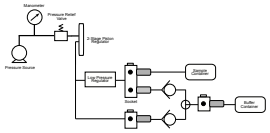

VI. HARDWARE

For controlling the hardware devices in the experiment, a small microcontroller platform was used. The Arduino Nano can easily be programmed and was plugged onto a purpose build printed circuit board (PCB) serving as an interface to the experiment.

VII. SOFTWARE

The interpreted programming language *Forth* was used to operate the instrument.[5] The program running on the microcontroller allows to operate the experiment interactively using so-called Words, which are small subroutines. *Forth* can easily be learned by non-professional programmers and applied for controlling complex experimental setups.

VIII. FURTHER PROJECTS

Portable CE instrument for field applications

IX. CONCLUSIONS

- The microfluidic breadboard approach can be used as a modular design tool for building CE instruments.
- The resulting CE instruments have a compact and flexible set-up. They can easily be rearranged for different applications.
- Possible applications are shown such as the determination of inorganic ions in water or biogenic amines by LIF.

REFERENCES

[1] Voeten, R. L. C., Ventouri, I. K., Haselberg, R. and Somsen, G. W., *Anal. Chem.*, **2018**, *90*, 1464-1481.

[2] Toraño, J. S., Ramautar, R., de Jong, G., *J. Chromatogr. B*, **2019**, *1118-1119*, 116-136.

[3] Koenka, I. J, Sáiz, J., Rempel, P. and Hauser, P. C., *Anal. Chem.*, **2016**, *88*, 3761-3767.

[4] Furter, J. S., Hauser, P. C., *Electrophoresis*, **2019**, *40*, 410-413.

[5] Furter, J. S., Hauser, P. C., *Anal. Chim. Acta*, **2019**, *1058*, 18-28.